Reduced Order Modeling for Smart Grids' Simulation and Optimization

Muhammad Haris Malik

UNIVERSITE BRETAGNE LOIRE

Thèse de Doctorat

Muhammad Haris MALIK

Mémoire présenté en vue de l'obtention
du grade de Docteur de l'École Centrale de Nantes
Docteur de la Universitat Politècnica de Catalunya
sous le sceau de l'Université Bretagne Loire

École doctorale : Sciences Pour l'Ingénieur, Géosciences, Architecture

Discipline : **Génie Mécanique, productique transport**
Unité de recherche : **Institut de Calcul Intensif**

Soutenue le 28 février 2017

Reduced Order Modeling for Smart Grids' Simulation and Optimization

JURY

Président :	**Ruth Vazquez SABARIEGO**, Professeur, Université KU Leuven (Belgique)
Rapporteurs :	**Elías CUETO**, Professeur, Université de Saragosse (Espagne) **Pierre JOYOT**, Maître de conférences- HDR, École Supérieure des Technologies Industrielles Avancées
Examinateurs :	**Manuel PINEDA-SÁNCHEZ**, Professeur, Université Polytechnique de Valence (Espagne) **Ruth Vazquez SABARIEGO**, Professeur, Université KU Leuven (Belgique)
Directeur de thèse :	**Francisco CHINESTA,** Professeur des Universités, École Centrale de Nantes
Co-directeur de thèse :	**Pedro DÍEZ**, Professeur, Université Polytechnique de Catalogne (Espagne)
Co-encadrant de thèse :	**Domenico BORZACCHIELLO**, Chargé de Recherche, École Centrale de Nantes

Acknowledgements

A very special gratitude goes out to all members of the consortium of SEED Erasmus Mundus Joint Doctorate for helping and providing the funding for the work and also to the coordinators at the two universities I spent time during my research.

I would like to specially thanks my thesis supervisors Prof. Francisco Chinesta, Prof. Pedro Díez and Dr. Domenico Borzacchiello. Especially Dr. Borzacchiello who helped me a lot in the understanding of an entire new engineering field of power systems. I would also like to thank Prof. Chinesta for his brilliant vision which guided me in the research carried out. I would also like to give special thanks to Prof. Pedro Díez who was always present and guided me during my thesis. With the constant support and guidance of all my thesis supervisors, I was able to carry out the research work during my doctoral studies.

I am grateful to my brother and mother and my wife, who have provided me through moral and emotional support in my life. I am also grateful to my friends in Ecole Centrale Nantes and Universitat Politècnica de Catalunya who have supported me along the way.

I am also grateful to the members of my thesis committee, especially Prof. Elías Cueto and Prof. Pierre Joyot. I am also grateful to Prof. Ruth Vazquez Sabariego and Prof. Manuel Pineda-Sánchez for their valuable comments that improved the quality of this dissertation.

Thanks for all your encouragement!

To my mother and my wife ...

Contents

List of Figures

List of Tables

Abstract

Résumé (French)

Cette thèse présente l'étude de la réduction de modèles pour les réseaux électriques et les réseaux de transmission. Un point de vue mathématique a été adopté pour la réduction de modèles. Les réseaux électriques sont des réseaux immenses et complexes, dont l'analyse et la conception nécessite la simulation et la résolution de grands modèles non-linéaires. Dans le cadre du développement de réseaux électriques intelligents (smart grids) avec une génération distribuée de puissance, l'analyse en temps réel de systèmes complexes tels que ceux-ci nécessite des modèles rapides, fiables et précis. Dans la présente étude, nous proposons des méthodes de réduction de de modèles à la fois a priori et a posteriori, adaptées aux modèles dynamiques des réseaux électriques.

Un accent particulier a été mis sur la dynamique transitoire des réseaux électriques, décrite par un modèle oscillant non-linéaire et complexe. La non-linéarité de ce modèle nécessite une attention particulière pour bénéficier du maximum d'avantages des techniques de réduction de modèles. Initialement, des méthodes comme POD et LATIN ont été adoptées avec des degrés de succès divers. La méthode de TPWL, qui combine la POD avec des approximations linéaires multiples, a été prouvée comme étant la méthode de réduction de modèles la mieux adaptée pour le modéle dynamique oscillant.

Pour les lignes de transmission, un modèle de paramètres distribués en domaine fréquentiel est utilisé. Des modèles réduits de type PGD sont proposés pour le modèle DP des lignes de transmission. Un problème multidimensionnel entièrement paramétrique a été formulé, avec les paramètres électriques des lignes de transmission inclus comme coordonnées additionnelles de la représentation séparée. La méthode a été étendue pour étudier la solution du modèle des lignes de transmission pour laquelle les paramètres dèpendent de la fréquence.

Mots-clés Réseaux Intelligents, Dynamique transitoire, Équations oscillantes, Lignes de transmission, Réduction de modèles, Décomposition orthogonale appropriée, Méthode d'incrémentation de grande longueur, Méthode linéaire par morceaux de trajectoire, Décomposition généralisée appropriée, Paramètres dépendants de la fréquence

Resumen (Spanish)

Esta tesis presenta un estudio de la reducción de modelos (MOR) para redes de transmisión y distribución de electricidad. El enfoque principal utilizado ha sido la dinámica transitoria y para la reducción de modelos se ha adoptado un punto de vista matemático. Las redes eléctricas son complejas y tienen un tamaño importante. Por lo tanto, el análisis y diseño de este tipo de redes mediante la simulación numérica, requiere la resolución de modelos no-lineales complejos. En el contexto del desarrollo de redes inteligentes, el objetivo es un análisis en tiempo real de sistemas complejos, por lo que son necesarios modelos rápidos, fiables y precisos. En el presente estudio se proponen diferentes métodos de reducción de modelos, tanto a priori como a posteriori, adecuados para modelos dinámicos de redes eléctricas.

La dinámica transitoria de redes eléctricas, se describe mediante modelos dinámicos oscilatorios no-lineales. Esta no-linearidad del modelo necesita ser bien tratada para obtener el máximo beneficio de las técnicas de reducción de modelos. Métodos como la POD y la LATIN han sido inicialmente utilizados en esta problemática con diferentes grados de éxito. El método de TPWL, que combina la POD con múltiples aproximaciones lineales, ha resultado ser el mas adecuado para sistemas dinámicos oscilatorios.

En el caso de las redes de transmisión eléctrica, se utiliza un modelo de parámetros distribuidos en el dominio de la frecuencia. Se propone reducir este modelo basándose en la PGD, donde los parámetros eléctricos de la red de transmisión son incluidos como coordenadas de la representación separada del modelo paramétrico. Este método es ampliado para representar la solución del modelos con parámetros dependientes de la frecuencia para las redes de transmisión eléctrica.

Palabras claves Redes Inteligentes, Dinámicas Transitorias, Ecuaciones de Movimiento Oscilatorio, Líneas de Transmisión, Reducción de Modelos, Descomposición Ortogonal Propia, Método de Incremento de Gran Tiempo, Método Lineal en Trayectoria Piece-wise, Descomposición Generalizada Propia, Parámetros Dependientes de la Frecuencia

Abstract

This thesis presents the study of the model order reduction for power grids and transmission networks. The specific focus has been the transient dynamics. A mathematical viewpoint has been adopted for model reduction. Power networks are huge and complex network, simulation for power grid analysis and design require large non-linear models to be solved. In the context of developing "Smart Grids" with the distributed generation of power, real time analysis of complex systems such as these needs fast, reliable and accurate models. In the current study we propose model order reduction methods both a priori and a posteriori suitable for dynamic models of power grids.

The model that describes the transient dynamics of the power grids is complex non-linear swing dynamics model. The non-linearity of the swing dynamics model necessitates special attention to achieve maximum benefit from the model order reduction techniques. In the current research, POD and LATIN methods were applied initially with varying degrees of success. The method of TPWL has been proved as the best-suited model reduction method for swing dynamics model; this method combines POD with multiple linear approximations.

For the transmission lines, a distributed parameters model in frequency-domain is used. PGD based reduced-order models are proposed for the DP model of transmission lines. A fully parametric problem with electrical parameters of transmission lines included as coordinates of the separated representation. The method was extended to present the solution of frequency-dependent parameters model for transmission lines.

Keywords Smart Grids, Transient Dynamics, Swing Equations, Transmission Lines, Model Reduction, Proper Orthogonal Decomposition, Large Time Increment Method, Trajectory Piece-wise Linear Method, Proper Generalized Decomposition, Frequency-Dependent Parameters

Chapter 1

Introduction

This chapter presents the literature review and establishes the state of the art in the model order reduction of electrical power systems. Also, it presents the various model order reduction methods employed in the field of power systems.

Contents

1.1 Smart Grids

The term smart grid instantaneously pops the image of high voltage electric power lines and power generation stations in mind, but what exactly does it mean. The term "smart grid" refers to the use of computers, communications, sensing, and control technology parallel to the electric grid [3]. It is a two way flow of electricity and information which is capable of monitoring and controlling all the aspects of a power distribution system from power plants to individual customers [4]. In a Smart Grid, power production from different types of generation units are integrated into the grid and the grid is connected to the production units and the consumers and the information is constantly exchanged. The concept of an interconnection and information flow in a smart grid is depicted in the Figure 1.1.

Electric power grids are among the most complex network systems possible due to the large number of nodes and the interconnection of various types of sources, loads, and controls. Current electricity distribution systems have a number of flaws such as voltage drops, blackouts, overloads and as well as environmental issues of electricity generation mainly through the burning of fossil fuels [5]. There is a hope in the smart grid solutions that these problems can be overcome. The economic and environmental factors make it necessary for the adoption of smart grids with the advancement in the renewable energies and efficient energy management solutions. The electricity delivery is comparatively more reliable using smart grids and offer minimization of cost of electrical energy to the consumers and facilitate the interconnection of new generating sources to the already available grid [3].

Countries like US, China, India, UK and several countries within European Union have already started working towards the introduction of smart grids. This field has shown a lot of potential and business opportunities and an early start resulting in better implementation and new infrastructure could propel emerging nations to the front. USA has invested about US $7 billion [3], while China has invested about US $7.3 billion and a further planned investment of US $96 billion by the year 2020 [3]. China is one of the fastest growing countries and its energy needs will double by 2020. China accounts for about 18.2% spending of global smart grid appliances by the end of 2015. In the country's 12th Five Year Plan (FYP) for 2011 through 2015, the investments were raised by 68% particularly in ultra-high-voltage transmission lines [6] . South Korea is another country that has invested about US $1 billion and with a small US $65 million pilot project already implemented for 6000 homes in Jeju Islands [3]. The South Korean leaders envisage a nationwide implementation of smart grids by 2030. Developing countries like India and emerging countries like Brazil are also at the forefront of this technology with increase in their renewable energy productions.

Smart grid technology is the integration of advances in digital and information technology. It is designed to be flexible with operational intelligence and connectivity. Due to the availability of sensing and data sources it is possible to have real time precision in operations and control to dynamically optimize grid operations. It allows for variable rates of electricity to be charged at different times depending upon the demand and supply, thus benefitting consumers as well as reducing

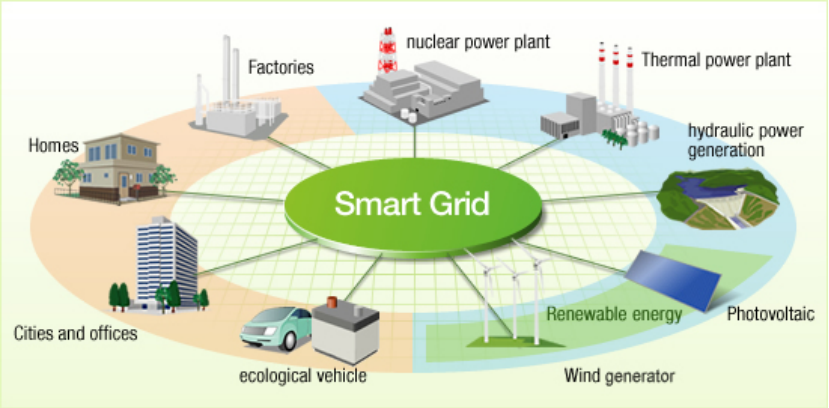

Figure 1.1: A graphic demonstration of the Smart Grid concept

loads during the peak hours. US department of energy (DOE) defined some of the main functionalities of the smart grids as self-healing, active participation from the consumers, resilient operations against physical and cyber attacks, accommodating different types of generation and storage options and most importantly optimized and efficient operations [3, 7].

1.1.1 Challenges and Opportunities

Transformation from traditional power generation systems and grids to smart grids is a major upgrade and a lot of challenges are ahead. The biggest challenge is the transition from the traditional grid to the smart grid with the grid running. There are security risks associated with the power grids in their current state, as well as the reliance on an old system with the ever growing complexity increases the probability of failures. The way forward is the gradual deployment of the smart grid solutions.

Optimum placement of distributed generation, determining failures and real time modification and self-healing are few to name. Modeling and analysis of electric power systems is another major challenge due to the large network size.

1.1.2 Distributed Generation

Distributed generation is one of the main components of accomplishing the smart grid concept. It is the decentralizing of the power generation capabilities from thermal or nuclear power plants to more environmental friendly renewable power generation, e.g. solar and wind power generation. An overview of the available literature reveals that there is no single consistent and agreed upon definition of distributed generation. It is generally considered as the generation of electricity from many small sources such as PV panels, small wind turbines etc. Apart from the definition, there are also multiple terminologies associated with the distribution generations such as Anglo-American countries often use “embedded generation” and in Europe and parts of Asia it is termed as “decentralized generation” [8]. The

definition of the distributed generation varies with the rating of the power units as well, as according to following definitions:

- The Electric Power Research Institute defines distributed generation from few kilowatts to 50 MW.
- Distributed generation is regarded as up to 25 MW according to the Gas Research Institute.
- Preston and Rastler define the size as ranging from a few kilowatts to over 100 MW [9].
- Others have defined similar power ratings of up to 100 MW as defining distributed generations.

Another important criterion in distributed generation is the location of the distributed generation plants. And also the manner this distributed generation is integrated with the grid.

Distributed generation can provide support for the primary network in the maintenance of a sustained and stable operation of the smart grid. It can supply directly to the customers or just provide a support and backup system [10].

1.1.3 Modeling and Simulation of Power Grids

Mathematical modeling of the electrical power systems is carried out in order to perform the simulation of the electric power systems. The objective of such simulations is to understand the behavior of the system under static and dynamic conditions [11]. Generally, power grids are large scale and complicated networks that have complicated, dynamic and nonlinear behavior changing continuously in both time and space [12]. The power system consists of many components like generators and loads and even these components are different from one another making the task of modeling and simulation further complicated because of the interdependence of heterogeneous components. The simulations are necessary to analyze the system weaknesses and to perform load flow and stability studies. These studies are extremely crucial because of the commercial and economic cost associated with the unreliability of power systems.

Mainly load flow or power flow studies are carried out for static analysis of the power grids and the data needed for such analysis consists of the topology of the network, transmission networks, model and parameters for transmission lines, location of power generation units and the loads. The details about these will be discussed in the subsequent chapters in the current thesis. In addition to this, dynamic studies must also be performed to ensure the uninterrupted and reliable power to the consumers. For such dynamic studies, the models are even more complicated and the level of required data increases further. All of this makes the modeling and simulation of power grids computationally expensive and therefore we see more and more applications of High Performance Computing (HPC) in the energy systems [13].

1.2 Model Reduction of the Power Grids

Power systems are typically large networks and very complicated engineering systems in operation in the present world. The analysis of such complex systems is computationally expensive. Real time analysis and study of dynamic stability of the system is a very difficult task numerically. As noted in the Sec. 1.1.3 about the applications of HPC in power systems has increased manyfolds. An alternative to the HPC is to make the model such that average computing capabilities can handle the problem. A reduced order model is therefore required for efficient simulation of the power grids. Reduced order models that replace a given mathematical model that is considerably smaller but still retains a reasonable level of accuracy and still contains the relevant dynamics of the system is an active area of research in power systems.

Traditionally, model order reduction of power systems can be categorized into two classes [14]. The first is based on the application of coherency and aggregation methods, which usually gives a reduced order non-linear model. The second method focuses on the external system that is less relevant to the part of the system under consideration and consider it as an input-output model and thus resulting in a lower order model.

In the electrical engineering community, dynamic equivalencing has been studied since 1970s as a means to perform model reduction. The earliest researchers in this field is Robin Podmare and the method proposed by Podmore [15] are still currently being employed in the industry in updated form. Dynamic equivalency method is a method based on the coherency and model reduction is achieved through aggregation of coherent generators or similar elements of the power system. The method works by identifying the elements of the power systems that are coherent and aggregating these coherent machines into equivalent single element. The distribution of the power system into the study system and an external system reduces the size of the model because the disturbances in the study system does not effect significantly the internal dynamics of the external system, although a sufficient level of connection between the two needs to be maintained in order to accurately model the system for the stability analysis. In large power grids, even after reduction the size of the model is still significant and usually more than 5000 buses and around 1000 generators [14].

Model reduction of power grids based on coherency technique was also presented in the study of Tanaka et al [16]. The main feature of their proposed model reduction method is the capability that the short circuit current in the reduced model remains equal to that of the original system and it reduces any radial or loop sub-systems. The focus on matching the short circuit current in the reduced and the original system is to retain the transient influence by the system disturbance. The proposed method is utilized in the Japanese market, the authors have concluded that the method is useful but there is little room for improvement in terms of accuracy and proposed the research should be focused on other areas to improve accuracy such as the modal truncation methods.

1.2.1 Static Equivalent Methods

Physical power systems are large networks and as already established by the discussion in the current chapter, need some kind of model reduction to perform simulation and analysis with available computing power in realistic time. Although the static analysis of the power flow analysis is less complicated than the dynamic problems encountered in the power system studies, researchers still thrive to form reduced models [17]. Static equivalent methods are developed simultaneously with dynamic equivalencing methods around 1970s [18, 19, 20, 21]. There is a rich collection of available literature and the study by Yu et al [17] have listed these categorizing them according to the methods. These methods include the Thevenin equivalent method, methods based on Ward equivalent [21] and REI equivalents. Müller and Nelles [22] have utilized the ability of Artificial Neural Networks (ANN) to model non-linear static systems and applied it on the static equivalent networks.

There are more recent work published on the topic of static equivalent methods, but considering our focus of research is on the dynamic systems we switch our focus to the model order reduction methods applied on the dynamic models of the power systems.

1.2.2 Dynamic Equivalencing

Dynamic Equivalencing is the earliest form of the model reduction in the research, analysis and design of power system dynamics with the earliest work available from Altalib and Krause [23], Podmore [15] and Rudnick et al [24]. With dynamic equivalencing, a part of the network termed as an external system is replaced by an equivalent system, a graphic example of this method is given in the manuscript of Feng et al [25]. In the study by Feng et al, they have presented the solution for dynamic equivalencing of networks in which distributed generation is present. The ever growing renewable energy generation increases the size and complexity of the power distribution network and it is very difficult to gather the exact data to model it properly. The focus of the study of Feng et al has been on such systems and presenting solutions for the dynamic equivalencing. The authors have used system identification methods based on input/output observances and regarded the system as a black box. The advantage in this technique is that with the unavailability of the actual network structure and parameters, the system can still be reduced. Methods used for system identification are ARX and State-Space from the MATLAB System Identification toolbox. The proposed method is proved to be accurate for the cases where the type and location of disturbances is same as for the system used for identification. If this changes, the accuracy levels drop which is the shortcoming of this proposed method. Nevertheless, the advantage is in the strength that without proper knowledge of the system parameters and structures, the method works.

Dynamic equivalencing methods are around since 1970s and Electric Power Research Institute (EPRI) developed DYNRED computer program which is still being employed in the industry. It has been updated and now includes online DSA (Dynamic Security Assessment) since 2010, this capability was tested by Ma et al and

the results were published in their study in 2011 [26].

Dynamic equivalent method's application depends upon the knowledge of the structure and the parameters of the power grid and its components. In the study by Feng et al [25], they proposed a method when these parameters are not known or difficult to know for certain. Other researchers presented ways to get these parameters, one such method is the use of phasor measurement units (PMU). Anderson and Chakrabortty [27] in their study presented their development of graph-theoretic algorithms for placement of PMUs which are used to identify the dynamic equivalent model. They have demonstrated their method on an IEEE 34-bus system, also they have shown the dependence of PMU locations and the computational time of these algorithms on network size and complexity. In an earlier paper by Chakrabortty et al [28] presented a methodology of reducing a two-area power system to a dynamic equivalent two machine system using the transient phasor measurements.

Takimoto [29] developed an algorithm for forming linear dynamic equivalents based on the modal analysis claiming that it has greater accuracy. The model order reduction is based on the aggregation of similar modes and also the elimination of the inferior modes, the author further claims that it has no significant effect on the frequency response of the subsystem and it is suitable for the steady-state and transient stability analysis studies. A brief description of the steady-state and transient stability analysis will be presented in the next chapter. The author has combined the mathematical techniques of model reduction, i.e., the modal analysis with the technique of dynamic equivalencing which is more prevalent in the electrical engineering field. As described earlier the techniques based on the coherency tends to have a lesser degree of accuracy compared with modal analysis but the author has chosen a coordinate system which is the same as the reference generator D-Q coordinate system instead of the R-J coordinate system. This allows the accuracy to be better even if the system becomes non-linear. The number of modes to be kept in the reduced system are managed in an intelligent way such that modes with similar eigenvalues are aggregated and the reduction is performed without damaging the frequency response. This means that some of the inferior modes have to be kept considering they are important for the frequency response. The method was verified using a power system consisting of 16 generators and it was shown that considerable reduction was achieved without a significant loss of accuracy. This paper is very interesting and it is suggested as a good read for researchers in the field of model reduction of power grids. It provides very good insight into the model reduction and its intricacies in the power system applications.

Singhavilai et al [30] presented a method to identify the dynamic equivalent of a power system using online measuement with the knowledge of coherent generators. The authors have used the graph model for knowing the number of coherent generators and their locations, thus eliminating the need for determination of the dynamic parameters of the power system. The authors have proposed five steps for the parameter identification which includes the graph model of the power system, identifying the coherent generators, aggregation and the network reduction. The method was demonstrated on a five bus power system and is shown to be reliable. There are other studies such as [31] which have proposed other methods for

the identification of parameters for the purpose of dynamic equivalent. They have demonstrated their approach on a 10 machine 39 bus New England test system and proved their method retains all the dynamics properties of the original network.

There are a lot of developments on the topic of dynamic equivalence [32, 33, 34, 35]. In the study by Zhou et al [34] introduced the dynamic characteristics of loads in the model reduction using the dynamic equivalent method. Hu et al [35] have also presented the work with inclusion of dynamic characteristics of loads instead of static load models.

Porkar et al [36] have presented a method using Frequency Domain method to find a network equivalent for the external system. The method they have used is the frequency dependent network equivalent (FDNE) and they have developed it by approximating the admittance matrix by vector fitting method.

Recent developments have also seen researchers working with artificial neural networks (ANN) [37] while Joo et al [38] have included the dynamics of the rotor and the voltage in the coherency based dynamic equivalencing for the model reduction purposes. Ouari et al [39] have proposed a method where the authors claim the coefficients matrices structure is preserved in the time domain representation. A detailed analysis and development through the years in the field of model reduction using the coherency principle is given in the book by Joe H. Chow [14].

1.2.3 Model Reduction by Mathematical Analysis

A number of approximation schemes are available for model reduction and selection of an appropriate scheme depends upon the problem to be tackled so that a suitable reduced order model is achieved [40]. The techniques defined by Bai et al [40] include Krylov-subspace techniques, Lanczos based methods such as MPVL algorithm and SyMPVL etc. In the subsequent discussion we will keep focus on the techniques used in model order reduction of the power grids' simulation. The methods presented in this section are other than the dynamic equivalencing methods and hence are more mathematical based model reduction. Takimoto [29] had categorized model reduction techniques in his study into one more engineering based and other mathematical based analysis and has presented a good reference base for both techniques that were available at that time. Here, we present studies which are published later than the study by Takimoto.

Chaniotis and Pai [41] have applied the Krylov Subspace methods in the model reduction of the power systems and have proposed a connection between the Krylov subspace model reduction and the previously discussed coherency in power systems. The authors have used the Krylov subspace method to reduce a linearized model of the external area of the power system and observed the effects of the model reduction by introducing a fault in the study area. Another objective of their study was to use this method for the identification of coherent generators in the external area. The authors have demonstrated the application of their method on a system that contains 50 machines in the external area of the power system.

The study by Parrilo et al. [42] presents the use of principal-orthogonal decomposition based methods to reduce the hybrid, non-linear model of a power network.

The focus of their study is to develop a reduced order model that is capable of approximating the global behavior of the hybrid non-linear power network. The authors used the "Swing Equations" which are the second order differential equations representing the rotor dynamics of the generator. These equations are used to represent each generator node and used along with an algebraic equation to denote each load bus. The models described in the study are hybrid and non-linear interconnected systems. To model a physical power grid, the simulation using this model becomes very large to handle and hence model reduction becomes important. The difficulties in the model reduction for this case are presented by the hybrid and non-linear nature of the model. In this paper, the Karhunen-Loéve decomposition is implemented. The Karhunen-Loéve decomposition provides for high dimensional systems with state space is R^n, a method to find the smallest dimensional subspace which contains observed points on the trajectories of the system. The subspace obtained through this decomposition is then used to project upon the dynamics from a Galerkin projection. Thus, the high-dimensional system is approximated by a small number of non-linear ordinary differential equations. The authors in this study also used the concept of external area and a study area, where the one half of the grid was reduced considering it as an external area while the area where the cascading failure was introduced was kept in original dimension, thus considering it as a study area. The results show excellent agreement between the original model with 100 states and the reduced model with 10 states only. It is one of the important studies which formed the basis of our current study.

In the study by Sturk et al [43], applied the structured model reduction on the power systems with an external area and a study area, the advantage the author claims is that it reduces the external area to a low order linear system keeping the nonlinear characteristic of the study system. In their study, the authors have linearized the external area before applying the model reduction algorithm on this part of the system. The method of structured model reduction is based on the concept of balanced truncation and there is a necessary requirement of being asymptotically stable. The authors in this study have used MATLAB's ode15s solver for the solution of the high fidelity and reduced order models as these DAEs are stiff, a phenomenon which contains both slow and fast dynamics. The same solver has also been used in our current study. The authors have demonstrated their algorithm using a 3 machine, 9 bus system and the system was reduced from 16 states to just 3 states. In another study by Sturk et al [44], the authors have presented the same methodology of structured model reduction to power systems without the need to identify the coherent group of generators.

Model reduction techniques like balanced truncation and optimal Hänkel are not recent and have been applied in the model reduction of the power systems. A good review of these and a couple of modified techniques have been presented in the study by Bettayeb and Al-Saggaf [45] and their application to a single machine infinite bus system. Comparison based on errors and transient responses are given between these techniques and it has been shown that the balanced, weighted balanced, optimal Hänkel and weighted optimal Hänkel are good model reduction methods. The two unweighted methods perform good in terms of transient responses but their steady

state behavior deteriorates which is improved in the weighted methods. Weighting also improves the transient performances. Detailed descriptions of these methods and their applications can be read from the chapter by Al-Saggaf and Bettayeb [46].

Cherid and Bettayeb [47] have presented reduced order models using balanced representations, the focus of their study is the single machine power system. The development is based on the state space representatiions and take into account the controllability and observability concept. The results show that the reduced model is accurate enough and a comparison with Davison reduction technique shows that the balanced reduction method adopted in this study performs better in both transient and steady state cases. In the study by Al-Saggaf [48], he has used the same balanced representations for the model reduction for the purpose of dynamic control of a power plant. The study by Al-Saggaf presented the development of dynamic equivalent model reduction which is presented in the previous section with the use of balanced state space representations.

Kashyap et al [49] have used model order reduction for the purpose of state estimation of phasor measurement units (PMU). The authors have proposed an algorithm based on reduced-dimension matrices which operate separately on PMU measurements and on conventional measurements. The proposed scheme is applicable to distributed implementation and is reported to be numerically stable. PMUs are used to measure electrical signals on an electric power grid and can be useful in real time management of the power grid, for the purpose of real time management state estimation (SE) is important. It is an initial step towards the implementation of the smarter grids. PMUs can provide accurate, synchronized measurements of voltage and current phasors sampled at upto 30 times per second, which is faster than the traditional measurement methods. PMU measurements are available as real and imaginary parts of the positive sequence voltage and current phasors. But, it is infeasible to cover the whole grid with PMUs and therefore the measurements are combined with the conventional instrument transformer measurements. The issue of combining these two measurements has been studied and presented an efficient algorithm. It is an iterative procedure where state vector is estimated using weighted least squares approach. The algorithm was applied on a IEEE 14-bus system and compared with existing schemes in the literature and demonstrated good accuracy.

Wille-Haussmann et al. [50] uses symbolic reduction approach to model lower order grid segments. Symbolic model reduction technique is based upon looking at the equations that describe the model and removing equations that do not influence the specified variables. Symbolic reduction works by starting with the detailed model and removing variables with negligible influence and aggregate the remaining equations into a reduced model. The reductions can be either algebraic, branch, switch reductions or term replacing or term cancellation. The study shows reduction by a factor of 2 for a typical grid. This algorithm was used for the optimal operation and control of smart grids.

The idea of using reduced order models for the real time control and optimization is based on the necessity of solving the huge network of nodes encountered in smart grids. The concept of proper generalized decomposition is applied for developing a reduced order model of the smart grids.

1.3 Motivation: Rationale and Advantages of Model Reduction

From the literature review presented in the previous sections, it can be deduced that most of the studies in the model reduction of power systems divide the power grid in two parts, namely, 1) study area and 2) external area. The model reduction albeit is applied only on the external area because its detailed study is not needed and therefore is considered for the model reduction because a loss of accuracy and details about the dynamics will not have a profound effect on the study area, while the study area has been modeled in detail as it has to be completely accurate and must capture the whole dynamic behavior.

The literature review presented in the previous sections demonstrates that there are a lot of challenges and hence opportunities available in the simulation of smart grids. The real time data available from the sensors in the distribution systems and the end user will make the real time operations of the smart grid advance and will enable customer engagement. The smart grids are the grids for the future and with advanced computation and visualizations; it will enable state estimation, real time contingency analysis and real time monitoring of dynamic behaviors in the system. The biggest hurdle in the simulation and optimal control is the sheer size of the grid network. This large domain makes traditional computational models inefficient and time consuming for this purpose. Therefore, the need for an efficient reduced order model so that the simulation and control of smart grids can be made possible in real time arises. PGD as shown in so many applications offers a potential in the reduced order modeling of the smart grids. It is demonstrated that the method of PGD can reduce the number of computations significantly and hence will allow the real time control possible and efficient.

In the current thesis, we endeavour to find a solution for the model reduction of the whole grid without the distinction between the external area and the study area. In doing so, our motivation is to have a reduced order model which is accurate enough compared to the high fidelity model and must capture the important dynamics of the power grid.

1.4 Objectives and Approach

The idea of having a model that can be used in real-time for control and prediction of the dynamic behavior of the power grids is of prime concern in this study. The design, analysis and optimization cycle for power grids require simulation models that can be run repeatedly and provide reliable and accurate results.

For this purpose, one cannot rely on full dimensional models for large complex problems. The answer to this kind of problem lies in the model order reduction. In the current research presented in this thesis, the objective is to search for such model order reduction techniques that can be applied to non-linear dynamic models involved in the simulation of power grids and develop reduced-order models. The main objectives of the current research can be summarized as:

1. Develop reduced-order model capable to efficiently simulate high order non-linear problems.

2. Develop reduced-order models that can be used with a broader range of input variables without the need of constantly updating.

3. Preferably, use a priori model order reduction methods and build a database of solutions that can be used in real-time analysis.

4. Present solutions for problems that are discovered during literature survey which have complex solutions. Present alternative computationally efficient model reduction solution techniques based on the methods of our expertise, i.e., LATIN and PGD.

The approach that is adopted in this research is using the methods that are well-understood for model order reduction on problems identified from the literature review of model order reduction in power grids. A priori methods which form the core competencies of our research group take the preference as the choice of method but a posteriori methods are also applied. Because, in power systems most of the studies focus on time-domain simulation we also approached the problem from time-domain. However, in some cases our experience suggest that some problems can be efficiently solved in frequency-domain and the model reduction methods are more effective, we transformed the problem in to frequency-domain and then applied our model reduction techniques. A general approach to the model order reduction adopted in the current thesis is shown through a flow-chart presented in Figure 1.2.

1.5 Scope of the Thesis

Keeping in view the objectives defined in Sec. 1.4 and the literature survey presented in Sec. 1.2, the thesis focuses on the transient dynamics of the power grids and transmission lines. The thesis is divided into six chapters as:

1. **Chapter 1** presents the literature survey and establishes the state of the art of model order reduction in power grids.

2. **Chapter 2** presents the models that are the focus of current research so that the reader gets familiar with the problem in hand. Some standard modeling techniques are introduced in this chapter and fast non-linear solver such as Alternating Search Directions (ASD) and Large Time Increment (LATIN) methods are presented. The test problems dealt with in the current thesis are also introduced and developed in this chapter.

3. **Chapter 3** gives an overview of the a posteriori model order reduction methods in the time-domain studied for the current research and also presented some initial results and discussions about the applications of the Proper Orthogonal Decomposition (POD) method. Then later in the chapter the method

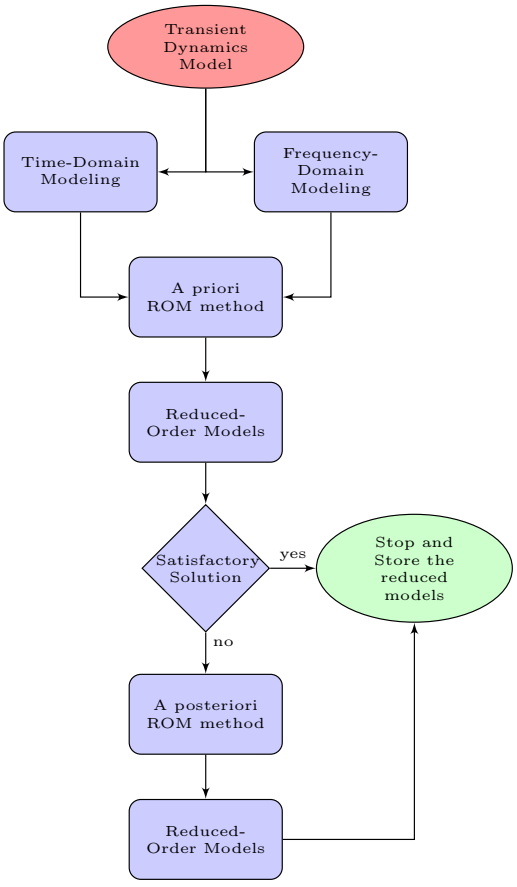

Figure 1.2: Thesis Flow Overview

of Trajectory Piece-wise Linear (TPWL) method which also is a posteriori method and its application on the swing dynamics model is presented. This also serves as the first major contribution of the current research.

4. **Chapter 4** and **Chapter 5** presents the a priori method of the Proper Generalized Decomposition (PGD) for the transmission line models and simulation. In Chapter 4, we present the PGD method as an harmonic solver using Distributed Parameters model for transmission lines and present it as an alternative model order reduction method. In Chapter 5, we present PGD as an efficient solver for problems with frequency dependent parameters and provide another major contribution of the current research.

Chapter 2

Basics of Power Systems and Problem Description

An introduction to the basics of the power systems and its elementary knowledge is vital for the understanding of the research presented in this thesis. In this chapter, we present a brief description of the power systems. The layout of the chapter is such that it starts with very basic definition of power systems and its constituents, later on in the chapter we will present different models used in the analysis and design of power systems that have been used in this thesis. Finally, we setup the test problem that will be the focus of research in the current study.

Contents

2.1 Power System

A general power system consists of sources of electrical energy usually generators or wind or solar powered renewable resources, a transmission and a distribution network and at the end the user generally termed as loads.

Electric power systems have some basic characteristics:

- Consists of three-phase AC systems at constant voltage.
- Traditionally, synchronous machines are used for electricity generation. These machines run on fossil fuel, some are nuclear powered and some are hydro powered and convert mechanical energy into electrical energy. Recently, renewable resources are added into electricity generation.
- Transmission of power from generators to end users over long distances. The transmission system for this purpose works on different voltage levels.

A schematic diagram of the components of the power system is given in Figure 2.1.

2.2 Definitions

In this section, we present some definitions that have been used in this thesis.

2.2.1 Current

Electric current can be defined as the flow of electric charge, the charge is basically the movement of electrons. The symbol for current is I and the SI units for current are Ampere named after André-Marie Ampère.

Generally, the currents are classified either as Direct Current (DC) or Alternating Current (AC). The difference between AC and DC is the direction of the flow of electric charge. DC is the unidirectional flow of the electric charge while in AC the electric charge periodically reverses direction, usually in a waveform defined by a sine wave.

2.2.2 Voltage

Voltage also called as the potential difference is the difference in electric potential energy between two points in a conductor. It represents the force that pushes the electric charge from one place to another. Voltage can be considered as the work done by per unit electric charge against a static electric field to move between two points. It is denoted by the symbol V and the SI units are volts. The units are named after the Italian scientist Alessandro Volta.

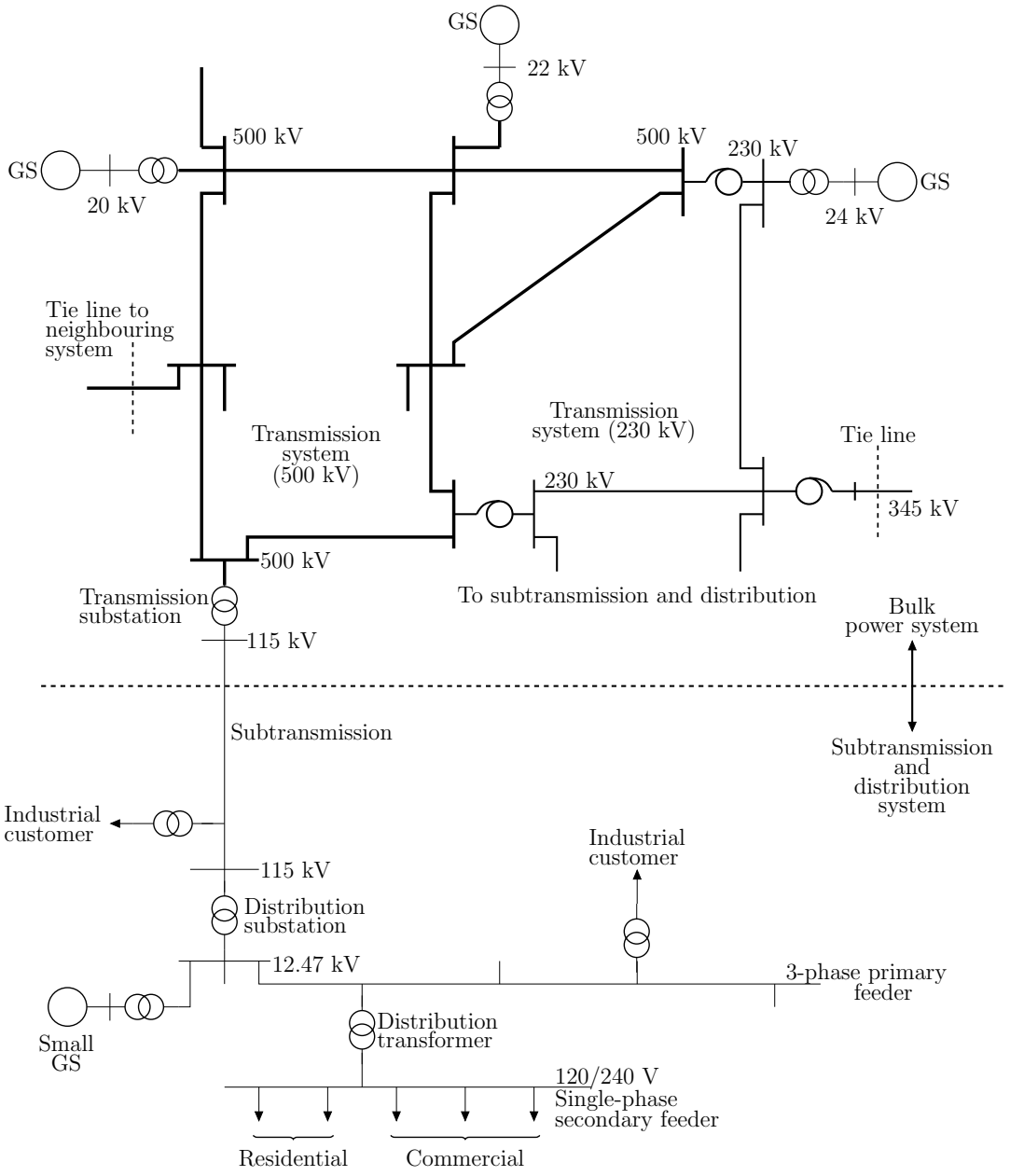

Figure 2.1: Basic elements of a power system [1]

2.2.3 Ohm's Law

Ohm's law is the relation between the current and the voltage, it states that the current passing through a conductor between two points is directly proportional to the voltage applied across these two points. The relationship is presented as:

$$V = IR \tag{2.1}$$

where, R is the proportionality constant defined as the resistance R with units of Ω (ohms). The resistance is usually a material parameter depending upon the conductor's material and geometry.

2.2.4 Power

Power is defined as the rate of energy E consumed or transferred by an electrical circuit per unit time. The SI unit of power is Watt (W) and is denoted by P.

$$P = \frac{E}{t} = VI \tag{2.2}$$

Since, power can be absorbed or supplied by a electrical component, there are two categories in which the components are placed.

2.2.4.1 Passive Devices

Passive devices or loads are devices which consume electric power and transform it into other forms of energy such as heat, light, mechanical work etc. Examples of passive devices are motors, light bulbs or electrical appliances.

For passive loads with linear relationship between current and voltage, Ohm's law can be used in the equation for power.

$$P = VI = I^2R = \frac{V^2}{R} \tag{2.3}$$

2.2.4.2 Active Devices

Active devices are components that generate power by converting other forms of energy to electrical energy for example, chemical energy from a battery or mechanical energy. These devices are called as power sources and common examples include generators and batteries.

2.2.4.3 Complex Power

For AC currents, the power takes the form of complex power denoted by S. Given voltage and current phasors V and I such that:

$$\begin{aligned} \boldsymbol{V} &= V\angle\delta \\ \boldsymbol{I} &= I\angle\phi \end{aligned} \tag{2.4}$$

Then the complex power S can be calculated as follows:

$$\begin{aligned} \boldsymbol{S} &= \boldsymbol{V}\boldsymbol{I}^* \\ &= V\angle\delta \times I\angle(-\phi) \\ &= VI\angle(\delta-\phi) \\ &= VI\angle(\theta) = VI\cos\theta - \iota VI\sin\theta \end{aligned} \tag{2.5}$$

where $\theta = \delta - \phi$ is the power angle (i.e phase difference between voltage and current).

The units of complex power are volt-ampere (VA). The power can be denoted as

$$\boldsymbol{S} = \boldsymbol{P} + \iota\boldsymbol{Q} \tag{2.6}$$

where, $\boldsymbol{P}$ is defined as the active or real power with units watt (W) while the $\boldsymbol{Q}$ is termed as the reactive power with the units of volt-ampere reactive (VAR). The magnitude of the complex power $|\boldsymbol{S}|$ is called the apparent power.

2.2.5 Bus

In load flow or power flow studies, the graph node of a single-line diagram typically with multiple connections at which voltage, current or power is to be calculated is called a bus.

2.2.6 Classification Of Buses

Generally, the buses are classified into three types depending upon the information known. A tabular representation of these buses is presented in Table 2.1.

2.2.6.1 Load Buses

As the name suggests, these buses are used to represent loads in the network. The loads draw power from the network defined be negative sign convention, real power $-P_{Li}$ and reactive power $-Q_{Li}$. In these buses, generated real power P_{Gi} and reactive power Q_{Gi} are taken as zero. This type of bus is also referred to as P-Q bus. The objective of the load flow studies is to find both the voltage magnitude $|Vi|$ and phase angle δ_i.

2.2.6.2 Voltage Controlled Buses

Buses where generators are connected are called as the voltage controlled buses. The power generation from the generators on these buses is controlled through prime mover while the terminal voltage is controlled through the generator excitation. At these buses, generated real power P_{Gi} and the voltage magnitude $|V_i|$ is kept constant. This is achieved by keeping the input power to the generator constant through turbine-generator control and the voltage is kept constant using automatic voltage regulator. These buses are also referred to as P-V buses. The reactive power Q_{Gi} supplied by the generator depends on the system configuration and is unknown along with the phase angle δ_i.

Node Type	$\lvert V_i \rvert$	δ_i	P_{Gi}	Q_{Gi}	P_{Li}	Q_{Li}
Slack (Reference)	✓	✓	×	×	✓	✓
PQ (Load Bus)	×	×	✓	✓	✓	✓
PV (Voltage Control Bus)	✓	×	✓	×	✓	✓

Table 2.1: Classification of buses with knowns and unknowns

2.2.6.3 Slack or Swing Bus

The slack bus acts as the angular reference for all the other buses. This is typically numbered as bus 1 for power flow analysis. Because the difference of angle between two voltage sources is important rather than the particular angle of a bus and this difference dictates the real and reactive power flow between them. Therefore, the particular angle of the slack bus is not important and is usually taken as 0°. Also, in power flow studies, voltage magnitude of slack is assumed to be known.

2.2.7 Kirchhoff's Laws

Kirchhoff's law are a set of two laws one for current and one for voltage, together with Ohm's law provides a tool for the analysis of electrical circuits. These are

2.2.7.1 Kirchhoff's Current Law

Kirchhoff's current law (KCL) states that at every node in a circuit, the sum of all currents entering must be equal to zero. It can be represented as:

$$\sum_{n=1}^{N} i_n = 0 \tag{2.7}$$

An alternative definition of KCL can be the sum of currents entering a node must be equal to the sum of currents leaving the node. This law is based on the law of conservation of charge.

2.2.7.2 Kirchhoff's Voltage Law

Kirchhoff's voltage law (KVL) states that the sum of voltages around a closed loop in an electrical circuit must be zero. It can be mathematically represented as:

$$\sum_{m=1}^{M} v_n = 0 \tag{2.8}$$

An alternative definition of KVL can be that the sum of voltage drops must be equal to the sum of voltage rises in a closed loop. It is based on the law of conservation of energy.

2.2.8 Admittance

Admittance is a measure of the ease with which an electrical current can pass through a circuit and also its possibility of getting polarized which is a dynamic quantity. It is a vector quantity comprised of two independent scalar quantities, namely, conductance G and susceptance B. The units of admittance are Siemens and it is given by the expression

$$Y = G + \iota B \tag{2.9}$$

Conductance G is the inverse of resistance and it is the quantity which represents the ease of passage of current through a circuit. The imaginary part of the admittance is called the Susceptance B, it is the AC counter part of the conductance. When an AC current passes through a component that has non-zero susceptance, energy is alternately stored and released either through a magnetic or an electric field. When the component through which current passes is an inductor, then it produces a magnetic field and the susceptance is inductive and is assigned a negative imaginary value. On the other hand if the component is a capacitor, an electric field is produced and the susceptance is called capacitive and is assigned positive imaginary values. Both conductance and susceptance have the same units as admittance, i.e., Siemens.

Admittance is the inverse of impedance Z

$$Y = \frac{1}{Z} \tag{2.10}$$

2.2.8.1 Bus Admittance Matrix

Bus admittance matrix or nodal admittance matrix (also called Y matrix or Y bus or admittance matrix) is an $N \times N$ matrix representing a power system containing N buses. The bus admittance matrix of a large power system has large number of zeros and hence is quite sparse. In the power flow study, the knowledge of Y matrix is fundamental. It provides a relation between the injected node currents and the node voltages.

$$\mathbf{I} = \mathbf{Y}_{bus}\mathbf{V} \tag{2.11}$$

where, $\mathbf{I}$ is the vector of injected node currents and $\mathbf{V}$ is the vector containing node voltages and $\mathbf{Y}_{bus}$ is the bus admittance matrix.

2.2.9 Impedance

Impedance is the inverse of admittance and it describes the opposition that an electric component or circuit offers to the flow of current. It is also a complex variable and consists of resistance R and reactance X. Impedance is denoted by symbol Z and the SI unit for impedance is ohms Ω. Mathematically,

$$Z = R + \iota X \tag{2.12}$$

In DC circuits, only the resistance R part of the impedance is present, but in the AC circuits, the imaginary part reactance X is also present. The reactance is the related to the energy stored and released in inductive and capacitive components with each AC cycle. Both resistance and reactance have the same units as impedance.

2.2.9.1 Bus Impedance Matrix

The inverse of the Bus Admittance Matrix is the Bus Impedance Matrix, also known as Z-matrix or impedance matrix. Unlike, the admittance matrix, impedance matrix can not be constructed by inspection.

$$\mathbf{V} = \mathbf{Z}_{bus}\mathbf{I} \tag{2.13}$$

The calculation of $\mathbf{Z}_{bus}$ can be done by inverting the admittance matrix, it is very useful in short-circuit calculations. Also, unlike the bus admittance matrix, bus impedance matrix is not sparse.

There are methods to build $\mathbf{Z}_{bus}$ and $\mathbf{Y}_{bus}$ which can be found in [51].

2.3 Power Flow Analysis

The most fundamental study of a power system is the solution for steady-state powers and voltages. It is important in system planning and operation and the most commonly performed study in power systems [51]. For the purpose of power flow analysis, the transmission system is modeled with nodes or buses representing generators or loads which inject and consume power respectively. These nodes are interconnected using transmission links and the topology of the network is given by either the bus admittance or bus impedance matrix.

The aim of the power flow study is to ensure that the power is delivered to the consumers within an acceptable voltage and frequency limits and reliably. In the power flow analysis, the complex power demanded by loads S_{Li} is known and constant. Power flow study requires the relationship between the complex power generated S_{Gi}, load demand S_{Li} and the bus voltages V_i across the network. This relation is given by the equations termed as "Power Flow Equations", which is presented in the Sec. 2.3.1.1.

In a few simple cases, power flow problems can be solved analytically but in most cases the power grid is too big to solve analytically and hence numerical methods are often applied for the solution. The numerical methods typically applied in the power flow analysis are:

- Gauss Iteration
- Gauss-Seidel Iteration
- Newton-Raphson Iteration

We explain the power flow problem using the standard method of Newton-Raphson in the next section.

2.3.1 Newton-Raphson

Newton-Raphson method is the second most commonly used power flow solution method after Gauss-Seidel Iteration method. The main idea behind Newton-Raphson is the linearization of the nonlinear power balance equations. We will explain the Newton-Raphson method using a general problem.

We assume a function $\mathbf{f}(\mathbf{x})$ n-dimensional function of variable $\mathbf{x}$ also an n-dimensional vector. Then, the problem is defined as find $\hat{\mathbf{x}}$ such that $\mathbf{f}(\hat{\mathbf{x}}) = 0$.

$$\mathbf{x} = \begin{bmatrix} x_1 \\ x_2 \\ \vdots \\ x_n \end{bmatrix} \quad , \quad \mathbf{f}(\mathbf{x}) = \begin{bmatrix} f_1(\mathbf{x}) \\ f_2(\mathbf{x}) \\ \vdots \\ f_n(\mathbf{x}) \end{bmatrix} \tag{2.14}$$

Newton-Raphson method is based on the first order linearization of the function. The linearization is carried out using the Taylor Series expansion, for multi-variable functions Taylor series is written as:

$$\begin{aligned} f_1(\hat{\mathbf{x}}) &= f_1(\mathbf{x}) + \frac{\partial f_1(\mathbf{x})}{\partial x_1}\Delta x_1 + \frac{\partial f_1(\mathbf{x})}{\partial x_2}\Delta x_2 + \cdots + \frac{\partial f_1(\mathbf{x})}{\partial x_n}\Delta x_n + \text{higher order terms} \\ &\vdots \\ f_n(\hat{\mathbf{x}}) &= f_n(\mathbf{x}) + \frac{\partial f_n(\mathbf{x})}{\partial x_1}\Delta x_1 + \frac{\partial f_n(\mathbf{x})}{\partial x_2}\Delta x_2 + \cdots + \frac{\partial f_n(\mathbf{x})}{\partial x_n}\Delta x_n + \text{higher order terms} \end{aligned} \tag{2.15}$$

In matrix terms, it can be represented as

$$\mathbf{f}(\hat{\mathbf{x}}) = \begin{bmatrix} f_1(\mathbf{x}) \\ f_2(\mathbf{x}) \\ \vdots \\ f_n(\mathbf{x}) \end{bmatrix} = \begin{bmatrix} \frac{\partial f_1(\mathbf{x})}{\partial x_1} & \frac{\partial f_1(\mathbf{x})}{\partial x_2} & \cdots & \frac{\partial f_1(\mathbf{x})}{\partial x_n} \\ \frac{\partial f_2(\mathbf{x})}{\partial x_1} & \frac{\partial f_2(\mathbf{x})}{\partial x_2} & \cdots & \frac{\partial f_2(\mathbf{x})}{\partial x_n} \\ \vdots & \ddots & \ddots & \vdots \\ \frac{\partial f_n(\mathbf{x})}{\partial x_1} & \frac{\partial f_n(\mathbf{x})}{\partial x_2} & \cdots & \frac{\partial f_n(\mathbf{x})}{\partial x_n} \end{bmatrix} \begin{bmatrix} \Delta x_1 \\ \Delta x_2 \\ \vdots \\ \Delta x_n \end{bmatrix} + \text{higher order terms} \tag{2.16}$$

The matrix with the partial derivatives is the Jacobian matrix $\mathbf{J}(\mathbf{x})$. The steps for the solution based on Newton-Raphson method are:

1. Make an initial guess $\mathbf{x}^i$.
2. Linearize the function $\mathbf{f}(\mathbf{x})$ using the Jacobian $\mathbf{J}(\mathbf{x})$ at $\mathbf{x}^i$.
3. Define the increment $\Delta\mathbf{x} \approx -\mathbf{J}(\mathbf{x})^{-1}\mathbf{f}(\mathbf{x})$
4. Update the previous value of $\mathbf{x}^i$ with the increment calculated from the first order approximation as $\mathbf{x}^{i+1} = \Delta\mathbf{x}^i + \mathbf{x}^i$
5. Iterate until convergence

There are certain advantages of the Newton-Raphson method. It has a quadratic rate of convergence, which means that when the error becomes small the solution converges very quickly. But, this has a negative side effect as well, the solution depends upon initial guess and it can diverge very quickly as well. In addition to this, the solution using Newton-Raphson method requires the computation of the derivative which in large systems can be computationally costly. We now discuss the application of Newton-Raphson method to Power Flow Analysis.

2.3.1.1 Power Flow Equations

The equations governing the power flow in a network are the power balance equations.

$$S_i = V_i I_i^* \tag{2.17}$$

where I_i^* is the complex conjugate of current I_i entering the node i. The current I_i can be replaced with the Kirchhoff's current law at node i:

$$I_i = \sum_{k=1}^{n} Y_{ik} V_k \tag{2.18}$$

The admittance Y_{ik} is the sum of conductances G_{ik} and the susceptances B_{ik} of the line connecting node i and k.

$$Y_{ik} = G_{ik} + \iota B_{ik} \tag{2.19}$$

The power S_i in terms of active and reactive powers is defined as:

$$S_i = P_i + \iota Q_i \tag{2.20}$$

Replacing the current in eq. (2.17) with the Kirchhoff's law given in eq. (2.18), and recalling the complex form of the voltage we have

$$\begin{aligned} S_i &= V_i \sum_{k=1}^{n} Y_{ik}^* V_k^* = \sum_{k=1}^{n} |V_i||V_k| e^{\iota\theta_{ik}} (G_{ik} - \iota B_{ik}) \\ &= \sum_{k=1}^{n} |V_i||V_k| (\cos\theta_{ik} + \iota \sin\theta_{ik})(G_{ik} - \iota B_{ik}) \end{aligned} \tag{2.21}$$

Writing the active and reactive power as the real and imaginary parts of the power balance equations

$$\begin{aligned} P_i &= \sum_{k=1}^{n} |V_i||V_k| (G_{ik}\cos\theta_{ik} + \iota B_{ik}\sin\theta_{ik}) = P_{Gi} - P_{Li} \\ Q_i &= \sum_{k=1}^{n} |V_i||V_k| (G_{ik}\sin\theta_{ik} - \iota B_{ik}\cos\theta_{ik}) = Q_{Gi} - Q_{Li} \end{aligned} \tag{2.22}$$

where subscripts G and L represent the power generated and the power load demanded at each node. So, now the power balance equations that are needed to be

solved to find the voltage magnitude and phases are defined, we apply the Newton-Raphson algorithm on this problem. Rewriting the eq. (2.22) as

$$\begin{aligned}\sum_{k=1}^{n}|V_i||V_k|(G_{ik}\cos\theta_{ik}+\iota B_{ik}\sin\theta_{ik})-P_{Gi}+P_{Li}=0\\ \sum_{k=1}^{n}|V_i||V_k|(G_{ik}\sin\theta_{ik}-\iota B_{ik}\cos\theta_{ik})-Q_{Gi}+Q_{Li}=0\end{aligned} \tag{2.23}$$

and adopting the notation of $P(x)$ for the first term in the first of the equations and $Q(x)$ for the first term in the second equation,

$$\begin{aligned}P_i(x)-P_{Gi}+P_{Li}=0\\ Q_i(x)-Q_{Gi}+Q_{Li}=0\end{aligned} \tag{2.24}$$

In power flow solution, one of the nodes is taken as the reference termed as the "slack bus", at the slack bus both the voltage magnitude and phase is known instead of the power generated and demanded. Once the voltage magnitudes and phases are calculated for each node the power demanded and generated at the slack node can be calculated. Therefore, for a network with n buses there are $2\times(n-1)$ unknowns and equations to be solved. The unknown variables are and the functions are then expressed as,

$$\mathbf{x}=\begin{bmatrix}\theta_2\\ \vdots\\ \theta_n\\ |V_2|\\ \vdots\\ |V_n|\end{bmatrix},\quad \mathbf{f}(\mathbf{x})\begin{bmatrix}P_2(x)-P_{G2}+P_{L2}\\ \vdots\\ P_n(x)-P_{Gn}+P_{Ln}\\ Q_2(x)-Q_{G2}+Q_{L2}\\ \vdots\\ Q_n(x)-Q_{Gn}+Q_{Ln}\end{bmatrix} \tag{2.25}$$

Applying the algorithm as described earlier, an initial guess for all the θ_i and $|V_i|$. The most difficult part and time-consuming part of the Newton-Raphson method is the evaluation of the Jacobian matrix at each iteration. This especially becomes problematic as the grid becomes larger and the complexity of the problem increases by the order of $\mathcal{O}(n^2)$. The Jacobian in the case of power flow problems, can be computed analytically by the expression given in eqs. (2.22). As an example we apply Newton-Raphson algorithm to a two bus system assuming bus one is the slack bus.

2.3.1.2 Example Problem

Unknowns: $\mathbf{x}=\begin{bmatrix}\theta_2\\ |V_2|\end{bmatrix}$

Given: $\boldsymbol{Y}=\begin{bmatrix}-\iota 10 & \iota 10\\ \iota 10 & -\iota 10\end{bmatrix}$, $\quad P_2=200MW\ Q_2=100MVR$

$|V_1|=1.0\ pu\ ,\theta_1=0^\circ$

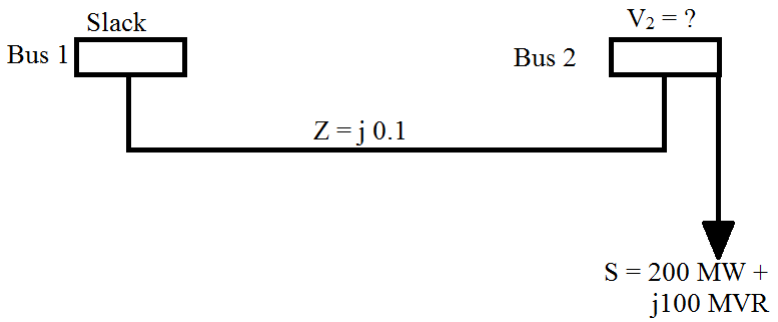

Figure 2.2: Example of a two bus problem

Solution:
An initial guess is made as
$\begin{bmatrix} \theta_2^{(0)} \\ |V_2|^{(0)} \end{bmatrix} = \begin{bmatrix} 0 \\ 1 \end{bmatrix}$

The iterations and the results are presented in Table 2.2.

Iteration	**New Solution**	**Error**
1	$\begin{bmatrix} -0.2 \\ 0.9 \end{bmatrix}$	$\begin{bmatrix} 0.2 \\ 0.1 \end{bmatrix}$
2	$\begin{bmatrix} -0.233 \\ 0.8586 \end{bmatrix}$	$\begin{bmatrix} 0.033 \\ 0.0411 \end{bmatrix}$
3	$\begin{bmatrix} -0.236 \\ 0.8554 \end{bmatrix}$	$\begin{bmatrix} 0.003 \\ 0.0035 \end{bmatrix}$

Table 2.2: Newton-Raphson Iterations for two bus example problem

Result: $\mathbf{x} = \begin{bmatrix} \theta_2 \\ |V_2| \end{bmatrix} = \begin{bmatrix} -13.52^\circ \\ 0.8554 \end{bmatrix}$

The results and iterations listed in Table 2.2 indicated the rapid convergence of the Newton-Raphson algorithm. But, as stated earlier the convergence to the correct solution inordinately depends on the initial guess. Just as an example, if we had chosen an initial condition to be $\begin{bmatrix} \theta_2^{(0)} \\ |V_2|^{(0)} \end{bmatrix} = \begin{bmatrix} 0 \\ 0.25 \end{bmatrix}$. The solution would then converged to a different solution that we call a low voltage solution. $\mathbf{x} = \begin{bmatrix} \theta_2 \\ |V_2| \end{bmatrix} = \begin{bmatrix} -49.91^\circ \\ 0.261 \end{bmatrix}$

This situation is explained through the Figure 2.3. The figure shows two hyperbolic curves representing the eq. (2.17) and a straight line representing eq. (2.18). The two points denoted by s_1 and s_2 are the two initial guesses which lead to different solutions on the hyperbolic curves of eq. (2.17), the solution converged in the

negative x-y quadrant is the low voltage solution while the solution converged in the positive x-y quadrant represents the correct high voltage solution.

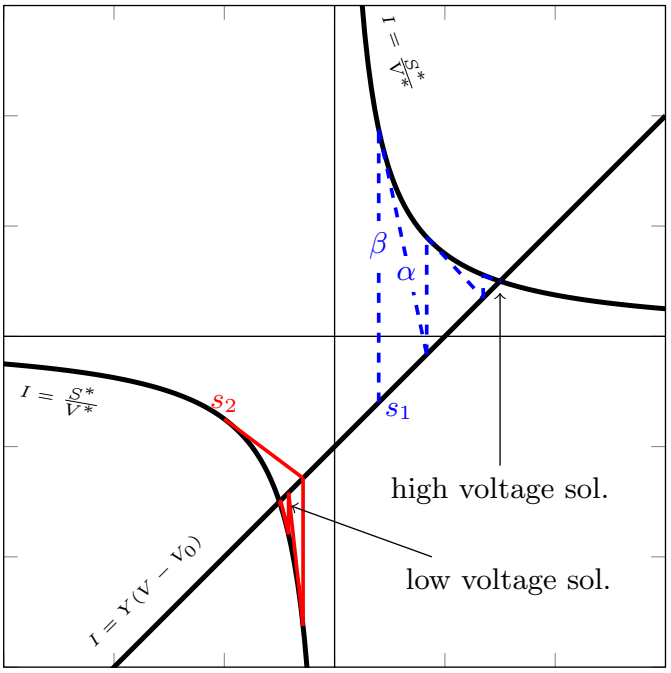

Figure 2.3: Convergence of the NR method w.r.t. initial guess

This is explained in detail in Figure 2.4 for what values of voltage magnitude and angle can be selected for the initial guess so that the method converges to the high voltage solution. On the x-axis is the phase angle and on the y-axis is the magnitude. Red region represents the convergence to the high voltage solution while the yellow region shows the initial value which leads to the low voltage solution.

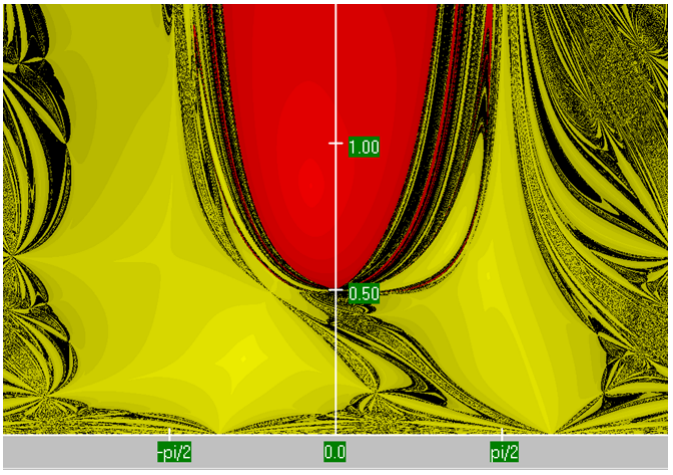

Figure 2.4: Region of convergence w.r.t. initial guess

2.3.2 Alternating Search Direction

A new method of Alternating Search Directions (ASD) was proposed for the solution of load flow problems. The motivation was that a method should be adopted in which the computationally cumbersome calculations of Jacobian matrix can be avoided instead a fixed direction should be selected for all iterations. Hence the computation of the search direction matrices can be done only once before the iteration process starts. There is an additional benefit of this method and it is the guaranteed convergence to the high voltage solution and hence the probability of wrong solution because of the initial guess is thus eliminated.

In order to better explain the method, we will forgo the index notation and present the equations in vector notation. Rewriting eq. (2.17) in vector notation and introducing I_0 as the constant current in the same equation.

$$\boldsymbol{Y}V = I_0 + I \tag{2.26}$$

A few symbols that are used in the future are defined here, $\odot$ denotes the Hadamard component-wise product of vectors and $\oslash$ denotes the component-wise quotient of vectors. The power balance equations in vector notation is written as:

$$S = V \odot I^* \tag{2.27}$$

In the method of alternating search directions, we use the equations described by (2.26) and (2.27) and introduce two additional linear equations. One single iteration of the method, involves solving these four equations in total in two steps. The additional equations that are introduced define the search directions and provide a linear relationship between the currents and voltages at each node. One of the each additional equation is paired with eq. (2.26) and eq. (2.27), for an iteration l, we can express the pair of equations as:

$$\begin{cases} I^{[l+(1/2)]} - I^{[l]} = \boldsymbol{\alpha}(V^{[l+(1/2)]} - V^{[l]}) \\ \boldsymbol{Y}V^{[l+(1/2)]} = I_0 + I^{[l+(1/2)]} \end{cases} \tag{2.28}$$

The superscript notation $[l+(1/2)]$ in eq. (2.28) represents the intermediate step at iteration l. The matrix $\boldsymbol{\alpha} \in \mathbb{C}^{n\times n}$ is known a priori and is the search direction for the first step. For the second step of the iteration, a matrix $\boldsymbol{\beta} \in \mathbb{C}^{n\times n}$ is used as the search direction and the second pair of equations is:

$$\begin{cases} I^{[l+1]} - I^{[l+(1/2)]} = \boldsymbol{\beta}(V^{[l+1]} - V^{[l+(1/2)]}) \\ V^{[l+1]*} \odot I^{[l+1]} = S^* \end{cases} \tag{2.29}$$

2.3.2.1 ASD method algorithm

The algorithm of alternating search direction method is simple, here we will briefly describe the algorithm and later apply it on a simple problem to demonstrate the method.

1. Given the system attributes like the admittance $\boldsymbol{Y}$ matrix, power demanded and generated at each node S_i and I_0.
2. Select the search direction matrices $\boldsymbol{\alpha}$ and $\boldsymbol{\beta}$, be sure they are not identical.
3. Evaluate the matrix $(\boldsymbol{Y} - \boldsymbol{\alpha})$, this is done only once at the beginning of the iteration procedure.
4. Calculate the initial voltage using the two equations in (2.29).
5. Using the pair of equations in (2.28) and (2.29), alternate between evaluating V and I until convergence is achieved.

2.3.2.2 Advantages of ASD method

Alternating search directions offer various advantages over the conventional methods used for power flow problems like Gauss-Seidel and Newton-Raphson methods.

1. The main advantage over the Newton-Raphson method is the computationally efficient algorithm without the need of evaluating Jacobian at each iteration.
2. The method converges quicker than Gauss-Seidel method and needs around similar iterations as Newton-Raphson. The comparison of iterations needed for convergence between these methods was studied in [52] by the author and other colleagues.
3. The method guarantees convergence to the high-voltage solution, a problem which requires attention in conventional methods. The eqs. (2.29) can be solved analytically and a quadratic equation is formed. The root with positive determinant of the resulting quadratic equation is selected to progress the solution, this results in the solution convergence to the high voltage solution. This is explained in the Figure 2.5 for an example problem that we used for the Newton-Raphson method.
4. The coupled non-linearity is tackled separately by dividing the problem in a global linear part and a local non-linear part, the equation pair (2.28) is the global linear part of the problem and the equation pair (2.29) is the non-linear problem solved locally at each nodes.

2.3.3 Application of ASD to an Example Problem

This is a simple explanation of the method of alternating search directions, a detailed insight into the method can be found in [53]. The method was applied to an example problem, the grid we consider in this study is a grid of 100 buses, same as the grid in the study of Parrilo et al [42]. The grid is represented by nodes in a square mesh of 10 by 10. We have 4 nodes representing generators and the rest are considered load buses. Node 1 was considered as the slack node and nodes 23, 28, 73 and 78 are

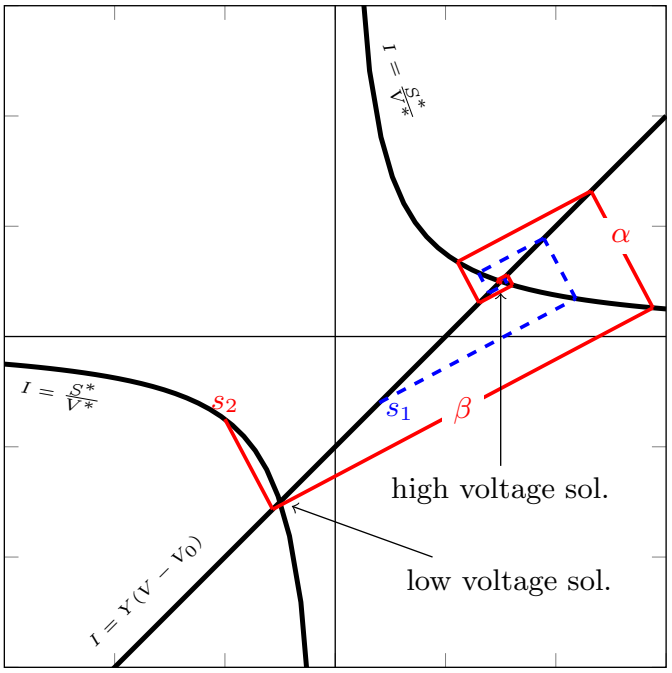

Figure 2.5: Convergence of the ASD method w.r.t. initial guess

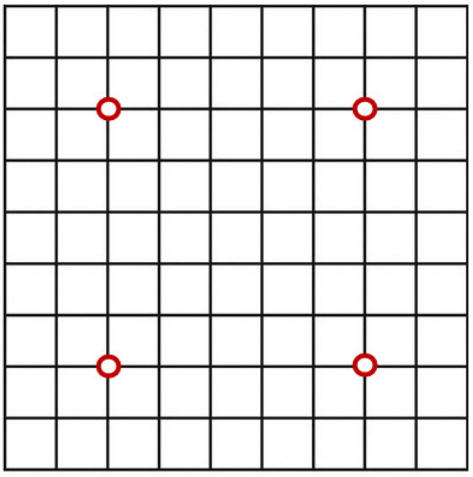

Figure 2.6: A 10 by 10 grid with 4 generators

Description	Symbol	Value
Total Buses	N	100
Number of Generators	N_{gen}	4
Number of Loads	N_{load}	96
Power Generated	S_{Gi}	$1 + 0\iota$ [p.u.]
Power Demanded at loads	S_{Di}	$-S_{Gi}/(N - N_{gen})$ [p.u.]
Slack bus Voltage	V_1	$1 + 0\iota$ [p.u.]

Table 2.3: Values used for parameters in POD model reduction

the generators. Figure 2.6 shows the grid with the positions of generators marked by red circles.

The generators are assumed to deliver 1 p.u. power each and the power demanded at each load buses is assumed equal and the sum of the demanded power at all the load buses is equivalent to the power generated by the generator buses. The admittances are considered real only and are selected randomly for the linkages between any buses. The values are listed in Table 2.3.

2.3.3.1 Search Directions

The matrices α and β are the search direction matrices of order $\mathbb{C}^{n\times n}$. The choice of these matrices depends upon the problem and can be selected without any restriction. The only limit on the choice of these matrices is that they should not be identical, which will lead the search directions to become parallel.

In the example problem discussed here, the choice of matrices $\boldsymbol{\alpha}$ and $\boldsymbol{\beta}$ has been based upon the admittance matrix $\boldsymbol{Y}$. The admittance matrices for the power systems in general are sparse matrix and therefore relying on the admittance matrix for the search direction matrices results in these matrices being sparse themselves. This is specially fruitful in terms of memory requirements for large power grids. The matrix $\boldsymbol{\alpha}$ is taken to be a diagonal only matrix with the entries equal to the inverse of the entries of the admittance matrix, while the $\boldsymbol{\beta}$ is a diagonal matrix also with the entries same as the diagonal entries of the admittance matrix, i.e.,

$$\alpha_{ij} = \begin{cases} 0 & \text{if } j \neq i \\ -\frac{1}{Y_{ii}} & \text{if } j = i \end{cases} \tag{2.30}$$

$$\beta_{ij} = \begin{cases} 0 & \text{if } j \neq i \\ Y_{ii} & \text{if } j = i \end{cases} \tag{2.31}$$

The choice of β is such that it should be close to the admittance matrix.

2.3.3.2 Steps of the Solution Procedure

Let us illustrate the method algorithm using the example we have chosen.

1. We begin with the calculation of voltages using the local non-linear set of equations (2.29).

$$\begin{aligned} V^{*[0]} \odot (I^{[0]} - I_0) &= S^* \\ \boldsymbol{\beta} V^{[0]} &= I^{[0]} \end{aligned} \tag{2.32}$$

2. Eliminate $I^{[0]}$ and derive a quadratic equation in terms of $V^{[0]}$

$$V^{[0]} = \frac{I_0 \pm \sqrt{I_0^2 + 4\boldsymbol{\beta} S}}{2\boldsymbol{\beta}} \tag{2.33}$$

3. Select the root with positive determinant $\sqrt{I_0^2 + 4\boldsymbol{\beta} S}$ because it represents the high voltage solution which is the physical solution.

4. Calculate $I^{[0]}$ using the power balance equations in (2.32).

5. Calculate $V^{[1/2]}$ from the linear set of the problem given in (2.28), eliminating I and forming the equations in terms of V, we have

$$-[\boldsymbol{Y} - \boldsymbol{\alpha}] V^{[1/2]} = I^{[0]} - \boldsymbol{\alpha} V^{[0]} + I_0 \tag{2.34}$$

6. Calculate $I^{[1/2]}$ using the Kirchhoff's law, the second equation in (2.28).

7. Now, we calculate the voltage $V^{[1]}$ using (2.29), again combining the two equations to eliminate $I^{[1]}$ and derive a quadratic equation whose solution can be

$$V^{[1]} = \frac{(\boldsymbol{\beta} - I^{[1/2]} + I_0) \pm \sqrt{(\boldsymbol{\beta} - I^{[1/2]} + I_0)^2 + 4\boldsymbol{\beta} S}}{2\boldsymbol{\beta}} \tag{2.35}$$

8. Selecting the root with positive determinant of eq. (2.35) and calculate $I^{[1]}$ using the power balance equation.

9. Iterate until convergence is achieved within a prescribed tolerance.

2.3.3.3 Results

The method converges very quickly for a grid which has admittance values in the order of $\mathcal{O}(10)$, the results are graphically illustrated in the Figure 2.7. The voltage magnitude is real as expected and the number of iterations required is 60 presented in the Figure 2.9 and the time for convergence is about 3 secs. The voltages in the whole grid is close to the voltage of the slack node and also the phase angles of all the buses are close to the phase of the slack bus which is an indication of the system in static stability as demonstrated in the Figure 2.7. Similarly, the solutions for current are presented in Figure 2.8.

For the case, with low admittance matrix the method is able to converge and has the ability to demonstrate the instability of the power grid, one by the number

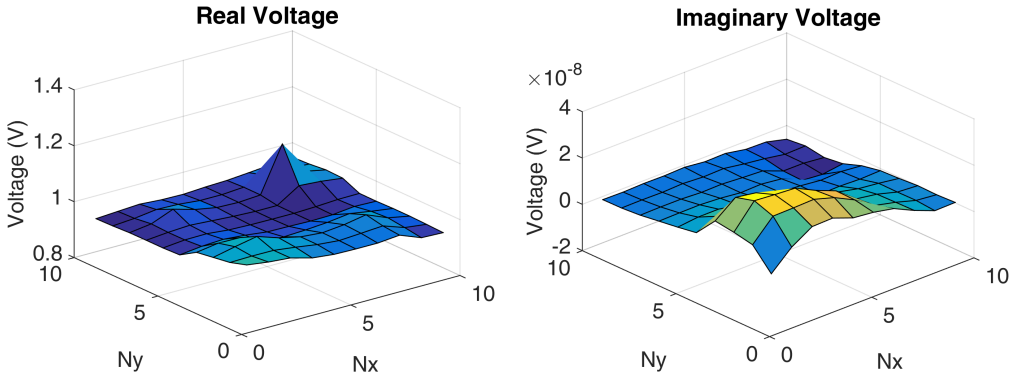

(a) Real Voltage

(b) Imaginary Voltage

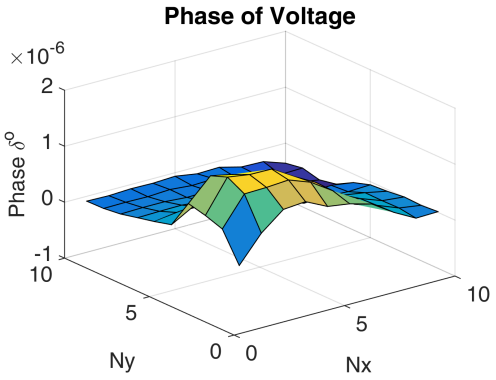

(c) Voltage Phase

Figure 2.7: Voltage magnitude and phase for high admittance values

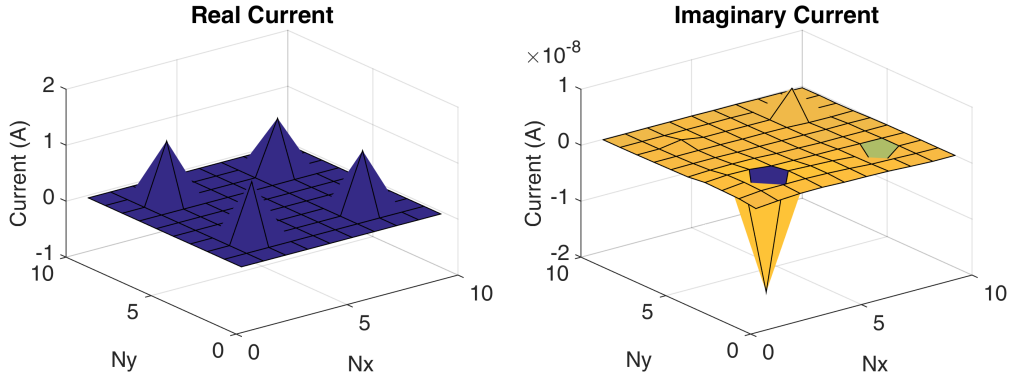

(a) Real Current

(b) Imaginary Current

Figure 2.8: Solution of Current for high admittance values

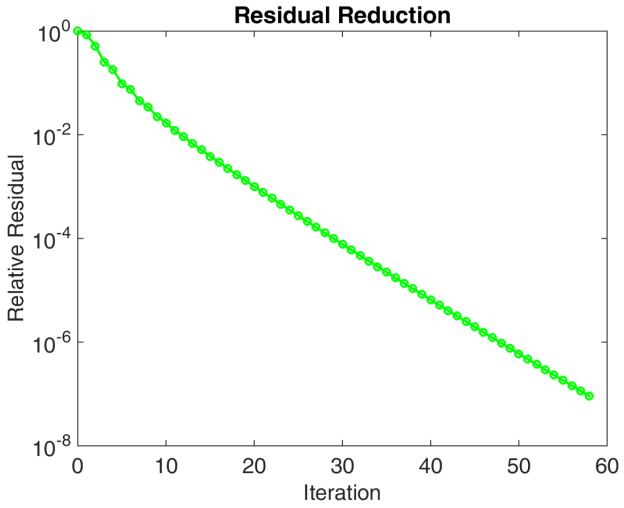

Figure 2.9: ASD iterations for high admittance values

of iterations increase several times to about 1600 iterations before the solution is converged. Although the number of iterations increase in the case of unstable solutions the time required is still around 5 secs. This demonstrates the potential of the alternating search direction method for the use of power flow analysis. The results for the low admittance case are presented in Figure 2.10 and the iterations required for convergence are presented in Figure 2.12. The graphic solution presented in the Figure 2.10 shows that the voltages in nodes other than slack bus become too large and also have an imaginary component as well as the phase angles of the buses are very high compared to the slack bus which leads to the coherent swing instability.

The method is applied to a couple of benchmark problems and has been published [52] with the comparison of the proposed method with Gauss-Seidel and Newton-Raphson methods.

2.4 Power System Stability

Power system stability has been an important area of research since 1920's [54]. The stability of power systems is of vital importance because of the financial losses can run into billions of dollars in case of instabilities leading to failure of the power grids [1]. Historically, the focus remained on the transient stability of the grids and hence we have also decided to focus our research and development of reduced order models for the study of transient stability. The transient stability is concerned with the issue of maintaining synchronism between generators after a severe disturbance [51]. The disturbance can come from many sources for example a lightning strike. Typically, there are procedures associated with the fault occurences such as these to clear the fault. The sequence of events called a fault sequence generates a transient through the power system [51].

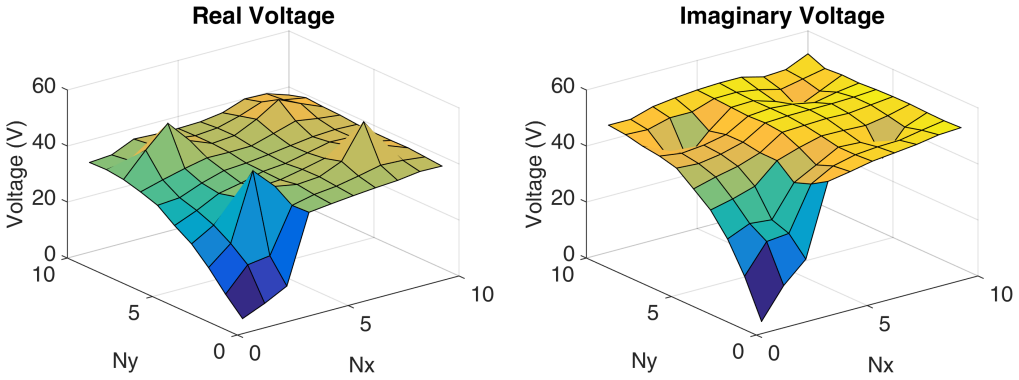

(a) Real Voltage

(b) Imaginary Voltage

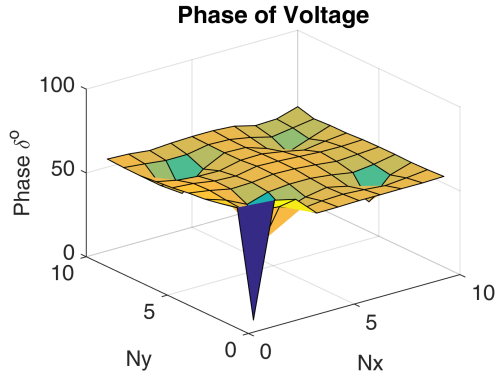

(c) Voltage Phase

Figure 2.10: Voltage magnitude and phase for low admittance values

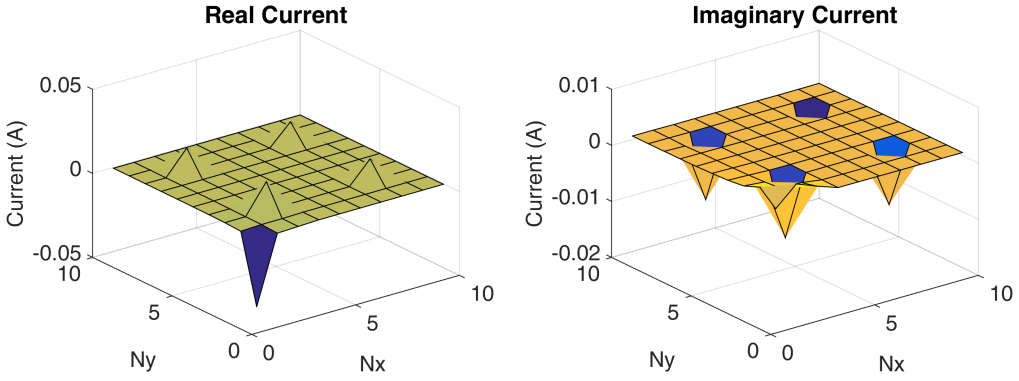

(a) Real Current

(b) Imaginary Current

Figure 2.11: Solution of Current for low admittance values

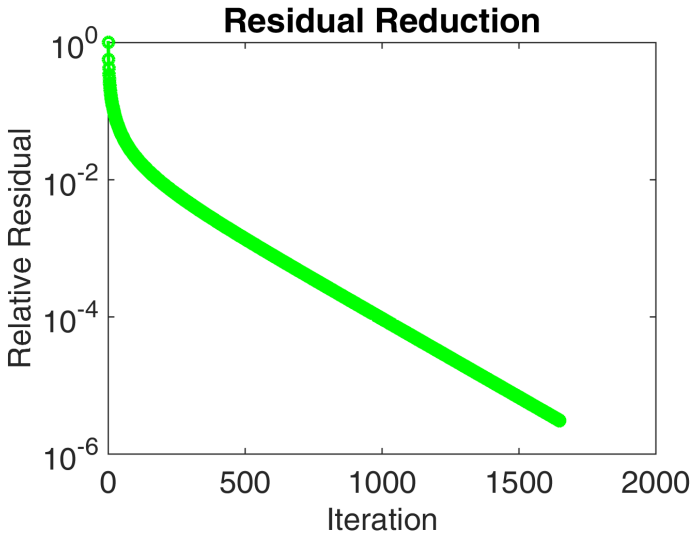

Figure 2.12: ASD iterations for low admittance values

2.5 Swing dynamics equations

A mathematical model to describe the transient dynamics of power systems is the "Swing Dynamics" [51]. It involves a second order differential equation representing the generator node or bus which originates from the rotor dynamics of the generator and an algebraic equation associated with the load bus. The differential equation for the i^{th} bus:

$$m_i\ddot{\delta}_i + d_i\dot{\delta}_i = p_i^m - p_i \quad \text{for} \quad i = 1, ..., N \tag{2.36}$$

The unknown in the eq. (2.36) is $\delta_i(t)$ and i varies from $i = 1, ..., N$ where N represents the number of nodes in the system. The variables δ_i represent the generator rotor angle deviations with respect to a synchronously rotating frame, while $\dot{\delta}_i$ and $\ddot{\delta}_i$ are respectively the first and the second time derivatives of the rotor angle. The quantities p_i^m and p_i are the mechanical power input and the electrical power output at node i and are given. The parameters m_i and d_i are the i^{th} generator's normalized inertia and damping coefficients.

The expression for the electrical power output is given by:

$$p_i = \sum_{k=1}^{N} |V_i||V_k|b_{ik}\sin(\delta_i - \delta_k) \quad \text{for} \quad i = 1, ..., N \tag{2.37}$$

In eq. (2.37), $V_i = |V_i|e^{\iota\delta_i}$, and $y_{ik} = g_{ik} + \iota b_{ik}$ represents the complex admittance matrix with b_{ik} is the line susceptance and g_{ik} is the line conductance, it is assumed that voltage magnitudes $|V_i|$ do not change and the transmission line losses are negligible, i.e. y_{ik} is purely imaginary ($g_{ik} = 0$). Using eq. (2.37) in eq. (2.36) gives, The term b_{ik} is the line susceptance between buses i and k, and is 0 if these two buses are not connected and also in the case i=k.

$$m_i\ddot{\delta}_i + d_i\dot{\delta}_i = p_i^m - \sum_{k=1}^{N} |V_i||V_k|b_{ik}\sin(\delta_i - \delta_k) \quad \text{for} \quad i = 1, ..., N \tag{2.38}$$

Until this point, we have considered the grid as consisting of only generators which are considered as PV buses and are represented by a differential equation given in eq. (2.38). However, general power grids consists of both generation units and loads where that power is consumed. For a node where we have a load, the equation representing the bus is an algebraic one which is a simple power balance equation

$$p_i^l = -p_i \tag{2.39}$$

In the limit when the motor constants are zero, we obtain a differential-algebraic equation (DAE) system, which can be interpreted as the singular perturbation limit of the model presented.

We can combine the differential equation of (2.36) and the algebraic equation of (2.39) in order to have a system of differential algebraic equations that represent the whole grid. In this case, we can write the swing equations in the form:

$$\gamma_i \left(m_i\ddot{\delta}(t) + d_i\dot{\delta}(t) - p_i^m\right) + (1 - \gamma_i)\, p_i^l = -p_i \tag{2.40}$$

Replacing p_i using eq. (2.37),

$$\gamma_i \left(m_i\ddot{\delta}(t) + d_i\dot{\delta}(t) - p_i^m\right) + (1 - \gamma_i)\, p_i^l = -\sum_{k} |V_i||V_k|b_{ik}\sin(\delta_i(t) - \delta_k(t)) \tag{2.41}$$

Where, γ_i represents the locations of generators, 1 for the generator node and 0 elsewhere. P_{L_i} is the power consumed at the i^{th} node.

Eq. (2.38) describes the transient dynamics of the power system under the assumption that the lines are purely reactive and voltage magnitudes are kept constant [42].

In the current study, several techniques are employed for the purpose of model order reduction. It is to be noted in the framework of POD and other model reduction methods, mathematical manipulations of system (2.38) are more easily handled using matrix and vector representations. Hence, we present the system of equations in matrix form:

$$[M]\{\ddot{\delta}\} + [D]\{\dot{\delta}\} = \{p^m\} - \{p(\{\delta\})\} \tag{2.42}$$

Where, $[M]$ and $[D]$ are $N \times N$ diagonal matrices, while $\{\ddot{\delta}\}$, $\{\dot{\delta}\}$ and $\{\delta\}$ are vectors in $\mathbb{R}^N$, N being the number of nodes in the grid. Note that, the notation $[M]\{\ddot{\delta}\}$ stands for the matrix-vector product. The vector $\{p(\{\delta\})\}$ is a nonlinear function of $\{\delta\}$. Eq. (2.42) is the high fidelity model of the swing dynamics in contrast to the reduced order model that is developed based on the high fidelity model.

The differential-algebraic equation (2.41) can also be written in matrix form as:

$$\{\gamma\}\left([M]\{\ddot{\delta}\}+[D]\{\dot{\delta}\}-\{p^m\}\right)+\left(\vec{1}-\{\gamma\}\right)\{p^l\}=-\{p(\{\delta\})\} \tag{2.43}$$

where $\{\gamma\}$ is a vector with indices equal to one coinciding the generator nodes and zero elsewhere.

2.5.1 Coherent Swing Instability

The transient stability of power grids is very important for the continuous function and transmission of power through the grid. The coupled nature of the synchronous rotating machines in a neighborhood make the grid susceptable to transient instabilities when one of the power generator is subjected to a disturbance. The coupled swing dynamics of rotating machines in a neighborhood can lead to coherent swing instability, which means that if one of the generator is subjected to a large enough disturbance that it causes it to loose synchronicity with the neighboring generators. If the generator that is the subject of disturbance doesn't reverse back to the original stable position with respect to the phase δ, it can cause other generators to follow and start oscillations. This loss of transient stability can cause large power outages such as the one in Italy [55].

2.5.2 Cascading Failure

A cascading failure is defined as the successive failure of most of the machines in a multi-machine system caused by a fault in a part of the system. This type of failure can occur in any system of interconnected parts including computer networking, financial markets etc. We are here focused on the power transmissions systems and cascading failure in power grids is the result of disturbances in the grid. Cascading failures can result in large blackouts of power supply [56]. In a study by IEEE PES CAMS task force has detailed various reasons that lead to cascading failures in [57].

The definition of cascading failures as given in [57] is that sequence of dependent failures of individual components that successively weakens the power system. Typically an overload of a transmission line leads to its failure which then overloads the neighboring transmission lines, if the failure is not contained then it can lead to a total failure of the grid and results in a blackout [56]. In the study by IEEE PES CAMS task force [57], they have adopted a wider view of cascading failures and included in addition to electrical components, other events such as software or control systems as well as human error in the propagation of cascading failure.

2.6 Non-linear Methods for Dynamic Problems

The results of the static problem gives the confidence in the application of fast non-linear solvers like the ASD and their ability to be used successfully in power grids simulations. Since, the main focus of this current research is in the dynamic cases of the power grids like the transient stability. We now present the methods and

results for the dynamic problems in power systems. For the dynamic problems, we have two options of time-domain simulation and frequency-domain simulations. We will present methods for both the domains, starting with the time-domain methods. Time-domain simulation is preferred more in the studies of power systems, even when the solution is easy to compute in frequency-domain the results are then transformed to the time-domain because the overall grid studies involve component-wise analysis which is comparatively simple to combine in time-domain.

Transient stability of the power grids is a keen area of research because of its implications in the power system planning, operation and control. Energy based methods for the transient analysis of power grids were developed originally by Mangnusson [58] and Aylett [59]. The substantial size of power grids makes the transient analysis computationally costly to simulate and therefore a need of model order reduction arises. Reduced order models need to be computationally cost-effective while retaining considerable accuracy of the full model in large network grids simulations.

Real time analysis and monitoring of non-linear swing dynamics of power grids requires simulation of very large number of nodes therefore a reduced order model of the network is a key for quick on the fly simulations. A number of model order reduction methods are discussed in the literature. In this section we would discuss some of these methods and their relevance in the model order reduction of the non-linear swing dynamics of the power grids.

A number of approximation schemes are available for model reduction and selection of an appropriate scheme depends upon the problem to be solved so that a suitable reduced order model is achieved [60]. Some of the earliest methods in the domain of model order reduction are Truncated Balance Realization proposed by Moore in 1981, Hankel-norm reduction published in 1984 by Glover [61], Proper Orthogonal Decomposition (POD) [62], Assymptotic Waveform Evaluation, PRIMA [61] and a more recent Proper Generalized Decomposition (PGD) [63]. There are more recent methods which are modified form of these fundamental methods tailored for specific problems such as the Laguerre-SVD method [64]. The techniques defined by Bai et al [40] includes Krylov-subspace techniques, Lanczos based methods such as MPVL algorithm and SyMPVL among others for the reduced order modeling in the electromagnetic applications.

As a precursor to the a priori model order reduction methods in time-domain for transient problems we start with the method of Large Time INcrement (LATIN) which is the predecessor of ASD method and is considered as a fast, non-iterative in time, solver for non-linear dynamic problems. Although, not strictly a model order reduction method but considering LATIN is a non-incremental method, it can result in significant savings in computational time.

2.7 Fast Solution Methods in Time-Domain

In time-domain dynamic problems, we are interested in the transient dynamics of the power grids. In this section, we present the method of LATIN for the solution of non-linear problem of transient dynamics of power grids.

2.7.1 Problem Statement

The mathematical model used to describe the dynamical behavior of buses in a power grid is the "Swing Dynamics" model that we described in Sec. 2.5. The swing equations are recalled here,

$$m_i\ddot{\delta}_i + d_i\dot{\delta}_i = p_i^m - \sum_{k=1}^{N} |V_i||V_k|b_{ik}\sin(\delta_i - \delta_k) \quad \text{for} \quad i = 1, ..., N \tag{2.44}$$

The variable of interest is the phase δ_i of voltages at each bus i. This is because the coherent swing instabilities defined in Sec. 2.5.1 are the result of the phase angles of the coherent generators loosing synchronocity due to some external disturbance. In the following discussion, we will focus on a grid termed as "ring grid". The grid is formed in such a way that all the nodes or buses are considered as PV nodes, i.e., all the nodes have generators and each generator is connected to only two generators such that in a ring, an example of such a grid is presented in Figure 2.13. Therefore, the term ring grid, additionally there is also a slack bus which is simultaneously connected with all the generators, similar to the ring grid presented in the study of Susuki et al. [55].

We are interested in this problem because of the potential it has to develop in to an unstable condition defined as the coherent swing instabilities, presented in Sec. 2.5.1. The grid in this part of our study is the same as in the study of Susuki et al. [55]. The swing equations presented in (2.44) are used to model the dynamics of the ring grid, since the grid does not include any load (PQ) buses, the equations are purely differential equations.

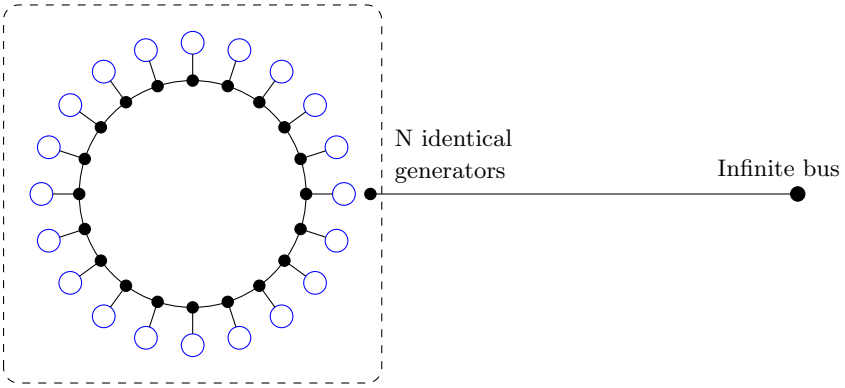

Figure 2.13: A ring grid power network. Blue circles representing generators connected to an infinite bus

A list of assumptions for the grid in the current study are:

- The power grid is loss-less
- The generators are small and the ratio between the length of transmission line joining generators to the infinite bus and the length of transmission line joining

Symbol	Description	Value
m_i	Mass of the generators	1 [p.u.]
$\|V_i\|$	Voltage Magnitude of generator	1 [p.u.]
p_i^m	Power generated by the generators	0.95 [p.u.]
b	Susceptance between generator and slack node	1 [p.u.]
b_{int}	Susceptance between consecutive generators	100 [p.u.]
N	Number of generators	20

Table 2.4: Grid Data

two consecutive generators is much bigger. Hence, the interaction between a generator and infinite bus is much smaller than the interaction between two neighboring generators

- Transmission lines joining two consecutive generators is shorter than the line joining the generators with the infinite bus
- Transmission lines between the infinite bus and all the generators are of same length
- Transmission lines connecting the generators are of same length

With the assumptions made above, the right hand side of eq. (2.44) representing the non-linear function of power demanded at bus i changes, recalling the power demanded $p_i(\delta)$ given by the eq. (2.37) in Sec. 2.5,

$$p_i(\delta) = \sum_{k=1}^{N} |V_i||V_k|b_{ik}\sin(\delta_i - \delta_k) \tag{2.45}$$

The generator at node i now connects with two other generators at buses $(i-1)$ and $(i+1)$ and also with the slack node. The susceptance between two consecutive generators is denoted by b_{int} and the susceptance between any generator and the slack node is denoted by b and it is assumed that the values of b_{int} and b are same for every connection between two generators and a generator and slack bus. Since, the nodes are considered as PV nodes, this means that the voltage magnitude at each node is known and for simplification it is taken to be one. The mass of the generators are assumed to be one and the system is assumed to be undamped. The properties of the grid are listed in Table 2.4. The eq. (2.45) for the ring grid is modified to be:

$$p_i(\delta) = b\sin\delta_i + b_{int}\{\sin(\delta_i - \delta_{i-1}) + \sin(\delta_i - \delta_{i+1})\} \tag{2.46}$$

Therefore, the swing dynamics equation takes the following form.

$$\ddot{\delta} = p_i^m - b\sin\delta_i - b_{int}\{\sin(\delta_i - \delta_{i-1}) + \sin(\delta_i - \delta_{i+1})\} \tag{2.47}$$

Symbol	Description	Value
T	Total time of simulation	2.5 [s]
ΔT	Time step	0.001 [s]
N_t	Total time snapshots	2500

Table 2.5: Training trajectories data

We initially apply Newton-Raphson method on this problem and then apply methods which should be computationally faster and cheaper than the Newton-Raphson's method.

2.7.2 Newton-Raphson

Newton's method (Newton-Raphson method) as described in the Sec. 2.3.1 is commonly used in the electrical engineering community. The method is very well known and simple to implement. In the current section, we make use of the MATLAB's built-in ODE solver ode15s to implement Newton's method and use it as a reference for the performance of other methods. MATLAB's ODE solver ode15s is based on the "Backward Differentiation" formulae of order 1 to 5. The solver is suited ideally for stiff problems or problems with differential-algebraic-equations (DAEs) which is the case in swing dynamics model when we consider both PQ and PV nodes, where PV nodes are represented by differential equations and PQ nodes are represented by non-linear algebraic equations.

The main concept of the Newton's method is to find the roots of a problem in an iterative solver. As defined in Sec. 2.3.1, the method requires the first derivative and in the current case this derivative is the Jacobian matrix. In order to implement, the equation given by (2.47) is divided into two first order differential equations by assuming $\dot{\delta}_i(t) = \omega_i(t)$, therefore,

$$\begin{aligned} \frac{d\delta_i}{dt} &= \omega_i \\ \frac{d\omega_i}{dt} &= p_i^m - b\sin\delta_i - b_{int}\{\sin(\delta_i - \delta_{i-1}) + \sin(\delta_i - \delta_{i+1})\} \end{aligned} \tag{2.48}$$

The time step and the total time of simulation are listed in the Table 2.5. The results are graphically presented in in Figure 2.14 where each line represents the dynamics of individual generator, an average value of the generators' phase angle is given in in Figure 2.15.

2.7.3 LATIN

LATIN stands for "LArge Time INcrement" method and the method of Alternating Search Direction (ASD) described in Sec. 2.3.2 is inspired by this method. As was the case in ASD, the method is divided into two parts, a global linear and the

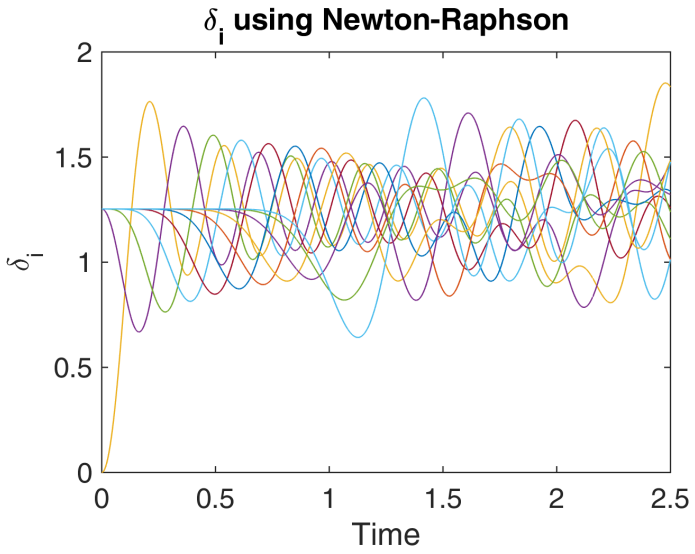

Figure 2.14: Evolution of phase angle δ_i after initial disturbance

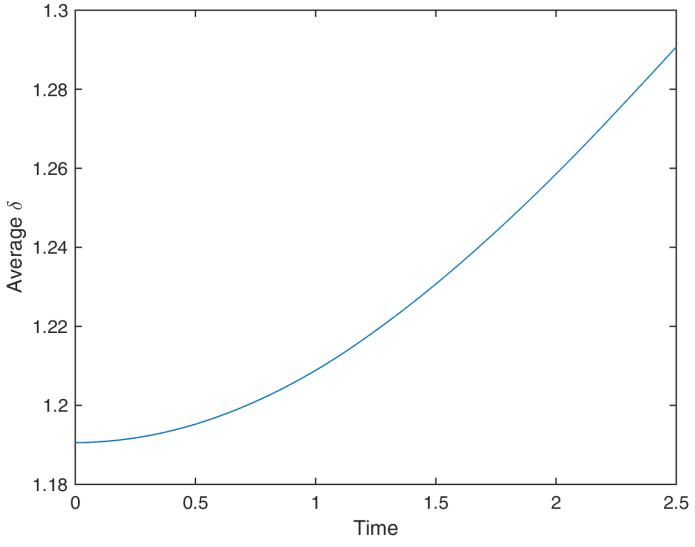

Figure 2.15: Average value of δ for all buses

other local non-linear part. The obvious difference between the two methods is that LATIN is adapted for dynamic problems. The biggest advantage of LATIN method is the non-incremental nature of the method, which means that this method is not an iterative solver in time-domain. It is an alternative to Newton-Raphson method which we have described is an iterative procedure in time-domain as well. One can argue that LATIN method itself uses iterations but that iterative procedure is needed to converge to the solution but the method is non-incremental in time. The time domain can be solved completely in one iteration. The method was initially developed for problems in mechanics of materials by Ladevèze [53]. The idea originated by Pierre Ladevèze for problems where the non-linear part was local in the physical space, the separation of the space-time representation was thus proposed where the global part was linear and the non-linearity was in the local part of the problem. The time-dependent non-linear function was integrated locally [65].

The problem we are dealing in the transient dynamics of power grids is given by eq. (2.48). Before, moving further, we transform our equation for voltage to the complex plane from the polar coordinate system, because the magnitude at each node is assumed to be known and fixed.

$$V = |V|(\cos\delta + \iota \sin\delta) \tag{2.49}$$

Also, we can write the right hand side of the eq. (2.48) in terms of the complex power formula, therefore eq. (2.48) can be written as:

$$\frac{d\omega_i}{dt} = p_i^m - \Re[VI^*] \tag{2.50}$$

The equations as per the procedure of LATIN method is divided into local non-linear and global linear parts as:

$$\text{Local} \begin{cases} \dot{\delta} = \omega \\ \dot{\omega} = p_i^m - \Re[V^{[l]} I^{[l]*}] \\ V^{[l]} = |V|(\cos\delta + \iota \sin\delta) \\ I^{[l+(1/2)]} - I^{[l]} = \boldsymbol{\beta}(V^{[l+(1/2)]} - V^{[l]}) \end{cases} \tag{2.51}$$

where I_0 represents the contribution from the slack bus. The superscript notation $[l+(1/2)]$ in eq. (2.28) represent the intermediate step in the iteration l. The matrix $\boldsymbol{\beta} \in \mathbb{C}^{n\times n}$ is known a priori, is the search direction for the first step. For the second step of the iteration, a matrix $\boldsymbol{\alpha} \in \mathbb{C}^{n\times n}$ is used as the search direction and the second pair of equation is:

$$\text{Global} \begin{cases} I^{[l+1]} - I^{[l+(1/2)]} = \boldsymbol{\alpha}(V^{[l+1]} - V^{[l+(1/2)]}) \\ \boldsymbol{Y} V^{[l+1]} = I_0 + I^{[l+1]} \end{cases} \tag{2.52}$$

The solution is initialized at the equilibrium position of the generators given by

$$\begin{aligned} \delta_i &= \sin^{-1}\left(\frac{p_i^m}{b}\right) \\ \omega_i &= 0 \end{aligned} \tag{2.53}$$

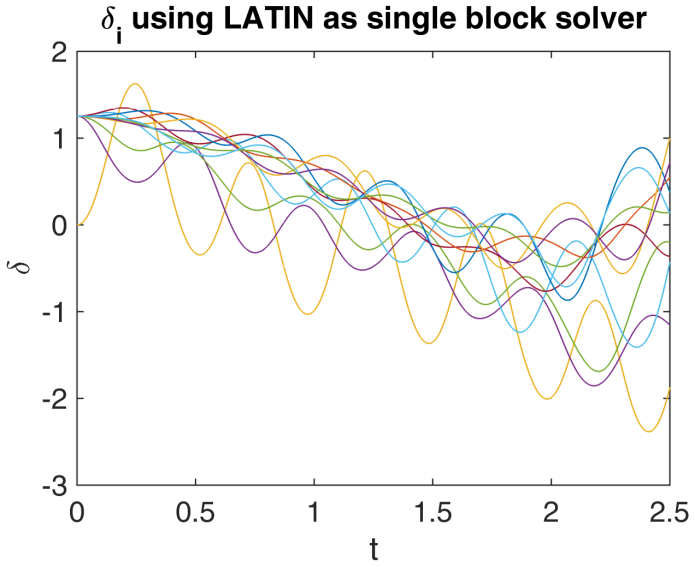

Figure 2.16: Evolution of phase angle δ_i after initial disturbance using LATIN

At the start of each local part of the iteration, the values of δ and ω are updated using high order finite difference formulas. Once, δ is updated the complex voltage is updated using eq. (2.49). With the updated voltage, we can perform the first part of the LATIN iteration from $[l]$ to $[l + 1/2]$. In the global part of the system, we use the Kirchhoff's current law to update the voltages and currents at all the buses from $[l + (1/2)]$ to $[l + 1]$.

The value of the phase angle of each bus δ_i of the first implementation of the LATIN method is presented in Figure 2.16 and the average δ is presented in the Figure 2.17. A quick comparison with the results from the Newton's method with the LATIN can conclude that the solution did not converge to the exact solution.

A probable cause of the error is the accumulation of error and a solution was thought to divide the time-domain into more sub-domains and iterate LATIN procedure over each sub-domain. The new procedure would first start with the first sub-domain in time and once the convergence is achieved the procedure would then follow on to the subsequent sub-domains. In an attempt to better converge to the exact solution, the total time-domain of 2.5 seconds was divided into 10 sub-domains.

The method of dividing the time-domain into smaller sub-domains inevitably makes the procedure computationally time consuming and the total number of iterations increase from 275 in the first case to about 700 iterations in total, with about 70 iterations for each sub-domain. The results are presented for δ_i in Figure 2.20 and for average δ in Figure 2.21. But the results show that the method has still not converged to the right solution, only a slight change is observed in the average value of δ.

A further modification of the procedure is performed, with the addition of domain overlap for the sub-domains. The size of sub-domains were also decreased and therefore the total number of iterations increased further to about 9225 iterations. But instead of reducing the error to the correct solution, the procedure converged

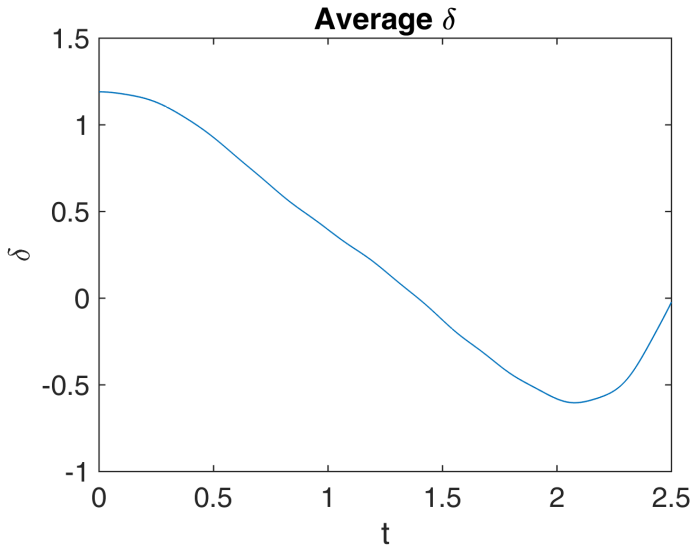

Figure 2.17: Average value of δ for all buses using LATIN

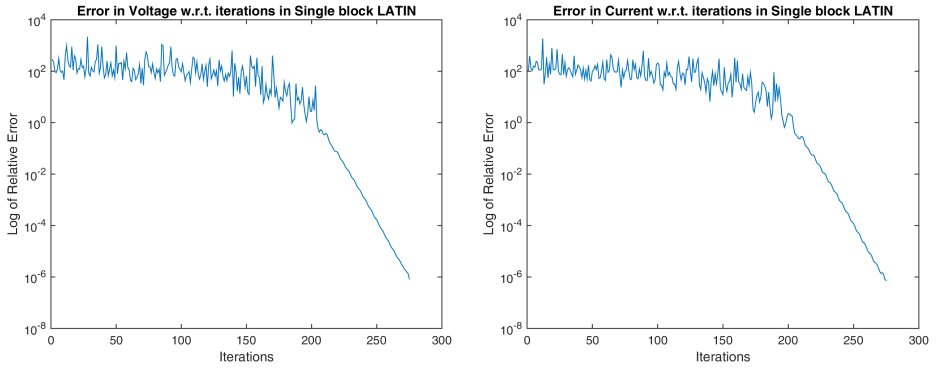

(a) Error convergence in voltage (b) Error convergence in current

Figure 2.18: Error Convergence with respect to iterations of LATIN procedure

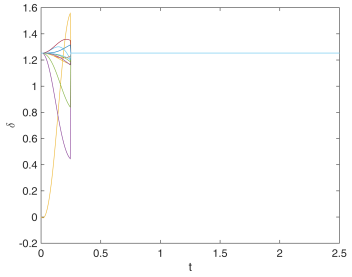

(a) Solution after convergence in 1^{st} sub-domain

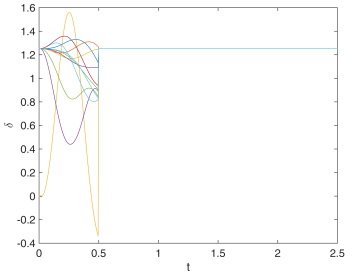

(b) Solution after convergence in 2^{nd} sub-domain

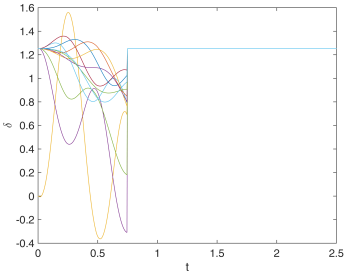

(c) Solution after convergence in 3^{rd} sub-domain

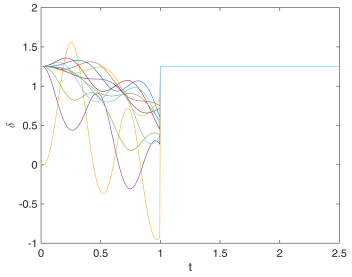

(d) Solution after convergence in 4^{th} sub-domain

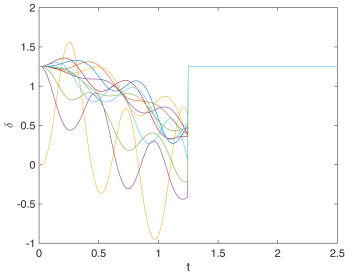

(e) Solution after convergence in 5^{th} sub-domain

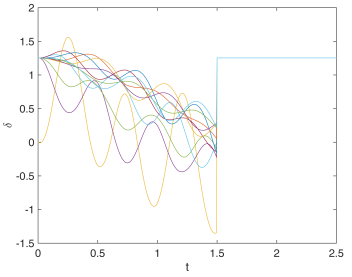

(f) Solution after convergence in 6^{th} sub-domain

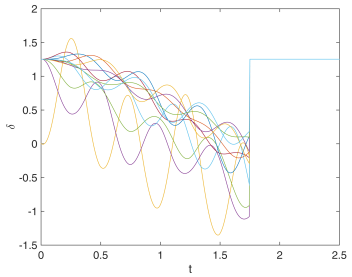

(g) Solution after convergence in 7^{th} sub-domain

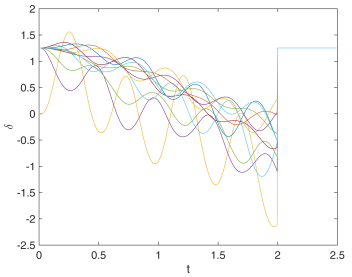

(h) Solution after convergence in 8^{th} sub-domain

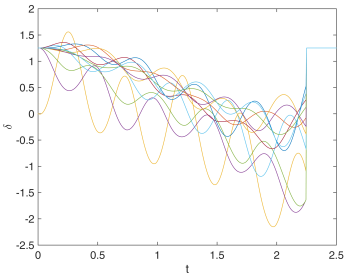

(i) Solution after convergence in 9^{th} sub-domain

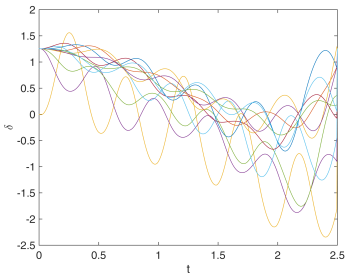

(j) Solution after convergence in 10^{th} sub-domain

Figure 2.19: Evolution of δ_i with convergence of each sub-domain

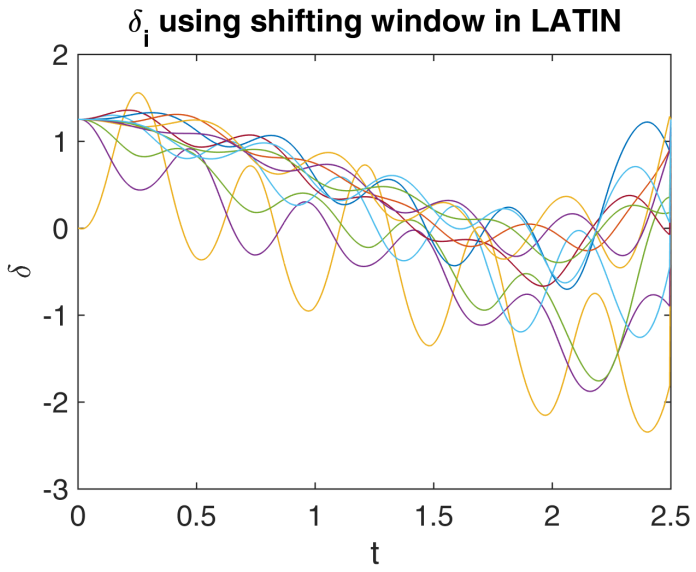

Figure 2.20: Evolution of phase angle δ_i after initial disturbance using LATIN

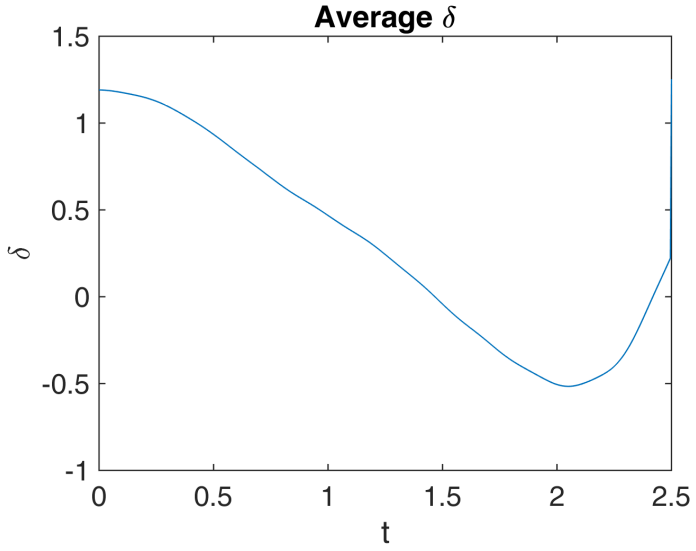

Figure 2.21: Average value of δ for all buses using LATIN

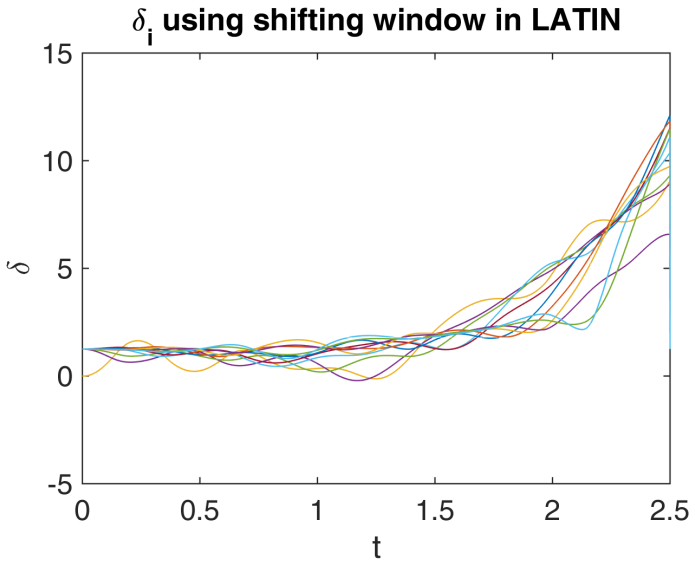

Figure 2.22: Evolution of phase angle δ_i after initial disturbance using LATIN

to a solution that is even further away and thus increasing the errors. The results are presented graphically in Figure 2.22 and Figure 2.23.

The divergence is observed to increase with the decrease in the time-domain solved in each LATIN iteration. This suggests that the divergence is not due to the numerical instability with the LATIN method but with the problem itself being unstable. Although there are some problems reported in the literature with the application of LATIN in problems with the snap-back behavior. In the study of Vandoren et al [66], they have compared this problem in LATIN method with the iterative procedure of Newton-Raphson method. The snap-back behavior is defined in mechanics as the failure in which initiation of damage results in the reduction of elongation and reduction of load instead of the increase in elongation and deformation [67]. The solution proposed by Vandoren et al [66, 68] is to use a constrain function in the equilibrium equation during the global stage of the LATIN procedure.

2.8 Conclusions

This chapter performs the task of setting up the problem that we discuss in the current thesis. The introduction to power system components and analysis is required in order to develop the problem of transient dynamics. The methods used in the Power System applications are introduced and explained which serves as the benchmark for the reduced order models. One of the early success in the current research is the application of ASD method for the power flow studies. The results are extremely encouraging and compares well with the already well known methods in the industry. The results of the ASD method were then expanded into another study which manifested in the publication of a journal article.

In the second part of the chapter, we presented the main focus of our study that is the transient dynamics problem. A fast non-incremental method of LATIN was

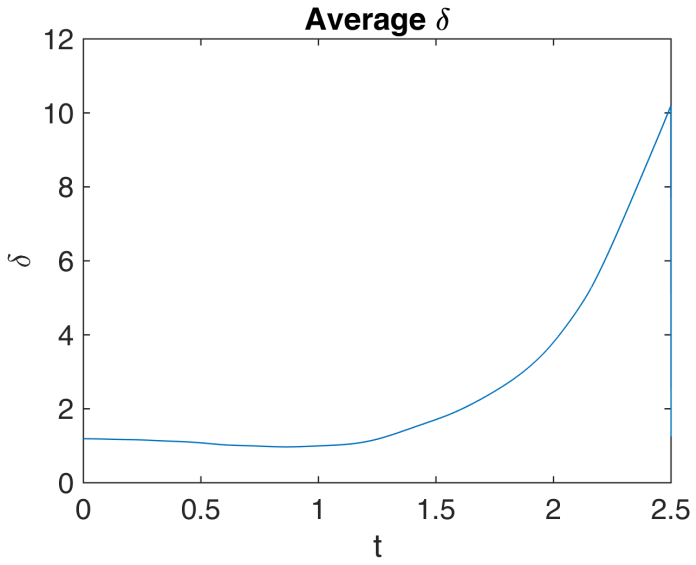

Figure 2.23: Average value of δ for all buses using LATIN

applied to the transient dynamics model represented by the swing dynamics model. Although, the results are not as encouraging as expected still it gave deep insight into the problem. In the case when the LATIN methods are applied, the solution becomes unstable and diverges in all the different variations of the method we applied. This is mainly due to the nature of the problem which is linearly unstable and can be observed from the fact that the solution diverges even more when the time-domain is decomposed into smaller sub-domains as compared to when the time integration was solved at once.

Chapter 3

Reduced order modeling of Power Systems

This chapter presents the a posteriori model order reduction methods for the transient problem of the swing dynamics. The chapter starts with the introduction to the POD method and its application to the problem. The chapter discusses the results of POD and introduces the method of Trajectory Piece-Wise Linear method.

Contents

3.1 Model Order Reduction of Swing Dynamics

In Chapter 1, we discussed the model order reduction in the power systems and presented a brief review of different categories of model order reduction techniques. In this chapter, we describe the a posteriori model order reduction methods we studied in the current research and applied to the transient dynamics problem of power systems represented by the swing dynamics, see Sec. 2.5. We start with the basic method of POD and discuss the method for transient problems.

3.2 A posteriori Reduced Order Modeling

A posteriori reduced order modeling methods require full scale simulation of problems using conventional numerical techniques before the model reduction can be applied. With the a priori method of LATIN described in Sec 2.7 not converging for the transient problems, we refer to a posteriori methods in search of a suitable method that can be applied to swing dynamics model. In the following sections, we will describe a posteriori methods and present some results for the same problem.

3.2.1 Proper Orthogonal Decomposition

Proper Orthogonal Decomposition is an "a posteriori" method for model order reduction. The study by Parrilo et al. [42] presents the use of POD to reduce the hybrid, nonlinear model of a power network. POD based model order reduction has applications in diverse fields and is the preferred method in electrical engineering applications such as in the study by Montier et al [69]. In their study, the POD is applied in combination with discrete empirical interpolation method.

The Karhunen-Loève decomposition allows for high dimensional systems with state space in $\mathbb{R}^n$, a method to find the smallest dimensional subspace which contains observed points on the trajectories of the system. The subspace obtained through this decomposition is then used to project upon the dynamics from a Galerkin projection. Thus, the high-dimensional system is approximated by a small number of nonlinear ordinary differential equations.

The objective is to find an orthonormal basis considerably smaller as compared to the high fidelity model using the information extracted from previously computed simulations. Say $\{\delta\}$ is a vector of dimension N containing all the state variables of the system, the objective of POD is to reduce the dimension from N to q where $q << N$. The mapping from the original to the reduced coordinates is expressed by the linear application:

$$\{\delta\} = [\tilde{U}]\{z\} \tag{3.1}$$

where $\{\delta\}$ is a $N \times 1$ vector, $[\tilde{U}]$ is a $N \times q$ matrix, and $\{z\}$ is a $q \times 1$ vector. The goal of POD is to compute matrix $[\tilde{U}]$ from the analysis of the principal components of the available solutions.

The matrix $[\tilde{U}]$ can be calculated using several techniques. In essence, POD is similar to the Karhunen-Loéve decomposition (KLD) and it is often referred to as KLD, principal component analysis (PCA) or the singular value decomposition (SVD) [70]. In the current study, SVD interpretation has been used to obtain a reduced order model.

Here, we will briefly describe the SVD reduction procedure which is available as a built-in function in MATLAB.

A selection of solution "snapshots" $\{\delta\}_k$, with $k = 1, 2, \ldots, n$, are arranged into the columns of the matrix $[Q] \in \mathbb{R}^{N\times n}$,

$$[Q] = [\{\delta\}_1, \{\delta\}_2, \ldots, \{\delta\}_n] \tag{3.2}$$

The number of snapshots must guarantee that they represent the complete set of solutions, i.e., n must be large enough. The set of n snapshots contains redundant information that have to be suppressed by keeping only the pertaining remaining modes q.

The factorization under SVD is given as:

$$\begin{aligned}[Q] &= [U][\Sigma][V]^* \\ &= \sum_{i=1}^{N} \sigma_i \{U_i\}\{V_i\}^T \approx \sum_{i=1}^{q} \sigma_i \{U_i\}\{V_i\}^T\end{aligned} \tag{3.3}$$

where, $[U]$ is a $N \times N$ matrix, $[\Sigma]$ is a $N \times n$ diagonal matrix with non-negative real numbers on the diagonal, and $[V]^*$ is a $n \times n$, unitary matrix, $[V]^*$ is the conjugate transpose of the $n \times n$ unitary matrix $[V]$. The left hand side of eq. (3.3) accurately estimate the full $[Q]$ matrix for i=1,...,N. The last sum is the truncation of first terms that sufficiently approximates the full $[Q]$ matrix.

To obtain a reduced order model which retains minimum energy required to accurately capture the behavior of the high fidelity model, it is truncated at q where $q << N$. Number of modes q are selected such that for any $j > q$, the quotient η is within some defined tolerance and $\sigma_j << \sigma_1$, where quotient η is defined as the difference of the relative energy retained, where $\eta = 0$ means that the total energy of the system is retained. It is usually the case that only few of the larger σ_j contain the most energy and the rest σ_j for $j = q, ..., N$ can be dropped from the reduced basis.

$$\eta = \left| \frac{\sum_{j=1}^{q} \sigma_j}{\sum_{k=1}^{N} \sigma_k} - 1 \right| \tag{3.4}$$

The quotient η is employed to find the size of the reduced basis which accurately mimics the original basis, typical values are between 10^{-1} and 10^{-5}. The matrix $[\tilde{U}]$ is given as:

$$[\tilde{U}] = [\{U\}_1, \{U\}_2, \ldots, \{U\}_q] \,, \qquad q < N < n \tag{3.5}$$

The columns of $[\tilde{U}]$ correspond to vectors $\{U\}_i$ representing the most characteristic *modes* in the solution, that is, the most recurrent structures.

For detailed insight into the method and the variations in the above mentioned procedures of KLD, PCA and SVD, the author refers to the studies by Liang et al. [70]. Additionally one can also refer to Kerschen et al. [71] and Berkooz et al. [72].

The reduced order model for the governing equations is obtained by replacing $\{\delta\}$ with the relation given by eq. (3.1) in eq. (2.44), writing the system given in eq. (2.44) in matrix form,

$$[M][\tilde{U}]\{\ddot{z}\} + [D][\tilde{U}]\{\dot{z}\} = \{p^m\} - \{p\} \tag{3.6}$$

and using Galerkin method to project the residual on the reduced basis

$$[\tilde{U}]^T[M][\tilde{U}]\{\ddot{z}\} + [\tilde{U}]^T[D][\tilde{U}]\{\dot{z}\} = [\tilde{U}]^T\{p^m\} - [\tilde{U}]^T\{p(\{\delta\})\} \tag{3.7}$$

Defining the following notations

$$\begin{aligned} [\widetilde{M}] &:= [\tilde{U}]^T[M][\tilde{U}] \\ [\widetilde{D}] &:= [\tilde{U}]^T[D][\tilde{U}] \\ \{\widetilde{p}^m\} &:= [\tilde{U}]^T\{p^m\} \\ \{\widetilde{p}(\{z\})\} &:= [\tilde{U}]^T\{p(\{\delta\})\} \end{aligned} \tag{3.8}$$

we obtain the governing equation (2.44) in the reduced basis as:

$$[\widetilde{M}]\{\ddot{z}\} + [\widetilde{D}]\{\dot{z}\} = \{\widetilde{p}^m\} - \{\widetilde{p}(\{z\})\} \tag{3.9}$$

Note that $\{\widetilde{p}\}$ is a nonlinear function of $\{z\}$.

3.2.2 High Fidelity Model

For the model order reduction with a-posteriori methods we start with the model reduction of the grid presented in the study of Parrilo et al. [42]. The grid contains both loads and generators as buses, thus the swing dynamics model represented by a system of differential-algebraic equations (DAEs), given by eq. (2.43) in the Sec. 2.5 is used. Recalling the equation here,

$$\{\gamma\}\left([M]\{\ddot{\delta}\} + [D]\{\dot{\delta}\} - \{p^m\}\right) + \left(\vec{1} - \{\gamma\}\right)\{p^l\} = -\{p(\{\delta\})\} \tag{3.10}$$

The starting point for the current research is based upon the work presented by Parrilo et al. [42]. The authors used Proper Orthogonal Decomposition (POD) for the model reduction of the network grid presented in the Fig 2.6. It has been noted in the study that the model reduction of this kind of grid is difficult because of the hybrid nature of the differential algebraic equations and the non-linearity of the system.

The study by Parrilo et al. [42] focused on the model reduction for the power grid suffering a cascading failure, defined in Chapter 2 Sec. 2.5.2. In the study by Parrilo et al., an initial known failure was induced in the grid by removing the

Description	Symbol	Value
Total Buses	N	100
Number of Generators	N_{gen}	4
Number of Loads	N_{load}	96
Power Generated	p_i^m	$1 + 0\iota$ [p.u.]
Power Demanded at loads	p_i^l	$-p_i^m/(N_{load})$ [p.u.]
Mass of the generators	m_i	1 [p.u.]
Damping of the generators	d_i	0.01
Voltage Magnitude	$\|V_i\|$	1 [p.u.]

Table 3.1: Values used for parameters in POD model reduction

corresponding connection between the buses, thus b_{ij} from the admittance matrix. This initial failure is known and its effect spread through the network was predicted using the POD model reduction. The reduction approach used in the study was to divide the domain in two parts $[x_1, x_2]$ where x_1 is the part of the grid where the states of the system were kept and x_2 were replaced by a lower-order approximation.

The results in the study of Parillo et al. [42] are limited in the sense that the reduced model is only used for the part of the grid where it remained unaffected by the cascading failure. In the current study, the endeavor is to apply the model reduction on the whole grid and the effects it has on the prediction of the cascading failure. The grid and the conditions are similar as defined in the study of Parrilo et al. [42]. Just as in the study by Parrilo et al. [42], two kinds of initial failures are implemented. The first kind of failure is that one of the connections between two buses is removed due to the overload on the line connecting the two buses and other is that one of the generators is perturbed and hence the generator phase becomes asynchronous with respect to other generators. Both of these initial problems lead to the cascading failure in the grid.

3.2.3 Numerical Integration of the High Fidelity Model

Swing equations are numerically integrated in the commercial software MATLAB. The values of the different parameters of the power grid are listed in Table 3.1.

The grid we consider in this study is the same as we used in the static case studied using the alternating search direction, presented in Sec. 2.3.2. This is a grid of 100 buses represented by nodes in a square mesh of 10 by 10. We have 4 nodes acting as generator and the rest are considered as load buses. Figure 2.6 shows the grid with the positions of generators. Eq. (3.10) is the system of differential-algebraic equations (DAEs) defining the behavior of the grid in the transient case.

3.2.4 Linear Approximation of Swing Equations

The non-linearity in the swing equations (3.10) is present in the power consumed term p_i. Recalling the swing equations in indicial notation here,

$$\begin{aligned}\gamma_i \left(m_i\ddot{\delta}_i(t) + d_i\dot{\delta}_i(t) - p_i^m\right) + (1-\gamma_i)\, p_i^l = \\ -\sum_j |V_i||V_j|b_{ij}\sin\left(\delta_i(t) - \delta_j(t)\right)\end{aligned} \tag{3.11}$$

Using the Taylor series expansion,

$$f(x) = f(a) + \frac{f'(a)}{1!}(x-a) + \frac{f''(a)}{2!}(x-a)^2 + \frac{f'''(a)}{3!}(x-a)^3 + \cdots \tag{3.12}$$

for a function $f(\delta) = \sin(\delta + \delta_0)$,

$$\sin\left(\delta + \delta_0\right) \approx \sin(\delta_0) + \cos(\delta_0)(\delta - \delta_0) \tag{3.13}$$

Using only the first order approximation, the linearization of the function p_i is simply,

$$\begin{aligned}p_i &= \sum_j |V_i||V_j|b_{ij}\sin\left(\delta_{0i} + \delta_i(t) - \delta_{0j} - \delta_j(t)\right) \\ &\approx \sum_j |V_i||V_j|b_{ij}\cos\left(\delta_{0i} - \delta_{0j}\right)\left(\delta_i(t) - \delta_j(t)\right)\end{aligned} \tag{3.14}$$

Using the linearized form of p_i given in eq. (3.14) and replacing it in eq. (3.11), the linearized equation is

$$\begin{aligned}\gamma_i \left(m_i\ddot{\delta}_i(t) + d_i\dot{\delta}_i(t) - p_i^m(t)\right) + (1-\gamma_i)\, p_i^l(t) \\ = -\sum_j |V_i||V_j|b_{ij}\cos\left(\delta_{0i} - \delta_{0j}\right)\left(\delta_i(t) - \delta_j(t)\right)\end{aligned} \tag{3.15}$$

Separately representing the differential and algebraic equations after linearization.

$$\begin{aligned}m_i\ddot{\delta}_i + d_i\dot{\delta}_i &= p_i^m - \sum_j |V_i||V_j|b_{ij}\cos\left(\delta_{0i} - \delta_{0j}\right)\left(\delta_i(t) - \delta_j(t)\right) \\ 0 &= -p_i^l - \sum_j |V_i||V_j|b_{ij}\cos\left(\delta_{0i} - \delta_{0j}\right)\left(\delta_i(t) - \delta_j(t)\right)\end{aligned} \tag{3.16}$$

In order to implement the system of equations in MATLAB to solve the linear system of equations (3.15) and assuming $\dot{\delta} = \omega$, we present the equations in matrix form.

$$\begin{bmatrix} M & 0 \\ 0 & I \end{bmatrix} \cdot \begin{bmatrix} \dot{\omega} \\ \dot{\delta} \end{bmatrix} + \begin{bmatrix} D & B \\ -I & 0 \end{bmatrix} \cdot \begin{bmatrix} \omega \\ \delta \end{bmatrix} = \begin{bmatrix} P \\ 0 \end{bmatrix} \tag{3.17}$$

where B is the matrix containing the line susceptances.

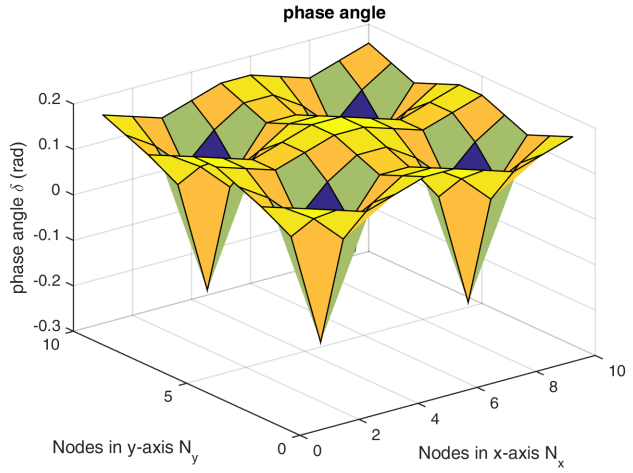

Figure 3.1: Equilibrium Solution for the linearized problem

3.2.5 Equilibrium Solution

The static solution presented in the section 2.3.2 showed that the power grid always settles to an equilibrium position. An initial solution of the problem for the equilibrium conditions was sought with the linearized equations as given here. The difference in the results presented in this section with the results presented in the Sec. 2.3.2 is due to the assumptions made for this case. In the study we presented in Sec 2.3.2, we considered the first node as the slack node where we fixed both the voltage magnitude $|V_1|$ and the phase angle δ_1. The rest of the nodes had both voltage magnitude $|V_i|$ and phase angles δ_i as unknown, instead we had power demanded or generated as given. Here, we are not considering any node as the reference node and instead of having both voltage magnitudes $|V_i|$ and phase angles δ_i as unknowns, we fix the voltage magnitudes as given in Table 3.1 and keeping only phase angles δ_i as unknown variable.

The linearzied equation was used to generate the equilibrium solution. This solution serves as an initial condition for the problems where an induced fault was introduced in the grid. The equilibrium solution for the grid studied is given in the Figure 3.1.

An interesting observation should be pointed out here, that the equilibrium solution depends upon the initial guess taken during the Newton's method. The solution presented in Figure 3.1 is the result when the initial guess was taken as $\delta_i = 0.1$ for all the buses. But for a random initial guess, the solution converges to the one presented in Figure 3.2. But, this should not be a cause of concern, as the important aspect in the swing dynamics model is the difference in the phase angles of the neighboring buses and as it can be observed the solution in Figure 3.2 is just a translated solution of Figure 3.1.

In the current study, POD based reduced order modeling was performed for three cases, namely;

1. Failure of a bus

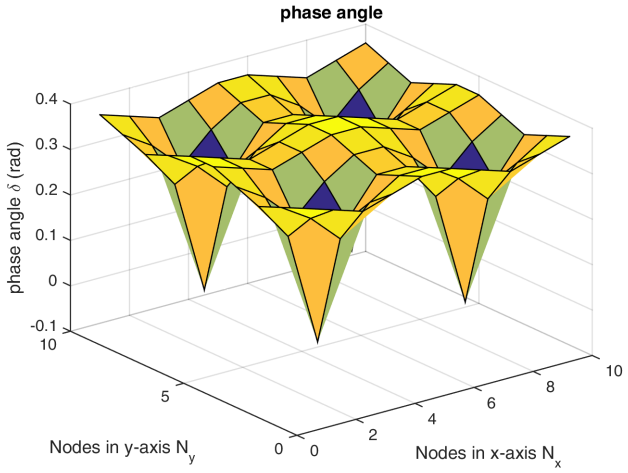

Figure 3.2: Equilibrium Solution for the linearized problem with random initial guess

2. Variable loads

3. Load Prediction

3.2.6 Connection Failure between buses

To simulate the behavior of the grid going through cascading failure, it was modeled that if the difference between the rotor angles between two adjacent buses grows beyond a certain value, the connection between the buses will be removed and therefore introducing a new fault in the grid.

In the first case, we try to simulate the failure of a bus and subsequent cascading failure initiated by this kind of failure. One of the buses is removed from the grid, this is achieved by making the corresponding susceptance matrix values to zero. Figure 3.3 shows the tribanded matrix B with some entries missing representative of lost connection between two loads and Figure 3.4 shows the position of the bus removed as the point of initial failure.

$$b_{ij} = 0 \quad \text{when line connecting nodes } i \text{ and } j \text{ is disconnected} \tag{3.18}$$

3.2.7 Variable loads

The aim is to perform simulations based on real time measurements of the demanded power. Since, the real time simulation based on the measurements from sensors on the grid require models that are capable of quick simulations, reduced order models based on the swing dynamics model will be necessary. Therefore, we start with a high fidelity model simulation with some assumptions and then use the methods like POD to find reduced order models. For this purpose, it is assumed that the power

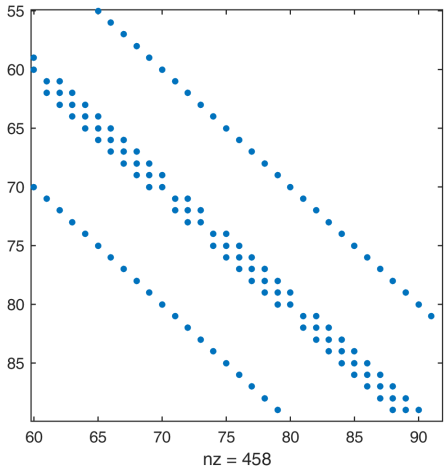

Figure 3.3: Banded B matrix with missing entries representing the removal of the bus

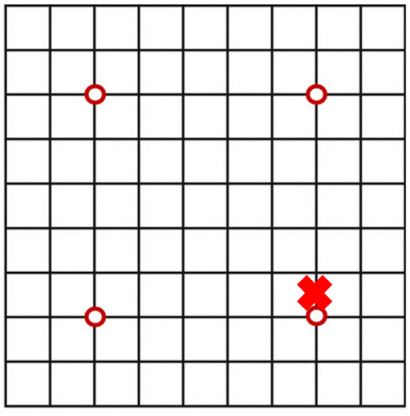

Figure 3.4: Network grid with cross representing the removal of the bus

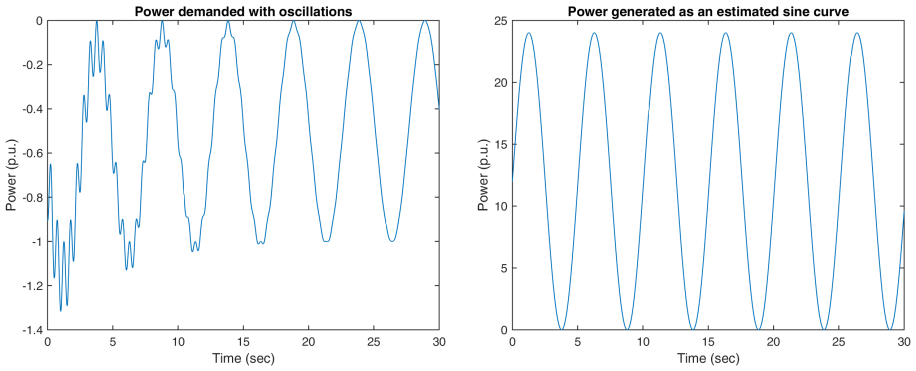

(a) Power demanded by a load (b) Power generated by a machine

Figure 3.5: Power oscillations for load and generator buses

demand at load buses vary with time and can be approximated by a combination of simple sinusoidal and exponential functions. To meet this fluctuation in the power demand the generators can also follow different yet close sinusoidal patterns for power generation.

The approach used in this case was to use a sinusoidal wave to mimic the generators response and a similar sinusoidal wave to represent the behavior of loads. In addition, another exponential sinusoidal function was superimposed on the loads with a high frequency. The functions for the power demand by loads and the power generated by machines is given as:

$$p_i^l = -[1 + \sin(\omega_1 t) + \gamma_1 \exp^{-t/2\pi}] - \gamma_2 \cos(\omega_2 t) \exp^{-t/2\pi} \tag{3.19}$$

where $\omega_2 < \omega_1$.

$$p_i^m = (1 + \sin(\omega_1 t)) \ \frac{(N_{load})}{N_{gen}} \tag{3.20}$$

Figure 3.5a graphically represents the profile of the power demand at load buses that we have used to simulate the high fidelity model while the power generator profile is shown in Figure 3.5b.

3.2.8 Load Prediction

Another situation, where reduced order models can be useful is in the prediction of load demand and generation for future and assess the dynamic behavior of the grid based on these simulations and carry out any precautionary measures required. The predictions can be based upon the historical data of the power grids in similar conditions.

A reduced order model is suitable for the quick estimation of the grid's dynamic response under the variable load. For the next day power demand prediction a small variation is added in a sinusoidal function. Note that, these are just assumptions to validate the model, in real time the power demand can be a complex combination of

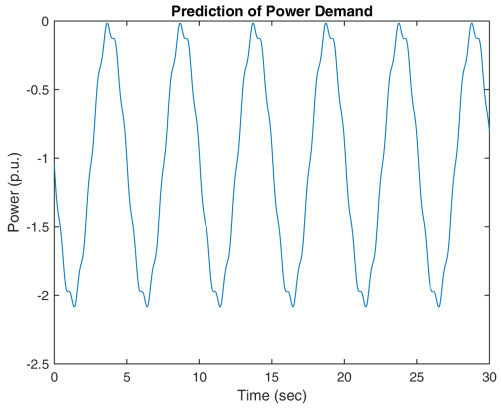

Figure 3.6: Power demanded by a load 'i'

several functions. Similar to the first case of load oscillations, we use another high frequency low amplitude sine wave given as:

$$p_i^l = -\left[(1+\gamma_1)\ \sin(\omega_1 t) + \gamma_1\ \sin(\omega_2 t)\right] \tag{3.21}$$

where $\omega_2 < \omega_1$

And the power generated can be estimated as:

$$p_i^m = (1+\gamma_1)\ N_{loads}/N_{gen} \tag{3.22}$$

The load curve generated by eq. (3.21) is represented in the Figure 3.6.

3.2.9 Divergence in the solution

One thing that was observed during the high fidelity model simulation with the linearized model of eq. (3.17) that the solution keeps on diverging. Even for solutions where the power demand and generated were forced to zero, the solution kept on diverging. To eliminate the possibility of divergence due to the functions we adopted for the power demand and generated in the Sec. 3.2.7 and 3.2.8 in eqs. (3.18) to (3.22), we modified the functions for power demand p_i^m and power generated p_i^l. The power functions for this purpose are approximated as a damped sinusoid given in eq. (3.23). The graphical representation of this function is given in Figure 3.7.

$$\begin{aligned} p_i^l &= -\left[\gamma_1\ \sin(\omega_1 t)\ \exp(-\omega_2 t)\right] \\ p_i^m &= \left[\gamma_1\ \sin(\omega_1 t)\ \exp(-\omega_2 t)\right] \end{aligned} \tag{3.23}$$

The solution of the linearized swing equations with the power functions of eq. (3.23) also diverges even though from Figure 3.7, it can be observed that the power at all the nodes vanishes around 10 secs. The time evolution of the solution is presented in the Figure 3.8.

The average phase angle δ_i of all the buses was computed and plotted against time along with the magnitude of the average power in Figure 3.9.

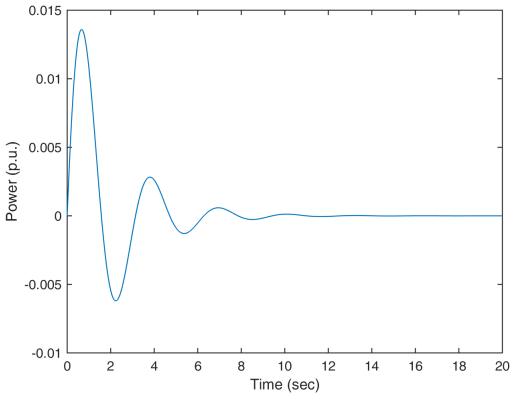

Figure 3.7: Power demanded by a load 'i'

To understand this behavior, a linear stability analysis was carried out on the system matrices to determine whether instability is caused by a numerical issue or is this system is linearly unstable. We solved the characteristic problem associated with our DAE system.

$$\left(\begin{bmatrix} M & 0 \\ 0 & I \end{bmatrix} + \mu \begin{bmatrix} D & B \\ -I & 0 \end{bmatrix} \right) \nu = 0 \tag{3.24}$$

The eigen-analysis of the system which is ill-conditioned shows that most of the eigenvalues are clustered around zero, but two of the eigenvalues are in the positive half of the complex plane. The eigenvalues are plotted in the Figure 3.10.

3.2.10 Results and Discussions about POD

Since, the solution keeps on diverging and from the results presented in Sec 3.2.9 it is evident that the system of equations is linearly unstable. We tried to increase the damping of the system in order to check if the system is stable for any value other than presented in the Table 3.1. With the damping equal to the mass of the generators, the system remains unstable but the values of the phase angles does not increase to very large values, therefore, the author applied the proper orthogonal decomposition on the solution obtained with $d_i = 1$. Although, this value of damping is unrealistic but it can give an insight into the effectiveness of the model reduction method.

The simulation of cascading failure as defined in Sec. 2.5.2 is initiated by a single failure which can then lead to multiple failures in the grid. In order to excite the cascading failure, one initial bus is removed by means of removing the corresponding entries in the susceptance matrix. This is assumed that it will redistribute the voltage and can result in the further failures. The other lines are removed when the phase difference between corresponding buses reaches a certain limit. To check the accuracy of the reduced model described by the POD, once we removed the line joining buses 73 and 74 and simulate the grid until the equilibrium state is achieved.

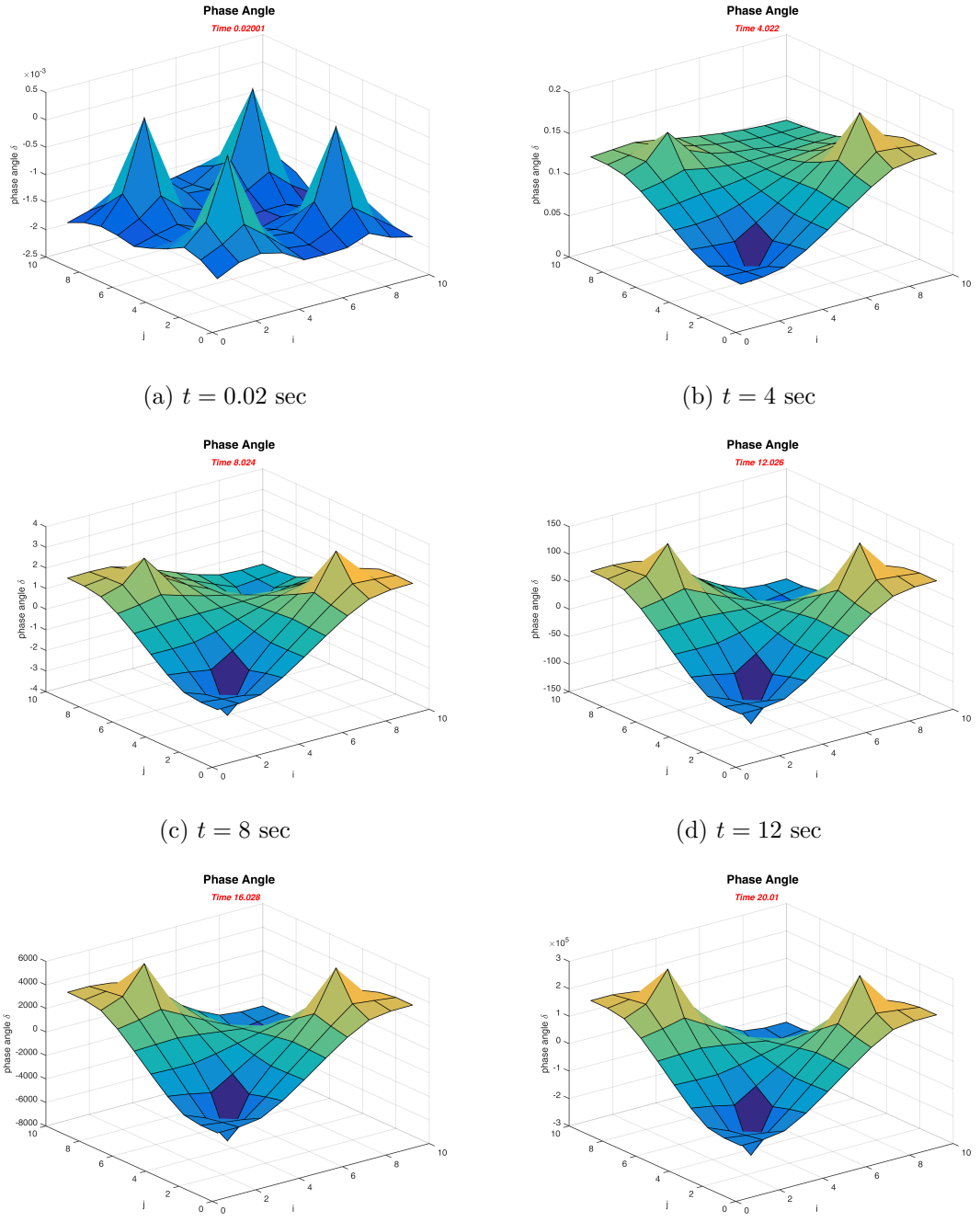

(a) $t = 0.02$ sec

(b) $t = 4$ sec

(c) $t = 8$ sec

(d) $t = 12$ sec

(e) $t = 16$ sec

(f) $t = 20$ sec

Figure 3.8: Evolution of the solution with time

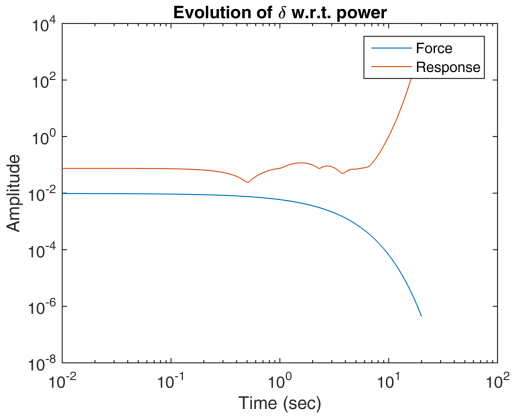

Figure 3.9: Average δ and average power w.r.t. time

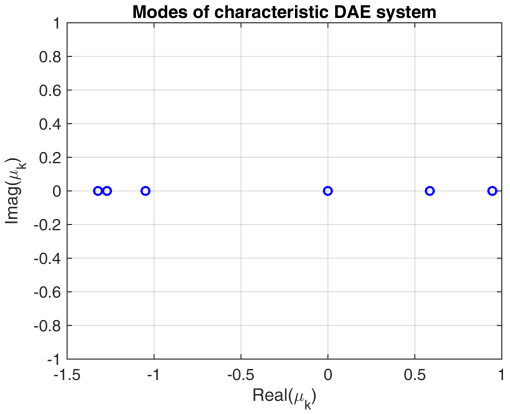

Figure 3.10: Eigenvalues of the characteristic problem

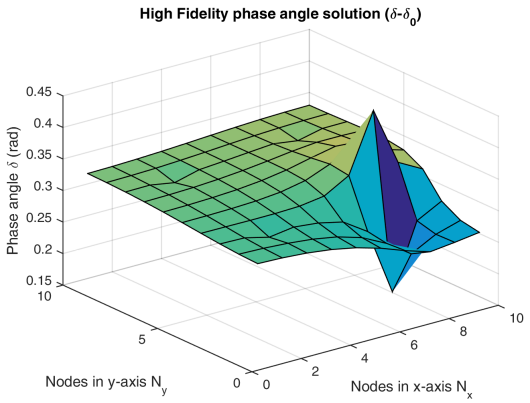

Figure 3.11: Difference between new and previous equilibrium for line 73-74 failure using high fidelity model

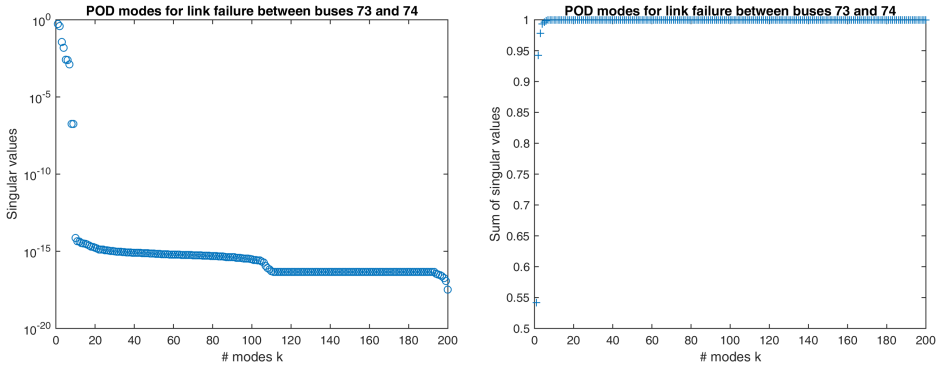

(a) Singular values

(b) Sum of the modes

Figure 3.12: SVD modes for the simulation of connection failure

The difference between the initial equilibrium state and this new equilibrium state is shown in the Figure 3.11 which is the exact solution.

Figure 3.12a and Figure 3.12b represent the modes and the sum of the modes obtained from the exact solution. It can be observed from the Figure 3.12a and Figure 3.12b that only 12 modes out of the total 200 modes are high energy modes and their sum is almost equal to 1. The POD basis created using these modes was tried to simulate cascading failures of the similar conditions. Various different buses were taken out and simulated using the reduced basis in order to ascertain the accuracy of the model. For the initial failure being at the same point as the one tested in the exact solution for the construction of this reduced basis, shows a very accurate result. The difference between the initial and final equilibrium states is shown in the Figure 3.13 which appears close to the solution presented in Figure 3.11 for the high fidelity model. Figure 3.14a shows the norm of the relative error for the case where the link between generator at bus 73 and load bus 74 is disconnected, for better graphical representation the norm is presented in a semi-log plot in Figure 3.14b.

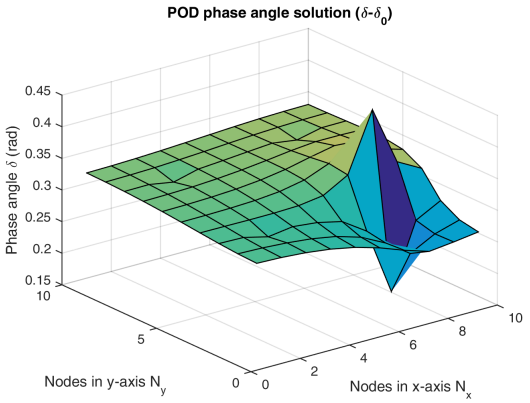

Figure 3.13: Difference between new and previous equilibrium for line line 73-74 failure using POD

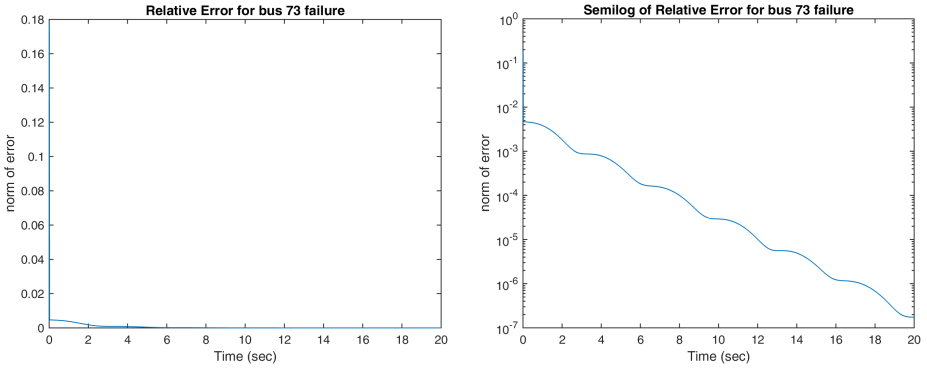

(a) Norm of the Relative Error (b) Semi-log plot of the Relative Error

Figure 3.14: Relative Error in the solution for line 73-74 failure using POD

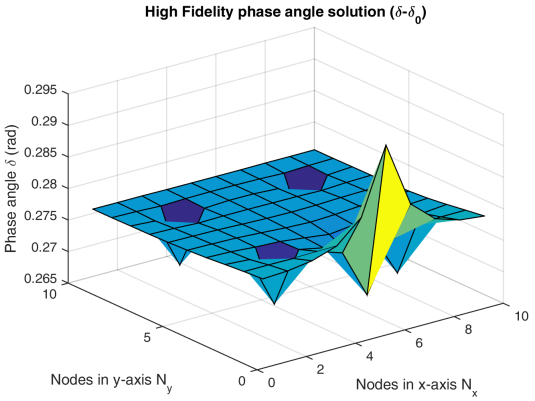

Figure 3.15: Difference between new and previous equilibrium for line 51-52 failure using high fidelity model

The above mentioned case shows good promise for the POD based reduced order modeling. However, in real world situation, it is not known where the fault may develop and how it will effect the grid. For this kind of unpredictable fault propagation, it is very critical for the reduced order model to accurately capture and simulate a failure in the network anywhere. To simulate this kind of unpredictable error, we have used the POD basis constructed previously to simulate when the initial bus failure is between loads 51 and 52 and compare it to the exact solution. The exact and the reduced model solutions are presented in the Figure 3.15 and Figure 3.16 respectively, while the norm of the error is shown in the Figure 3.17a and the semi-log plot of the relative error in Figure 3.17b.

The results show that although POD basis accurately models the scenario when the same case was used to construct the basis it fails to accurately model the other failures. The promise of POD based model reduction is immense when the grid size is small and all the probable combinations of failures can be used to construct the reduced basis. However, in the practical applications, network grids are much larger and the network topology is complex and varied and hence it will be impractical to incorporate all the probable failures in the construction of the reduced basis.

The second case where we wanted to predict the day ahead load variation in the realtime analysis. We developed a sinusoidal profile for the loads and the generators given by the eq. (3.19) and eq. (3.20). The profiles for the load and generator powers are given by the graphs in Figure 3.5a and Figure 3.5b. These variable loads were used in the full solution and used to build a POD reduced order basis.

The modes and the sum of these modes are represented in Figure 3.18a and Figure 3.18b. Only the first four modes were dominant out of the total 200 modes. The results for the simulation from the reduced order basis for the same problem, generates good results. The norm of the relative error and the semi-log plot are presented in the Figure 3.19a and Figure 3.19b.

To predict the next day load using the reduced basis generated from the high fidelity model simulation of Sec 3.2.7, another sinusoidal wave superimposed with high frequency low amplitude sine wave was used for the loads represented in Figure 3.6.

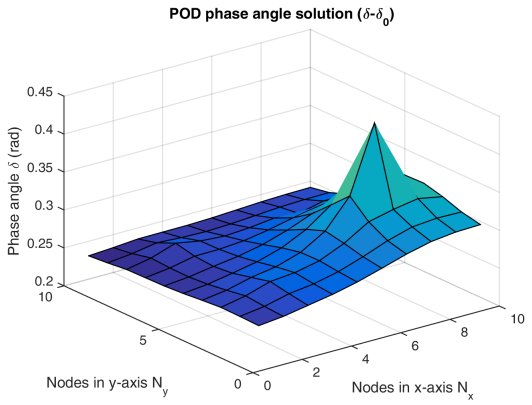

Figure 3.16: Difference between new and previous equilibrium for line 51-52 failure using POD

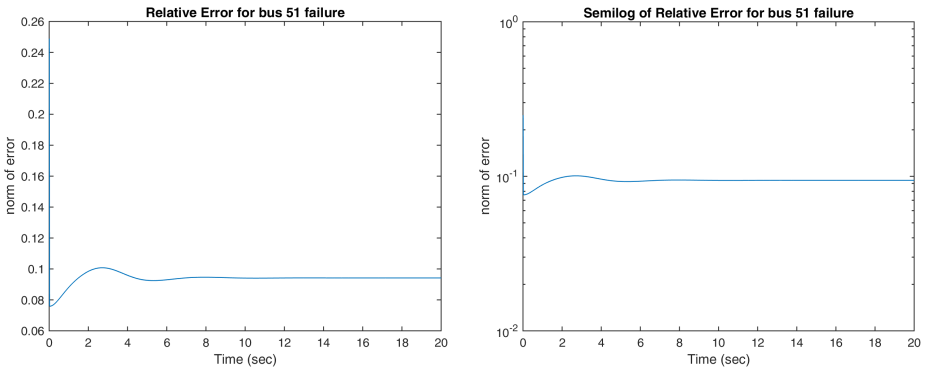

(a) Norm of the Relative Error (b) Semi-log plot of the Relative Error

Figure 3.17: Relative Error in the solution for line 51-52 failure using POD

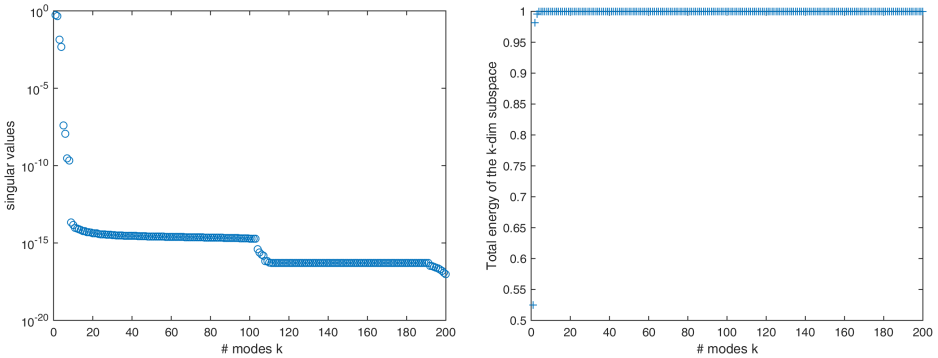

(a) Singular values for the case of variable load (b) Sum of the modes for the case of variable load

Figure 3.18: Singular Value Decomposition of the high fidelity solution of variable load

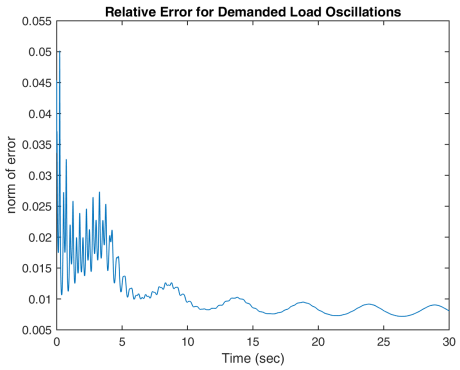

(a) Norm of the Relative Error

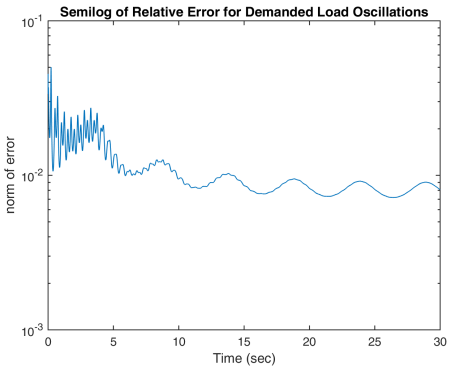

(b) Semi-log plot of the Relative Error

Figure 3.19: Relative Error in the Solution of Variable Load using POD for Variable Load

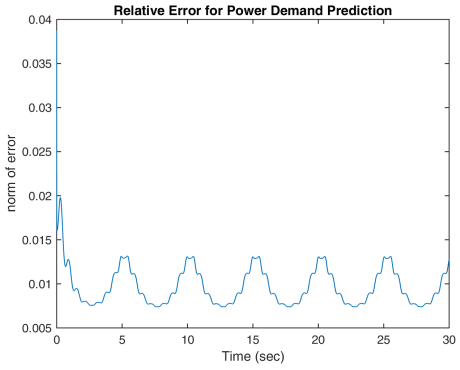

(a) Norm of the Relative Error

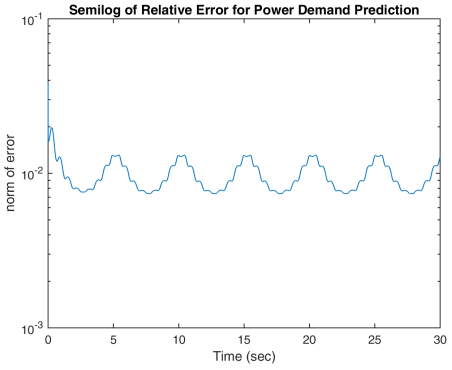

(b) Semi-log plot of the Relative Error

Figure 3.20: Relative Error in the Solution of Load Prediction using POD from Variable Load

The norm of the error is acceptably low although varies slightly with each time step and depends upon the profile of the power demanded curve used in the prediction simulation. This behavior is illustrated in the Figure 3.20a and Figure 3.20b.

3.2.11 Treating Non-linearity

Although it is possible to use POD on nonlinear problems for model order reduction, the necessity of evaluating the nonlinear function renders it less practical in terms of computational complexity. In the current study, we are using MATLAB based ODE solver 'ode15s', which requires that the nonlinear function to be defined analytically. Recalling the equation for p_i describing the nonlinear function,

$$p_i = -\sum_{k=1}^{N} |V_i||V_k|b_{ik}\sin(\delta_i - \delta_k) \quad \text{for} \quad i = 1, ..., N$$

The nonlinear function here depends upon the original basis δ, in the reduced

basis it has to be defined as:

$$\begin{aligned} p_i(\tilde{U}z) &= -\sum_{k=1}^{N} |V_i||V_k| b_{ik} \sin(\sum_{j=1}^{q} (\tilde{U}_{ij} - \tilde{U}_{kj}) z_j) \quad \text{for} \quad i = 1, ..., N \\ \tilde{p}_l(z) &= \sum_{i=1}^{N} \tilde{U}_{il}\ p_i(\tilde{U}z) \quad \text{for} \quad l = 1, ..., q \end{aligned} \tag{3.25}$$

The nonlinear function $\tilde{p}(z)$ in the reduced basis therefore becomes,

$$\tilde{p}_l(z) = -\sum_{i=1}^{N} \tilde{U}_{il} \sum_{k=1}^{N} |V_i||V_k| b_{ik} \sin(\sum_{j=1}^{q} (\tilde{U}_{ij} - \tilde{U}_{kj}) z_j) \quad \text{for} \quad l = 1, ..., q \tag{3.26}$$

It is evident from the eq. (3.26), it requires $\mathcal{O}(N^2 \times q^2)$ operations, which is counter-productive to the reduced order modeling. To save computation costs and truly exploit the benefits of reduced order modeling, it would be necessary to eliminate the N^2 number of operations which is the dimension of original basis. Therefore, a method of Trajectory Piece-Wise Linear Method (TPWL) has been proposed. The solution of the reduced basis using the TPWL method is presented in Chapter 4. Here, in the following section 3.3 we will briefly present the method of Trajectory Piece-wise Linear Method.

As an example of the problem with increased computational cost, we performed a simulation with POD based reduced model for the high fidelity model presented in Sec. 2.7.3. The full simulation without the model reduction required around 202 seconds, with POD and the nonlinear function as defined in eq. (3.26) the simulation took about 290 seconds.

3.3 Trajectory Piece-Wise Linear Method

From the results presented in the Sec. 3.2.1, it is clear that the method of linearization is not applicable because the system becomes linearly unstable. And it is demonstrated through the discussion in the Sec. 3.2.11 that inclusion of the nonlinear function in the reduced model is counter-productive in terms of computational time. Therefore, a method should be adopted which addresses the issue of non-linearity in the system.

Model order reduction of non-linear dynamic systems is a challenging problem and there are issues that are intuitive in the model reduction of non-linear systems. The foremost problem is the accurate and computationally efficient method that approximates the high fidelity model in the reduced basis [73]. Therefore, for any reduced order model to work efficiently on a non-linear problem such as the swing dynamics model, it must be able to construct a basis which is of lower dimension than the original model and approximate the non-linear functions of the system in a way that is computationally efficient [74].

The Trajectory Piece-wise Linear method is a method which combines the positive aspects of the proper orthogonal decomposition and the linearized model for the swing dynamics equations. The first requirement of any model reduction method is to construct a reduced basis of order q smaller than the order of the original basis N, such that, $q << N$. The method of proper orthogonal decomposition (POD) is very good at reducing the dimension of the problem, the other question of an efficient approximation of the non-linear function is what we need an answer for. We present in this method which tries to solve the issue of approximating the non-linear function. The main concept of the TPWL method is to use the linear approximation of the non-linear function using the Taylor Series expansion but not just at the starting point. The trick is to find multiple linear approximations throughout the domain and combine them in such a way that it covers the whole domain of interest. The non-linear function in the original model is replaced with a weighted sum of linearized models in the reduced model.

The method of TPWL offers several advantages for the kind of problem we are dealing with in the current research. First and foremost, it offers an accurate approximation of the non-linearity of the problem by using linear approximations at several points in the domain, without compromising the computational efficiency too much. Even though, we have used POD for the model reduction, the method of TPWL can easily incorporate any of the other well known model reduction techniques [73] such as Empirical Interpolation Method (EIM) [75] and Discrete Empirical Interpolation Method (DEIM) [76].

3.4 Literature Review of TPWL

The main hurdle in the effective model order reduction of the power grids is the strong non-linearity appearing in swing dynamics models. Trajectory Piecewise-Linear method (TPWL) is a well-defined method for the model order reduction of nonlinear time varying applications [74]. This method proposes a suitable strategy for treatment of nonlinearities which presents the real bottleneck of model order reduction. This method has been applied on several nonlinear problems especially to electronics engineering applications [77, 78, 79, 80, 81, 82, 83, 84].

The method of TPWL originated for the non-linear problems in electrical circuits [85]. The method was initially used in the model order reduction of non-linear dynamical systems by Rewienski and White [86]. The method was developed by Rewienski [74] as his PhD dissertation and used this method on various applications including electrical circuits, MEMS and fluid problems. The method has thus been adopted for problems in subsurface flow simulations [87, 88], computational fluid dynamics [89] and chemical process controls [90].

A similar method to the one adopted in this paper is found in the work of Bugard et al [91] and Panzer et al [92] who have proposed a parametric model order reduction. The main idea presented in these works is to reduce several local models and then produce a parametric reduced order model using a suitable interpolation strategy. Compared to these methods, TPWL has one global reduced basis and uses

interpolation of locally linearized models just to represent the nonlinear term in the reduced variables space. More than one training trajectories can be added together to form the single global reduced basis similar to the concept of POD.

Non-linearity is recurrent in the electronics engineering applications, Hao et al. [93] implemented TPWL macromodeling in their study of the analog mismatch for the large-scale stochastic differential-algebraic equations (SDAE). They implemented TPWL with an improved incremental aggregation of sub-spaces and named it as “isTPWL". Their results indicate tremendous gains in terms of computational speed compared to the Monte-Carlo method with similar level of accuracy. Zong et al. [94] applied TPWL macromodeling methods for the time-dependent non-linear models of the circuits. The authors in this study have proposed MOR in time domain rather than frequency domai based on wavelet-collocation method. Farooq et al. [82] have used Chebyshev interpolating polynomials in each piece-wise region in their implementation of TPWL method.

TPWL method has been implemented in non-linear control of integrated circuits and MEMS [79]. Xie and Theodoropoulos [90] have used the capability of TPWL of reducing large scale non-linear dynamic models and demonstrated it through the stabilization of the oscillatory behavior tubular reactors as the case study. They have demonstrated the use of linear MPC for non-linear distributed-parameter systems. The study combines the use of POD and finite element Galerkin projection to gather low order nonlinear models of the system, then TPWL was applied to get a piece-wise linear representation of the reduced model.

Trajectory piecewise-linear methods are not limited to just power electronics and control systems applications, indeed there are vast areas of research where the application of TPWL based model order reduction will be beneficial [87, 88]. The study by He et al. [87] involves the implementation of TPWL macromodeling for subsurface flow simulations. In another study by Cardoso and Durlofsky [88] the work on model order reduction using TPWL methods for subsurface flow simulations is presented. The authors have applied their proposed method on two examples of 24,000 and 79,200 grid blocks and comparing it with experimental results have shown the method produces results accurately. Also, the saving in terms of computational time is given in the range of 100-2000 times which is significant.

In the current study, we implemented TPWL method to accurately obtain a reduced order model for the nonlinear transient dynamics of power grids, mathematically modeled by swing dynamics. The swing dynamics model is highly non-linear and it is very difficult to have accurate results with linearized reduced order models and the nonlinear POD is inefficient with respect to time consumption. Therefore, the adoption of TPWL method in the current study is suitable for the model order reduction of power grids.

3.5 Model Order Reduction using TPWL

In this section, we present the model order reduction based on the Trajectory Piecewise Linear (TPWL) method, which combines the typical proper orthogonal decom-

position with the linearization of the non-linear functions at multiple points in the solution manifold.

3.5.1 Proper Orthogonal Decomposition

The method of proper orthogonal decomposition has already been presented in the Section 3.2.1. Here, we recall that from the results of Sec. 3.2.9, it was concluded that the method of POD is not suitable for effective model order reduction of swing dynamics model because of the non-linearity.

Although, we discussed in the Sec. 3.2.9 that POD with the linearized approximation of the swing dynamics problem does not work as intended because of the system becoming linearly unstable. It is primarily because of the linear approximation making the system unstable, we have shown from the results that POD as a method itself shows some encouraging results. In the method of TPWL, POD is used for the model reduction part. Therefore, at this point we refer the readers back to Sec. 3.2.1 to recall the method of POD if not familiar.

3.5.2 Trajectory Piece-Wise Linear method

An approach based on TPWL method has been adopted in the current study to reap the benefits of reduced order modeling while also maintaining a good approximation of the nonlinear function.

Evaluation of $\{\tilde{p}(z)\}$ requires $N^2 \times q^2$ operations which results in similar time consumption as high fidelity model. The objective of introducing TPWL method is to construct a locally affine mapping $\{\tilde{L}_p(z)\}$ from $\mathbb{R}^q$ to $\mathbb{R}^q$ at some time steps s where $s << n$ which involves less operations and such that $\{\tilde{L}_p(z)\} \approx \{\tilde{p}(z)\}$.

Trajectory piece-wise linear method is a method combining the model order reduction and the linearization of the non-linear functions. The system in the current study given by swing dynamics equation, recalled here in eq. (3.27), has strong non-linear characteristic and as described in earlier sections, nonlinear reduced order model does not reduce the time consumption. The TPWL method provides a combination of linearized models obtained at selected snapshots.

$$m_i\ddot{\delta}_i + d_i\dot{\delta}_i = p_i^m - \sum_{k=1}^{N} |V_i||V_k|b_{ik}\sin(\delta_i - \delta_k) \quad \text{for} \quad i = 1, ..., N \tag{3.27}$$

To accurately capture the behavior of nonlinear function, it is important that the points selected for the linearization should be such that they span the whole manifold in which the system trajectories evolve. As an example of this, Figure 3.21 shows the typical trajectory in the space of reduced variable $\{z\}$ and in this the selection of linearization points is made to ensure that the trajectory is completely covered.

The proposed method takes advantage of multiple linearized points instead of relying on the linearization of the initial point, this combination of linearization models enhances accuracy considerably and solves the issue of linear instability

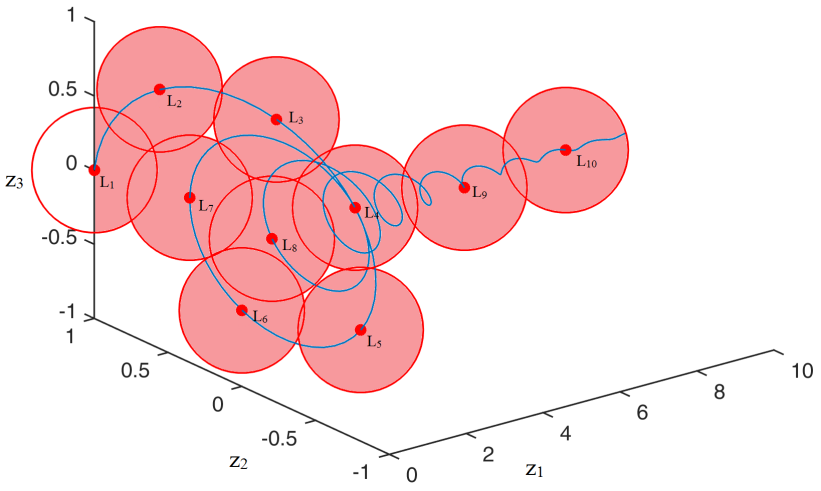

Figure 3.21: Linearization points on a sample curve in reduced basis (z_1,z_2,z_3)

encountered in the implementation of POD based reduced order modeling methods, presented in Sec. 3.2.1.

3.5.2.1 Steps of TPWL Simulation

TPWL method can be separated into an offline and an online stage. The steps during the offline phase are below:

- Step 1: Simulation of the high fidelity model used as the training trajectories (See details in sec. 3.5.2.2).
- Step 2: Generation of reduced basis using POD.
- Step 3: Linearization of the nonlinear function and construction of the set of linearization points S (See details in sec. 3.5.2.3). During the construction of set S, weights have to computed for the combination of linear functions which is detailed in the sec. 3.5.2.4.
- Step 4: Reduction of the linearized system and the storage of $\{\delta\}^j, \{\tilde{p}\}^j, [\tilde{J}]^j$ and S, where j is the element in the set of linearization points S.

Once the above steps are performed and we have a reduced linear system with $\{\delta\}^j, \{\tilde{p}\}^j, [\tilde{J}]^j$ and S available, we can perform the simulation of the reduced system in an online phase of TPWL. The following steps comprise the online phase of TPWL.

- Step 1: Load the stored reduced basis.
- Step 2: Calculate weighting functions.
- Step 3: Combine the linearized systems in a convex combination.

- Step 4: Solve the reduced linearized system.

The general algorithm of the TPWL method is graphically represented in the Figure 3.22.

In the following sections we will present the methodology to select the linearization points and also the weighting procedure for the combination of the linearization points.

3.5.2.2 Selection of Training Trajectories

Training trajectories form an integral part of the TPWL method which theoretically, should be able to cover all the domain of the nonlinear function. The selection of training trajectories, therefore, requires careful selection of initial conditions upon which the trajectories of the swing model depend. One may consider it is inefficient to compute so many nonlinear functions to cover the whole domain. However, in practice there are only a few possible conditions a system can achieve in real time applications. Training trajectories provide the points at which the nonlinear system has to be linearized (see Sec. 3.5.2.3). It is to be stressed that the TPWL method can interpolate between the training trajectories but not to extrapolate. Therefore, it is necessary to include all the trajectories in the training set that are considered to be visited by the nonlinear function [73].

3.5.2.3 Selection of Linearization Points

The selection of the linearization points has been done during the offline stage of the TPWL method and is performed on the full original dimension of the system. This is due to the reason that the construction of the linear approximation $\{\tilde{L}_p(z)\}$ is done with the information already available from the training trajectories. Therefore, we present the equations in terms of the original basis $\{\delta\}$, the nonlinear function $\{p(\delta)\}$ in eq. (3.10) is linearized at certain points in time. This function at a generic snapshot is given by local approximation $\{L_p^j(\{\delta\})\}$ as:

$$\{L_p^j(\{\delta\})\} \approx \{p\}^j + [J]^j \left(\{\delta\} - \{\delta\}^j\right) \quad \text{for} \quad j = 1, ..., s \tag{3.28}$$

This is the first step in the TPWL simulation after the full nonlinear solutions have been obtained at the predefined training trajectories. The initial conditions are represented by $\{\delta\}^0$ and it is by default the first point selected for the linearization. The Jacobian is given by:

$$[J] = \frac{\partial\{p\}}{\partial\{\delta\}} = \begin{bmatrix} \frac{\partial\{p\}}{\partial\delta_1} & \cdots & \frac{\partial\{p\}}{\partial\delta_N} \end{bmatrix} \tag{3.29}$$

Note that the Jacobian can be derived analytically for the swing equations.

The linearized function approximates the actual nonlinear function using the Jacobian at the specified linearization points, represented by j in the superscript. The idea behind the TPWL method is that a number of linearization points are selected and the linearized functions at those snapshots are summed up by a weighting

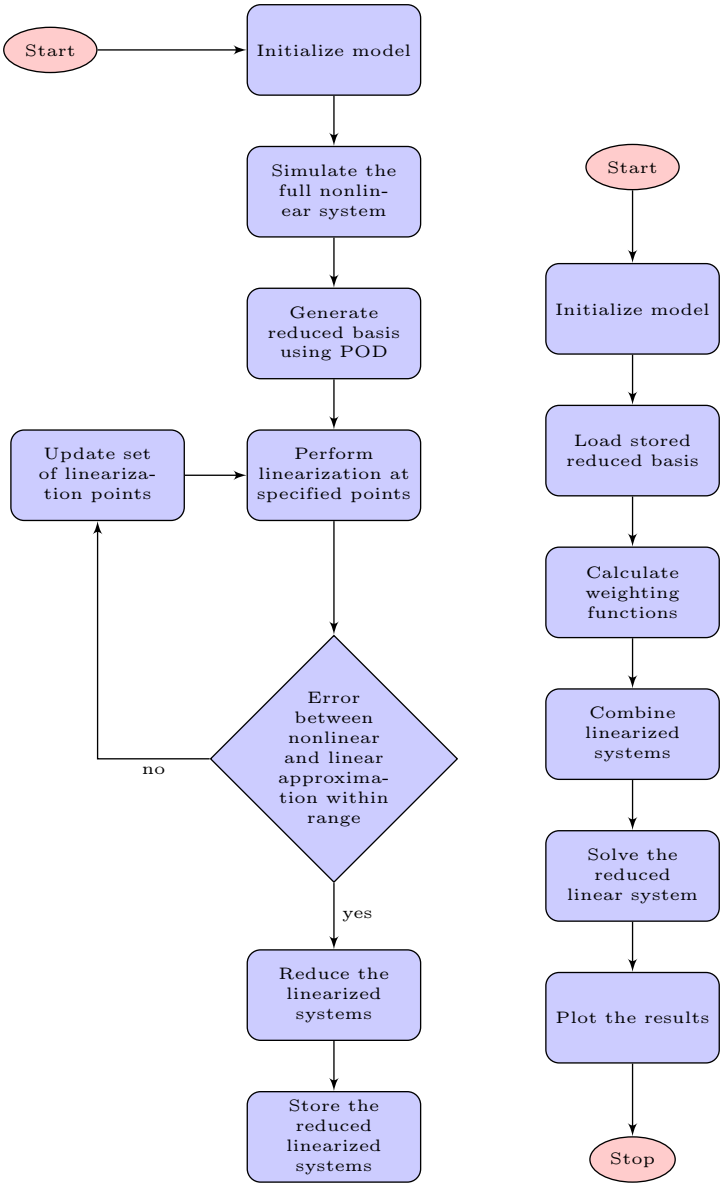

(a) Offline stage (b) Online stage

Figure 3.22: Two stages of TPWL Simulation

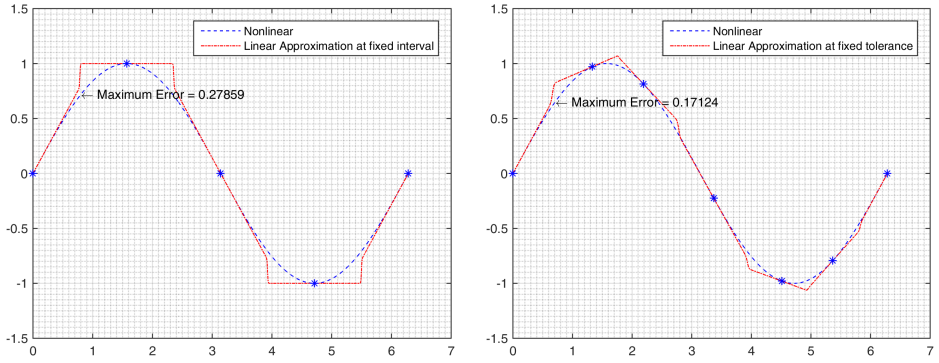

(a) Linearization at Fixed intervals (b) Linearization using tolerance

Figure 3.23: Two methods for selection of linearization points

function given a global approximation as presented in eq. (3.30). A detail on the selection of linearization points has been presented in Algorithm 1.

$$\{L_p(\{\delta\})\} \approx \sum_{j=1}^{s} w^j \cdot \left(\{p\}^j + [J]^j \left(\{\delta\} - \{\delta\}^j\right)\right) \tag{3.30}$$

where, L_p is the linear approximation, $\{p\}^j$, $[J]^j$ are the nonlinear function and Jacobian matrix evaluated at the j^{th} linearization point, and $\{\delta\}^j$ is the j^{th} linearization point. The weight $\hat{w}^j$ is given by eq. (3.31), which depends on the distance d^j between $\{\delta\}$ and linearization point $\{\delta\}^j$, and the normalized form is denoted by w^j which appears in eq. (3.30).

$$\hat{w}^j = e^{-\beta d^j / d^{min}} \tag{3.31}$$

where β is a positive constant and it can be adjusted to reduce the error and smooth the affine function $\{L_p\}$, d^j is the distance between $\{\delta\}$ and linearization point $\{\delta\}^j$ and d^{min} is the minimum among d^j.

The strategy to select the linearization points is traditionally based on the difference between the phase differences between the successive time steps, i.e., $(\delta_i - \delta_{i-1})^j - (\delta_i - \delta_{i-1})^{j-1}$. If the phase difference is greater than some angle, e.g. 10 degrees, than this point j will be added to the set of linearization points. This method is widely used in the studies referenced in our work as presented in the works of Albunni [73] and Rewienski et al. [86]. The limitation in this method is that when the selection is based on the distance between points, there is no control over the error. This can lead to significant error especially if the Jacobian is close to singular. The alternative method adopted in this study is to place the linearization points adaptively based on an error indicator. This is obtained by the difference between the nonlinear function and the approximation obtained by TPWL method. When a point is encountered for which the error is greater than a given threshold, the TPWL model is enriched with a new point. This procedure is applied recursively to all the snapshots of the training simulations, starting with a single point that is the initial condition.

A simple nonlinear trigonometric function and its linear approximation based on the concept of fixed distance in the context of its norm is plotted in Figure 3.23a while a new method developed in the current study is shown in Figure 3.23b. As it is observable from Figure 3.23a and Figure 3.23b, the number of linearization points are comparable as 5 in the first case to 7 in the current case has reduced the approximation error by about 40 %. Generally, the increase in number of linearization points is of no significant loss in computation time as the selection is done during the offline phase while in the online phase the computation of linear functions is very quick.

This approach is similar to the method proposed in the study of Liu et al [77] in which the authors have used a global maximum error for linearization point selection.

Algorithm 1 Build set of linearization points

Input $\{\delta\}^i,\ \{p\}^i,\ [J]^i,\ i = 1, ..., n$
Initialize set of linearization points with initial condition as the first point $\{\hat{\delta}\}^1 = \{\delta\}^0$
$S = \{\hat{\delta}\}^1,\ s = 1$
$\{\hat{p}\}^1 = \{p\}^1,\ [\hat{J}]^1 = [J]^1$
Set tolerance ϵ_s for the selection of new point of linearization
$\epsilon_s = 0.005$
while $i < n$ **do**
  Linearize $\{p\}$ and combine in a weighted sum
  for $j = 1$ **to** s **do**
    Compute $\hat{\boldsymbol{w}}^{\boldsymbol{j}}$ according to eq. (3.31) and normalize to get $\boldsymbol{w}^{\boldsymbol{j}}$
    $\{L_p(\{\delta\}^i)\} = \sum_{j=1}^{s} w^j \cdot (\{p\}^j + [J]^j (\{\delta\}^i - \{\delta\}^j))$
    if $\{\{p(\{\delta\}^i)\} - \{L_p(\{\delta\}^i)\}\} > \epsilon_s$ **then**
      Increase the size of set of linearization points
      $\{\hat{\delta}\}^s = \{\delta\}^i,\ \{\hat{p}\}^s = \{p\}^i,\ [\hat{J}]^s = [J]$
      $S \leftarrow S \cup \{\hat{\delta}\}^s$
    end if
  end for
end while
Output $S = \{\{\hat{\delta}\}^1, ..., \{\hat{\delta}\}^s\}, s = card(S),\ \{\hat{p}\}^j,\ [\hat{J}]^j, j = 1, ..., s$

The modified version of the selection of linearization points is more time consuming then the original method proposed by Albunni [73]. However, selection of linearization points is performed during the offline phase where time is not a constraint, the proposed method in the current study has higher accuracy with the problem discussed here.

A very important note that the nonlinear function $\{\tilde{p}\}^j$ and the Jacobian matrix $[\tilde{J}]^j$ are stored in the reduced basis.

3.5.2.4 Weighting Function

TPWL method combines the linearized model in a convex combination approximating the original nonlinear system. In a convex combination all the coefficients are greater or equal to zero with the sum of all the coefficients equal to one. If there are 's' linearized models and 'q' is the order of the linearized system, then the computation of these weights is in the order of $O(sq)$ (for detailed study on the weighting function refer to thesis of Rewienski [74]). The calculation of weights is carried out during both the online and offline phases in the current study.

Given the set of linearization points S and β, the weights can be calculated for any point with respect to the points in the linearization set. The value of β should be a positive constant, in the current study its value is 25 . A smaller value smooths the function and make its appearance continuous, while a higher value results in kinks in the function. The necessity of adjusting β is that it helps to reduce the error between the nonlinear function and its approximation. The first step is to compute the distance d^j between a point $\{\delta\}$ and all the points in the set S using,

$$d^j = ||\{\delta\} - \{\delta\}^j||_2 \quad \text{for} \quad j = 1, ..., s \tag{3.32}$$

The weights are then calculated as,

$$\hat{w}^j = e^{-\beta d^j / d^{min}} \quad \text{for} \quad j = 1, ..., s \tag{3.33}$$

where, $d^{min} = \min_{j=1,...,s} \ d^j$

Once, the weights are calculated with respect to all the points in the set S, the weights are normalized as:

$$w^j = \frac{\hat{w}^j}{\sum_{i=1}^{s} \hat{w}^i} \ , \quad \text{for} \quad j = 1, ..., s \ , \ i = 1, ..., s \tag{3.34}$$

During the online phase, in place of $\{\delta\}$ reduced basis $\{z\}$ is used to calculate the distance and the points in the set S consists of linearization points in the reduced basis as well.

3.5.2.5 Numerical Integration of the Reduced Model

Once a linear model has been obtained from the training trajectories during the offline phase, the values of the nonlinear function and the Jacobian matrix evaluated at the selected linearization points are reduced and stored to be used during the online phase along with the set of linearization points. The nonlinear function and the Jacobian is projected in the reduced space as:

$$\begin{aligned} \{\tilde{p}(\{z\})\} &= [\tilde{U}]^T \{p(\{\delta\})\} \\ [\tilde{J}] &= [\tilde{U}]^T [J][\tilde{U}] \end{aligned} \tag{3.35}$$

Since, we replace the nonlinear function with an approximation containing sum of linearized functions, we have

$$\begin{aligned} &\{\tilde{L}_p(\{z\})\} = [\tilde{U}]^T\{L_p([\tilde{U}]\{z\})\} \\ &\Rightarrow \{\tilde{L}_p(\{z\})\} \approx \sum_{j=1}^{s} w^j \cdot \left(\{\tilde{p}\}^j + [\tilde{J}]^j \left(\{z\} - \{z\}^j\right)\right) \end{aligned} \tag{3.36}$$

In the above equation, the weights w^j are evaluated afresh in the reduced dimension. The weights are calculated exactly as described in the section 3.5.2.4 with $\{z\}$ replacing the $\{\delta\}$.

With the above information, we now have a system in reduced basis which fully exploits the benefits of reduced order modeling. As it can be observed from eq. (3.36), the number of operations now depend on s rather than N^2.

3.6 Numerical experiments

The network grid studied here is termed as the “Ring Grid" consisting of only generators with one reference node connected to all the generators, represented in Figure 3.24. The mathematical model describing the ring grid is the swing dynamics given by the eq. (3.27).

The grid in this study is a ring grid containing all the generator nodes and a slack node in a topology such that the slack node is connected with all the generators. A slack node or bus in electrical power system is a bus where both $|V|$ and δ are known and is used to balance the power losses or power demand shortage while performing a power flow study [95]. Here, the slack bus is modeled as an infinite bus which is a simplifying assumption that the voltage at this bus is always constant and it has infinite power capacity as the impedance is zero for this bus. A list of assumptions for the grid in the current study are:

- The power grid is loss-less
- The generators are small and the ratio between the length of transmission line joining generators to the infinite bus and the length of transmission line joining two consecutive generators is much bigger. Hence, the interaction between a generator and infinite bus is much smaller than the interaction between two neighboring generators
- Transmission lines joining two consecutive generators is shorter than the line joining the generators with the infinite bus
- Transmission lines between the infinite bus and all the generators are of same length
- Transmission lines connecting the generators are of same length

The non-linear function p_i in eq. (3.27) is different from its form given in eq. (2.37) in Sec. 2.5 due to the assumptions described earlier and is given as eq. (2.46) in Sec. 2.7.2, recalling the non-linear term here,

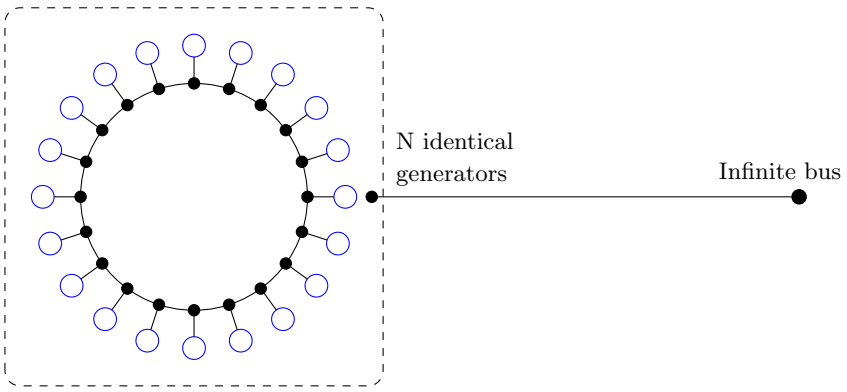

Figure 3.24: A ring grid power network. Blue circles representing generators connected to an infinite bus

Symbol	Description	Value
m_i	Mass of the generators	1 [p.u.]
d_i	Damping of the generators	0.25 [p.u.]
p^m	Power generated by the generators	0.95 [p.u.]
b	Susceptance between generator and slack node	1 [p.u.]
b_{int}	Susceptance between consecutive generators	100 [p.u.]
N	Number of generators	1000

Table 3.2: Grid Data

$$p_i = b\sin(\delta_i) + b_{int}[\sin(\delta_i - \delta_{i+1}) + \sin(\delta_i - \delta_{i-1})] \text{ for } i = 1, ..., N \tag{3.37}$$

where, b is line susceptance between generators and the reference node and b_{int} is the line susceptance between two connected generators.

The eq. (3.27) takes the following form,

$$\begin{aligned} m_i\ddot{\delta}_i + d_i\dot{\delta}_i = p_i^m - b\sin(\delta_i) - b_{int}[\sin(\delta_i - \delta_{i+1}) + \sin(\delta_i - \delta_{i-1})] \\ \text{for } i = 1, ..., N \end{aligned} \tag{3.38}$$

The grid studied consists of 1000 generators and one slack node connected to all the generators. The data used in the study is given in Table 3.2, all the values are given in per-unit system.

The values used in the current study are adapted from the study of Susuki et al. [55] with the addition of damping to ensure the steady state stability of the power grid. Also, the number of generators in the study of Susuki et al. are only 20 and the focus of their study is to demonstrate the coherent swing instabilities. Although different from the study by Susuki et al., the grid loop as described in their study presented a good opportunity to showcase the ability of TPWL method for the model order reduction and fast simulation of electrical power grids.

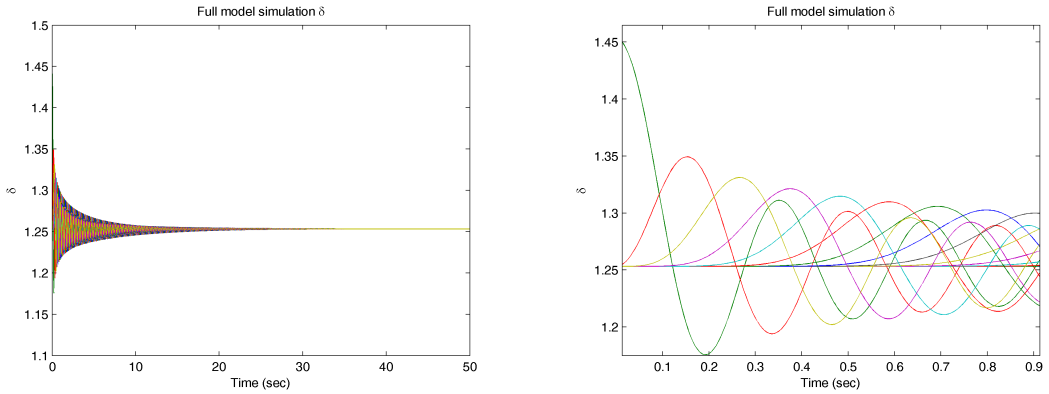

(a) Complete trajectory

(b) Zoomed in view

Figure 3.25: First training trajectory: Initial condition of equilibrium with one node perturbed

3.6.1 Training Trajectories and Reduced order models

In the current study, there are three different scenarios of initial conditions that must be taken into account for the training trajectories, these are listed in Table 3.4. The dependence of the trajectories on the initial conditions is evident since the trajectory will be different in each case as shown in the Figure 3.25 to Figure 3.27.

As described in section 3.5.2.2, multiple training trajectories have been employed for the generation of reduced order models. These training trajectories were categorized into three different types. The total time of simulation and the step size are listed in Table 3.3 and Table 3.4 lists the perturbation amount and the node for each case.

1. Initial conditions at the equilibrium point for all the generators bar one. This is illustrated in Figure 3.25a and in Figure 3.25b a zoomed in view of Figure 3.25a is presented where the effect of non-synchronous generator on its neighboring generators can be observed.

2. All the generators start from a non-equilibrium point and one generator out of synchronicity. This is illustrated in Figure 3.26a and a zoomed in view is presented in Figure 3.26b.

3. All the generators start from the same non-equilibrium state and are synchronous. This case is demonstrated by Figure 3.27

The Jacobian is a tri-banded diagonal matrix in the case under study here.

$$\begin{aligned} J_{k,l} = \frac{\partial p_k}{\partial \delta_l} &= \frac{\partial}{\partial \delta_l}\left[b\sin(\delta_k) + b_{int}\sin(\delta_k - \delta_{k+1}) + b_{int}\sin(\delta_k - \delta_{k-1})\right] \\ &= \hat{\delta}_{k,l}\{b\cos(\delta_k)\} + \{b_{int}\cos(\delta_k - \delta_{k+1})\}(\hat{\delta}_{k,l} - \hat{\delta}_{k+1,l}) \\ &+ \{b_{int}\cos(\delta_k - \delta_{k-1})\}(\hat{\delta}_{k,l} - \hat{\delta}_{k-1,l}) \end{aligned} \tag{3.39}$$

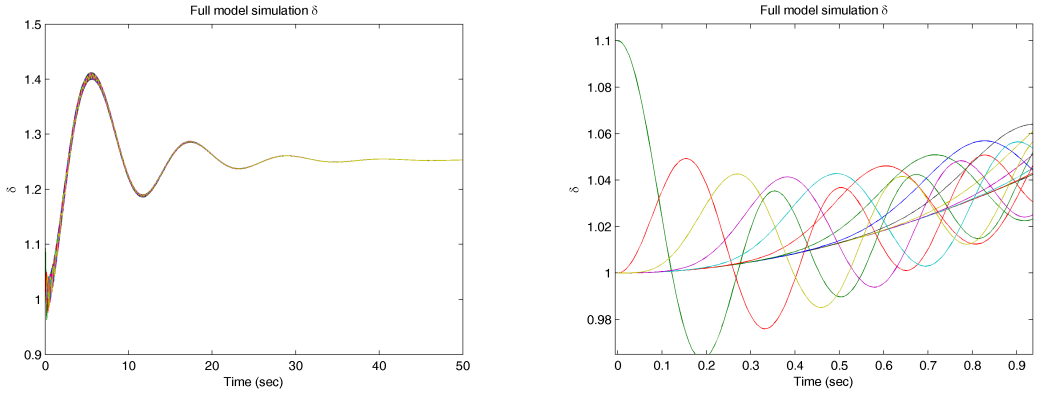

(a) Complete trajectory

(b) Zoomed in view

Figure 3.26: Second training trajectory: Initial condition of non-equilibrium with one node perturbed

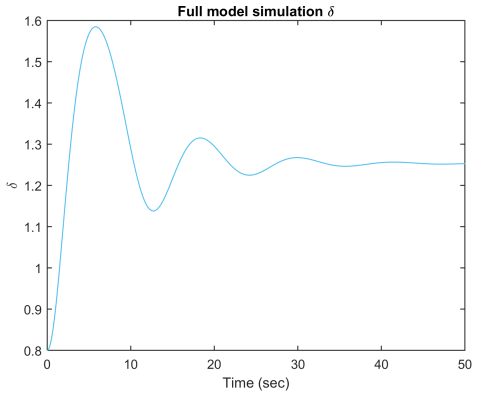

Figure 3.27: Third Training trajectory: Initial condition of equilibrium with all nodes synchronous

Symbol	**Description**	**Value**
T	Total time of simulation	50 [s]
ΔT	Time step	0.005 [s]

Table 3.3: Training trajectories data

Training Trajectory	$\boldsymbol{\delta_2}$	$\boldsymbol{\delta_i}$ $\forall i \neq 2$
Trajectory 1	1.45	1.25
Trajectory 2	1.1	1
Trajectory 3	0.8	0.8

Table 3.4: Initial conditions

Training Trajectory	Quotient 'η'	Modes 'q'	Tolerance 'ϵ_s'	Lin pts 's'
1	1×10^{-4}	312	0.01	26
	1×10^{-2}	203	0.005	47
	2×10^{-2}	171	0.005	47
2	1×10^{-4}	312	0.005	16
	1×10^{-2}	199	0.005	16
	1×10^{-2}	199	0.001	49
3	1×10^{-4}	130	0.005	8
	2×10^{-2}	62	0.005	8
	2×10^{-2}	62	0.001	17

Table 3.5: Number of modes and linearization points for all training trajectories

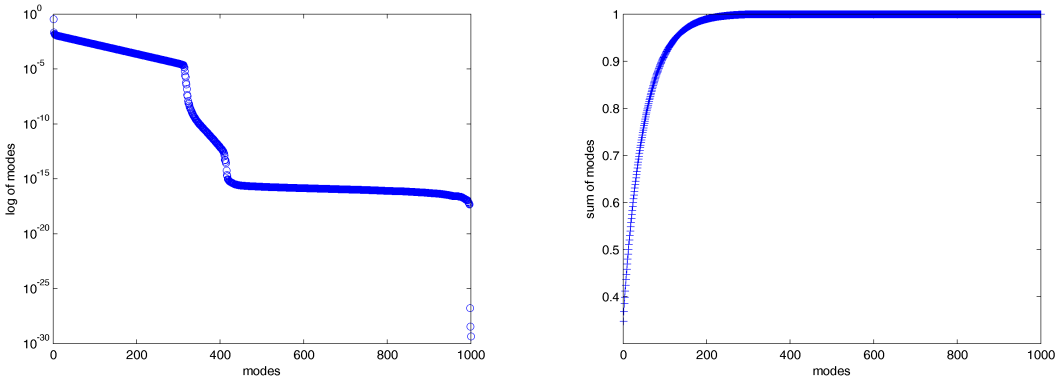

(a) Singular Modes

(b) Sum of the Modes

Figure 3.28: 1st training trajectory

Figure 3.25a represents the first case where the system was initially in equilibrium state except one generator the phase of which was disturbed from the equilibrium position by 0.2 radians. The second case is represented in Figure 3.26a which is the one where all the generators start off from non-equilibrium position and in addition one of the generator's phase angle is different from the rest by an angle of 0.1 radians. The third case is the one where all the generators are synchronous but they are not at the equilibrium position and hence the system oscillates before settling down to a steady state equilibrium, this case is shown in Figure 3.27.

Reduced order models obtained using the POD technique are listed in the Table 3.5 along with the number of linearization points selected, the order of the reduced model depends upon the individual cases. The Figure 3.28a to Figure 3.30b represents the modes and the sum of modes for case 1, case 2, and case 3 respectively.

It is intuitive that the more the number of modes and the number of linearization points the more time the reduced model takes to simulate. The time consumption data along with number of modes and linearization points of the training trajectories

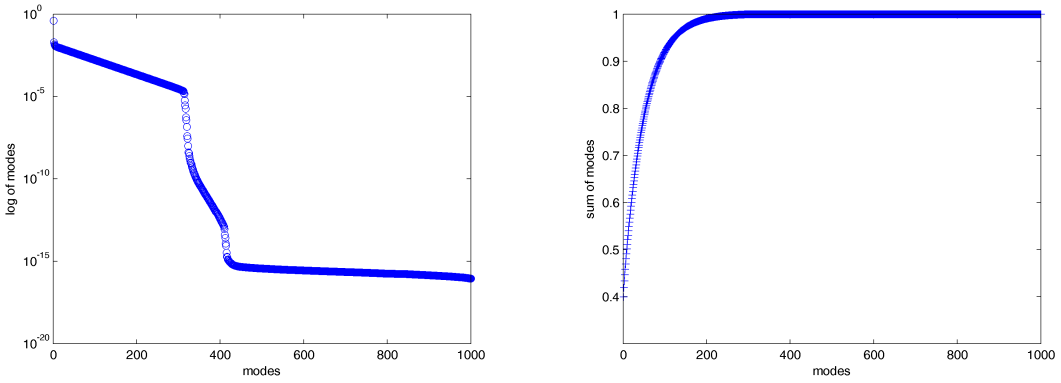

(a) Singular Modes (b) Sum of the Modes

Figure 3.29: 2nd training trajectory

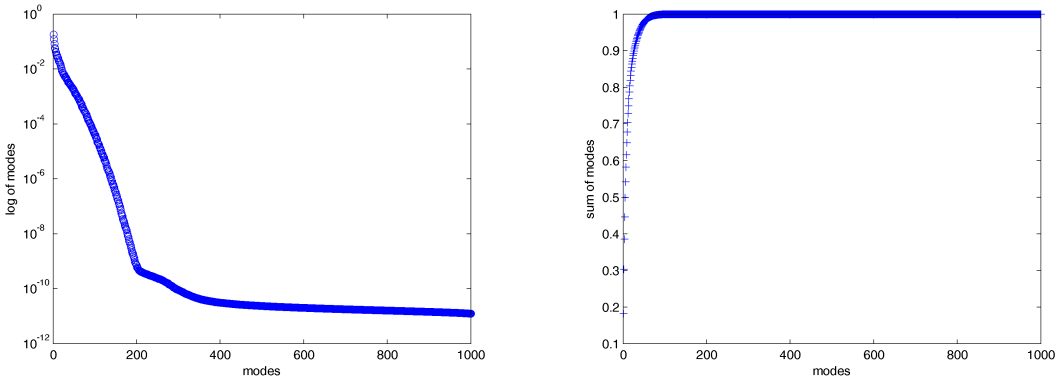

(a) Singular Modes (b) Sum of the Modes

Figure 3.30: 3rd training trajectory

Training Trajectory	Modes 'q'	Lin Pts 's'	Time (sec)		
			Full Model	POD	Lin Pts Sel
1	312 ($\eta < 10^{-4}$)	26 ($\epsilon_s = 0.01$)	202	33	276
	312 ($\eta < 10^{-4}$)	47 ($\epsilon_s = 0.005$)			632
	203 ($\eta < 10^{-2}$)	47 ($\epsilon_s = 0.005$)			580
2	312 ($\eta < 10^{-4}$)	16 ($\epsilon_s = 0.005$)	191	27	155
	199 ($\eta < 10^{-2}$)	16 ($\epsilon_s = 0.005$)			150
	199 ($\eta < 10^{-2}$)	49 ($\epsilon_s = 0.001$)			850
3	130 ($\eta < 10^{-4}$)	8 ($\epsilon_s = 0.005$)	60	30	105
	62 ($\eta < 2 \times 10^{-2}$)	8 ($\epsilon_s = 0.005$)			100
	62 ($\eta < 2 \times 10^{-2}$)	17 ($\epsilon_s = 0.001$)			200

Table 3.6: Time Consumption Data

is listed in Table 3.6. It is to be noted that all the simulations have been run on a laptop with a i5-4200 CPU with a 1.6 GHz processor and 8 GB RAM.

The combination of the above described number of modes and number of linearization points gave us has given some varied performance in terms of time and errors. The errors mentioned in the Table 3.7 are both the absolute errors and the relative errors in the δ of corresponding generators where we have listed the maximum error in cases where we simulated the same case with TPWL as the case in training trajectories. This way we gain confidence in the model selected for the cases that differ from the training trajectories. The modes and number of linearization points selected are based on the minimum error while keeping the time of computation minimum. A comparison of average δ from the full non-linear simulation and the TPWL simulation is presented in Figure 3.31 to Figure 3.33.

The comparison between the reduced linearized model from TPWL and the full non-linear model was carried out on the average δ, which is termed as collective-phase variable and its time derivative is ω. These are defined for loop power systems as:

$$\delta = \frac{1}{N} \sum_{i=1}^{N} \delta_i \tag{3.40}$$

$$\omega = \frac{d\delta}{dt} = \frac{1}{N} \sum_{i=1}^{N} \omega_i \tag{3.41}$$

These variables are well-known in power system stability analysis as the Center of Angle (COA) or Center of Inertia (COI) [55]. These variables demonstrate the collective dynamics of the system and are useful in the study of stability of the power grids.

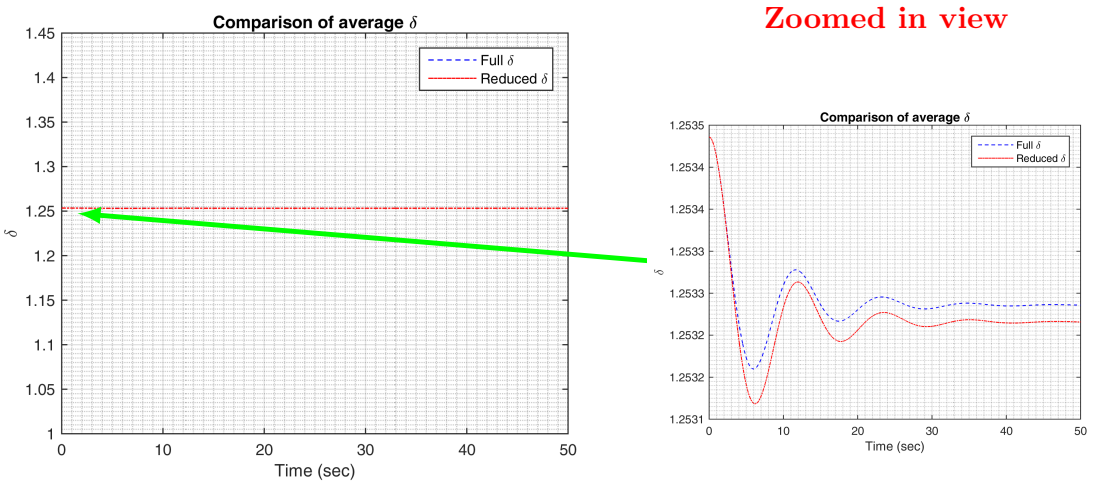

Figure 3.31: Comparison of the average δ for the 1st training trajectory

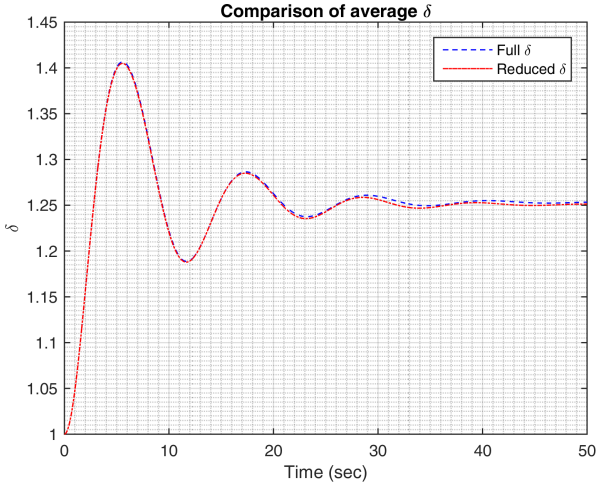

Figure 3.32: Comparison of the average δ for the 2nd training trajectory

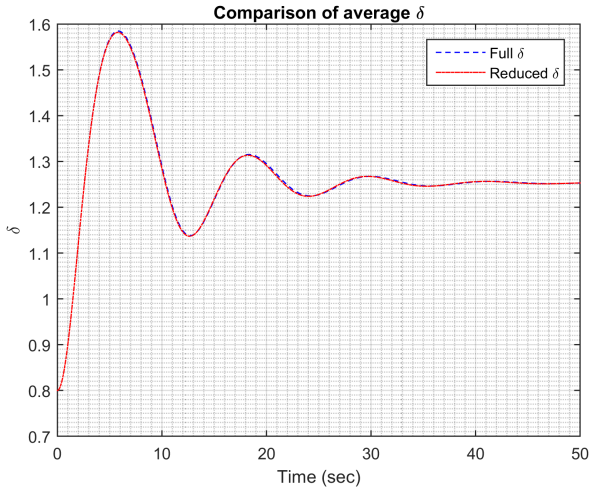

Figure 3.33: Comparison of the average δ for the 3rd training trajectory

Training Trajectory	**Modes 'q'**	**Lin Pts 's'**	**TPWL Time (sec)**	**Error in δ**	
				Abs	**Rel**
1	312	26	90 s	0.0011	8.97×10^{-4}
	312	47	123 s	8.55×10^{-4}	6.85×10^{-4}
	203	47	61 s	8.56×10^{-4}	6.85×10^{-4}
2	312	16	26 s	0.0044	0.0035
	199	16	13 s	0.0046	0.0036
	199	49	17 s	8.71×10^{-4}	6.75×10^{-4}
3	130	17	5 s	0.0014	0.0011
	130	8	3 s	0.0061	0.0046
	62	17	2 s	0.0014	0.0010

Table 3.7: Specifics of Reduced Order Models and the Error w.r.t. Training Trajectories

Test Cases	**Generator Disturbed** j	$\boldsymbol{\delta_j}$	$\boldsymbol{\delta_i}$ $\forall i \neq j$
Test Case 1	2	1.12	1
Test Case 2	2	1.15	1.15
Test Case 3	2	1.37	1.25
Test Case 4	100	1.45	1.25

Table 3.8: Initial conditions for test cases

The modes and the linearization points from the training trajectories were saved and then used with cases which are different from the training cases. The results we obtained are encouraging for this kind of model order reduction for the nonlinear functions. The variations in the values of phase angles δ_i of the disturbed node used for the test cases are listed in Table 3.8.

3.6.2 First test case: Single Node perturbation in non-equilibrium conditions

This is the case which is closely related to the second training trajectory. We have all the nodes starting from a non-equilibrium point $\delta_i = 1\ \forall i \neq 2$ and in addition one node was perturbed by about 0.12 radians, i.e., $\delta_2 = 1.12$. The initial conditions used for this test case are presented in Table 3.8.

The results are very promising and the TPWL simulation is considerably faster than the full simulation in a similar case which takes about 240 seconds while the TPWL simulation took about 18 with good accuracy. The errors are measured according to the difference in the individual phase of each generator between the high fidelity model and reduced model and the absolute and relative errors are listed in the Table 3.9. The comparison of the average δ between the original and reduced order models are presented in Figure 3.34.

3.6.3 Second test case: Synchronous non-equilibrium

This is a case similar to the third training trajectory where we had all the nodes starting from a synchronous non-equilibrium position, in this case we gave the initial conditions of 1.15 rather than 0.8 in the training case $\delta_i = 1.15\ \forall i$. The initial conditions used for this test case are presented in Table 3.8.

The results are excellent and the TPWL simulation is considerably faster as the full simulation in this case takes about 60 seconds while the TPWL simulation takes about 4 seconds with very high accuracy. The errors are listed in the Table 3.9 and the comparison of the average δ between the original and reduced order models are presented in Figure 3.35. A slight phase shift is observed between the average δ of high fidelity and reduced model, this phase shift can be removed with the addition of more linearization points.

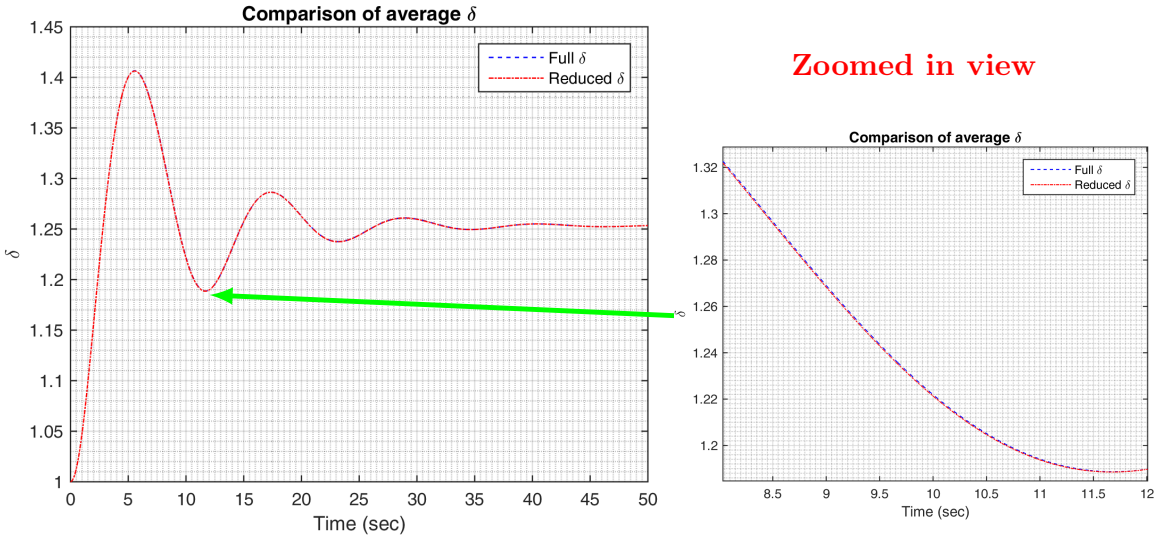

Figure 3.34: Comparison of the average δ for the 1st test case

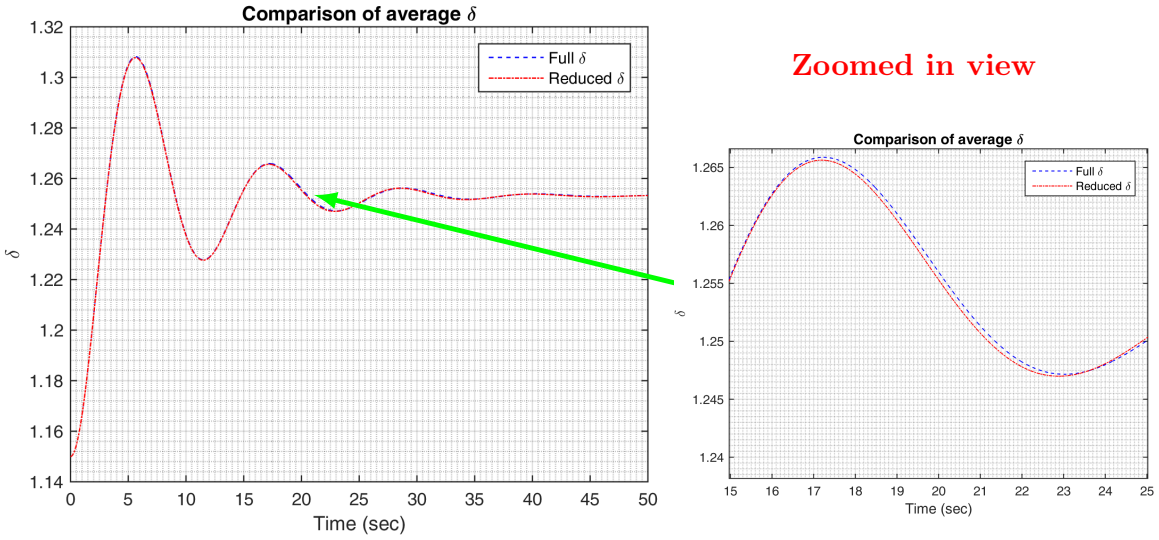

Figure 3.35: Comparison of the average δ for the 2nd test case

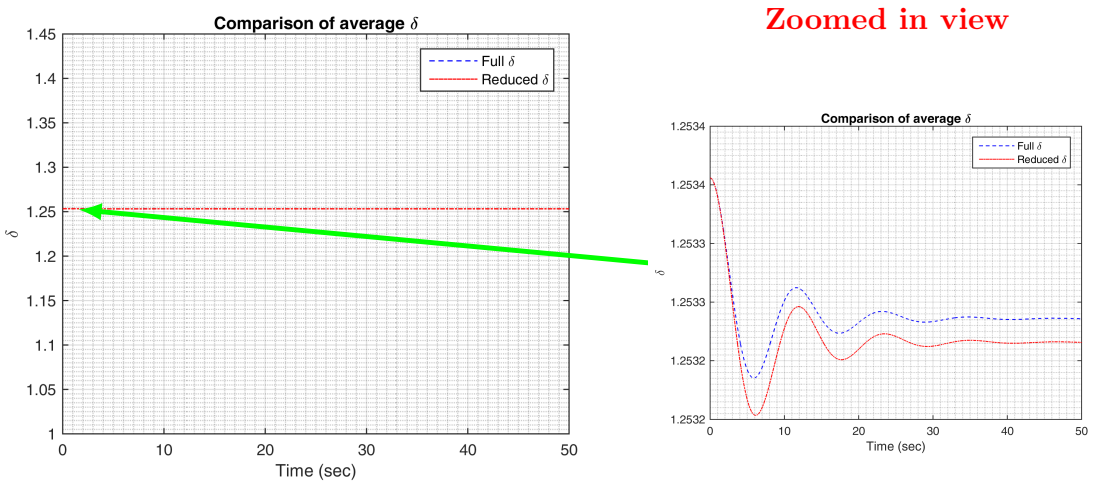

Figure 3.36: Comparison of the average δ for the 3rd test case

3.6.4 Single node perturbation with low intensity

Since the perturbations can be random, a common case which can occur is that the disturbance of different magnitudes in the same node. In this case we disturb the node at position 2 same as in the training trajectory by 0.12 radians rather than the 0.2 radians in the training case. The results are excellent and the TPWL simulation is considerably faster as the full simulation in this case takes about 215 seconds while the TPWL simulation took about 66 seconds. The errors listed in the Table 3.9 designated as test case 3 and the comparison between the average δ between the original and reduced order models are presented in Figure 3.36.

3.6.5 Single node perturbations in Equilibrium conditions

One of the most common case which we can encounter is that there is a random perturbation in one of the nodes while the system was in equilibrium position, i.e., all the generators were initially synchronous. It is similar to the case 1 from the training trajectories except that the position of the disturbed node is changed, in this case we disturb the node at position 100 rather than the node 2 in the training case. The results are close and the TPWL simulation is considerably faster as the full simulation in this case takes about 270 seconds while the TPWL simulation took about 64 seconds. The errors listed in the Table 3.9 designated as test case 4 and the comparison between the average δ between the original and reduced order models are presented in Figure 3.37.

3.6.6 Additional tests in Non-Equilibrium conditions

A few other variations were also tested for similar cases as the third training trajectory. For example, changing the node position of the disturbed generator and changing both the node position and the disturbance value. The results for this case

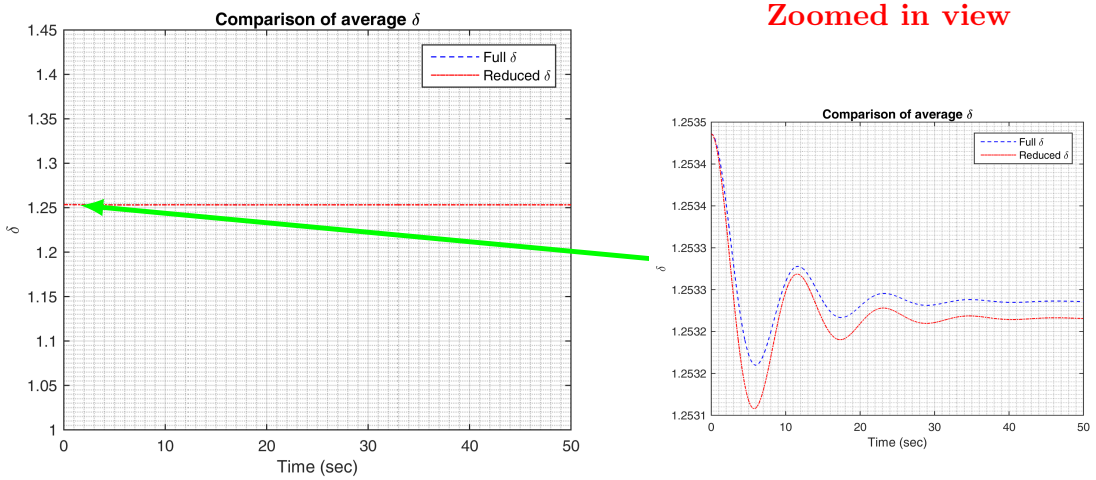

Figure 3.37: Comparison of the average δ for the 4th test case

Test Case	Modes 'q'	Lin Pts 's'	Time (sec)		Error in δ	
			Full Model	TPWL	Abs	Rel
1	199	49	240	18	8.75×10^{-4}	6.75×10^{-4}
2	62	17	60	4	6.62×10^{-4}	5.27×10^{-4}
3	203	47	215	66	7.31×10^{-4}	5.84×10^{-4}
4	203	47	270	64	0.1177	0.0810

Table 3.9: Error in Test cases of TPWL Simulations

Pert Node	Pert Value	Modes 'q'	Lin Pts 's'	TPWL Time (sec)	Error in δ	
					Abs	Rel
500	0.07	199	16	20 s	0.0699	0.0653
800	0.07	199	16	28 s	0.0504	0.0471
800	0.1	199	16	28 s	0.0504	0.0471

Table 3.10: Maximum error in different tests of TPWL

is listed in the following Table 3.10.

3.6.7 Convergence Analysis

It is important to analyze the source of error in the current study. As the results from the previous section show that the error is small but not small enough in comparison with the machine precision level. In order to understand how the error diminishes and its dependency on various factors, we studied different factors namely, the number of modes, number of linearization points and the time step size. It is evident from the results presented in previous sections that the number of modes used has little impact on the error but considerable impact on computation time. The behavior of the maximum relative error in the reduced linearized variable δ with respect to the time step and the number of linearization points is shown in the Figure 3.38a and Figure 3.38b, respectively. The non-monotonic behavior of the relative error as a function of time step in Figure 3.38a is due to the fact that for a larger time step compared to the one adopted for the training trajectory ($\Delta T = 0.005$) the reduced order model might skip some linearization points. Hence, it is inferred that the time step used for the reduced model simulation should be at least equal to the time step used in the training simulation. For smaller time steps the error is bounded by the truncation error of the reduced basis.

It can be conclusively said that the major impact on the accuracy of the reduced order linearized model depends on having more linearized point. This is quite intuitive, since adding more points around which the linearization of the non-linear function is performed it will be able to capture the non-linear behavior more effectively and hence reducing the error.

3.6.8 Confidence Interval

In order to give an idea of how the reduced model generated using TPWL compares with the high fidelity model, we carried out a simple analysis similar to sensitivity analysis. For this analysis, all the parameters were kept constant bar one. This is repeated for all the parameters. This analysis is performed using reduced basis generated using one training trajectory. The details of the training trajectory are similar to as listed in Table 3.2 and the initial values of the phase angles are listed

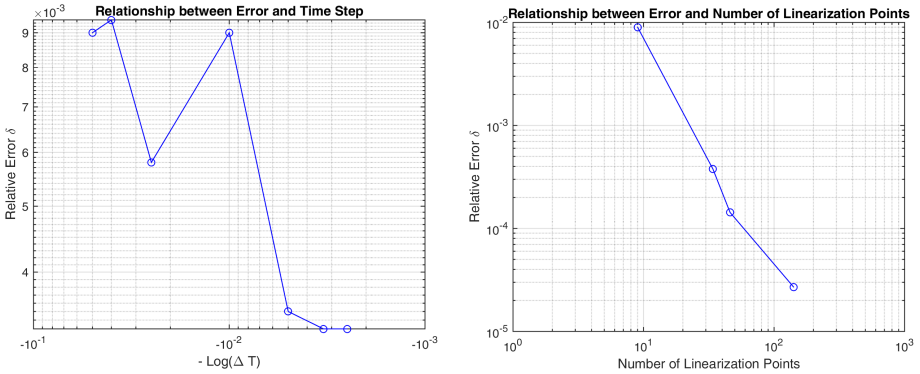

(a) Relationship between Error and Time Step

(b) Relationship between Error and Linearization Points

Figure 3.38: Maximum Relative Error in δ

Trajectory for Confidence Interval	$\boldsymbol{\delta_2}$	$\boldsymbol{\delta_i}$ $\forall i \neq 2$
Trajectory 1	1.5	1

Table 3.11: Initial conditions used in the build up for confidence interval

in Table 3.11. The number of linearization points (s) in the reduced basis for this case is 205 and the modes (q) selected are 199 out of 1000.

In Table 3.12 we presented the upper limit and the lower limit wherever applicable that we can use with confidence having a maximum relative error in $\{\delta\}$ of 5% or less. Due to the nature of the problem, the lower limit in the case of p^m and upper limit of d are open-ended as the error is always bounded on these limits. The number of generators N and the susceptances b are not included in this exercise because they depend upon the network topology and changes in these will have to be incorporated through a new reduced model. The mass of the generator is also not included since the equation is always normalized with the mass of the generator. The variation in the phase angle δ_2 depends upon the initial condition, the performance of the reduced model simulation improves with the inclusion of more than one training trajectory and hence, the range for δ_2 increases from what is given in Table 3.11.

As we have described earlier that in this method several training trajectories can be included in the offline phase to generate the reduced basis. This implies that for

Parameter	Upper Limit	Lower Limit
p^m	0.97 [p.u.]	-
d_i	-	0.15 [p.u.]
δ_2	2.25	1
b_{int}	105 [p.u.]	95 [p.u.]

Table 3.12: Confidence Interval for parameters with training trajectory of Table 3.11

values over the limits in the Table 3.12, we can add another training trajectory so that the error remains acceptable.

3.7 Conclusions

In this chapter, we presented the a posteriori model order reduction methods and adopted it for the swing dynamics problem. Based on the simulations presented for the linearized high fidelity model, it is concluded that the process of linearization of the swing dynamics model makes the system unstable. This was also the case in LATIN method presented in Chapter 2, and also when we applied the linearization procedure on the high fidelity model for the a posteriori model reduction using POD. Hence, it was evident that it was more related to system itself being unstable which was confirmed through the linear stability study we performed and presented in Sec. 3.2.9.

Therefore, we propose to use TPWL to deal with the non-linearity in a manner that not only solves the problem of instability but also keeps the model order reduction computationally efficient.

TPWL proves to be a robust method for model order reduction of models containing non-linear functions. It has been proved as a fast, reliable and accurate MOR technique as observed from the results presented by the test cases in Section 3.6. The method as described is separated into offline and online phases, where in the offline phase the selection of linearization points is carried out. That is the only time consuming part of the method and as it is performed only once during offline phase the time penalty on the overall procedure is not severe.

For the confidence interval, some other values of disturbances in $\{\delta\}$, and different values of p^m, d_i, b_{int} were trialed and the results as shown in section 3.6.8 proves the robustness of the method considering the large variations possible for simulation with reduced model. Note that, the confidence interval simulations were performed with only one training trajectory and if more trajectories are included in the reduced basis the interval where the method can be applied increases and the results improves.

The method is well adapted to the problem discussed in this study and more application for example, for the differential-algebraic equations (DAEs) of the network grids containing both generators (PV nodes) and the loads (PQ nodes), can further consolidate the current method as a well established model reduction method. A journal article [96] was published based on the results presented in this chapter.

Chapter 4

Model Order Reduction of Transmission Line Models in Power Systems

The major part of power systems are the complex transmission networks. A similar argument for the model reduction of transmission systems is valid as for the power grids. In this chapter, we present model reduction of transmission line models using the a priori method of PGD. A frequency-domain distributed parameters model for transmission lines is used and a full parametric problem is developed using PGD.

Contents

4.1 Introduction

Reduced order models for transmission lines have been studied widely for decades. There are a number of methods proposed for reduced order modeling of transmission line models, these methods are often based on modeling limited part of a transmission system or a simplification of the system [97]. The details of these methods can be found in a number of studies [98, 99, 100]. These studies consider model order reduction through application of a number of methods such as the balanced truncation, modal truncation or Hankel singular values. But most of them have limitations in the capturing of the whole range of relevant frequencies.

Morched and Brandwajn [97] have presented a method to generate an equivalent network from the frequency response. The authors have used lumped parameter models and developed a network equivalent which is simple and is able to approximate the network's behavior over a wide frequency range. Models are developed to reduce the complexity of the transmission system and save computation time in a number of analysis required for the power system studies [100, 101]. Lefebvre [100] have developed a reduced order model of the state space representation of transmission lines for the eigenanalysis. The authors have used the state-space equivalencing technique based on the balanced truncation. Clerici and Marzio [101] have focused their research on the evaluation of the transient behavior of switching overvoltages. They have presented results for transmission lines with intermediate or long length as the length of the transmission line has a significant effect on the transients because of the frequency of the AC currents [102]. There are several model order reduction methods applied and an overview can be found in the study by Ionutiu et al [103]. Soysal and Semlyen [104] have presented the linear least squares approach to model order reduction of transmission lines. On the other hand, Remis [105] has used the Lanczos-type reduction method for multi-conductor transmission lines. Belhocine and Marinescu [98] have developed a mixed balanced-modal truncation method for the model order reduction of transmission lines.

In the current study, the distributed parameters model is used to model the transmission lines, there are other models available for the transmission lines such as the π-equivalent model [102]. Distributed parameters models are not exclusive to the power system transmission lines but also used in mechanical engineering like heat equations and transport equations [106, 107]. Jang et al [106] have used the truncated balanced realization and singular perturbational model for a MIMO system. Opmeer [107] presented model reduction of the distributed parameters model for three different problems. Opmeer has used the Hankel singular values in order to reduce distributed parameters model. But, as noted in the study by Opmeer [107] the Hankel singular values decay asymptotically and therefore present a difficulty in balanced truncation method because then all the modes become important to achieve accurate results [98] a problem that Belhocine and Marinescu discuss also present in the modal truncation method.

In this chapter, we propose a PGD based solution of the distributed parameters (DP) model considering space-frequency as the separated representation coordinates. The chapter is divided into four major sections, first section presents the DP model

and the analytical solution in frequency-domain. The second section presents the PGD formulation, while third section extends PGD for parametric problem. In the last section, we present results of PGD based reduced order model developed.

4.2 DP Model

The electrical transmission lines provide the path for the voltage and current waves to propagate, the dynamics of the propagation is described by a distributed parameters (DP) model. This model depends upon the considerations taking into account like the losses and the frequency dependence of the parameters.

The distributed parameters model for a lossy transmission line with constant parameters can be written in the time domain as:

$$\begin{aligned} \frac{\partial v(x,t)}{\partial x} &= -L\frac{\partial i(x,t)}{\partial t} - Ri(x,t), \\ \frac{\partial i(x,t)}{\partial x} &= -C\frac{\partial v(x,t)}{\partial t} - Gv(x,t) \end{aligned} \tag{4.1}$$

For $0 \leq x \leq l$, where $v(x,t)$ and $i(x,t)$ are the voltage and current in the line respectively, and the resistance, the inductance, the capacitance and the conductance are represented by R, L, C, G respectively and these constants are assumed positive and independent of frequency. The parameters R, L, C, G are given in per unit length and in distributed parameters model are used without multiplication with the length of the line. However, these parameters must be converted into respective admittance and impedance values and multiplied by the length of the line in case one is using any lumped circuit model for transmission lines e.g. π-equivalent model. The effect of transverse conductance of the line is neglected in this model, i.e., $G = 0$. The interconnection between the transmission line, the load and the generator is performed using the Kirchhoff's laws and the boundary values are given by,

$$\begin{aligned} v(x,t)|_{x=0} &= V_0(t) - Z_0 i(x,t)|_{x=0} \\ v(x,t)|_{x=l} &= Z i(x,t)|_{x=l} \end{aligned} \tag{4.2}$$

The terms V_0 is the voltage source assumed to represent a generator behind an impedance represented by Z_0. The eq. (4.1) and eq. (4.2) represents the full model of the power system, written in state space representation the system is

$$\begin{aligned} \begin{bmatrix} \dot{z_1} \\ \dot{z_2} \end{bmatrix} &= \begin{bmatrix} 0 & -\frac{1}{C}\frac{\partial}{\partial x} \\ -\frac{1}{L}\frac{\partial}{\partial x} & -\frac{R}{L} \end{bmatrix} \begin{bmatrix} z_1 \\ z_2 \end{bmatrix} \\ Bz(t) = V_0(t), Cz(t) &= y(t), z(0,x) = z_0(x) \end{aligned} \tag{4.3}$$

In eq. (4.3) $z_1(t) = v(x,t)$ and $z_2(t) = i(x,t)$ and with $B[z_1(t) \quad z_2(t)]^T = v(0,t) - Z_0 i(0,t) = V_0(t)$ the input and $C[z_1(t) \quad z_2(t)]^T = v(l,t)$ the output. Matrices B and C are given as $B = [1 \quad -Z_0]$ and $C = [0 \quad Z]$.

Initial conditions are not fixed as described in the paper by Belhocine and Marinescu [99]. In the current study, we employ homogeneous initial conditions, i.e.

$$\begin{aligned} v(x,t)|_{t=0} &= 0 \\ i(x,t)|_{t=0} &= 0 \end{aligned} \tag{4.4}$$

We transform the Distributed Parameters model for transmission lines from time-domain to frequency-domain to convert the partial differential equations of (4.1) to ordinary differential equations in only one variable, that is only in space dimension. The benefit is in the availability of an easy analytical solution in addition to the well-defined PGD formulation for such equations. Moreover, as noted in the study of Morched and Brandwajn [97], that typically the electromagnetic transient studies are focused on the equivalent models around power frequency. Morched and Brandwajn argue that this decreases the accuracy of these studies for frequencies different from the power frequency. Therefore, by transforming the model into the frequency-domain and using PGD as a harmonic analysis tool which includes all the frequencies of interest, we can have a very accurate model for studying the electromagnetic transients in transmission systems.

Consider the Fourier transformation with respect to the time domain for the unknowns $v(x,t)$ and $i(x,t)$ in eq. (4.1),

$$\begin{aligned} \mathscr{F}_t\left\{v(x,t)\right\} &= \hat{V}(x,\omega) = \int_{-\infty}^{\infty} v(x,t)e^{-\iota\omega t} \\ \mathscr{F}_t\left\{i(x,t)\right\} &= \hat{I}(x,\omega) = \int_{-\infty}^{\infty} i(x,t)e^{-\iota\omega t} \end{aligned} \tag{4.5}$$

Applying Fourier transformation on the first derivatives with respect to time present in eq. (4.1), without going into details we present.

$$\begin{aligned} \mathscr{F}_t\left\{\frac{\partial v(x,t)}{\partial t}\right\} &= (\iota\omega)\hat{V}(x,\omega) \\ \mathscr{F}_t\left\{\frac{\partial i(x,t)}{\partial t}\right\} &= (\iota\omega)\hat{I}(x,\omega) \end{aligned} \tag{4.6}$$

The above definitions of eq. (4.5) and eq. (4.6) then transform the PDE in eq. (4.1) to an equivalent equation in frequency-domain,

$$\begin{aligned} \frac{\partial \hat{V}(x,\omega)}{\partial x} &= -\hat{I}(x,\omega).(R+\iota L\omega), \\ \frac{\partial \hat{I}(x,\omega)}{\partial x} &= -\hat{V}(x,\omega).(\iota C\omega) \end{aligned} \tag{4.7}$$

with boundary conditions as

$$\begin{aligned}\hat{V}(x,\omega)|_{x=0} &= \hat{V}_0(\omega) - Z_0\hat{I}(x,\omega)|_{x=0}\\ \hat{V}(x,\omega)|_{x=l} &= Z\hat{I}(x,\omega)|_{x=l}\end{aligned} \tag{4.8}$$

Eliminating $\hat{I}(x,\omega)$ from eq. (4.7)

$$\frac{d^2\hat{V}(x,\omega)}{dx^2} + (LC\omega^2 - \iota RC\omega)\hat{V}(x,\omega) = 0 \tag{4.9}$$

The boundary conditions for the differential equations in frequency domain are different from the boundary conditions given in eq. (4.2) for the time domain. In the eqs. (4.1) and the corresponding boundary conditions eq. (4.2) are given for a transmission line connected with a power system i.e. generator at one end and a load at other end. In the current study, we are more inclined in solving the system for a generic case where at the end of the transmission lines can be a generator and a load or loads at both ends. Therefore, following set of boundary condition is employed in the study.

$$\begin{aligned}\left.\frac{\partial\hat{V}(x,\omega)}{\partial x}\right|_{x=0} &= -\hat{I}|_{x=0}.(\iota L\omega + R)\\ \left.\frac{\partial\hat{V}(x,\omega)}{\partial x}\right|_{x=l} &= 0\end{aligned} \tag{4.10}$$

where

$\hat{I}|_{x=0} = 1$

A mirror image of the boundary condition is given as:

$$\begin{aligned}\left.\frac{\partial\hat{V}(x,\omega)}{\partial x}\right|_{x=0} &= 0\\ \left.\frac{\partial\hat{V}(x,\omega)}{\partial x}\right|_{x=l} &= -\hat{I}|_{x=l}.(\iota L\omega + R)\end{aligned} \tag{4.11}$$

where

$\hat{I}|_{x=l} = 1$

Of course, the two versions of boundary conditions defined in eq. (4.10) and eq. (4.11) are mirror images of each other. We expect to solve the aforementioned problem only once with one set of boundary conditions while the other will be a mirror image about $x = L/2$.

A similar second order differential equation in terms of $\hat{I}$ can be derived with the following boundary conditions.

$$\frac{\partial^2\hat{I}(x,\omega)}{\partial x^2} + (LC\omega^2 - \iota RC\omega)\hat{I}(x,\omega) = 0 \tag{4.12}$$

$$\left.\frac{\partial \hat{I}(x,\omega)}{\partial x}\right|_{x=0} = -\hat{V}|_{x=0}.(\iota C\omega)$$
$$\left.\frac{\partial \hat{I}(x,\omega)}{\partial x}\right|_{x=l} = 0 \tag{4.13}$$

where

$\hat{V}|_{x=0} = 1$

or

$$\left.\frac{\partial \hat{I}(x,\omega)}{\partial x}\right|_{x=0} = 0$$
$$\left.\frac{\partial \hat{I}(x,\omega)}{\partial x}\right|_{x=l} = -\hat{V}|_{x=l}.(\iota C\omega) \tag{4.14}$$

where

$\hat{V}|_{x=l} = 1$

4.2.1 Analytical Solution

There exists an analytical solution for the second order differential equation of the form given in eq. (4.9).

$$\frac{\partial^2 \hat{V}(x,\omega)}{\partial x^2} + (LC\omega^2 - \iota RC\omega)\hat{V}(x,\omega) = 0 \tag{4.15}$$

With the boundary conditions as:

$$\left.\frac{\partial \hat{V}(x,\omega)}{\partial x}\right|_{x=0} = -\hat{I}_1|_{x=0}.(\iota L\omega + R)$$
$$\left.\frac{\partial \hat{V}(x,\omega)}{\partial x}\right|_{x=l} = -\hat{I}_2|_{x=l}.(\iota L\omega + R) \tag{4.16}$$

Using commercial software MAPLE, we get the analytical solution of the ordinary differential equation with the boundary condition defined as in eq. (4.16). The analytical solution although is not separable.

The solution is,

$$\hat{V}(x,\omega) = c_1 e^{\sqrt{LC\omega^2 - \iota RC\omega}\ x} + c_2 e^{-\sqrt{LC\omega^2 - \iota RC\omega}\ x}$$

where

$$c_1 = \frac{(\iota L\omega + R)}{\sqrt{-LC\omega^2 + \iota RC\omega}} \left[\frac{\hat{I}_1 e^{-\sqrt{-LC\omega^2+\iota RC\omega}\ l} - \hat{I}_2}{e^{\sqrt{-LC\omega^2+\iota RC\omega}\ l} - e^{-\sqrt{-LC\omega^2+\iota RC\omega}\ l}}\right]$$
$$c_2 = \frac{(\iota L\omega + R)}{\sqrt{-LC\omega^2 + \iota RC\omega}} \left[\frac{\hat{I}_1 e^{\sqrt{-LC\omega^2+\iota RC\omega}\ l} - \hat{I}_2}{e^{\sqrt{-LC\omega^2+\iota RC\omega}\ l} - e^{-\sqrt{-LC\omega^2+\iota RC\omega}\ l}}\right] \tag{4.17}$$

If either of the boundary condition is replaced with a homogeneous Neumann boundary condition, i.e., $\hat{I}_1 = 0$ or $\hat{I}_2 = 0$, then we have boundary conditions as defined in eq. (4.10) and eq. (4.11) respectively. In such cases, the values of c_1 and c_2 becomes,

For $\hat{I}_2 = 0$,

$$\begin{aligned} c_1 &= \frac{(\iota L\omega + R)}{\sqrt{-LC\omega^2 + \iota RC\omega}} \left[\frac{\hat{I}_1 e^{-\sqrt{-LC\omega^2+\iota RC\omega}\ l}}{e^{\sqrt{-LC\omega^2+\iota RC\omega}\ l} - e^{-\sqrt{-LC\omega^2+\iota RC\omega}\ l}} \right] \\ c_2 &= \frac{(\iota L\omega + R)}{\sqrt{-LC\omega^2 + \iota RC\omega}} \left[\frac{\hat{I}_1 e^{\sqrt{-LC\omega^2+\iota RC\omega}\ l}}{e^{\sqrt{-LC\omega^2+\iota RC\omega}\ l} - e^{-\sqrt{-LC\omega^2+\iota RC\omega}\ l}} \right] \end{aligned} \tag{4.18}$$

For $\hat{I}_1 = 0$,

$$\begin{aligned} c_1 &= \frac{(\iota L\omega + R)}{\sqrt{-LC\omega^2 + \iota RC\omega}} \left[\frac{-\hat{I}_2}{e^{\sqrt{-LC\omega^2+\iota RC\omega}\ l} - e^{-\sqrt{-LC\omega^2+\iota RC\omega}\ l}} \right] \\ c_2 &= \frac{(\iota L\omega + R)}{\sqrt{-LC\omega^2 + \iota RC\omega}} \left[\frac{-\hat{I}_2}{e^{\sqrt{-LC\omega^2+\iota RC\omega}\ l} - e^{-\sqrt{-LC\omega^2+\iota RC\omega}\ l}} \right] \end{aligned} \tag{4.19}$$

The analytical solution for the eq. (4.12) given here,

$$\frac{\partial^2 \hat{I}(x,\omega)}{\partial x^2} + (LC\omega^2 - \iota RC\omega)\hat{I}(x,\omega) = 0 \tag{4.20}$$

With the boundary conditions as:

$$\begin{aligned} \left.\frac{\partial \hat{I}(x,\omega)}{\partial x}\right|_{x=0} &= -\hat{V}_1|_{x=0}.(\iota C\omega) \\ \left.\frac{\partial \hat{I}(x,\omega)}{\partial x}\right|_{x=l} &= -\hat{V}_2|_{x=0}.(\iota C\omega) \end{aligned} \tag{4.21}$$

The analytical solution is given by,

$$\hat{I}(x,\omega) = c_1 e^{\sqrt{-LC\omega^2+\iota RC\omega}\ x} + c_2 e^{-\sqrt{-LC\omega^2+\iota RC\omega}\ x}$$

where

$$\begin{aligned} c_1 &= \frac{\iota C\omega}{\sqrt{-LC\omega^2 + \iota RC\omega}} \left[\frac{\hat{V}_1 e^{-\sqrt{-LC\omega^2+\iota RC\omega}\ l} - \hat{V}_2}{e^{\sqrt{-LC\omega^2+\iota RC\omega}\ l} - e^{-\sqrt{-LC\omega^2+\iota RC\omega}\ l}} \right] \\ c_2 &= \frac{\iota C\omega}{\sqrt{-LC\omega^2 + \iota RC\omega}} \left[\frac{\hat{V}_1 e^{\sqrt{-LC\omega^2+\iota RC\omega}\ l} - \hat{V}_2}{e^{\sqrt{-LC\omega^2+\iota RC\omega}\ l} - e^{-\sqrt{-LC\omega^2+\iota RC\omega}\ l}} \right] \end{aligned} \tag{4.22}$$

If either of the boundary condition is replaced by a homogeneous boundary conditions,i.e., $\hat{V}_1 = 0$ or $\hat{V}_2 = 0$, then we have boundary conditions as defined

in eq. (4.13) and eq. (4.14) respectively. In such cases, the values of c_1 and c_2 becomes,

For $\hat{V}_2 = 0$,

$$\begin{aligned} c_1 &= \frac{\iota C\omega}{\sqrt{-LC\omega^2 + \iota RC\omega}} \left[\frac{\hat{V}_1 e^{-\sqrt{-LC\omega^2+\iota RC\omega}\ l}}{e^{\sqrt{-LC\omega^2+\iota RC\omega}\ l} - e^{-\sqrt{-LC\omega^2+\iota RC\omega}\ l}} \right] \\ c_2 &= \frac{\iota C\omega}{\sqrt{-LC\omega^2 + \iota RC\omega}} \left[\frac{\hat{V}_1 e^{\sqrt{-LC\omega^2+\iota RC\omega}\ l}}{e^{\sqrt{-LC\omega^2+\iota RC\omega}\ l} - e^{-\sqrt{-LC\omega^2+\iota RC\omega}\ l}} \right] \end{aligned} \tag{4.23}$$

For $\hat{V}_1 = 0$,

$$\begin{aligned} c_1 &= \frac{\iota C\omega}{\sqrt{-LC\omega^2 + \iota RC\omega}} \left[\frac{-\hat{V}_2}{e^{\sqrt{-LC\omega^2+\iota RC\omega}\ l} - e^{-\sqrt{-LC\omega^2+\iota RC\omega}\ l}} \right] \\ c_2 &= \frac{\iota C\omega}{\sqrt{-LC\omega^2 + \iota RC\omega}} \left[\frac{-\hat{V}_2}{e^{\sqrt{-LC\omega^2+\iota RC\omega}\ l} - e^{-\sqrt{-LC\omega^2+\iota RC\omega}\ l}} \right] \end{aligned} \tag{4.24}$$

4.3 A priori Reduced Order Modeling in Frequency Domain

A priori model order reduction is considerably faster than the a posteriori model reduction because it eliminates the need to perform the simulation of high fidelity model. Therefore, a priori model reduction remains the method of choice. As presented in the Sec. 2.7.3 a priori methods weren't able to converge to the right solution in the time-domain. There remains a possibility of achieving success with a priori methods in the frequency-domain modeling. For this purpose, we introduce the method of Proper Generalized Decomposition (PGD) as a priori method for model reduction in frequency-domain. The method of PGD is well-suited for both time-domain and frequency-domain problems, here we have used it for the frequency-domain problems.

4.3.1 Proper Generalized Decomposition

Proper Generalized Decomposition (PGD) belongs to a family of a priori model reduction methods. The method is based on the a priori separation of variable of the unknown field [63]. PGD can be considered as a model reduction technique in which the reduced basis are constructed progressively by enriching the reduced basis by adding a single mode per iteration of the method. The accuracy of the method is analyzed after each enrichment and if necessary, more enrichment modes can be added [108]. Suppose, our unknown field is a variable $u(x_1, x_2, \cdots, x_D)$ defined in a D-dimensional space $\mathbb{C}^D$. PGD works by separating the solution for u in each coordinate basis x_i, a tremendous advantage of PGD is that the coordinate x_i can

be a parameter as well like the boundary conditions or the material parameters. The solution in PGD framework is represented as:

$$u(x_1, \cdots, x_D) = \sum_{i=1}^{n} F_i^1(x_1) \times \cdots \times F_i^D(x_D) \tag{4.25}$$

The number of terms n are referred to as the enrichment modes are unknown a priori. The enrichment terms are added successively until a solution is achieved, converged to a preset tolerance. The separated representation achieved through PGD and the previously discussed POD is different that unlike POD, PGD does not need a solution of the original high-dimensional problem before the solution can be separated.

A quick solution steps in the PGD method as a priori differential solver is provided here, for more insight into the method of PGD, one can refer to a wealth of publications by Chinesta et al [63, 109, 110, 111, 112, 113]. The works that involve PGD in the frequency-domain problems are by Modesto et al [114]. For solving nonlinear problems with PGD, we can combine the method of LATIN described in Sec. 2.7.3 with PGD. In the study by Ladevèze et al. [115], PGD method has been used with the LATIN method. One of the advantages of the PGD method is that it is capable of handling parametric problems as discussed in the study by Raquel et al in [116, 117]. It should be noted that PGD can be used as an algebraic solver. The steps in PGD method are:

1. Given a PDE with appropriate boundary conditions, formulate a weak formulation.

2. Represent the variable of interest in separated representation. The separated representation can include parameters in addition to the coordinates.

3. Insert the separated representation in the weak formulation and obtain weak formulations for each coordinate separately.

4. Initialize the first mode such that it satisfies the boundary value in case of Dirichlet boundary conditions.

5. Make an initial guess for the enrichment mode and apply the Greedy algorithm.

6. Set a tolerance as a convergence criteria of enrichment modes.

7. Define a stopping criteria for the enrichment process.

8. Analyze the solution and if it does not satisfy the stopping criteria defined in Step 6, add another enrichment mode until convergence is achieved with respect to the stopping criteria.

4.3.1.1 Example Problem

We explain the method of PGD using an example of second order partial differential equation, namely the Poisson equation.

$$\Delta u(x,y) = f(x,y) \quad \forall\ x \in \Omega_x = (0,2),\ y \in \Omega_y = (0,1) \tag{4.26}$$

with a homogeneous Dirichlet boundary condition. For a given forcing function $f(x,y) = 1$, we have analytical solution for Poisson's equation. The analytical solution is given as:

$$u_{exact}(x,y) = \sum_{m,n\ odd} \frac{64}{\pi^4 mn(4n^2+m^2)} \sin\left(\frac{m\pi x}{2}\right) \sin(n\pi y) \tag{4.27}$$

The surface plot using the analytical solution is given in Figure 4.2a. In order to compare the PGD method with the analytical solution, we present the development of the PGD formulation.

The weak formulation for Poisson's equation with test function $u^*(x,y)$, is given as:

$$\int_{\Omega_x \times \Omega_y} u^*.(\Delta u - f)\ dx\ dy = 0 \tag{4.28}$$

Since, we need a solution in separated form, we define our variable of interest as,

$$u(x,y) = \sum_{i=1}^{n} X_i(x).Y_i(y) \tag{4.29}$$

similarly for the test function

$$u^*(x,y) = X^*(x)Y(y) + X(x)Y(y)^* \tag{4.30}$$

Now, for a n^{th} enrichment mode with previous modes already computed, we have

$$u(x,y) = \sum_{i=1}^{n-1} X_i(x)Y_i(y) + X_n(x)Y_n(y) \tag{4.31}$$

Consider, we are at an iteration p of the enrichment mode n, we have the solution converged so far as:

$$u^{n,p}(x,y) = u^{n-1} + X_n^p(x)Y_n^{p-1}(y) \tag{4.32}$$

The process of converging the n^{th} enrichment mode is performed using alternating direction strategy. The process starts with an initial guess, let's assume $Y_n^0(y)$ and calculate $X_n^1(x)$ and so on until convergence is achieved. At the end of the process, the values of $X_n^p(x)$ and $Y_n^p(y)$ are added to the database of previously computed modes as $X_n(x)$ and $Y_n(y)$. To calculate $X_n^p(x)$ from $Y_n^{p-1}(y)$, we use eq. (4.32). The test function can be written as:

$$u^*(x,y) = X_n^*(x)Y_n^{p-1}(y) \tag{4.33}$$

Replacing eq. (4.32) and eq. (4.33) into eq. (4.28), we have the weighted residual form.

$$\begin{aligned}
&\int_{\Omega_x\times\Omega_y} X_n^* Y_n^{p-1}\left(\frac{d^2X_n^p}{dx^2}\ Y_n^{p-1}+\frac{d^2Y_n^{p-1}}{dy^2}\ X_n^p\right)dx\ dy\\
&=-\int_{\Omega_x\times\Omega_y} X_n^* Y_n^{p-1}\sum_{i=1}^{n-1}\left(\frac{d^2X_i}{dx^2}\ Y_i+\frac{d^2Y_i}{dy^2}\ X_i\right)dx\ dy\\
&+\int_{\Omega_x\times\Omega_y} X_n^* Y_n^{p-1}\ f\ dx\ dy
\end{aligned} \tag{4.34}$$

Since, all the functions of y are known, we can define the following expressions.

$$\begin{cases}
\alpha^x = \int_{\Omega_y}\left(Y_n^{p-1}\right)^2 dy\\
\beta^x = \int_{\Omega_y} Y_n^{p-1}\frac{d^2Y_n^{p-1}}{dy^2}dy\\
\gamma_i^x = \int_{\Omega_y} Y_n^{p-1}Y_i dy\\
\delta_i^x = \int_{\Omega_y} Y_n^{p-1}\frac{d^2Y_i}{dy^2}dy\\
\xi^x = \int_{\Omega_y} Y_n^{p-1} f\ dy
\end{cases} \tag{4.35}$$

Inserting the definitions from eq. (4.35) in eq. (4.34).

$$\begin{aligned}
&\int_{\Omega_x} X_n^*\left(\alpha^x\frac{d^2X_n^p}{dx^2}+\beta^x X_n^p\right)dx =\\
&-\int_{\Omega_x} X_n^*\sum_{i=1}^{n-1}\left(\gamma_i^x\frac{d^2X_i}{dx^2}+\delta_i^x X_i\right)dx+\int_{\Omega_x} X_n^*\xi^x\ dx
\end{aligned} \tag{4.36}$$

Eq. (4.36) represents the weighted residual form in one dimension which can be solved by any numerical scheme like finite element method. The system of equations obtained from finite elements method can be represented in matrix form as:

$$\begin{aligned}
&\alpha^x[K_x]\{X_n^p\}+\beta^x[M_x]\{X_n^p\} =\\
&-\sum_{i=1}^{n-1}\left(\gamma_i^x[K_x]\{X_i\}+\delta_i^x[M_x]\{X_i\}\right)+\xi^x[M_x]\{1,\cdots,1\}^T
\end{aligned} \tag{4.37}$$

Once, X_n^p is known, we can calculate Y_n^p using the same procedure.

$$u^{n,p}(x,y) = u^{n-1} + X_n^p(x)Y_n^p(y) \tag{4.38}$$

The test function can be written as:

$$u^*(x,y) = X_n^p(x)Y_n^*(y) \tag{4.39}$$

Replacing eq. (4.38) and eq. (4.39) into eq. (4.28), we have the weighted residual form.

$$\begin{aligned}
&\int_{\Omega_x \times \Omega_y} X_n^p Y_n^* \left(\frac{d^2 X_n^p}{dx^2}\ Y_n^p + \frac{d^2 Y_n^p}{dy^2}\ X_n^p \right) dx\ dy \\
&= -\int_{\Omega_x \times \Omega_y} X_n^p Y_n^* \sum_{i=1}^{n-1} \left(\frac{d^2 X_i}{dx^2}\ Y_i + \frac{d^2 Y_i}{dy^2}\ X_i \right) dx\ dy \\
&+ \int_{\Omega_x \times \Omega_y} X_n^p Y_n^*\ f\ dx\ dy
\end{aligned} \tag{4.40}$$

Since, all the functions of x are known, we can define the following expressions.

$$\begin{cases}
\alpha^y = \int_{\Omega_x} \left(X_n^p\right)^2 dx \\
\beta^y = \int_{\Omega_x} X_n^p \frac{d^2 X_n^p}{dx^2} dx \\
\gamma_i^y = \int_{\Omega_x} X_n^p X_i dx \\
\delta_i^y = \int_{\Omega_x} X_n^p \frac{d^2 X_i}{dx^2} dx \\
\xi^y = \int_{\Omega_x} X_n^p f\ dx
\end{cases} \tag{4.41}$$

Inserting the definitions from eq. (4.35) in eq. (4.34).

$$\begin{aligned}
&\int_{\Omega_y} Y_n^* \left(\alpha^y \frac{d^2 Y_n^p}{dy^2} + \beta^y Y_n^p \right) dy = \\
&- \int_{\Omega_y} Y_n^* \sum_{i=1}^{n-1} \left(\gamma_i^y \frac{d^2 Y_i}{dy^2} + \delta_i^y Y_i \right) dy + \int_{\Omega_y} Y_n^* \xi^y\ dy
\end{aligned} \tag{4.42}$$

Using the finite element methods, the eq. (4.42) can be solved and can be expressed in matrix form as:

$$\begin{aligned}
&\alpha^y [K_y]\{Y_n^p\} + \beta^y [M_y]\{Y_n^p\} = \\
&- \sum_{i=1}^{n-1} \left(\gamma_i^y [K_y]\{Y_i\} + \delta_i^y [M_y]\{Y_i\} \right) + \xi^y [M_y]\{1, \cdots, 1\}^T
\end{aligned} \tag{4.43}$$

At this we define, a stopping criteria which can be used to judge the convergence of the alternating direction. A tolerance ϵ is predefined such that the iterations are stopped when the following equation holds true.

$$\frac{||X_n^p(x) Y_n^p(y) - X_n^{p-1}(x) Y_n^{p-1}(y)||}{||X_n^{p-1}(x) Y_n^{p-1}(y)||} < \epsilon \tag{4.44}$$

The enrichment modes are stopped when the residual $R(n)$ is acceptably low within a predefined tolerance.

$$R(n) = \sum_{i=1}^{n} \left(\frac{\partial^2 X_i}{\partial x^2} Y_i(y) + \frac{\partial^2 Y_i}{\partial y^2} X_i(x) \right) - f \tag{4.45}$$

Any other method can also be adopted. One stopping criteria for the enrichment process is the ratio between the last mode and the first mode. In this way, it can

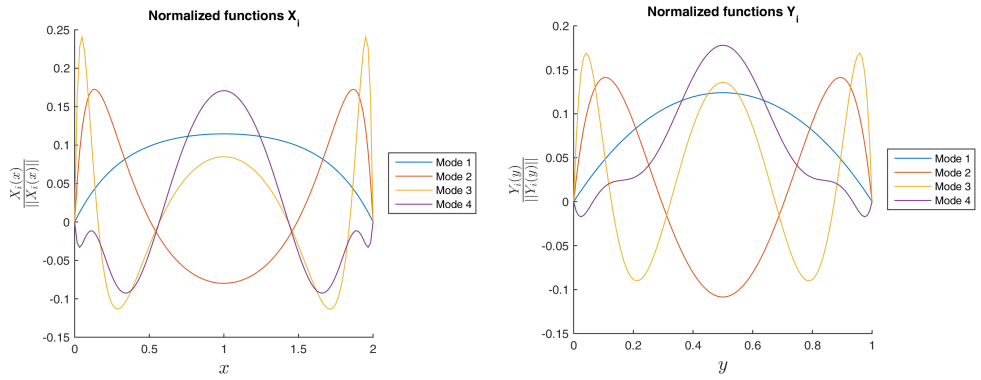

(a) X-axis (b) Y-axis

Figure 4.1: Modes in separated x-y dimensions

be observed that what improvements are added to the solution by the new modes. This is denoted by $\varepsilon(n)$ and defined as:

$$\varepsilon(n) = \frac{||X_n(x)Y_n(y)||}{||X_1(x)Y_1(y)||} \tag{4.46}$$

The modes computed for the Poisson's equation from the PGD formulation are presented in Figure 4.1. The results from the PGD based separated solutions Figure 4.2b and the analytical solution Figure 4.2a along with the error between the PGD solution and the analytical solution in Figure 4.2c.

4.3.2 PGD formulation for DP Model

We are seeking a separable solution to the eq. (4.15), representing the DP model in single variable of voltage, in the form of,

$$\hat{V}(x,\omega) = \sum_{i=1}^{n} X_i(x)O_i(\omega) \tag{4.47}$$

Eq. (4.15) along with the boundary conditions given in eq. (4.10) and eq. (4.11). In order to develop a PGD formulation, first we must have a weak formulation of the problem.

Multiply eq. (4.15) with a test function $\delta V^*(x)$ where, δV represents the test function and * represents the complex conjugate.

$$\int_{\Omega_x \times \Omega_\omega} \delta V^* \frac{\partial^2 \hat{V}}{\partial x^2}\, dxd\omega - \int_{\Omega_x \times \Omega_\omega} \delta V^* f(\omega)\hat{V}\, dxd\omega = 0 \tag{4.48}$$

where, $f(\omega) = (LC\omega^2 - \iota RC\omega)$.

Integrating by parts gives,

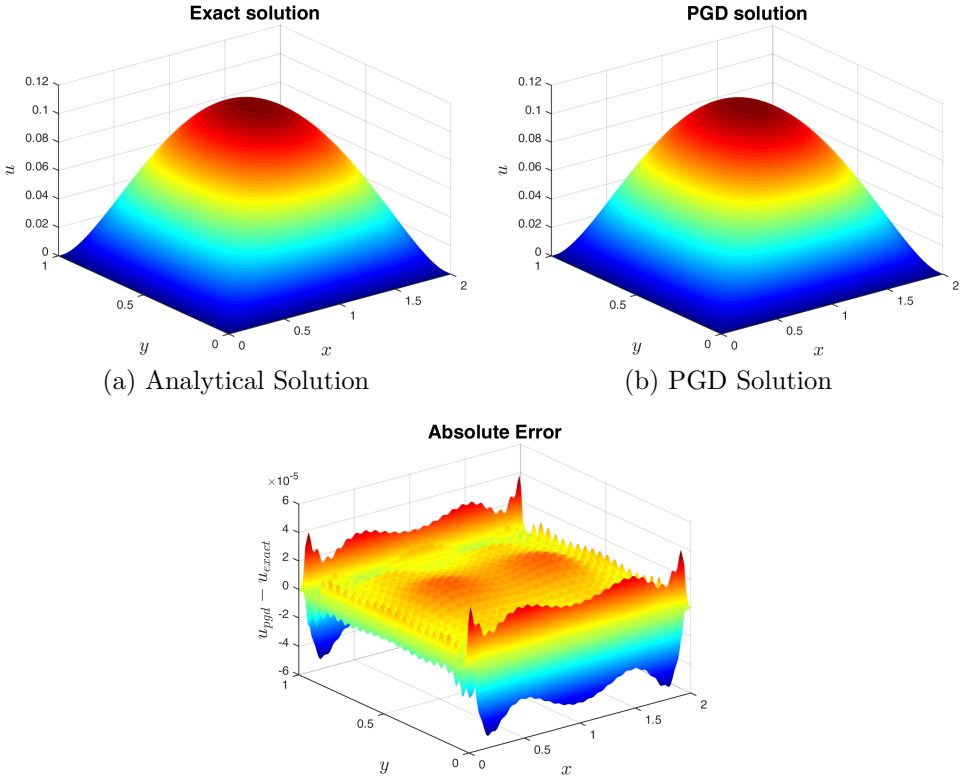

(a) Analytical Solution

(b) PGD Solution

(c) Error between PGD and Analytical solutions

Figure 4.2: Relative Error in the Solution of Variable Load using POD for Variable Load

$$\int_{\Omega_x\times\Omega_\omega} \delta V^* \frac{\partial^2 \hat{V}}{\partial x^2}\, dxd\omega = \int_{\Omega_\omega} \delta V^* \frac{\partial \hat{V}}{\partial x}\bigg|_{x=l} d\omega - \int_{\Omega_\omega} \delta V^* \frac{\partial \hat{V}}{\partial x}\bigg|_{x=0} d\omega - \int_{\Omega_x\times\Omega_\omega} \frac{\partial \delta V^*}{\partial x}\frac{\partial \hat{V}}{\partial x}\, dxd\omega \tag{4.49}$$

With the boundary conditions given in eq. (4.10) or eq. (4.11), one of the terms in the eq. (4.49) becomes zero. For example, with boundary condition of eq. (4.10), we have

$$\int_{\Omega_x\times\Omega_\omega} \delta V^* \frac{\partial^2 \hat{V}}{\partial x^2}\, dxd\omega = -\int_{\Omega_\omega} \delta V^* \frac{\partial \hat{V}}{\partial x}\bigg|_{x=0} d\omega - \int_{\Omega_x\times\Omega_\omega} \frac{\partial \delta V^*}{\partial x}\frac{\partial \hat{V}}{\partial x}\, dxd\omega \tag{4.50}$$

Therefore, the weak form of eq. (4.48) after inserting the boundary condition becomes

$$\int_{\Omega_x\times\Omega_\omega} \frac{\partial \delta V^*}{\partial x}\frac{\partial \hat{V}}{\partial x}\, dxd\omega + \int_{\Omega_x\times\Omega_\omega} f(\omega)\delta V^* \hat{V}\, dxd\omega = \int_{\Omega_\omega} \delta V^*(x=0,\omega).\hat{I}_1.(\iota L\omega + R)\, d\omega \tag{4.51}$$

The generic weak form is:

$$\begin{aligned} &A(\hat{V},\delta V) = L(\hat{V}) \\ &\text{where} \\ &A(\hat{V},\delta V) = A_1(\hat{V},\delta V) + A_2(\hat{V},\delta V) \end{aligned} \tag{4.52}$$

And the bilinear form is defined as:

$$\begin{aligned} A_1(\hat{V},\delta V) &= \int_{\Omega_x\times\Omega_\omega} \frac{\partial \delta V^*}{\partial x}\frac{\partial \hat{V}}{\partial x}\, dxd\omega \\ A_2(\hat{V},\delta V) &= \int_{\Omega_x\times\Omega_\omega} f(\omega)\delta V^* \hat{V}\, dxd\omega \\ L(\delta V) &= \int_{\Omega_\omega} \delta V^*(x=0,\omega).\hat{I}_1.(\iota L\omega + R)\, d\omega \end{aligned} \tag{4.53}$$

As stated earlier, we need a separated representation of the variable $\hat{V}$, assuming $n-1$ converged modes, we have:

$$\hat{V}(x,\omega) = \sum_{i=1}^{n-1} X_i(x)O_i(\omega) + X_n^p(x)O_n^{p-1}(\omega) \tag{4.54}$$

We assume the test function $\delta V^*(x,\omega)$ in the separated form as,

$$\delta V^*(x,\omega) = O_n^{p-1*}(\omega)\delta X_n^*(x) + X_n^*(x)\delta O_n^{p-1*}(\omega) \tag{4.55}$$

The generic bilinear form in separated representation is given as:

$$\begin{aligned} &m_1(O,\delta O).a_1(X,\delta X) + m_2(O,\delta O).a_2(X,\delta X) = \\ &-\sum_{i=1}^{n-1} m_1(O,\delta O).a_1(X,\delta X) - \sum_{i=1}^{n-1} m_2(O,\delta O).a_2(X,\delta X) + l_1(\delta O).l_1(\delta X) \end{aligned} \tag{4.56}$$

And the bilinear form is defined as:

$$\begin{aligned} a_1(X,\delta X) &= \int_{\Omega_x} \frac{d\delta X(x)^*}{dx}\frac{dX(x)}{dx}\ dx \\ a_2(X,\delta X) &= \int_{\Omega_x} \delta X(x)^* X(x)\ dx \\ l_1(\delta X) &= \delta X(x)^*(x=0,\omega) I_1 \\ m_1(O,\delta O) &= \int_{\Omega_\omega} O(\omega)^* O(\omega)\ d\omega \\ m_2(O,\delta O) &= \int_{\Omega_\omega} f(\omega) O(\omega)^* O(\omega)\ d\omega \\ l_1(O) &= \int_{\Omega_\omega} O(\omega)^*.(\iota L\omega + R)\ d\omega \end{aligned} \tag{4.57}$$

The PGD solution methodology is based upon an alternating strategy with the separated form of $\hat{V}(x,\omega)$ given above in eq. (4.47). We assume that the solution is converged until the step $n-1$, and the solution is in the enrichment step n in the p^{th} iteration,

Since, we are employing the Greedy Algorithm and made the assumption that the solution is converged until the enrichment step n in the p^{th} iteration,

$$\delta V^*(x,\omega) = O_n^{p-1*}(\omega)\delta X_n^*(x) \tag{4.58}$$

Substituting eq. (4.54) and eq. (4.58) in eq. (4.51), we get

$$\begin{aligned} &\int_{\Omega_x\times\Omega_\omega} \frac{d\delta X_n^*}{dx}\frac{dX_n^p}{dx} O_n^{p-1*} O_n^{p-1}\ dxd\omega + \int_{\Omega_x\times\Omega_\omega} f(\omega)\delta X_n^* X_n^p O_n^{p-1*} O_n^{p-1}\ dxd\omega = \\ &-\int_{\Omega_x\times\Omega_\omega} \sum_{i=1}^{n-1} \frac{d\delta X_n^*}{dx}\frac{dX_i}{dx} O_n^{p-1*} O_i\ dxd\omega - \int_{\Omega_x\times\Omega_\omega} f(\omega)\sum_{i=1}^{n-1} \delta X_n^* X_i O_n^{p-1*} O_i\ dxd\omega \\ &+\int_{\Omega_\omega} \delta X_n^* O_n^{p-1*}\hat{I}.(\iota L\omega + R)\ d\omega \end{aligned} \tag{4.59}$$

In the above equation, all functions of the parameter ω are known, and we can evaluate the corresponding one-dimensional integrals.

$$\begin{aligned}
\alpha^x &= \int_{\Omega_\omega} O_n^{p-1*} O_n^{p-1}\ d\omega \\
\beta^x &= \int_{\Omega_\omega} f(\omega) O_n^{p-1*} O_n^{p-1}\ d\omega \\
\gamma_i^x &= \int_{\Omega_\omega} O_n^{p-1*} O_i\ d\omega \\
\delta_i^x &= \int_{\Omega_\omega} f(\omega) O_n^{p-1*} O_i\ d\omega \\
\mu^x &= \int_{\Omega_\omega} O_n^{p-1*} \hat{I}.(\iota L\omega + R)\ d\omega
\end{aligned} \tag{4.60}$$

Hence, we have a weighted residual form in the variable X_n^p,

$$\begin{aligned}
&\int_0^l \alpha^x \frac{d\delta X_n^*}{dx}\frac{dX_n^p}{dx}\ dx + \int_0^l \beta^x \delta X_n^* X_n^p\ dx = \\
&-\int_0^l \sum_{i=1}^{n-1} \gamma_i^x \frac{d\delta X_n^*}{dx}\frac{dX_i}{dx}\ dx - \int_0^l \sum_{i=1}^{n-1} \delta_i^x \delta X_n^* X_i\ dx + \delta X_n^* \mu^x|_{x=0}
\end{aligned} \tag{4.61}$$

The solution to eq. (4.61) can be found using finite elements which will give us X_n^p.

$$\begin{aligned}
&\alpha^x [K_x]\{X_n^p\} + \beta^x [M_x]\{X_n^p\} = -\sum_{i=1}^{n-1} (\gamma_i^x [K_x]\{X_i\} + \delta_i^x [M_x]\{X_i\}) \\
&+ \{1, 0, ..., 0\}^T \mu_x
\end{aligned} \tag{4.62}$$

$$\begin{aligned}
\alpha^x &= \{O_n^{p-1}\}^T [M_w^1]\{O_n^{p-1}\} \\
\beta^x &= \{O_n^{p-1}\}^T [M_w^2]\{O_n^{p-1}\} \\
\gamma_i^x &= \{O_n^{p-1}\}^T [M_w^1]\{O_i\} \\
\delta_i^x &= \{O_n^{p-1}\}^T [M_w^2]\{O_i\} \\
\mu^x &= \hat{I}\{O_n^{p-1}\}^T [M_w^1]\{(\iota L\omega + R)\} \\
&\text{where} \\
[M_w^2] &= \int_{\Omega_\omega} f(\omega)\{N_w\}^T\{N_w\}\ d\omega
\end{aligned} \tag{4.63}$$

In the matrix operations in MATLAB, the transpose of a complex valued vector/matrix also conjugates it. In other softwares, it must be made sure that the transpose is the conjugated transpose.

The next step will be to evaluate O_n^p, since we already evaluated the term X_n^p. We assume the solution in the separated form is now given as:

$$\hat{V}(x, \omega) = \sum_{i=1}^{n-1} X_i(x) O_i(\omega) + X_n^p(x) O_n^p(\omega) \tag{4.64}$$

We assume the test function $V^*(x,\omega)$ in the separated form as,

$$\delta V^*(x,\omega) = X_n^{p*}(x)\delta O_n^*(\omega) \tag{4.65}$$

Substituting eq. (4.64) and eq. (4.65) in eq. (4.51) and simplifying we get:

$$\begin{aligned}
&\int_{\Omega_x\times\Omega_\omega} \frac{dX_n^{p*}}{dx}\frac{dX_n^p}{dx}\delta O_n^* O_n^p \; dx d\omega + \int_{\Omega_x\times\Omega_\omega} f(\omega) X_n^{p*} X_n^p \delta O_n^* O_n^p \; dx \; d\omega = \\
&- \int_{\Omega_x\times\Omega_\omega} \sum_{i=1}^{n-1} \frac{dX_n^{p*}}{dx}\frac{dX_i}{dx}\delta O_n^* O_i \; dx d\omega - \int_{\Omega_x\times\Omega_\omega} f(\omega) \sum_{i=1}^{n-1} X_n^{p*} X_i \delta O_n^* O_i \; dx \; d\omega \\
&+ \int_{\Omega_\omega} X_n^{p*}|_{x=0} \delta O_n^* \hat{I}.(\iota L\omega + R) \; d\omega
\end{aligned} \tag{4.66}$$

In this step, all the functions of the parameter x are known, and we can evaluate the following integrals.

$$\begin{aligned}
\alpha^\omega &= \int_{\Omega_x} \frac{dX_n^{p*}}{dx}\frac{dX_n^p}{dx} \; dx \\
\beta^\omega &= \int_{\Omega_x} X_n^{p*} X_n^p \; dx \\
\gamma_i^\omega &= \int_{\Omega_x} \frac{dX_n^{p*}}{dx}\frac{dX_i}{dx} \; dx \\
\delta_i^\omega &= \int_{\Omega_x} X_n^{p*} X_i \; dx \\
\xi^\omega &= X_n^{p*}|_{x=0}\hat{I}
\end{aligned} \tag{4.67}$$

Hence, we have eq. (4.66) as,

$$\begin{aligned}
&\int_{\Omega_\omega} \alpha^\omega \delta O_n^* O_n^p \; d\omega + \int_{\Omega_\omega} f(\omega)\beta^\omega \delta O_n^* O_n^p \; d\omega = - \int_{\Omega_\omega} \sum_{i=1}^{n-1} \gamma_i^\omega \delta O_n^* O_i \; d\omega \\
&- \int_{\Omega_\omega} f(\omega) \sum_{i=1}^{n-1} \delta_i^\omega \delta O_n^* O_i \; d\omega + \int_{\Omega_\omega} \xi^\omega \delta O_n^* (\iota L\omega + R) \; d\omega
\end{aligned} \tag{4.68}$$

The eq. (4.68) giving the weighted residual form doesn't involve any differential operators. The corresponding strong form results as:

$$\alpha^\omega O_n^p + f(\omega)\beta^\omega O_n^p = - \sum_{i=1}^{n-1} \gamma_i^\omega O_i - f(\omega) \sum_{i=1}^{n-1} \delta_i^\omega O_i + \xi^\omega(\iota L\omega + R) \tag{4.69}$$

$$(\alpha^\omega + f(\omega)\beta^\omega) O_n^p = - \sum_{i=1}^{n-1} (\gamma_i^\omega + f(\omega)\delta_i^\omega) O_i + \xi^\omega(\iota L\omega + R) \tag{4.70}$$

This is a set of algebraic equations solving which gives the unknown function $O_n^p(\omega)$.

Parameter Name	Symbol	Value	Units
Inductance	L	1.3×10^{-8}	H/km
Capacitance	C	8.87×10^{-9}	F/km
Resistance	R	0.105	ohm/km
Length of line	l	900	km
Minimum Frequency	ω_1	300	rad/sec
Maximum Frequency	ω_n	1300	rad/sec

Table 4.1: Distributed Parameters Values

Quantity	Value
Absolute Error	0.0864
Relative Error	$1.7924\ \times10^{-4}$
Number of Modes	12

Table 4.2: Error between Analytical and PGD Solutions

Alternatively, we can solve eq. (4.68) using FEM.

$$(\alpha^{\omega}[M_{\omega}] + \beta^{\omega}[M_{\omega}^{A}])\{O_n^p\} = -\sum_{i=1}^{n-1}(\gamma_i^{\omega}[M_{\omega}] + \delta_i^{\omega}[M_{\omega}^{A}])\{O_i\} + \xi^{\omega}\{(\iota L\omega + R)\} \quad (4.71)$$

A similar PGD formulation for the differential equation in terms of current has been formulated and is listed in Appendix A.1.

4.3.3 Validity of PGD Solution

In order to implement the PGD solution, we first must validate the PGD solution and its accuracy. For a simple case, we have the analytical solution for the problem given in eq. (4.8) and the boundary conditions of eq. (4.10). The parameters used for the validation purposes are adopted from the book of Bergen and Vittal [118] for a line of 138 kV line and are listed in the Table 4.1.

Solutions obtained using analytical expression and PGD are plotted in Figure 4.3a to Figure 4.3f as well as the error plots in Figure 4.3g to Figure 4.3i between the PGD solution and the solution obtained from the analytical solution. The maximum absolute and relative errors are listed in the Table 4.2.

The solution from PGD is accurate as evident from the errors listed in the Table 4.2. Also from the number of modes, presented in Figure 4.4, it is proved that PGD provides a fast as well as accurate alternative solution to the analytical solution. The analytical solution can also be presented in separated representation using SVD but the actual benefit of using PGD over SVD is in its ability to use it as a parametric solver which we present in the next section.

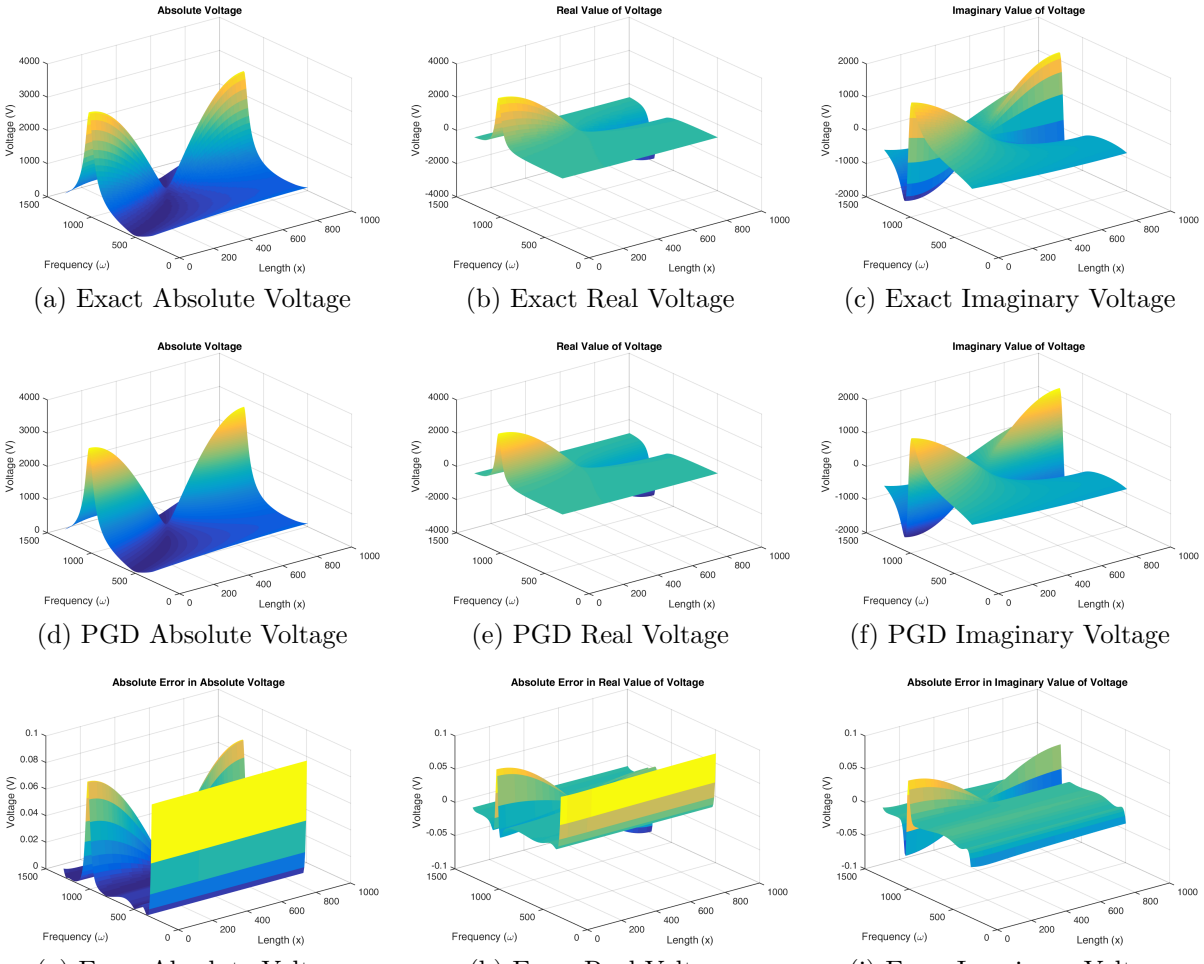

(a) Exact Absolute Voltage (b) Exact Real Voltage (c) Exact Imaginary Voltage

(d) PGD Absolute Voltage (e) PGD Real Voltage (f) PGD Imaginary Voltage

(g) Error Absolute Voltage (h) Error Real Voltage (i) Error Imaginary Voltage

Figure 4.3: Analytical and PGD Solution for the DP Model

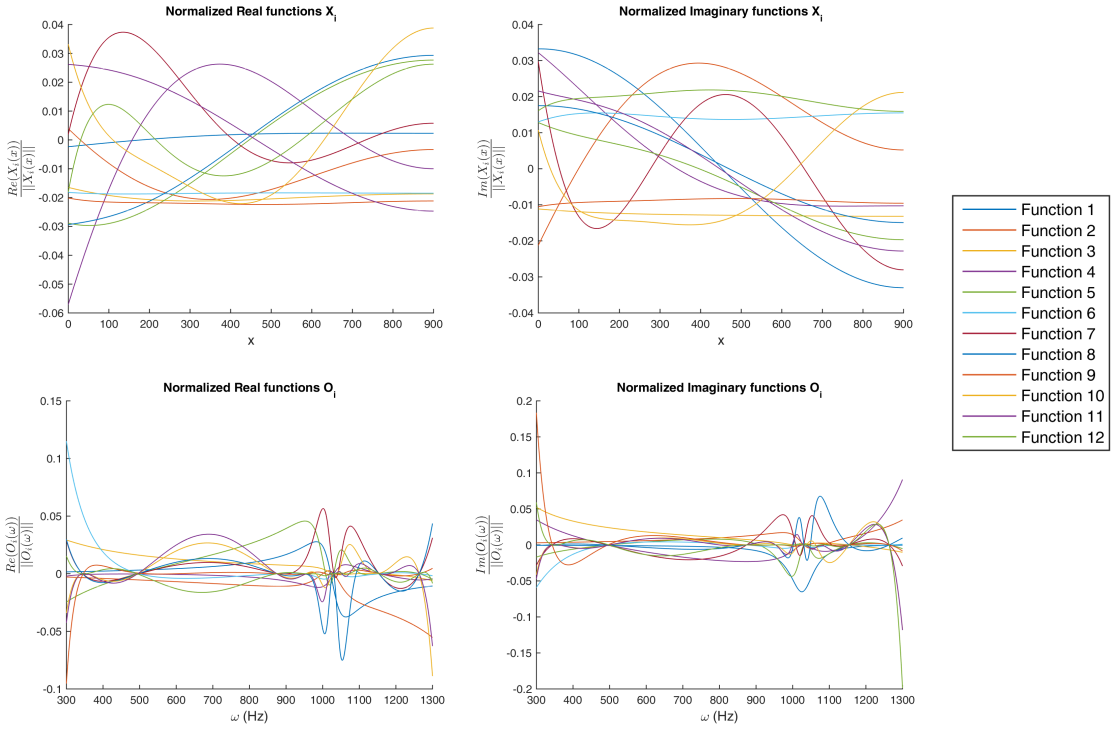

Figure 4.4: Modes of PGD Solution

4.3.3.1 PGD Residual Evaluation

Residual of the PGD solution is important to evaluate so that the progress of the solution and the quality of the enrichment modes can be assessed. The residual can be evaluated as:

$$Res(\delta V) := -A(V_{PGD}, \delta V) + L(\delta V) \tag{4.72}$$

The solution and the operator given in separated representation as:

$$V_{PGD}(x,\omega) = \sum_{m=1}^{N} X_m(x) O_m(\omega) = \sum_{m=1}^{N} \vec{X_m} \otimes \vec{O_m} \tag{4.73}$$

$$A(V_{PGD}, .) = \sum_{m=1}^{N} a_1(X_m, .) m_1(O_m, .) - a_2(X_m, .) m_2(O_m, .) \rightarrow \boldsymbol{C} \tag{4.74}$$

$$L(.) = l_1^O(.) l_1^X(.) \rightarrow \boldsymbol{B} \tag{4.75}$$

Therefore, the equation for residual calculation is

$$\begin{aligned} \boldsymbol{R} &= \sum_{m=1}^{N} \boldsymbol{C_m} - \boldsymbol{B} \\ \boldsymbol{R} &= \sum_{m=1}^{N} (\boldsymbol{M_w^1}.\boldsymbol{O_m} \otimes \boldsymbol{K_x}.\boldsymbol{X_m} - \boldsymbol{M_w^2}.\boldsymbol{O_m} \otimes \boldsymbol{M_x}.\boldsymbol{X_m}) - \boldsymbol{B} \end{aligned} \tag{4.76}$$

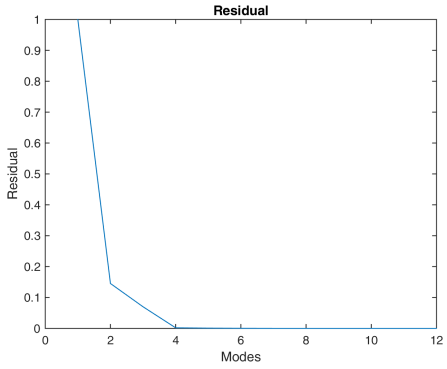

Figure 4.5: Residual w.r.t. Enrichment Modes

The residual for the case presented in this section, the residual decreases steeply after first mode. The residual steadily keeps on decreasing with more enrichment modes as presented in the Figure 4.5.

4.3.3.2 Effect of Tolerances on PGD Performance

Before moving further with the application of PGD based separated representation on the transmission line model, first we must quantify the effectiveness of the method. In this section, we study the effects of tolerances for the alternating directions and the tolerance for the enrichment process and their relation with the error, number of enrichment modes, number of iterations and the residual. Two studies were performed, first the tolerance for the enrichment process was kept constant at 1×10^{-10} and the tolerance for fixed point iterations was varied. The results of the first case is reported in Table 4.3.

The second set of analysis was carried out with tolerance for fixed point iterations kept constant at 1×10^{-10} and the tolerance for enrichment process was varied over a range from 1×10^{-6} to 1×10^{-15}, the results are presented in the Table 4.4. In order to explain the results presented in Table 4.3 and Table 4.4, it is imperative that the implementation of the algorithm and the tolerances within the algorithm are explained. To guarantee the convergence of each of the dimension in the fixed point iterations, both the amplitudes of the basis and the norm of the basis were checked for convergence. The tolerance for the amplitude of the basis was always kept below 1×10^{-6}, this partially explains the variation in the required number of iterations before the convergence during the fixed point iterations.

As observed in the Table 4.3, when the tolerance for fixed point iterations was very small, the required number of iterations were too many which gradually gets fewer as the tolerance is set higher. Also, the maximum number of iterations were fixed at 99 before terminating the fixed point iterations. This restriction on the number of iterations was applied so that the fixed point iterations do not get stuck in an infinite loop and because of the nature of PGD method, the error in one mode can be reduced in the following modes.

The results for the effect of tolerance on enrichment process presented in Table 4.4 is intuitive, as the tolerance is getting smaller the number of modes required to

Tolerance of Alternating Directions	10^{-10}	10^{-9}	10^{-8}	10^{-7}	10^{-6}	10^{-5}	10^{-4}	10^{-3}	10^{-2}	10^{-1}
Iterations	32	14	27	40	56	8	7	7	6	6
	99	95	85	82	99	81	69	63	57	48
	55	29	93	29	40	16	13	12	11	10
	99	99	99	99	99	99	99	99	99	99
	99	18	7	7	11	7	6	5	5	4
	42	12	30	22	24	12	11	10	9	8
	99	99	99	99	99	14	8	6	6	5
	99	99	38	15	26	6	6	5	5	5
	99	99	19	10	14	10	9	8	7	6
	99	99	99	99	24	23	20	16	13	9
	99	99	99	16	7	7	6	5	4	3
	99	99	99	99	99	20	16	10	10	5
Modes	-12-									
Abs Err	0.0864									
Rel Err	1.7924×10^{-4}									
Residual	1.59×10^{-10}									

Table 4.3: Performance of PGD solution w.r.t. tolerance of alternating directions

Tol for Enrich	10^{-6}	10^{-7}	10^{-8}	10^{-9}	10^{-10}	10^{-12}	10^{-15}
Iterations	99	69	69	22	29	44	76
	99	99	99	68	99	75	33
	16	15	54	48	40	41	99
	99	99	99	99	99	99	7
	15	8	12	8	8	11	35
	48	18	35	13	20	39	81
	99	46	78	48	22	99	16
		26	14	20	17	9	10
		13	12	10	12	12	37
		38	46	47	96	27	9
					9	8	68
					34	99	8
						9	99
						99	99
						99	99
						99	12
							99
							99
Modes	7	10	10	10	12	16	19
Abs Err	3.42	0.11	0.11	0.11	0.09	0.08	0.08
Rel Err	0.007	2.2×10^{-4}			1.8×10^{-4}	2.6×10^{-5}	
Residual	4.2×10^{-7}	2.8×10^{-9}			1.6×10^{-10}	3.5×10^{-11}	6.4×10^{-15}

Table 4.4: Performance of PGD solution w.r.t. tolerance of enrichment modes

achieve the accuracy increases.

4.4 PGD as Parametric Solver

The strength of PGD is not only its ability to reduce models in a priori sense but also to include parameters in the basis. In this section, we present the parametric solution of the DP model of transmission lines. First, we begin with including only one parameter and study the results. Then we will present the PGD formulation including all the parameters.

4.4.1 Inductance L as an extra parameter

As a first instance, we introduce inductance L as a parameter in PGD separated representation. The solution in separated representation will be then written as,

N_x	N_ω	N_L	L_1	L_{N_L}
1801	2001	1001	1×10^{-3}	1.5×10^{-3}

Table 4.5: Number of elements and range for PGD with L as a parameter

Modes	Maximum Error		Frobenius Norm of Error Matrices	
	Absolute	Relative	Absolute	Relative
25	175.5276	0.3639	6.3595×10^4	203.0935
50	16.6750	0.0327	7.9057×10^3	22.7360
100	13.8586	0.0287	3.9136×10^3	16.1839
150	2.1991	0.0052	814.6762	1.2063

Table 4.6: Error of PGD solutions with L as a parameter

$$\hat{V}(x, \omega, L) = \sum_{i=1}^{n} X_i(x) O_i(\omega) L_i(L) \tag{4.77}$$

The formulation is the same as previously defined and is detailed in the Appendix A.2. Here, we just present our results based on the PGD separated representation with inductance L as a parameter in addition to the space and frequency coordinates.

The values of R and C are kept fixed as listed in the Table 4.1. The range of values of L and the discretization used in the parametric space are listed in Table 4.5.

We present the errors for a specific value of inductance $L = 1.302 \times 10^{-3} H/km$ in the Table 4.6, values of resistance R and capacitance C are kept the same as in Table 4.1. The results indicate that the parametric solution depends upon the parameter range and the discretization size. Increasing the modes of PGD solution improves the accuracy of the solution which is intuitive. The results are graphically presented in the Figure 4.6. The number of modes for improved accuracy are quite large which can be reduced by using a post PGD compression. The convergence of the PGD solution with the addition of enrichment modes is presented in the Figure 4.7.

Frobenius Norm (commonly termed Euclidean norm) defined in the Table 4.6 is the matrix norm defined as the square root of the sum of the absolute squares of its elements $\|A\|_F = \sqrt{\sum_{i=1}^{m} \sum_{j=1}^{n} |a_{i,j}|^2}$.

The inclusion of inductance L as an extra parameter has provided good results from the parametric solution. Although, the number of enrichment modes have increased considerably compared with the solution where the solution was sought separated only in the space-frequency domain. The additional number of modes did not have significant impact on the memory or the computational time. Nevertheless, the number of modes can be reduced using post-PGD compression.

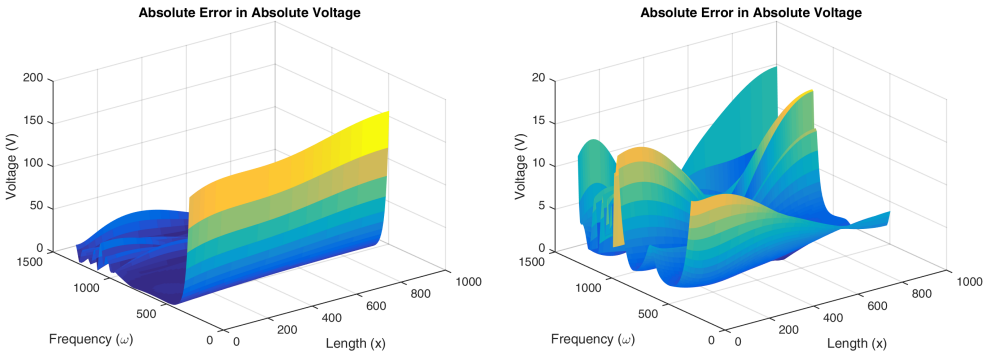

(a) With 25 modes

(b) With 50 modes

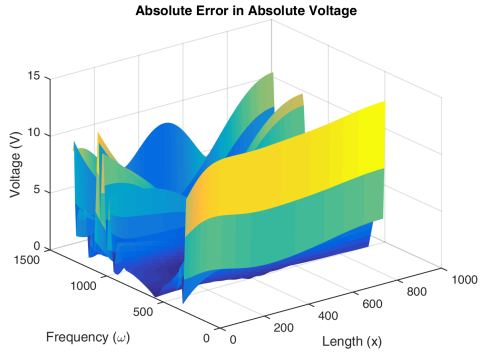

(c) With 100 modes

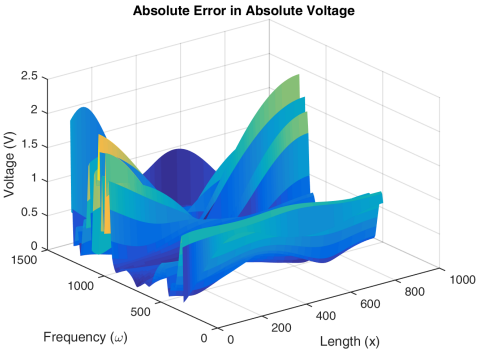

(d) With 150 modes

Figure 4.6: Effect of enrichment modes on error with inductance as parameter

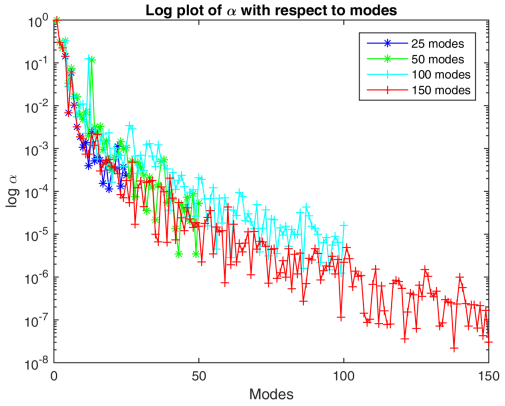

Figure 4.7: Effect of enrichment modes on ratio α of 1st mode to last mode

Parameter	Symbol	Range		Discretization
		Initial	Final	
Inductance	L	1×10^{-3}	1.5×10^{-3}	$N_L = 1001$
Resistance	R	1×10^{-1}	2×10^{-1}	$N_R = 1001$
Capacitance	C	8.5×10^{-9}	9×10^{-9}	$N_C = 1001$
Space	x	0	900	$N_x = 1801$
Frequency	ω	300	1300	$N_\omega = 2001$

Table 4.7: Parameter Space

Modes	Maximum Error		Frobenius Norm of Error Matrices	
	Absolute	Relative	Absolute	Relative
25	255.9129	0.6884	1.2172×10^5	391.7488
50	120.4323	0.0589	6.6426×10^4	288.9914
100	58.3446	0.1544	2.5890×10^4	142.9241

Table 4.8: Error of parametric PGD with values of L, R, C as listed in Table 4.7

4.4.2 Extending PGD for Parameters R,L and C

The next step is to develop a full parametric solution with all the electrical parameters of the transmission line as extra coordinates of the separated representation. This separated representation is of great significance in terms of real time evaluation of any type of commercially available transmission lines. In this way, we will have a database prepared in offline mode which we can then use in real time.

The formulation is presented in Appendix A.3.

Now, we have defined the PGD formulation for a fully parametric problem, we present some solutions and compare with the analytical results presented earlier in the chapter. The range of parameters used and the discretization for each parameter is presented in the Table 4.7.

The results for the full parametric solution using PGD is presented in the Table 4.8. The results are compared with the exact solution of the parameters presented in the book of Bergen and Vittal [118] and presented throughout this chapter.

The results presented in the Table 4.8 highlighted the fact that with the parametric solution, the choice of parameter range has to be carefully selected. In the results presented in Section 4.3.3, the separated solution needs only 12 modes, while the solution with only inductance L as a parameter needs upto 150 modes. With 150 modes, the accuracy is very good and the error is about 0.5 %, but for the full parametric solution this much modes are insufficient for accurate solutions. Therefore, we reduce the size of the parameters domain and are presented in the Table 4.9.

With the reduced range for parameters, the results are presented in Table 4.10. The errors have reduced below 1 % with only 50 modes and with more enrichment modes included the Frobenius norm with 100 modes is also very low. This indicates

Parameter	Symbol	Range		Discretization
		Initial	Final	
Inductance	L	1.25×10^{-3}	1.35×10^{-3}	$N_L = 1001$
Resistance	R	1×10^{-1}	1.1×10^{-1}	$N_R = 1001$
Capacitance	C	8.8×10^{-9}	8.9×10^{-9}	$N_C = 1001$
Space	x	0	900	$N_x = 1801$
Frequency	ω	300	1300	$N_\omega = 2001$

Table 4.9: Reduced range for Parameter Space

Modes	Maximum Error		Frobenius Norm of Error Matrices	
	Absolute	Relative	Absolute	Relative
25	39.0809	0.0767	1.1461×10^4	38.9270
50	13.7160	0.0044	5.8392×10^3	24.1773
100	7.5472	0.0024	1.0306×10^3	5.1648
150	5.4543	0.0113	1.1869×10^3	3.0289

Table 4.10: Error of parametric PGD with reduced range of L, R, C as listed in Table 4.9

that with 100 modes the error at each node is reduced to a very manageable level. The reduction in error with the increase in number of modes is shown in Figure 4.8a to Figure 4.8d while the solution using PGD formulation is presented in Figure 4.8e.

The reduction in absolute and relative errors with the increase in number of modes is evident and is presented in Figure 4.9. An observation from the Figure 4.9 is that when the number of modes are increased from 100 to 150, the relative error seems to increase. This is due to the fact that we are presenting the maximum error in both absolute and relative errors. The maximum error is now at a different value of distance and frequency as observed from the evolution of errors in the Figure 4.8. From the results presented in Table 4.10, it is observed that the overall accuracy of the solution increases as the Frobenius norm of the relative errors is decreasing. However, the increase in accuracy is small from 100 to 150 modes and we can be satisfied with the solution with 100 modes as a best compromise between computational effort and the accuracy level achieved.

4.5 PGD Solution as Generalized Transfer Function

The transfer function for a transmission line connecting a voltage source '$\hat{V}_0$' at one end and a load represented by 'Z' at the other end is studied in this section. The purpose of this study is twofold, one which is of concern in this section is the model

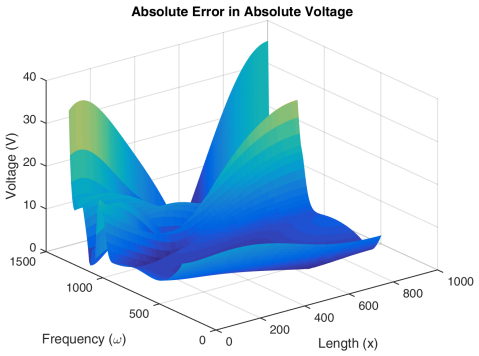

(a) Error with 25 modes

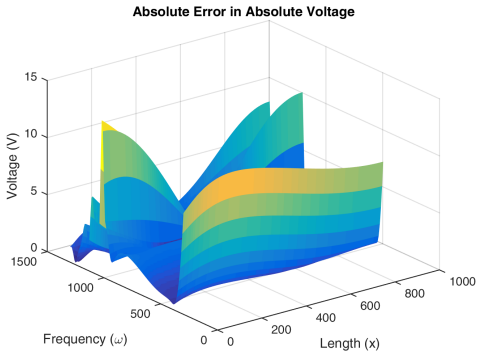

(b) Error with 50 modes

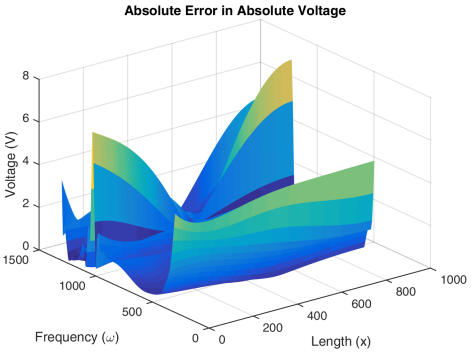

(c) Error with 100 modes

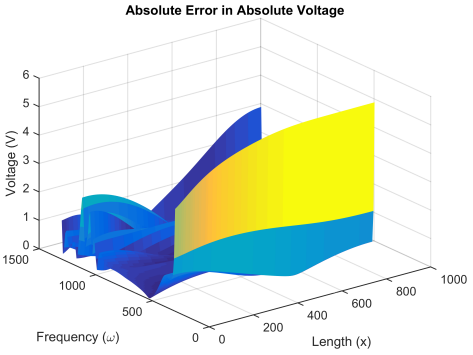

(d) Error with 150 modes

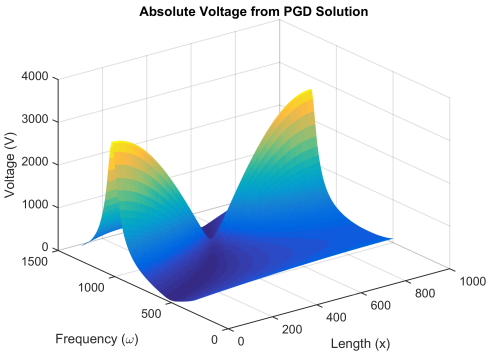

(e) Solution with 150 modes

Figure 4.8: Evolution of Parametric PGD solution for parameters listed in Table 4.1

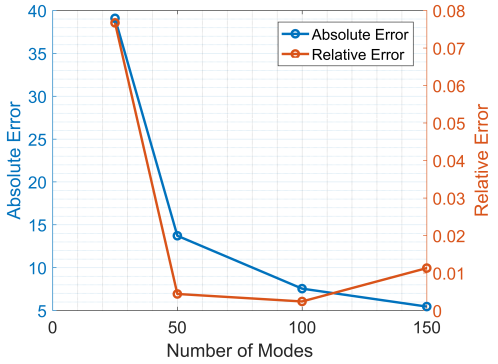

Figure 4.9: Effect of enrichment modes on maximum absolute and relative errors

reduction of the transfer function of a power transmission line. The other purpose is the validation of the separated representation obtained by the application of PGD which is to be utilized in the study of power grids harmonics analysis presented in the next chapter. The boundary conditions for the harmonic analysis are different than the current study and are presented in the eq. (4.10) and eq. (4.11).

In the study by Belhocine and Marinescu [99], the transfer function is obtained using the Laplace transfer. The differential equations representing the DP model is given in eq. (4.1) as recalled here.

$$\frac{\partial v(x,t)}{\partial x} = -L\frac{\partial i(x,t)}{\partial t} - Ri(x,t),$$
$$\frac{\partial i(x,t)}{\partial x} = -C\frac{\partial v(x,t)}{\partial t}$$

For an ideal voltage source $Z = 0$ and the line opened at extremity i.e. $Z = \infty$, the boundary conditions are given as

$$\begin{aligned} v(x,t)|_{x=0} &= V_0(t) \\ i(x,t)|_{x=l} &= 0 \end{aligned} \tag{4.78}$$

For such a system, the transfer function for the output $\hat{V}(l,s)$ at $x = l$ in the Laplace domain is given in the study by Belhocine and Marinescu [99] as:

$$\frac{\hat{V}(l,s)}{\hat{V}_0(s)} = \frac{1}{\cosh\left(l\sqrt{Cs(R+Ls)}\right)} \tag{4.79}$$

The transfer function in the spectral approach as described in the study by Belhocine and Marinescu [99], can be written in an infinite form

$$\frac{\hat{V}(l,s)}{\hat{V}_0(s)} = \frac{1}{\prod_{n=1}^{\infty}\left(\frac{4l^2LC}{(2n-1)^2\pi^2}s^2 + \frac{\left(\frac{R}{L}\right)4l^2LC}{(2n-1)^2\pi^2}s + 1\right)} \tag{4.80}$$

The detailed explanation of the spectral approach method is given in the references by B. Ya. Levin [119] and R.F. Curtain and H.J. Zwart [120]. In the next section, the model reduction of the transmission line models are discussed and the separated representation obtained using PGD is presented.

4.5.1 Model Reduction of the Transmission Line Model

Transmission line models should be able to fully describe the transients of the power systems. DP model has this capability but it is very difficult to use this model except for very few cases which is not practical. Hence, the other finite dimensional models like the π-model and multiple π-sections model are developed, but these models are not able to describe the wave propagation and have limitations in terms of its applications. The model reduction depends upon the application and the need to keep specific dynamics of the system keeping in view the type of study to be performed.

In the study [98] by Belhocine and Marinescu, they have presented the modal truncation and balanced truncation approach. Their goal was to present a model reduction technique which preserves the dynamics of the system the analysts are interested in. The authors first presented the two models of balanced and modal truncation and discussed. Later they have presented their own developed method, which is a mix of balanced and modal trunctations. The reduced order model obtained by combining the balanced and modal truncations as presented in the study by Belhocine and Marinescu [99] has still 171 modes. The number of modes are still high, even though the reduced model has closely matched the DP model.

We can use the ability of PGD to develop a separated representation of the DP model which has far fewer modes. As presented in the section 4.2, the Fourier transformation of the differential equations of (4.1) and the boundary conditions gives us the ordinary boundary value problem with mixed boundary conditions.

$$\frac{d^2\hat{V}(x,\omega)}{dx^2} + (LC\omega^2 - \iota RC\omega)\hat{V}(x,\omega) = 0 \tag{4.81}$$

$$\begin{aligned} \hat{V}(x,\omega)|_{x=0} &= V_0(t) \\ \left.\frac{\partial\hat{V}(x,\omega)}{\partial x}\right|_{x=l} &= 0 \end{aligned} \tag{4.82}$$

The transfer function in the separated representation is given by the product of the separated representation of the ODE.

4.5.2 Step Response

First, we present the time-domain simulation and present the results for a step input and a sinusoidal wave with a 100 Hz frequency. The same values are used in the study by Belhocine and Marinescu [99]. The results are graphically represented in the Figure 4.10.

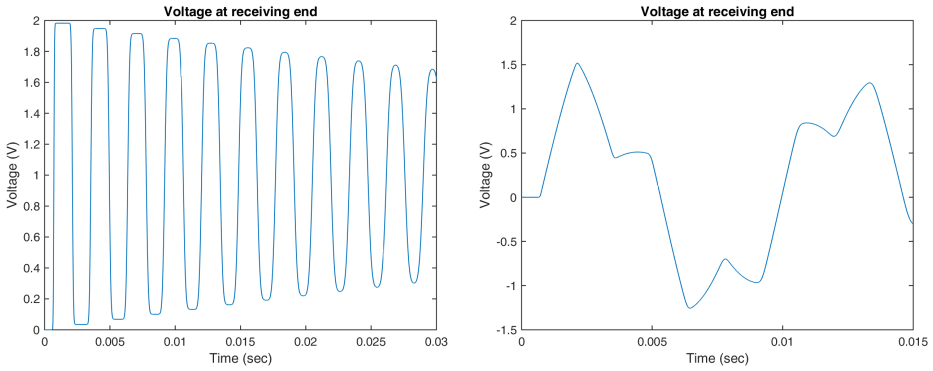

(a) Step Response (b) Response to a sinosuidal input

Figure 4.10: Time simulation of transmission line transient behavior

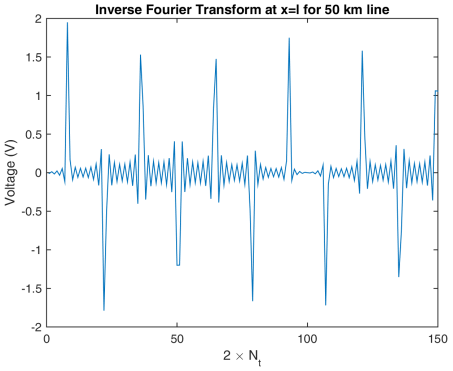

Figure 4.11: Impulse Response

In this section, we employed the PGD for space-frequency separated representation to obtain the generalized transfer function. The impulse response, i.e., the generalized transfer function response is given in the Figure 4.11.

Multiplying the impulse response with the given input function, gives the appropriate response which is equivalent to convolution in time domain. The results are presented graphically in Figure 4.12a and Figure 4.12b.

Comparing our results with the results presented in the study by Belhocine and Marinescu [99] and obtained from our time simulation and are presented in Figure 4.13a and Figure 4.13b, we can observe the PGD solution matches quite well.

4.6 Conclusions

In this chapter, we have presented the PGD formulation for space-frequency domain and compare the results of PGD separated representation with the analytical result. The PGD solution compares well and provides a reliable, accurate and robust method. The PGD formulation was then extended for the parametric problem. The results obtained are encouraging, parametric space, discretization and the number of

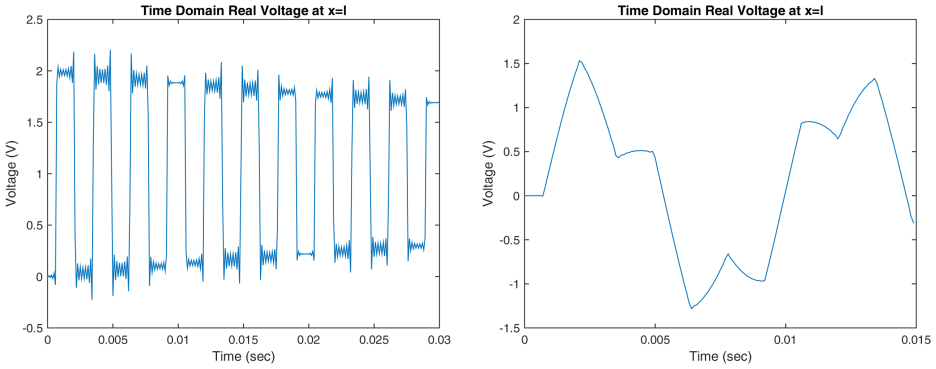

(a) Step Response (b) Response to a sinosuidal input

Figure 4.12: Time simulation using Inverse Fourier on the solution from space-frequency domain

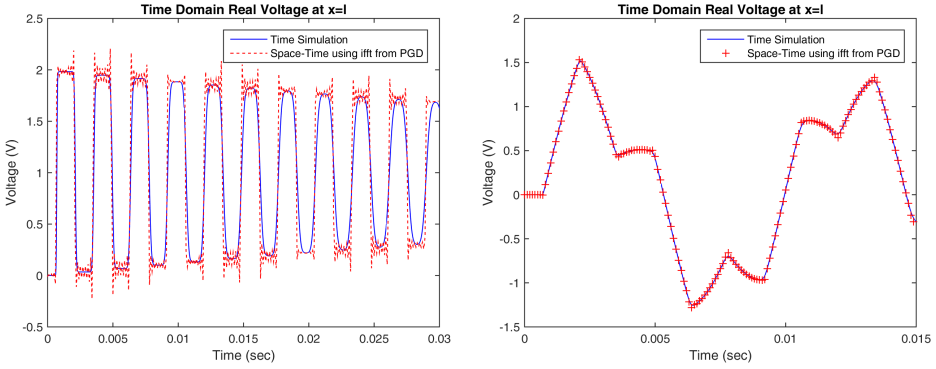

(a) Step Response (b) Response to a sinosuidal input

Figure 4.13: Comparison of solution from time-domain and inverse Fourier of solution from frequency-domain

enrichment modes all have effect on the accuracy of the results. In the last section, the PGD formulation is applied to a problem from the literature and demonstrated the method on this problem effectively.

Chapter 5

Model Reduction of DP Model with Frequency-Dependent Parameters

This chapter presents the application of Proper Generalized Decomposition on transmission line models involving frequency dependent parameters. Frequency dependence of parameters can be due to a number of reasons including the phenomenon known as "Ground Return Effects", "Proximity Effects" and "Skin Effects". In the current study, simplified methods of skin effects based on Bessel functions are used in order to showcase the method. The method can easily accommodate other effects which induces frequency dependence in the transmission line parameters. In time domain modeling, the parameters are assumed constant and these models prove inefficient when incorporating these parameters as function of frequency. Therefore, a frequency domain simulation is implemented using harmonic analysis. PGD presents a separated representation and provides a quick and accurate solution for such problems.

Contents

5.1 Introduction

Accurate modeling of transmission lines is important in the simulation and subsequent transient analysis of power grids. In this framework, frequency dependence of the line parameters should be accounted for [121]. The parameters of transmission lines in practice are highly frequency dependent and it is necessary to accommodate the frequency dependence over the whole frequency range of interest.

AC transmission lines are affected by the frequency of the AC voltage which produces a secondary effect on the line resistance and inductance. This effect is related to the non uniform distribution of the current which tends to concentrate more towards the outer surface of the line away from the center as the frequency increases [122]. Skin effects results in the reduction of the effective cross-section of the line used for the transmission of current and hence the resistance increases. This concentration of current at the surface has an inverse relation with the internal inductance of the line, as the frequency increases the inductance decreases [123, 124]. There are other phenomena like ground return and proximity which also have an effect on the transmission line parameters resulting in the frequency dependence of these parameters [123]. If the phenomena which produce frequency dependence are ignored and the parameters are assumed to be constant, this results in a magnification of the higher harmonics [125]. The wave shapes are distorted and at higher frequency the peaks have higher magnitudes than that are observed in practice. There are a wide range of frequencies presented in the signals during the transient phase and this can be modeled with the frequency-dependent parameters.

The challenge in time domain modeling is to incorporate the frequency dependence in an efficient manner and as such, several formulations have been proposed. As it will be discussed later in this paper, many of these result in profound modifications of the original model that are sometimes difficult to interpret in the light of their physical meaning. Accounting for frequency related effects is obviously more natural when the governing equations are formulated in the frequency domain rather than in time. However, this implies that incremental time stepping strategies for transient simulation can no longer be applied and harmonic components have to be solved individually, each requiring the solution of a different problem.

In this work we propose a robust parametric solver that allows to determine at once all the harmonics in a given frequency range. While this step is performed “off-line", the actual time response can be efficiently computed “on-line". The rest of this chapter is organized as follows, Section 5.2 presents the literature review. Section 5.3 presents the method proposed in the current study to deal with the frequency dependent parameters in the frequency domain. In the Section 5.4 we present the skin effects model for the transmission lines and in Section 5.5 we present the distributed parameters model of transmission lines that we adopted in this study. Finally, we present the results of our proposed approach in the Section 5.7 and extend it to the commercial transmission lines in Section 5.8.

5.2 Related Work

The frequency dependence of the parameters is the consequence of the assumption made in the derivation of Telegrapher's equations from the Maxwell's equations [126]. It is assumed that the conductor carries a uniform current in a uniform time-harmonic magnetic field. Furthermore, it is assumed that the curvature of the wire is negligible and there is no field variation in the wire direction i.e. x-axis in this case. It is considered that the current flows in x-direction only [127]. These assumptions simplify the 3-D Maxwell's equation to a manageable 1-D equation known as Telegrapher's equation given by:

$$\frac{\partial v(x,t)}{\partial x} = -Ri(x,t) - L\frac{\partial i(x,t)}{\partial t}\ , \quad \frac{\partial i(x,t)}{\partial x} = -Gv(x,t) - C\frac{\partial v(x,t)}{\partial t} \tag{5.1}$$

where, $v,\ i$ are the voltage and current, $R,\ L,\ G$ and C are the resistance, inductance, conductance and the capacitance per unit length respectively. Eliminating i and combining the two equations in (5.1) give

$$LC\frac{\partial^2 v(x,t)}{\partial t^2} + (LG + RC)\frac{\partial v(x,t)}{\partial t} + RGv(x,t) = \frac{\partial^2 v(x,t)}{\partial x^2} \tag{5.2}$$

In order to retain the correct physical behavior, the model parameters like resistance and inductance are often considered as functions of frequency in order to compensate for the simplifications introduced by the assumptions in the derivation of the 1-D model. The other scenario in which these parameters are kept constant will then require the 3-D partial differential equations to be solved.

Several numerical methods have been proposed for the solution of frequency dependent models [128]. An overview is listed in the Table 5.1.

There are mainly two families of solution procedures, i.e., a time-domain and a frequency-domain simulation. There are arguments in favor of both these methods. Time-domain modeling is delicate and some numerical instabilities and accuracy issues have been reported in the literature [125, 131]. But, the advantage it provides is the straightforward compatibility with the the models for components of the power system.

Most of the studies, reported in Table 5.1, avoid convolutions and developed intelligent models to circumvent the difficulties in time-domain modeling by modifying the formulation of the equations in time. For example, in the study by Semlyen and Dabuleanu [129], the authors have used approximations based on the exponential functions. The study by Chu-Sun et al [130] uses equivalent circuit with each section is a combination of equivalent resistances and inductances to include the skin effects. Some recent studies like Marques da Costa et al [123] used fitting methods to include skin effects in lumped parameters model of transmission line.

On the other hand, research studies in favor of frequency-domain modeling points out the ease of formulation. Instead of time convolutions, we can readily multiply the harmonic response of the system with the desired input function. Then obtaining the solution in time-domain is simply just a matter of inverse transformation. Wilcox

Authors	Phenomena	Methods
Time Domain Modeling		
Semlyn and Dabuleanu [129]	Ground return effect	Approximation of time variable characteristic admittance using exponential functions
J. R. Marti [125]	Ground return effect	Weighting Functions, Characteristic Impedance
Chu-Sun et al [130]	Skin effect	Equivalent Circuit using parallel equivalent resistors and inductors
Suk Oh [131]	Skin effect	Difference Approximation Method
Marques da Costa et al [123]	Ground return, skin and corona effects	Fitting Procedure for state space lumped parameters models
Dávila et al [132]	Corona and Skin Effects	Differential Integral Equation (Radulet Line Equations)
Frequency Domain Modeling		
Meyer and Dommel [133]	Ground return effect	Linear Superposition of all frequency components
Wilcox and Condon [134]	Skin Effects	Modal Analysis, Conversion to time-domain using Auto-Regressive-Moving-Average (ARMA) as fitting method
Kurokawa et al [121]	Ground return effect	Clarke's matrix as the modal transformation matrix
Machado et al. [128]	Skin and Proximity Effects	Magnetic Field Analysis using Bessel function development
Bormann and Tavakoli [124]	Skin and Proximity Effects	Reluctance networks
Gatous and Pissolato [135]	Skin Effects	Simplified expressions of R and L based on Bessel Functions
Kim and Neikirk [136]	Skin Effects	Compact Circuit Model in form of Ladder Circuit
Admane et al [122]	Skin Effects	Reduced order differential model based on Kim's Ladder Circuit

Table 5.1: Literature Review

and Condon [134] proposed a inverse transformation method based on ARMA (Auto-Regressive-Moving-Average) fitting method to obtain time-domain model, where ARMA is a statistical model used in several fields to fit model to observed data. While other studies like by Kurokawa et al [121] used modal transformation matrix. In frequency-domain analysis, as described in the study of Meyer and Dommel [133], we have to use linear superposition of all the frequency components. The solution is performed for every individual frequency present in the transients, as the unit impulse response in time, "translates" as the unit Heaviside response in frequency-domain.

In the current study, we present a simple yet efficient frequency-domain method based on the Proper Generalized Decomposition for the solution of transmission line including the frequency-dependence of parameters due to skin effects. We propose a method based on PGD's separated representation as a monolithic solver for all the frequencies.

5.3 Proposed Approach

Referring to eq. (5.2), the second term is referred as the dissipation term and the last term is the dispersion term. For a loss-less transmission line, we assume $G = 0$. By introducing a suitable finite element basis, the function $v(x,t)$ can be approximated as:

$$v(x,t) \approx \sum_{i=1}^{n} v_i(t)\phi_i(x) \tag{5.3}$$

Then, imposing Galerkin orthogonality of the residual of eq. (5.2) on the basis functions $\phi_i(x)$ leads to the following system of ordinary differential equations in time

$$[M]\{\ddot{v}(t)\} + [C]\{\dot{v}(t)\} + [K]\{v(t)\} = \{f(t)\} \tag{5.4}$$

where, $[M], [C]$ and $[K]$ are referred to as the mass, damping and stiffness matrices by analogy with structural dynamics. The unknowns of the problem are arranged into the vector $\{v(t)\} = \{v_1(t), v_2(t), \ldots, v_n(t)\}$.

Time integration of eq. (5.4) requires the solution of a $n \times n$ algebraic system for every time increment. Modal analysis provides an efficient strategy to reduced the numerical complexity of the system by transforming into a set of n uncoupled equations.

Transforming the problem from time-domain to frequency-domain using either Laplace or Fourier transformation. We show here for a Fourier transformation with $\hat{X} = xe^{\iota\omega t}$ and $\hat{F} = fe^{\iota\omega t}$,

$$\left(-\omega^2[M] + \iota\omega[C] + [K]\right)\hat{X} = \hat{F} \tag{5.5}$$

For a system with no damping, i.e. $[C] = 0$, the diagonalization of the system leads to the following generalized eigenvalue problem which corresponds to solving for the free response of the system in modal analysis.

$$\left(-\omega^2[M] + [K]\right)\hat{X} = 0 \tag{5.6}$$

However, for a system with constant parameters and damping, this means solving a quadratic complex eigenvalue problem. In this case, modal analysis works only if the damping is a linear combination of mass and stiffness matrices such as $[C] = a_0[M] + a_1[K]$.

$$\left(-\omega^2[M] + \iota\omega[C] + [K]\right)\hat{X} = 0 \tag{5.7}$$

In case of a system with frequency dependent parameters, the mass and stiffness matrix are no longer symmetric and frequency ω becomes a parameter. This is the case we address here when the parameters resistance $R(\omega)$ and inductance $L(\omega)$ becomes frequency dependent because of skin effects. In cases with parameters depending upon frequency, the problem cannot be solved using direct time integration as the time formulation started with constant parameters and in frequency domain, frequency dependent parameters are introduced which violates the causality. In the study by Crandall [137], the author discusses the effect of choosing frequency dependent parameter on time formulation, the argument is that even if the frequency dependence correlates with the experimental data, the inverse transformation to the time domain results in the loss of causality and the concept of non-equations is introduced for such equations in time-domain. In addition, the modal analysis is no longer a viable option for solution. The better option is to solve the harmonic analysis problem using eq. (5.5) for every frequency ω.

$$\left(-\omega^2[M(\omega)] + \iota\omega[C(\omega)] + [K(\omega)]\right)\hat{X}(\omega) = \hat{F}\ \forall\ \omega \tag{5.8}$$

Now, the harmonic analysis problem requires solution of n number of linear equations to be solved where let n represent the order of discrete frequencies involved. A similar problem involving the fractional damping was discussed in the study by [138]. The use of proper generalized decomposition (PGD) as a parametric solver as presented in earlier studies by Chinesta et al. [109] and [63] is considered here as well. PGD provides a strong tool as a single monolithic solver as compared to solving the harmonic problem using eq. (5.8) individually for every frequency. Note that if we solve the linear problem of eq. (5.8) we have to compute the matrices for every single frequency as they are no longer constant compared to the case where the constant parameters was considered and depend upon the frequency. Therefore, in this study, we present the Proper Generalized Decomposition (PGD) as a parametric solver, a method capable to solve the harmonic analysis.

5.4 Skin Effects Model

Skin Effect results in frequency dependence of the transmission line parameters; resistance and inductance. At this point, it is necessary to make the distinction between the internal inductance of the conductor and the external inductance. The evaluation of external inductance is based on the assumption that the total current

flow is on the surface of the transmission line, i.e., external inductance is maximum when the skin effect is maximum. However, the external inductance is the result of the current flow in the neighboring transmission line and therefore remains constant. In the current case, we are dealing with the single transmission line and in the succeeding discussion wherever inductance is mentioned it is assumed internal inductance unless explicitly mentioned.

A model derived from Maxwell's equations is presented here for a solid cylindrical conductor. Here, an assumption worth mentioning is that we consider a solid cylindrical conductor, typically transmission lines are bundled aluminum strands twisted together with some transmission lines consisting of steel strands in the core to increase the strength of the transmission line. However, here for the sake of simplicity the discussion is limited to a solid cylindrical conductor to effectively demonstrate the method. This model presents the complex internal impedance as the ratio of the voltage drop along the surface to the total current enclosed [139].

$$\begin{aligned} Z(\omega) &= \frac{\iota\omega\mu}{2\pi r}\frac{\mathrm{ber}(u)+\iota\mathrm{bei}(u)}{(\sqrt{2}\,/\,\sigma)(\mathrm{ber}'(u)+\iota\mathrm{bei}'(u))} \\ Z(\omega) &= R(\omega)+\iota\omega L_{in}(\omega) \end{aligned} \tag{5.9}$$

where

$$u = \frac{r\sqrt{2}}{\delta} \tag{5.10}$$

and

$$\delta = \left(\frac{2}{\omega\mu\sigma}\right)^{1/2} \tag{5.11}$$

r is the radius of the cross-section of the conductor, ω is the angular frequency and related to frequency in Hz as $\omega = 2\pi f$, μ is the magnetic permeability and σ is the electrical conductivity of the conductor. The terms ber(.) and ber$'$(.) are the real part of the Bessel function and its first derivative respectively and similarly bei(.) and bei$'$(.) are the imaginary parts. The bessel real and imaginary functions defined here are the historic names of the Kelvin functions, defined for a Bessel function of first kind J_ν with the phase of $(3/4)\pi$:

$$J_\nu(e^{\iota(3/4)\pi}u) = \mathrm{ber}_\nu(u)+\iota\mathrm{bei}_\nu(u) \tag{5.12}$$

The real and imaginary parts of the internal impedance give the resistance and inductance respectively.

$$\begin{aligned} R(\omega) &= \frac{1}{r}\left(\frac{\mu f}{2\pi\sigma}\right)^{1/2}\left[\frac{\mathrm{ber}(u)\mathrm{bei}'(u)+\mathrm{bei}(u)\mathrm{ber}'(u)}{(\mathrm{ber}'(u))^2+(\mathrm{bei}'(u))^2}\right] \\ \omega L_{in}(\omega) &= \frac{1}{r}\left(\frac{\mu f}{2\pi\sigma}\right)^{1/2}\left[\frac{\mathrm{ber}(u)\mathrm{bei}'(u)+\mathrm{bei}(u)\mathrm{ber}'(u)}{(\mathrm{ber}'(u))^2+(\mathrm{bei}'(u))^2}\right] \end{aligned} \tag{5.13}$$

Several researchers have presented simple models to include skin effects in the transmission line models [131], [135] and [122]. Since, our focus in the current study is not to model the skin effects but rather use the existing model and present a solution that is able to perform transient simulations with skin effects, we present here some of the simplified models and use them in our study.

For a transmission line with large radius compared to the skin depth [140], $\delta << 4r$ where skin depth δ is calculated as eq. (5.11).

$$R(\omega) = \frac{1}{\sigma(2\pi r)\delta} \ , \qquad L(\omega) = \frac{1}{\sigma(2\pi r)\delta\omega} \tag{5.14}$$

In the technical report by Phil Lucht [140], a low frequency limit is defined after which the resistance and inductance become functions of frequency, below this limit resistance and inductance are given as,

$$R = \frac{1}{\sigma\pi r^2} \ , \qquad L = \frac{\mu}{8\pi} \tag{5.15}$$

The low frequency resistance is the same as the DC resistance of a conductor in per unit length given by,

$$R = \frac{\rho}{\pi r^2} \tag{5.16}$$

where ρ is the resistivity of the conducting material.

The article by Monteiro et al [141] presents a simplified formulation for the calculation of skin effects on the transmission line wires. The formulation is based upon the Fourier transformation of Maxwell's equation presented above in eq. (5.9). The methodology presented by Monteiro et al is simple in terms of its application without the need to use Bessel functions and also presents good accuracy as it is directly developed from Maxwell's wave equations.

$$R(\omega) = \frac{\sum_{k=1}^{\infty} \left(R_k/(R_k^2 + \omega^2 L^2)\right)}{\left(\sum_{k=1}^{\infty} R_k/(R_k^2 + \omega^2 L^2)\right)^2 + \omega^2 \left(\sum_{k=1}^{\infty} L/(R_k^2 + \omega^2 L^2)\right)^2} \tag{5.17}$$

$$L(\omega) = \frac{\sum_{k=1}^{\infty} \left(L/(R_k^2 + \omega^2 L^2)\right)}{\left(\sum_{k=1}^{\infty} R_k/(R_k^2 + \omega^2 L^2)\right)^2 + \omega^2 \left(\sum_{k=1}^{\infty} L/(R_k^2 + \omega^2 L^2)\right)^2} \tag{5.18}$$

where

$$R_k = \frac{\xi_k^2}{4\pi\sigma r^2}; \quad L = \frac{\mu}{4\pi} \quad \text{and} \quad \xi_k = \frac{(2k-1)\pi}{2} + \frac{\pi}{4} \tag{5.19}$$

The units of R_k is $\Omega.m$ and L is H/m. The units of electrical conductivity σ is S/m and of the magnetic permeability μ is H/m. The term ξ_k is the k^{th} Bessel function root and is directly proportional to k. As mentioned previously, the transmission line in this study is considered to be a solid cylindrical copper wire, its radius and the electrical properties of the copper are listed in Table 5.2.

A comparison of different models was performed and the results were compared with the results from the study of Monteiro et al [141]. The results for the resistance and inductance with respect to frequency as presented in the Figure 5.1a and Figure 5.1b.

Parameter	**Value**	**Units**
Radius (r)	30	mm
Length (l)	300	km
Electrical Conductivity (σ)	5.96×10^7	S/m
Magnetic Permeability (μ)	1.26×10^{-6}	H/m

Table 5.2: Copper conductor wire properties

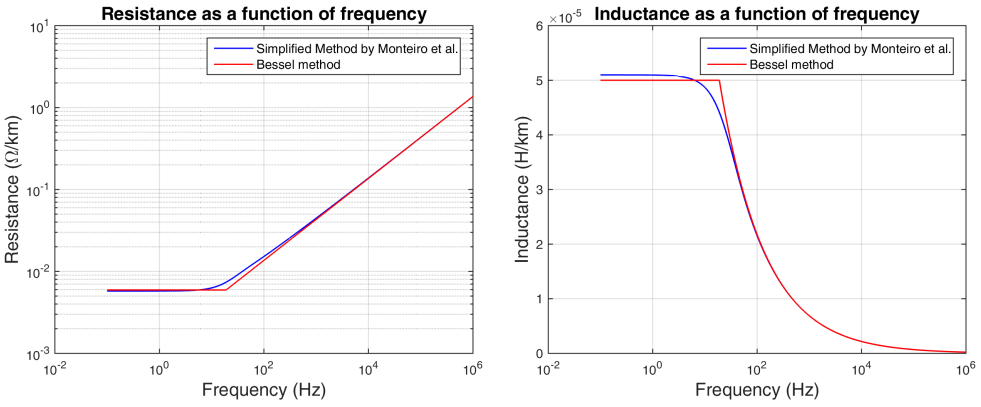

(a) Step Response (b) Sine Response

Figure 5.1: Frequency dependent resistance and inductance of a conductor

5.5 Distributed Parameters Model

5.5.1 Time Domain Simulation

We start with the time domain distributed parameters (DP) model. The electrical transmission lines provide the path for the voltage and current waves to propagate, the dynamics of the propagation is described by a distributed parameters model. This model depends upon the considerations taking into account like the losses and the frequency dependence of the parameters.

The distributed parameters model for a lossy transmission line with constant parameters can be written in the time domain as:

$$\begin{aligned} \frac{\partial v(x,t)}{\partial x} &= -L\frac{\partial i(x,t)}{\partial t} - Ri(x,t), \\ \frac{\partial i(x,t)}{\partial x} &= -C\frac{\partial v(x,t)}{\partial t} \end{aligned} \tag{5.20}$$

for $0 \leq x \leq l$, where $v(x,t)$ and $i(x,t)$ are the voltage and current in the line respectively, and the resistance, the inductance and the capacitance are represented by R, L, C respectively and these constants are positive and independent of frequency. The parameters R, L, C are given in per unit length and in distributed parameters model are used without multiplication with the length of the line. However, these parameters must be multiplied by the length of the line in case one is using any lumped circuit model for transmission lines e.g. *pi*-equivalent model. The effect of transverse conductance G of the line is neglected in this model. The interconnection between the transmission line, the load and the generator is performed using Kirschhoff's laws and the boundary values.

$$\begin{aligned} v(x,t)|_{x=0} &= V_0(t) \\ i(x,t)|_{x=l} &= 0 \end{aligned} \tag{5.21}$$

The term V_0 is the voltage source assumed to represent a generator, the boundary condition given above assumes that the voltage source is ideal, that is, the impedance is zero ($Z_0 = 0$) and the impedance at the receiving end ($x = l$) is infinite ($Z_l = \infty$).

The equation is converted to a single variable second order differential equation in time and space.

$$\frac{\partial^2 v}{\partial x^2} - LC\frac{\partial^2 v}{\partial t^2} - RC\frac{\partial v}{\partial t} = 0 \tag{5.22}$$

The eq. (5.22) is then discretized in time and space, using finite difference scheme for the time integration and finite elements for the space.

For a copper conductor wire, we can calculate the resistance and inductance from the eqs. (5.15), these values are listed in the Table 5.3. Solving a space time problem for these values, with a boundary condition representing a step as an input voltage V_0.

Parameter	Value	Units
Resistance (R)	5.7603×10^{-3}	Ω/km
Inductance (L)	5.0980×10^{-5}	H/km
Capacitance (C)	1.00×10^{-8}	F/km
Length (l)	300	km
Space Discretization (Δx)	1.0×10^{-1}	km
Total Time (T)	3.0×10^{-2}	sec
Time Step (Δt)	1.0×10^{-5}	sec

Table 5.3: Electrical Properties of a Copper Wire

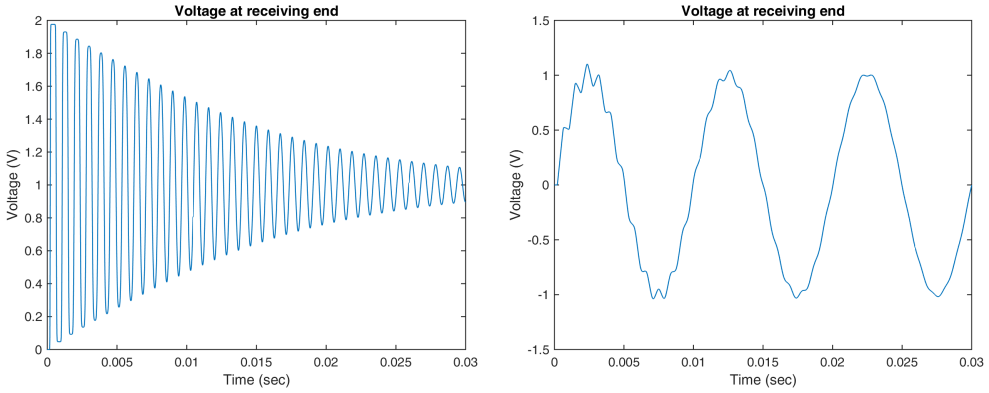

(a) Step Response (b) Sine Response

Figure 5.2: Time Simulation of constant parameters model in space-time domain

$$V_0 = \begin{cases} 0 \text{ for } t \leqslant 0 \\ 1 \text{ for } t > 0 \end{cases} \tag{5.23}$$

Also, a sine function with a frequency of $f = 100Hz$ was used as an input voltage for the same system

$$V_0 = \begin{cases} 0 \text{ for } t \leqslant 0 \\ \sin(2\pi 100t) \text{ for } t > 0 \end{cases} \tag{5.24}$$

The results of time simulation for the receiving end voltage $x = l$ is presented graphically in the Figure 5.2a and Figure 5.2b.

5.6 PGD Formulation

Skin effects phenomena resulting in frequency dependence of DP model cannot be numerically integrated in the time domain using the DP model presented in Sec. 4.2. As discussed in Sec. 5.2, the model has to be modified significantly in order to account for frequency dependence of parameters while using time domain models.

But, the problem in the frequency domain becomes a linear second order differential equation, where the parameters resistance and inductance are now a function of frequency. Fourier transformation of the time domain distributed parameters model gives the equation in the frequency domain as:

$$\begin{aligned} \frac{\partial \hat{V}(x,\omega)}{\partial x} &= -\hat{I}(x,\omega).(R + \iota L\omega), \\ \frac{\partial \hat{I}(x,\omega)}{\partial x} &= -\hat{V}(x,\omega).(\iota C\omega) \end{aligned} \tag{5.25}$$

Combining the two equations given in (5.25), we get a second order ordinary differential equations for voltage.

$$\frac{\partial^2 \hat{V}(x,\omega)}{\partial x^2} + (LC\omega^2 - \iota RC\omega)\hat{V}(x,\omega) = 0 \tag{5.26}$$

Corresponding boundary conditions in the frequency domain is given as,

$$\begin{aligned} \hat{V}(x,\omega)\Big|_{x=0} &= V_0 \\ \frac{\partial \hat{V}(x,\omega)}{\partial x}\Big|_{x=l} &= 0 \end{aligned} \tag{5.27}$$

This problem can be solved using PGD. A solution in separated representation as per PGD formulation is given as:

$$\hat{V}(x,\omega) = \sum_{i=1}^{n} X_i(x) O_i(\omega) \tag{5.28}$$

For the details about PGD formulation and its advantage, one can refer to several publications for example, [63, 109]. In Chapter 4 we presented the PGD formulation in detail for eq. (5.26) with Neumann boundary conditions.

Once, a separated solution using PGD with the boundary conditions given in eq. (5.27) is obtained, it is straightforward to get the desired time response using the discrete inverse Fourier function available in MATLAB. Using the separated representation of eq. (5.28), the differential equation of the DP model can be expressed in separated representation. In order to develop a PGD formulation, we derive a weak formulation of the problem.

Multiply eq. (5.26) with a test function $\delta V^*(x)$ where, δV represents the test function and $\delta V^*(x)$ represents the complex conjugate.

$$\int_{\Omega_x \times \Omega_\omega} \delta V^* \frac{\partial^2 \hat{V}}{\partial x^2}\, dx d\omega - \int_{\Omega_x \times \Omega_\omega} \delta V^* f(\omega) \hat{V}\, dx d\omega = 0 \tag{5.29}$$

where, $f(\omega) = (LC\omega^2 - \iota RC\omega)$.

We assume the test function $\delta V^*(x,\omega)$ in the separated form as,

$$\delta V^*(x,\omega) = O^*(\omega)\delta X^*(x) + X^*(x)\delta O^*(\omega) \tag{5.30}$$

Entity	Constant Parameters	Frequency Dependent
ε_p	10^{-10}	10^{-10}
ε_n	10^{-10}	10^{-10}
n	40	14
Residual	5×10^{-16}	4×10^{-19}
Computation time	250 sec	50 sec

Table 5.4: PGD Criteria

Since, the problem is now separated in the space $X(x)$ and the frequency $O(\omega)$, we have to solve two problems using FEM once for the space domain and then for the frequency domain. The weak formulation for the one dimensional problem in space is,

$$\begin{aligned}
&\int_{\Omega_x \times \Omega_\omega} \frac{d\delta X_n^*}{dx}\frac{dX_n^p}{dx} O_n^{p-1*} O_n^{p-1}\, dx\, d\omega + \int_{\Omega_x \times \Omega_\omega} f(\omega)\delta X_n^* X_n^p O_n^{p-1*} O_n^{p-1}\, dx\, d\omega = \\
&- \int_{\Omega_x \times \Omega_\omega} \sum_{i=1}^{n-1} \frac{d\delta X_n^*}{dx}\frac{dX_i}{dx} O_n^{p-1*} O_i\, dx\, d\omega - \int_{\Omega_x \times \Omega_\omega} f(\omega) \sum_{i=1}^{n-1} \delta X_n^* X_i O_n^{p-1*} O_i\, dx\, d\omega \\
&+ \int_{\Omega_\omega} \delta X_n^* O_n^{p-1*} \hat{I}.(\iota L\omega + R)\, d\omega
\end{aligned} \tag{5.31}$$

and for the problem to be solved in the frequency domain, the weak formulation will be

$$\begin{aligned}
&\int_{\Omega_x \times \Omega_\omega} \frac{dX_n^{p*}}{dx}\frac{dX_n^p}{dx} \delta O_n^* O_n^p\, dx\, d\omega + \int_{\Omega_x \times \Omega_\omega} f(\omega) X_n^{p*} X_n^p \delta O_n^* O_n^p\, dx\, d\omega = \\
&- \int_{\Omega_x \times \Omega_\omega} \sum_{i=1}^{n-1} \frac{dX_n^{p*}}{dx}\frac{dX_i}{dx} \delta O_n^* O_i\, dx\, d\omega - \int_{\Omega_x \times \Omega_\omega} f(\omega) \sum_{i=1}^{n-1} X_n^{p*} X_i \delta O_n^* O_i\, dx\, d\omega \\
&+ \int_{\Omega_\omega} X_n^{p*}|_{x=0} \delta O_n^* \hat{I}.(\iota L\omega + R)\, d\omega
\end{aligned} \tag{5.32}$$

The tolerances selected for the termination of the greedy algorithm ε_p and the tolerance for termination of enrichment process ε_n, along with the number of modes n in both the constant parameters and frequency-dependent parameters are listed in Table 5.4.

The boundary condition in eq. (5.27) is an equivalent of having an impulse function at the source which gives the impulse response or the transfer function $\hat{H}$ of the transmission line. The voltage impulse response at the receiving end is given as:

$$\hat{H}(x = l, \omega) = \sum_{i=1}^{n} X_i(x = l) O_i(\omega) \tag{5.33}$$

Once, this is done, the time response to any arbitrary condition at the source node is then straightforward multiplication of the voltage function in frequency domain

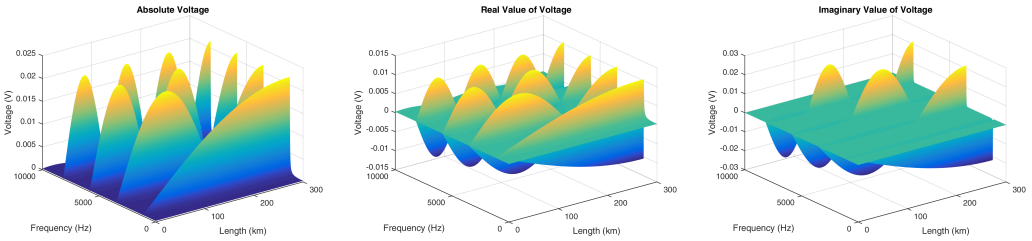

(a) Absolute Value (b) Real Value (c) Imaginary Value

Figure 5.3: Voltage in space-frequency domain with constant parameters

with the particular solution of the PGD at the receiving node. Then the frequency response to an arbitrary function $\hat{V}_0$ is given as

$$\hat{V}(x = l, \omega) = \hat{H}(x = l, \omega) \cdot \hat{V}_0 \tag{5.34}$$

5.6.1 Verification of PGD results

In this section, we first present the time response using inverse Fourier transform of the PGD solution particularized at the receiving end.

The PGD solution in terms of voltage on a space-frequency domain is presented in Figure 5.3a to Figure 5.3c and only the first ten enrichment modes from PGD solutions for the sake of clarity are presented in the Figure 5.4. While Figure 5.5a and Figure 5.5b shows the time response to a unit step function and a sinusoidal wave respectively obtained from the separated solution of PGD.

The results from Figure 5.6a and Figure 5.6b shows good correlation between the solution from time integration and the PGD solution. Therefore, it is established that the PGD solution is an accurate representation of the DP model of transmission lines. As seen in Figure 5.6a the time-space simulation is affected by artificial damping due to the low order finite difference scheme used to integrate the equation in time. On the other hand this effect is avoided when using space-frequency formulation.

5.7 PGD for frequency dependent parameters

The benefit of solving DP model in the frequency domain in the separated representation of PGD is the easy, fast and accurate solution with the option of a parametric solution. PGD methods provide the best option for parametric problems both in terms of computational efficiency and ease of solving the problem. In the case of skin effects, the eq. (5.26) now has parameters resistance R and inductance L as a function of frequency ω. As explained earlier time integration of such problems is almost impossible to achieve and hence PGD provides real accurate option to solve such problems. The problem is similar to the case of fractional derivatives which is similar to the fractional RLC circuit [142].

Eq. (5.26) with R and L as functions of frequency reads as:

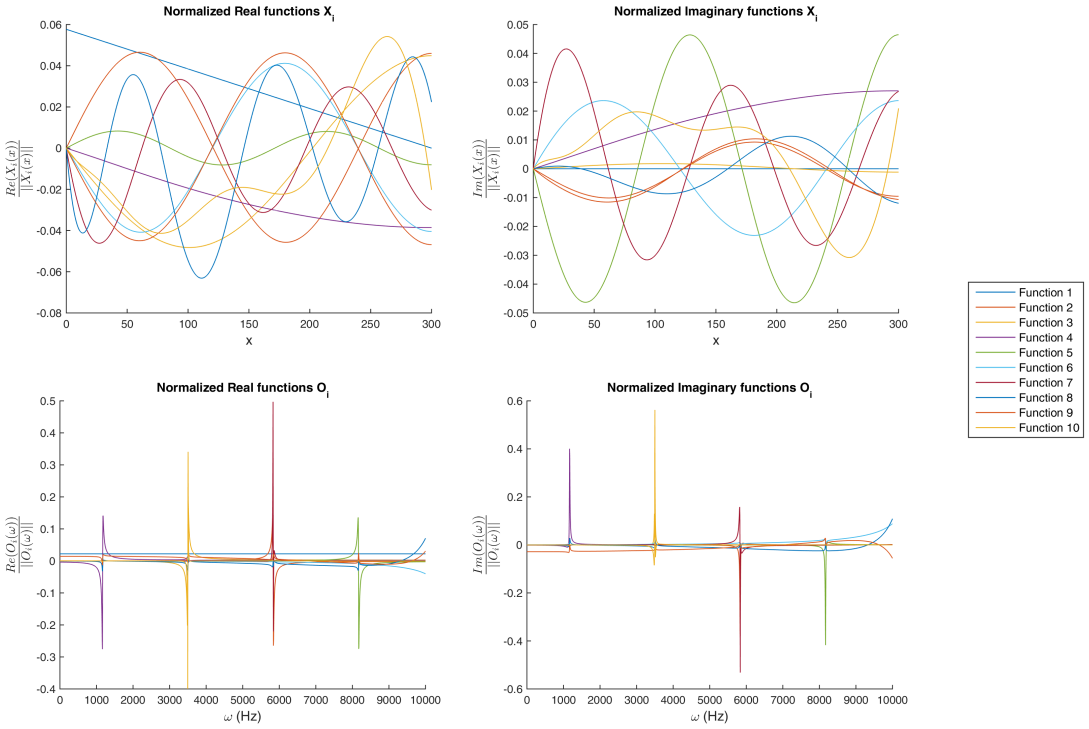

Figure 5.4: Modes of PGD Solution

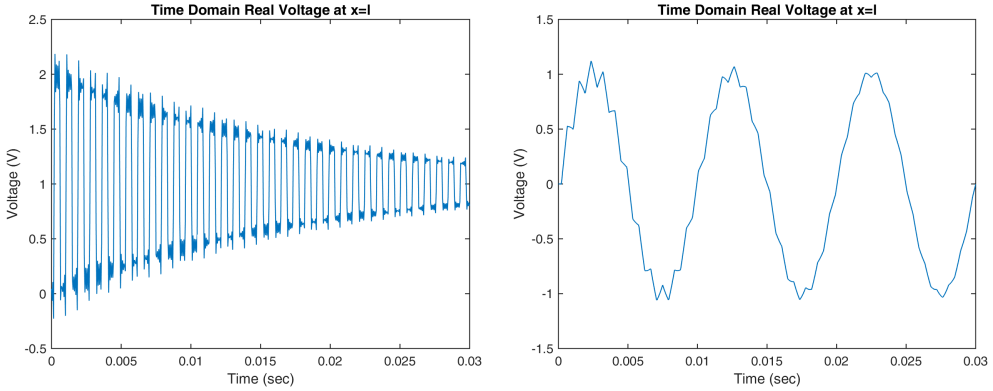

(a) Step Response (b) Sine Response

Figure 5.5: Time Response by Inverse Fourier of the PGD Solution

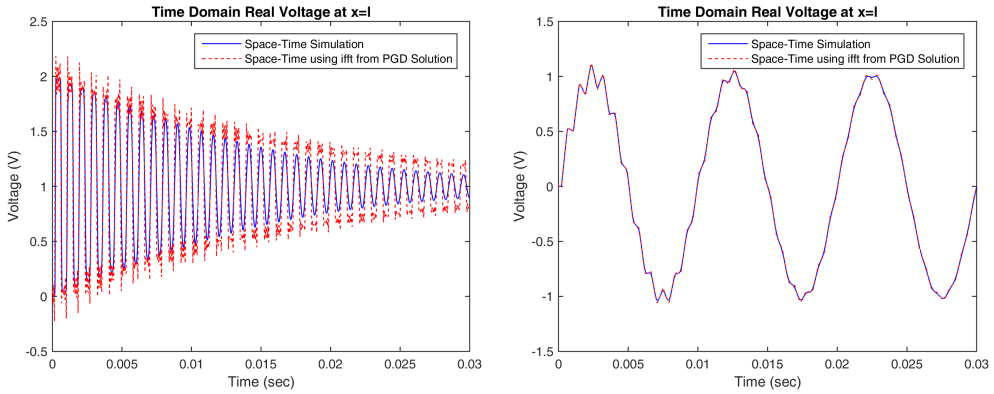

(a) Step Response (b) Sine Response

Figure 5.6: Comparison of Time Response between PGD Solution and Time Integration

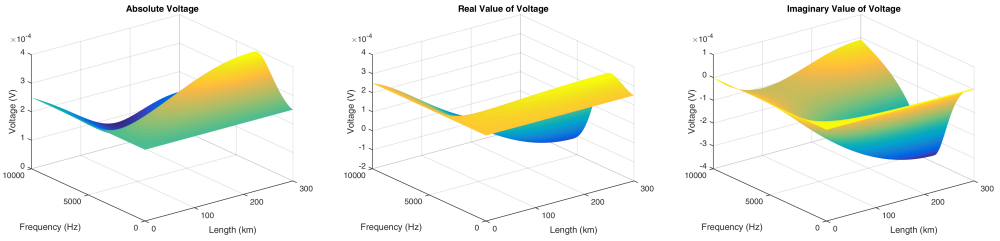

(a) Absolute Value (b) Real Value (c) Imaginary Value

Figure 5.7: Voltage in space-frequency domain with skin effects included

$$\frac{\partial^2 \hat{V}(x,\omega)}{\partial x^2} + (L(\omega)C\omega^2 - \iota R(\omega)C\omega)\hat{V}(x,\omega) = 0 \tag{5.35}$$

The increase in the resistance with the frequency and a simultaneous decrease in the inductance results in a system more damped than the system with constant resistance and inductance. This effect can be noticed in the Figure 5.7a to Figure 5.7c showing the voltage in the space-frequency domain, there is only one peak visible with a much less amplitude.

From the modes presented in Figure 5.8, it is also observed the number of enrichment modes for the PGD solution are only 14 including the first mode which includes the effect of the Dirichlet boundary condition. Performing inverse Fourier transform on the PGD solution for step and sin function as the input voltage at the sending end, the receiving end voltages are obtained as:

The effect of increased damping due to the increase in resistance can be compared in the receiving end voltage for the frequency dependent and constant parameters solution given in the Figure 5.9. In Figure 5.10, the two responses from the constant parameters and frequency dependent parameters are plotted on top of each other for a direct comparison. The increased damping removes almost all the oscillations observed in the constant parameters solution of Figure 5.5a and Figure 5.5b.

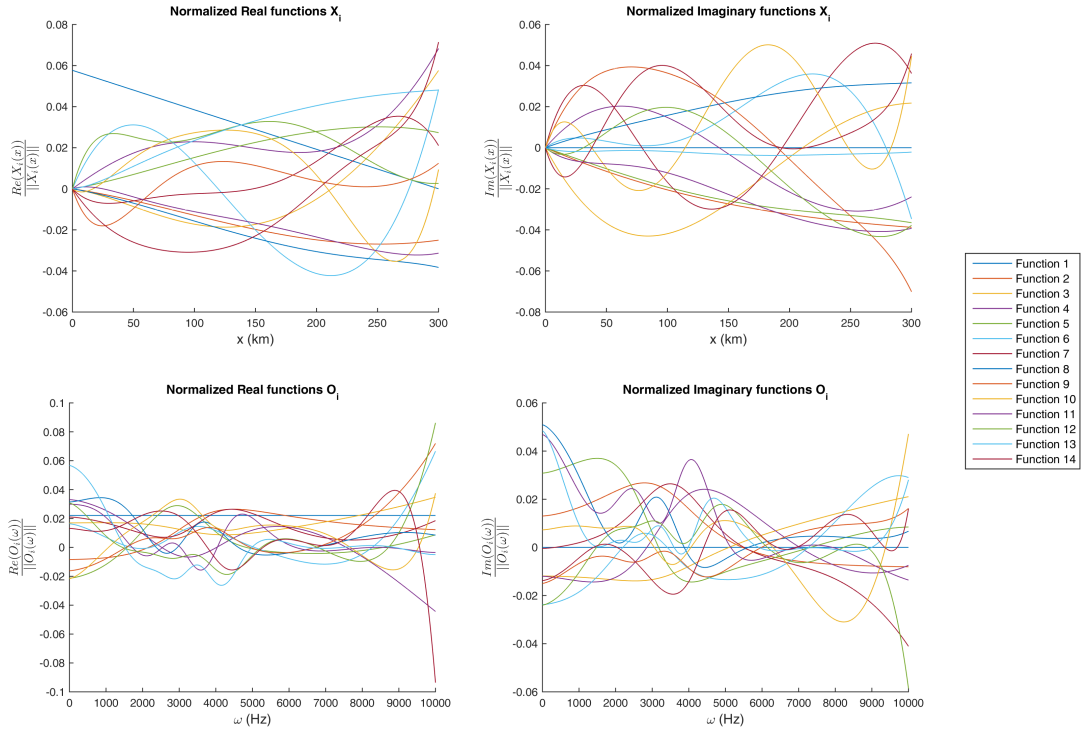

Figure 5.8: Modes of PGD Solution for frequency dependent problem

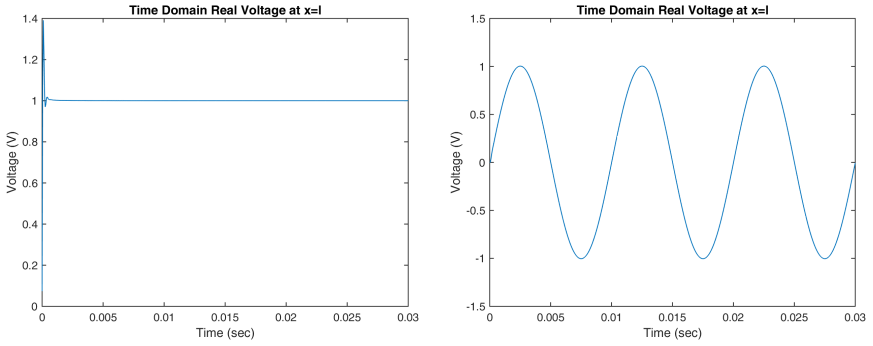

(a) Step Response (b) Sine Response

Figure 5.9: Time response from PGD solutions for frequency dependent parameters

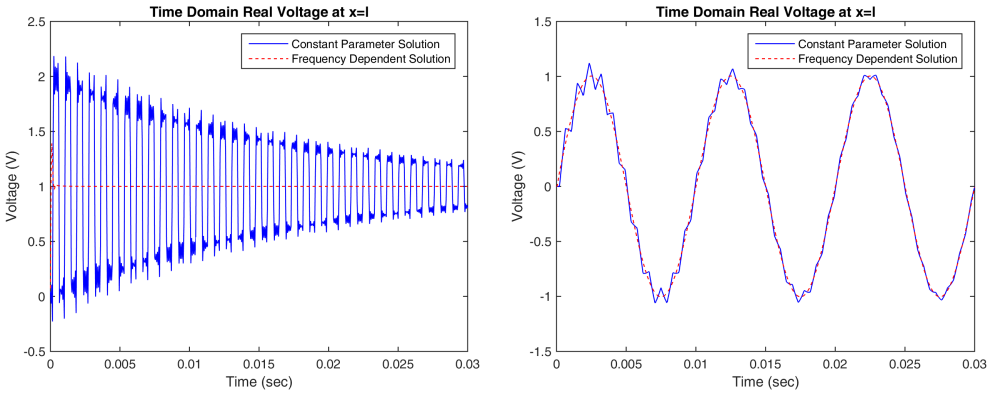

(a) Step Response (b) Sine Response

Figure 5.10: Comparison of response between constant and frequency dependent parameters

Entity	Parametric Frequency Dependent PGD
Δl	0.05
ε_p	10^{-10}
ε_n	10^{-10}
n	67
Residual	1×10^{-7}
Computation time	700 sec

Table 5.5: PGD Criteria

5.7.1 Parametric Solution

The advantage of PGD based harmonic analysis is that any parameter can be introduced as an added dimension to the separated representation. As an initial step, we introduce length of the transmission line as a new dimension for the parametric problem. The solution now is given as:

$$\hat{V}(x, \omega, l) = \sum_{i=1}^{n} X_i(x) O_i(\omega) D_i(l) \tag{5.36}$$

where D_i represents the modes of the dimension introduced to represent length.

The mathematical formulation of the problem remains similar and there is no significant additional computational cost to the problem. For the case, we have reported in this study, the new dimension of transmission line length is considered for a range $(200, 300)$ km. The discretization for the space and frequency have been kept the same as in previous case. The discretization and the other information valuable to gauge the PGD solution is listed in Table 5.5. Only the first ten modes of the PGD solution for the three dimensions are presented in Figure 5.11, the total number of enrichment modes are 67.

The advantage of parametric solution is presented in Figure 5.12 where the vari-

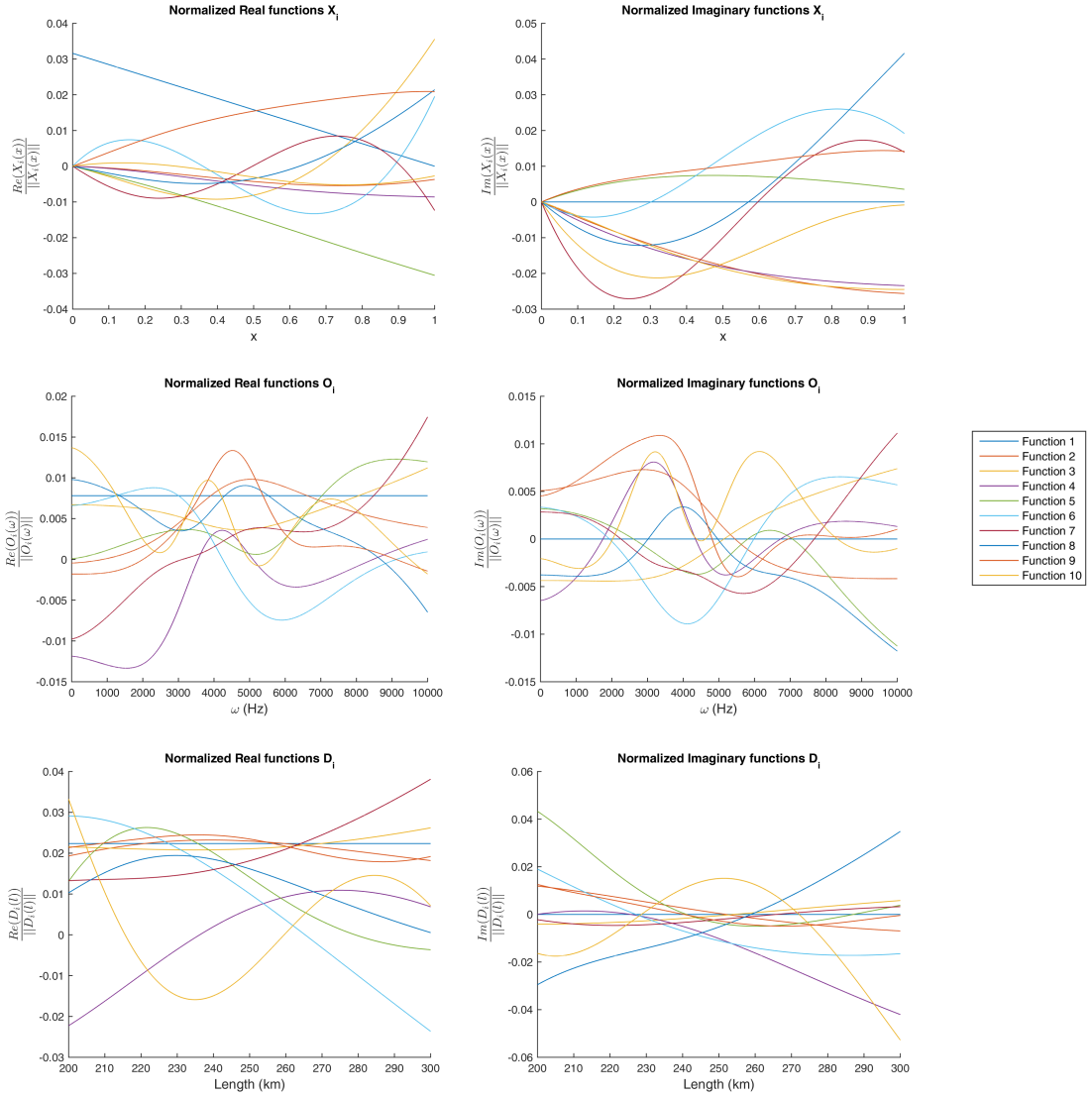

Figure 5.11: Modes of PGD Solution for frequency dependent problem with length as parameter

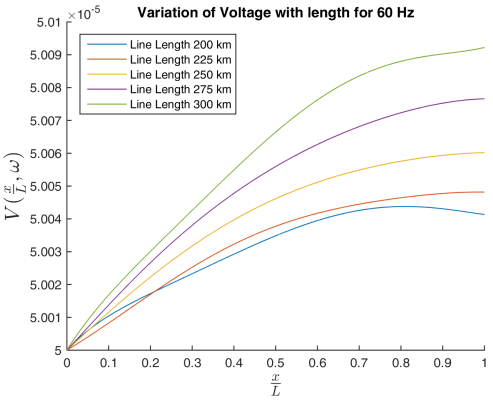

Figure 5.12: Variation of Voltage along the transmission line for different lengths at 60 Hz

Modes	**Maximum Error**		**Frobenius Norm of Error Matrices**	
	Absolute	Relative	Absolute	Relative
67	1.08×10^{-8}	2.26×10^{-4}	6.45×10^{-5}	0.8164

Table 5.6: Error of PGD solution with length as a parameter

ation of voltages along the transmission line with different lengths for a frequency of 60 Hz is plotted. Another advantage of such a solution is in the sensitivity or uncertainty analysis, in such an analysis a fixed point is selected and a variation of usually 5% in the independent variable and its effect on the variable of interest is studied. With a PGD solution, we already have a complete solution as a curve and the derivative can be easily evaluated for the sensitivity analysis.

For a specific case with transmission line length of 300 km, the solution can be particularized from the parametric PGD solutions and the results and the corresponding errors are presented in Figures 5.13. The length of 300 km is chosen such that it can be compared with the solution provided earlier in Figure 5.7 and the errors presented are compared with this solution. The errors are listed in the Table 5.6.

5.8 Application to Commercial Transmission Lines

As stated in the earlier Section 5.4 in this chapter, transmission lines used commercially are different in geometry and construction to the one presented previously. The above discussion is presented for the simplification provided by the assumption that the transmission line is a solid cylindrical conductor. The method can be applied to the transmission lines that are commonly used in the power grids worldwide, here we apply the method on two such types of transmission lines known with their trade names as “Falcon” and “Grosbeak”. First, we introduce some concepts related to the transmission lines.

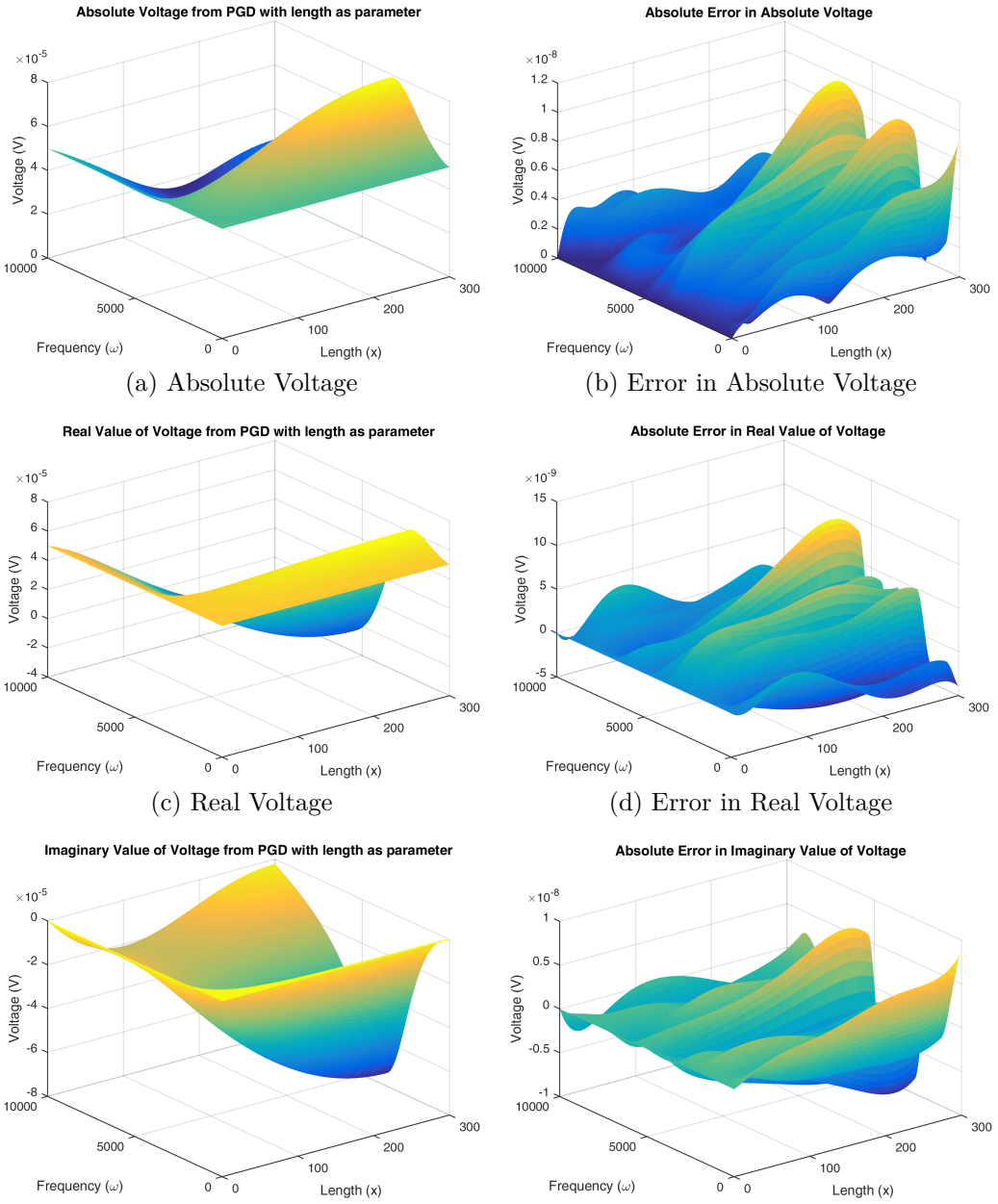

(a) Absolute Voltage

(b) Error in Absolute Voltage

(c) Real Voltage

(d) Error in Real Voltage

(e) Imaginary Voltage

(f) Error in Imaginary Voltage

Figure 5.13: Parametric PGD Solution for line of 300 km length

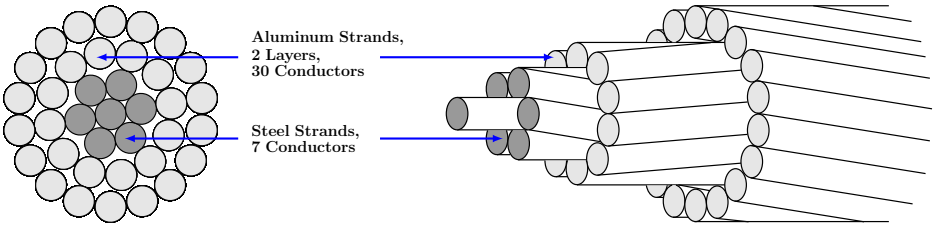

Figure 5.14: Typical construction of ACSR [2]

5.8.1 Transmission Line Construction and Materials

Typical overhead transmission lines use aluminum as the conducting materials. There are several types of commercial transmission lines using aluminum as the conductors; aluminum-conductor-steel-reinforced (ACSR), aluminum-conductor-alloy-reinforced (ACAR), all-aluminum-conductor (AAC), and all-aluminum-alloy-conductor (AAAC). These transmission lines especially ACSR are the most preferred ones, these are concentrically stranded conductor of one or more layers of aluminum wires wrapped around high strength steel wires. The steel wires are used to provide strength without comprising on the current carrying capacity known as 'Ampacity'. A typical construction of ACSR transmission lines is shown in Figure 5.14.

5.8.2 Resistance

The DC resistance for a transmission line is given as:

$$R_{DC} = \frac{\rho l}{A} \tag{5.37}$$

where, ρ is the resistivity (Ωm) of the conducting material, l is the length (m) of the line and A is the cross-sectional area (m^2). Considering $A = \pi r^2$ and $\rho = 1/\sigma$, eq. (5.37) is similar to eq. (5.16).

As described earlier, the frequency of the AC current produces a skin effect resulting in increase of the resistance. In general, for a 60 Hz an empirical skin correction factor k is estimated to be around 1.02 [2].

$$R_{AC} = kR_{DC} \tag{5.38}$$

The value of resistance at 60 Hz and at a specified temperature is given in the chapter by Manuel Reta-Hernández [2]. Besides frequency, the resistance of a transmission line is effected by temperature, spiraling of stranded conductors and arrangement of bundle conductors. Although, eq. (5.37) is primarily for the solid cylindrical conductor it can be used to estimate the resistance per unit length of the ACSR transmission line given the effective cross-sectional area and the conductivity of aluminum. These values are provided in most of the fact sheets by the manufacturers of the transmission line wires. The typical values of conductivity and magnetic permeability of different materials is presented in the Table 5.7.

Material	Conductivity at 20° C (S/m)	Permeability (H/m)
Aluminum	3.50×10^7	1.256665×10^{-6}
Copper	5.96×10^7	1.256629×10^{-6}
Steel	6.99×10^6	1.26×10^{-4}

Table 5.7: Electrical Properties of conductor materials

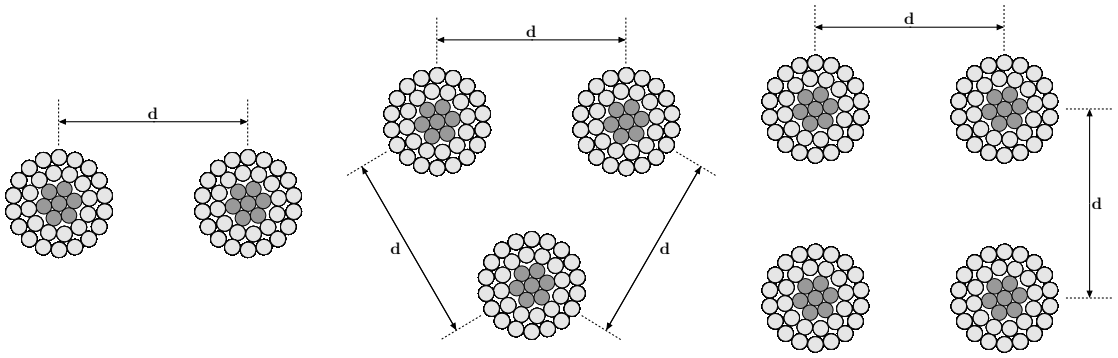

Figure 5.15: Example of stranded conductors in bundles per phase of two, three or four [2]

5.8.3 Inductance

For a solid cylindrical conductor of radius r with a current I across it. The material is assumed to be non-magnetic and the current distribution to be uniform, i.e., no skin effect present. As described in the earlier section, the internal inductance of a solid cylindrical conductor is given by second of the two in eq. (5.15).

$$L_{int} = \frac{\mu}{8\pi} \quad (H/m) \tag{5.39}$$

The effect of frequency is felt on internal inductance which tends to diminish with the increasing frequency. However, for high voltage transmission lines there are more than one stranded conductors arranged in bundles per phase. An example of the bundles is given in the chapter of transmission line parameters [2] and presented here in Figure 5.15.

The presence of more than one stranded conductor results in another type of inductance categorized as the external inductance. The calculation of the external inductance is based on the assumption that the current in the neighboring conductor is at the surface of the neighboring conductor, i.e., the skin effect is maximum. Therefore, this external inductance is considered constant with increase in frequency. The total inductance at any point D on the conductor L_{tot} which is the sum of internal L_{int} and external inductance L_{ext} is given as:

$$L_{tot} = \frac{\mu_0}{2\pi} \ln\left(\frac{D}{GMR}\right) \quad (H/m) \tag{5.40}$$

where, GMR is the geometric mean radius, radius of a fictional conductor that has

no internal flux but having same inductance as the actual conductor with radius r and is given as:

$$GMR = e^{-1/4}r = 0.7788r \tag{5.41}$$

Therefore, the external inductance can be calculated from the total inductance ($L_{ext} = L_{tot} - L_{int}$). Generally, the manufacturers do not provide the total inductance but the inductive reactance.

5.8.4 Inductive Reactance

The value of the inductive reactances given by the manufacturers is the sum of the external and internal inductive reactance. Inductive Reactance is the resistance of an inductor when an AC current is applied across it. It is fairly simple to calculate inductance from inductive reactance and vice versa using the following relation.

$$X_L = \omega L = 2\pi f L \tag{5.42}$$

5.8.5 Capacitance

For a solid cylindrical conductor with radius r, the capacitance between two points P_1 and P_2 is given as,

$$C = \frac{2\pi\varepsilon_0}{\ln\left[\frac{x_2}{x_1}\right]} \quad (F/m) \tag{5.43}$$

where, ε_0 is the free space permittivity. For a coaxial cable with outer radius R_2 and inner radius R_1, the capacitance is given as,

$$C = \frac{2\pi\varepsilon_0}{\ln\left[\frac{R_2}{R_1}\right]} \quad (F/m) \tag{5.44}$$

5.8.6 Capacitive Reactance

Similar to the inductive reactance, the values provided by the manufacturer for capacitance is in terms of resistance known as capacitive reactance X_C. The relationship between capacitive reactance and capacitance is given as,

$$X_C = \frac{1}{\omega C} = \frac{1}{2\pi f C} \tag{5.45}$$

Now, we have presented the basic information needed to explain the transmission lines that we have used in this study, we can apply our methodology to two ACSR transmission lines Grosbeak and Falcon. Table 5.8 gives the information that is available from the manufacturers for these and similar transmission lines. The reason to choose two different types of ACSR transmission line is to provide a comparison for very different types of transmission lines. From the data provided in Table 5.8, it can be observed that Falcon type line is thicker than the Grosbeak but its resistance and reactances are small as compared to the Grosbeak line.

Code	**Cross-Section Area**		**Resistance** $25°C$ **(mΩ/km)**		**GMR**	**Reactances (60 Hz)**	
	Total (mm^2)	Aluminum (mm^2)	DC	AC (60 Hz)		X_L (Ω/km)	X_C (Ω/km)
Falcon	908	806	35.9	37.4	15.91	0.312	0.187
Grosbeak	375	322	91.7	92.2	10.21	0.346	0.209

Table 5.8: ACSR Data

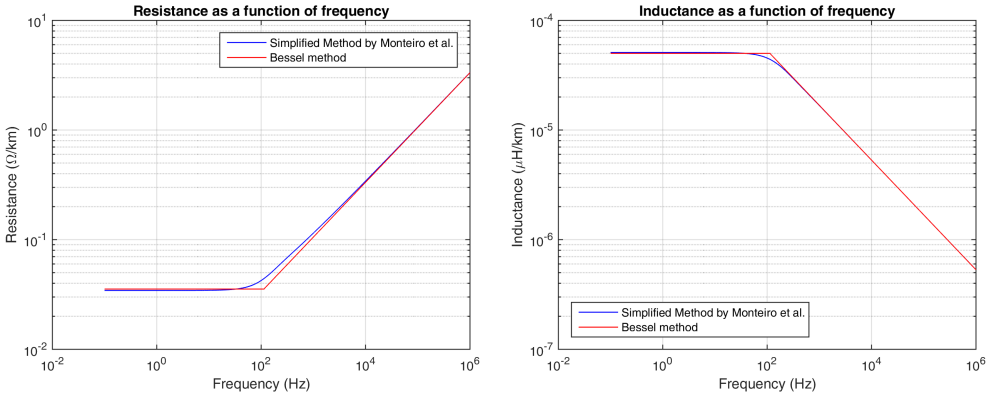

(a) Resistance (b) Internal Inductance

Figure 5.16: Skin Effect for ACSR Falcon transmission line

5.8.7 Skin Effects for ACSR Transmission Lines

The skin effect on the ACSR transmission lines resistance and inductance is presented in the Figure 5.16 and Figure 5.17 for Falcon and Grosbeak respectively. Here, the internal inductance is presented which decreases with increase in frequency. Thus, the total inductance which is the sum of internal and external inductance also decreases because of the vanishing contribution from the internal inductance.

5.8.8 PGD Results for Constant Parameters Model of Transmission Lines

The PGD modes for the two types of transmission lines are given here and the voltage distribution in the space-frequency domain with visible resonances are presented in the following figures. For Falcon type ACSR transmission lines the first 10 modes of the total 187 modes are presented in Figure 5.18. The voltage distribution from the PGD solution is presented in Figure 5.19.

For Grosbeak type ACSR transmission lines the modes are given in Figure 5.20. Again only first 10 modes of total 200 are presented to demonstrate the trend in

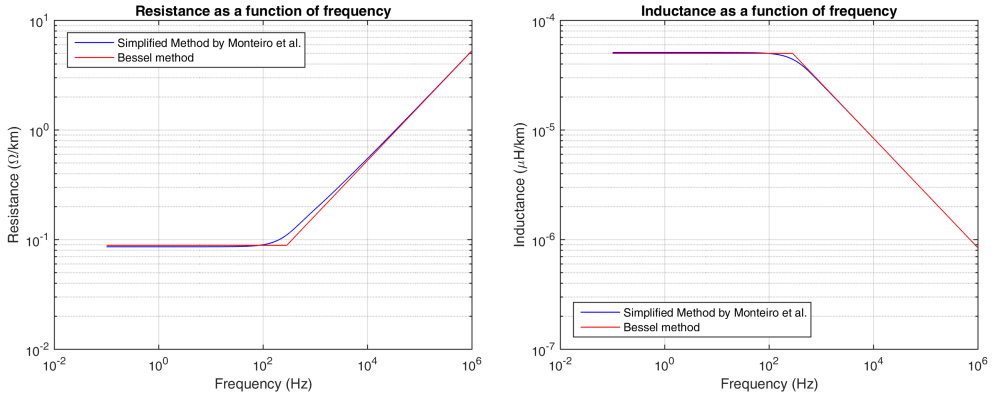

(a) Resistance (b) Internal Inductance

Figure 5.17: Skin Effect for ACSR Grosbeak transmission line

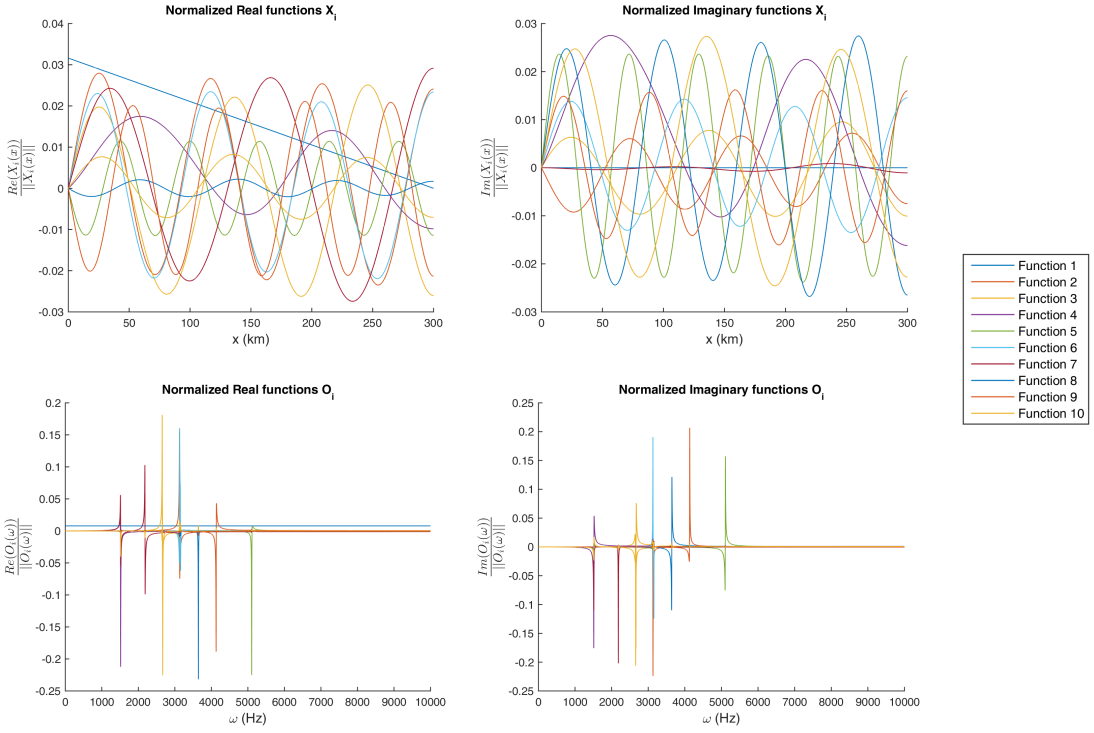

Figure 5.18: PGD modes for ACSR Falcon transmission line

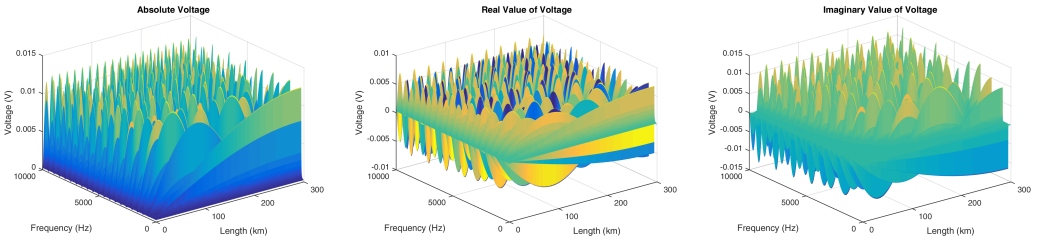

(a) Absolute Voltage (b) Real Voltage (c) Imaginary Voltage

Figure 5.19: Voltage in space-frequency domain with constant parameters for ACSR Falcon line

the enrichment process of PGD. The voltage distribution from the PGD solution is presented in Figure 5.21a to Figure 5.21c.

5.8.9 Time Simulation for Constant Parameters Model of ACSR Lines

The response to step and sinusoidal input voltage from the time simulation for the Falcon line is given in Figure 5.22a and Figure 5.22b. The time response for the Grosbeak line for similar inputs is given in Figure 5.23a and Figure 5.23b. The time results from the solution using PGD approach and applying inverse Fourier transform for Falcon transmission line are presented in Figure 5.22c and Figure 5.22d and compared in Figure 5.22e and Figure 5.22f. Similarly, the results for Grosbeak transmission line are presented in Figure 5.23c to Figure 5.23f.

5.8.10 PGD Results for Frequency-Dependent Model of Transmission Lines

The results with the skin effects included for the Falcon line are presented in Figure 5.25. It is evident from these figures that the skin effect dampens the system. The first 10 modes from the PGD solution is presented in Figure 5.24. The general trend is mirrored in the results for the Grosbeak transmission line which can be observed from the voltage distribution of Figures 5.27. Again, only the first 10 modes are presented for the Grosbeak line are given in Figure 5.26. In both the cases the total number of modes are 200.

5.8.11 Time Simulations for Frequency-Dependent Model of Transmission Lines

The time response for skin effects is very difficult to obtain however J. R. Marti [125] has presented a methodology to overcome the issues of instability and accuracy albeit for the ground return effect. The effect of the ground return is similar to the skin effects that we have presented in the current study.

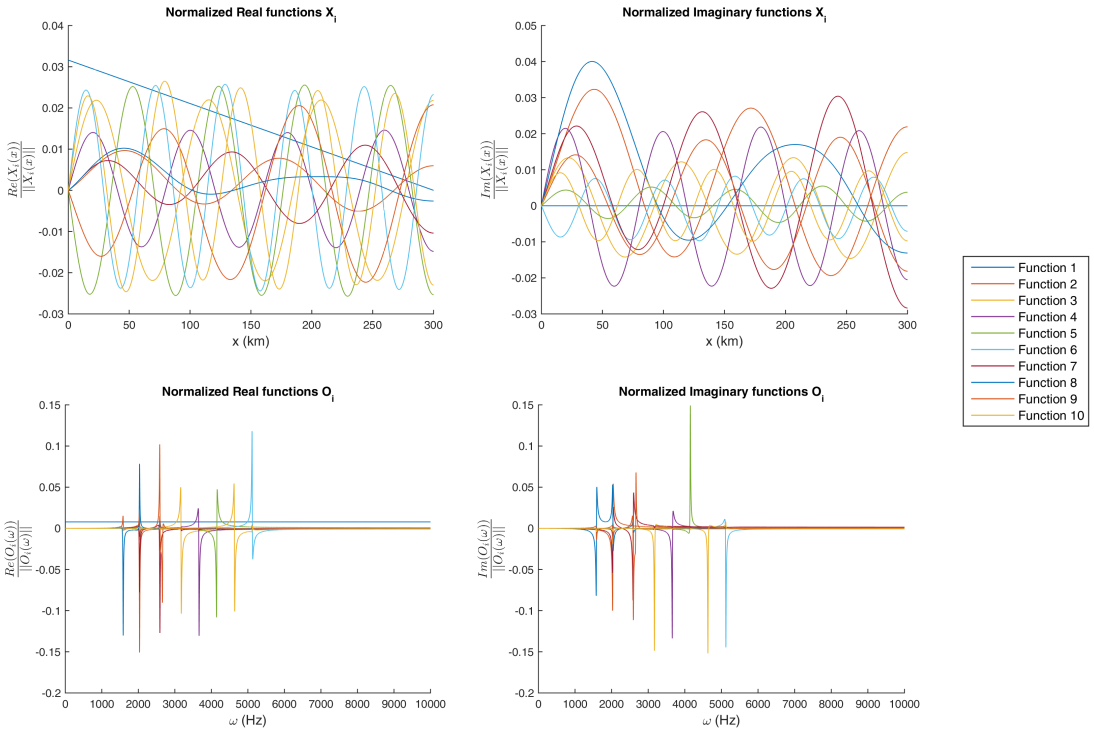

Figure 5.20: PGD modes for ACSR Grosbeak transmission line

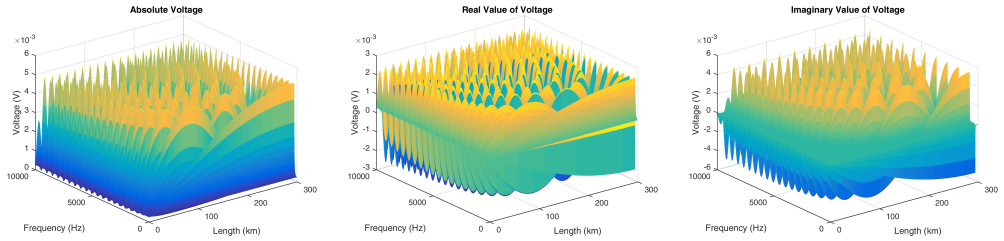

(a) Absolute Voltage (b) Real Voltage (c) Imaginary Voltage

Figure 5.21: Voltage in space-frequency domain with constant parameters for ACSR Grosbeak line

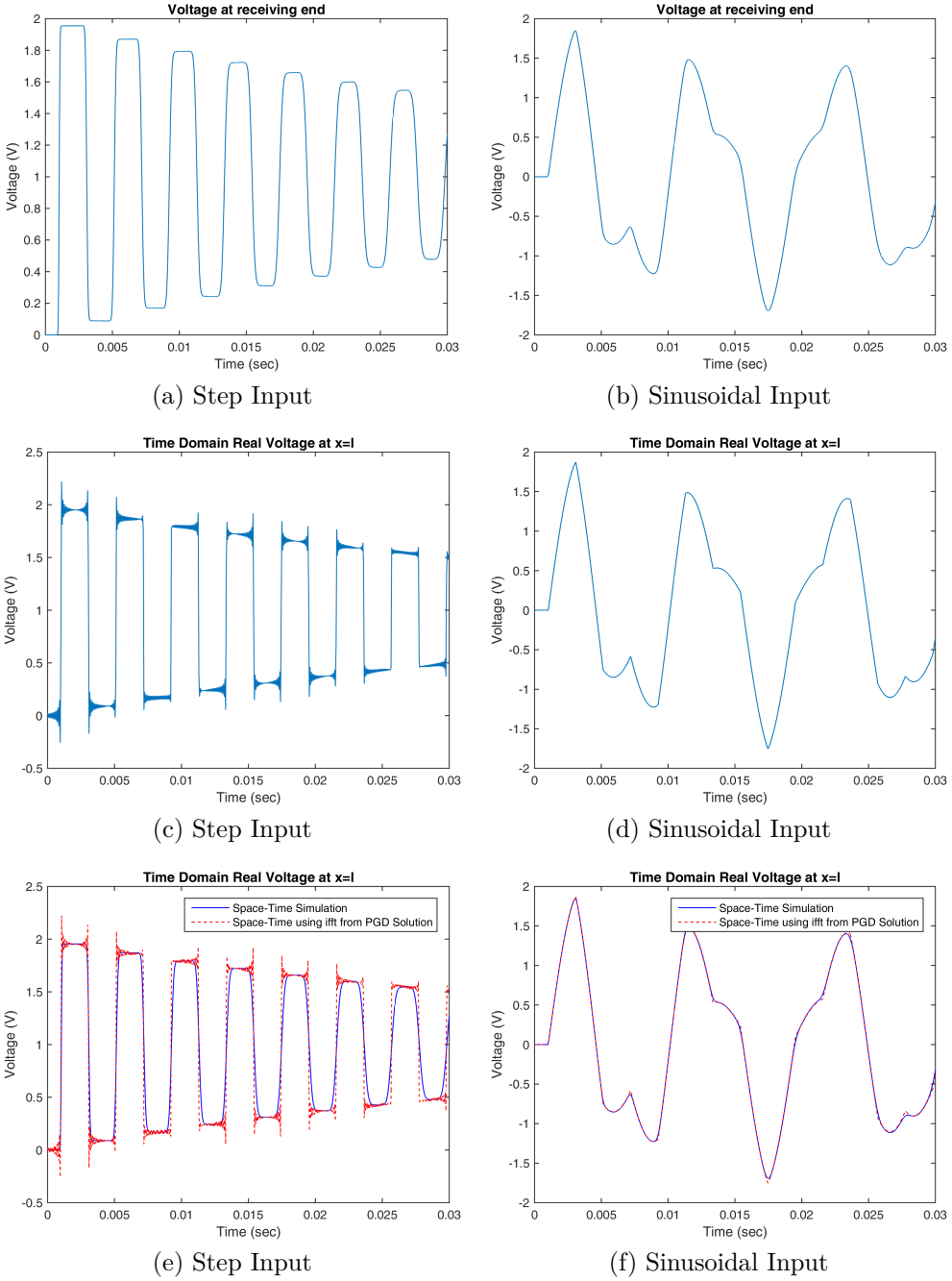

(a) Step Input (b) Sinusoidal Input

(c) Step Input (d) Sinusoidal Input

(e) Step Input (f) Sinusoidal Input

Figure 5.22: Time Response for Falcon Transmission Line, (a) and (b) using Time-Domain simulations, (c) and (d) using inverse Fourier on PGD and (e) and (f) comparison of two approaches

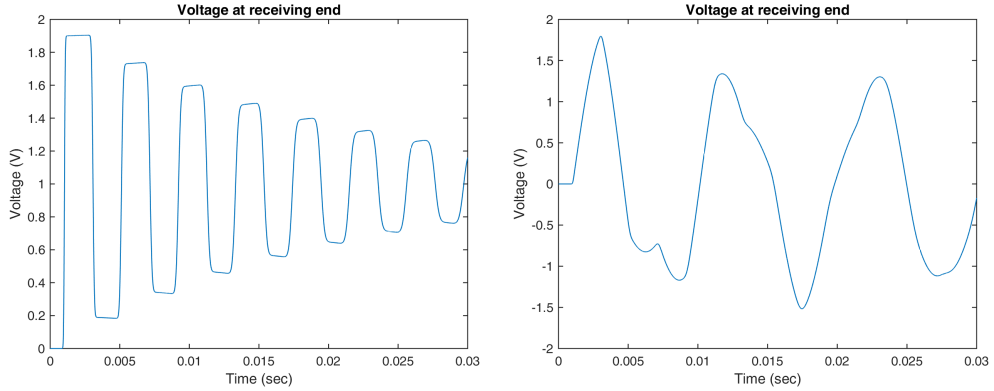

(a) Step Input

(b) Sinusoidal Input

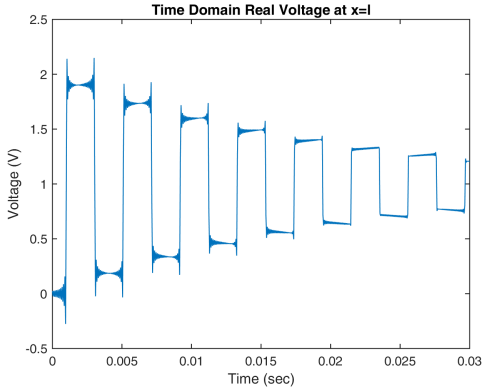

(c) Step Input

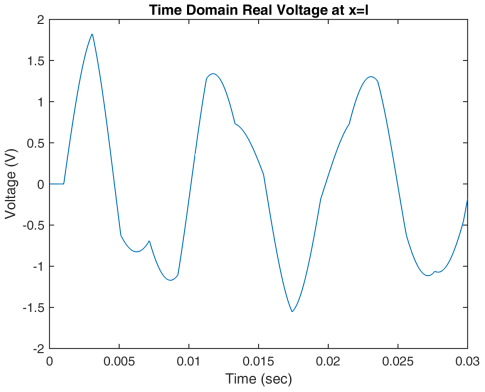

(d) Sinusoidal Input

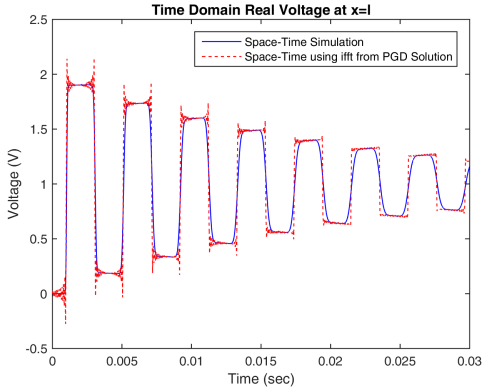

(e) Step Input

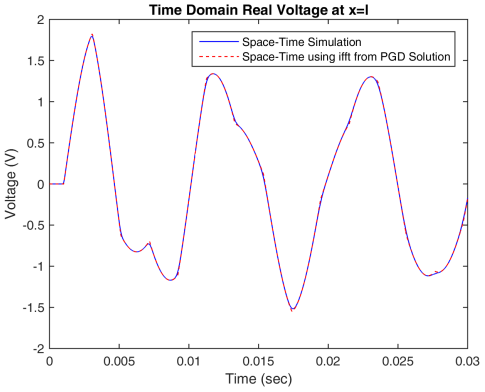

(f) Sinusoidal Input

Figure 5.23: Time Response for Grosbeak Transmission Line, (a) and (b) using Time-Domain simulations, (c) and (d) using inverse Fourier on PGD and (e) and (f) comparison of two approaches

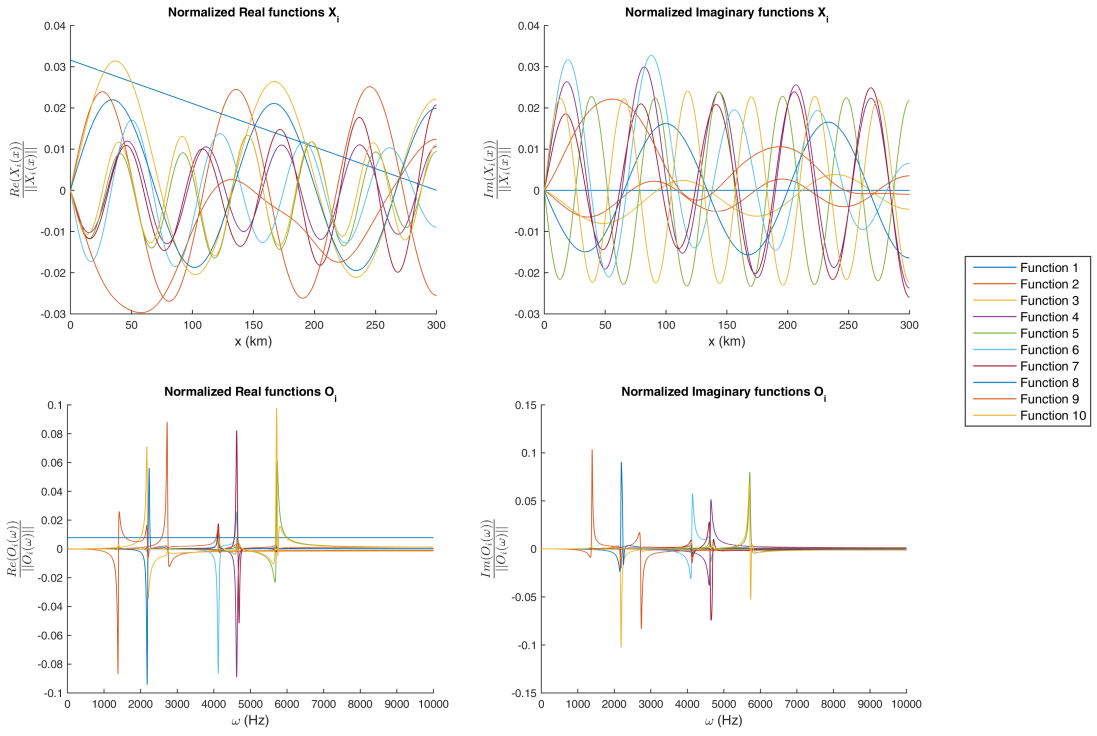

Figure 5.24: PGD modes for ACSR Grosbeak transmission line

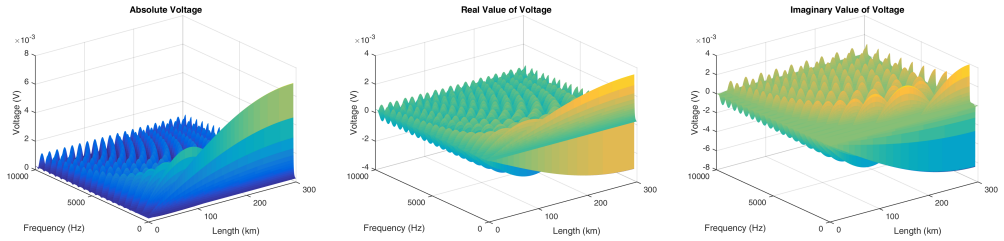

(a) Absolute Voltage (b) Real Voltage (c) Imaginary Voltage

Figure 5.25: Voltage in space-frequency domain with skin effects for ACSR Falcon line

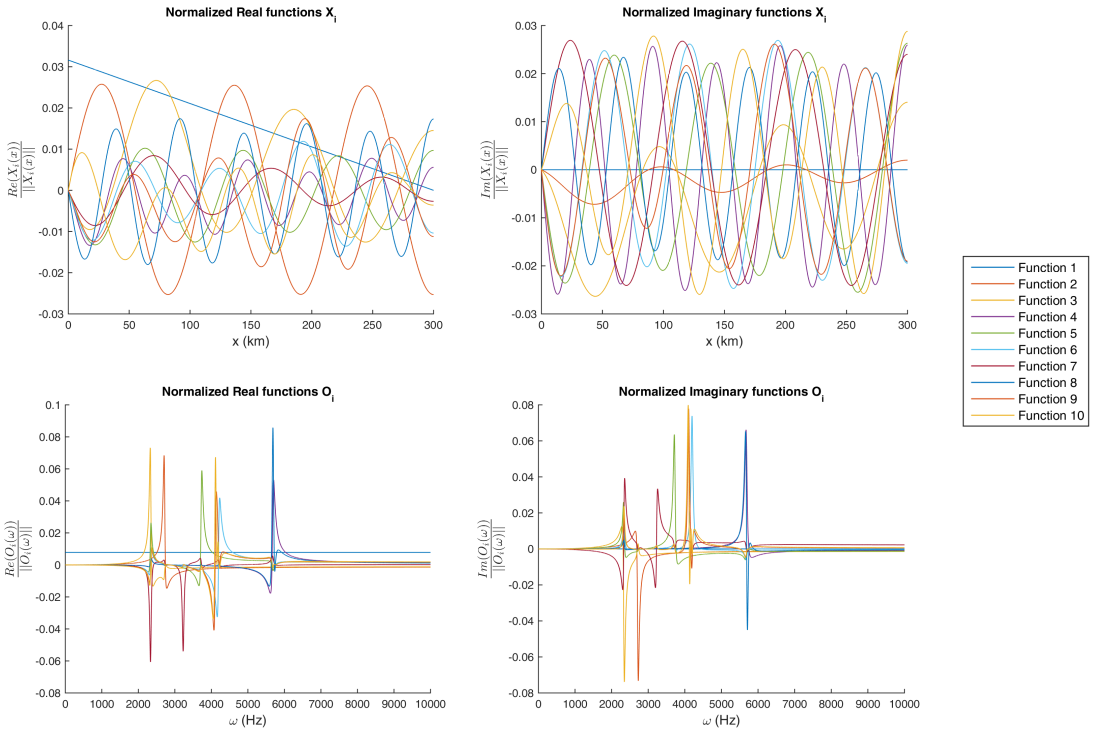

Figure 5.26: PGD modes for ACSR Grosbeak transmission line

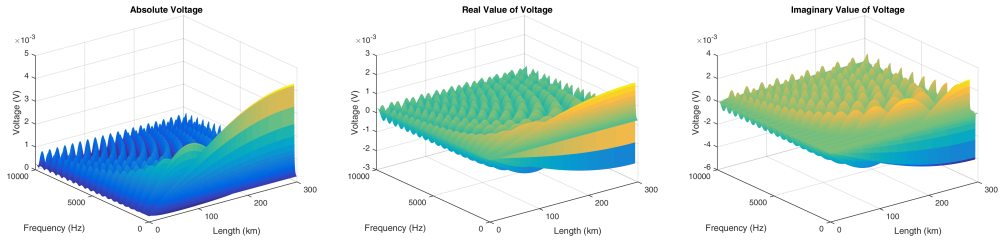

(a) Absolute Voltage (b) Real Voltage (c) Imaginary Voltage

Figure 5.27: Voltage in space-frequency domain with skin effects for ACSR Grosbeak line

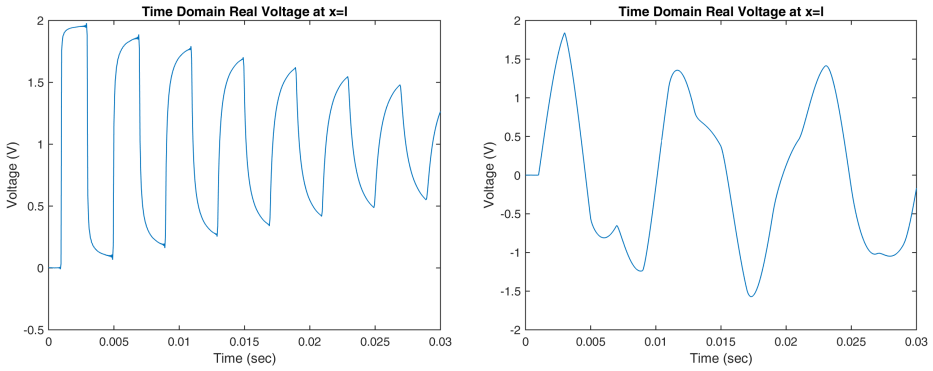

(a) Step Input (b) Sinusoidal Input

Figure 5.28: Time Response from PGD Solution with skin effects for Falcon line

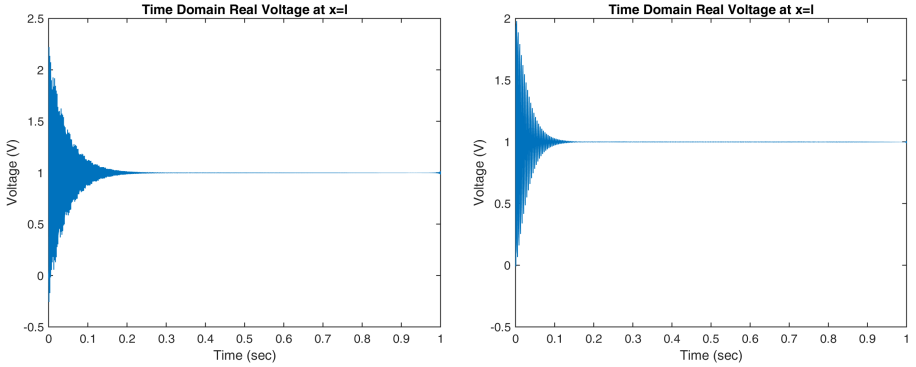

(a) Constant Parameters Model (b) Frequency-Dependent Parameters Model

Figure 5.29: Time Response from PGD Solution without and with skin effects for Falcon line for a step input

The time response for the step and sinusoidal input of the same magnitude and phase is presented for the frequency-dependent model in Figure 5.28a and Figure 5.28b. The effect of increased resistance and less inductance is visible as the voltage transients diminishes quickly and as demonstrated in the Figure 5.29a and Figure 5.29b for step response for constant parameters and frequency-dependent parameters respectively and the system reaches stationary conditions faster than the one where parameters are assumed constant.

The comparison between the two models also shows the much more damped response even in the transient phase. These are presented in the Figure 5.30a and Figure 5.30b.

Similar results are obtained for the Grosbeak transmission line and are presented in Figure 5.31 to Figure 5.33.

The skin effects have less impact on the Grosbeak transmission line compared to the impact on the Falcon line. There are two reasons, first the radius of the Grosbeak transmission line is small compared to the Falcon line and hence the ratio

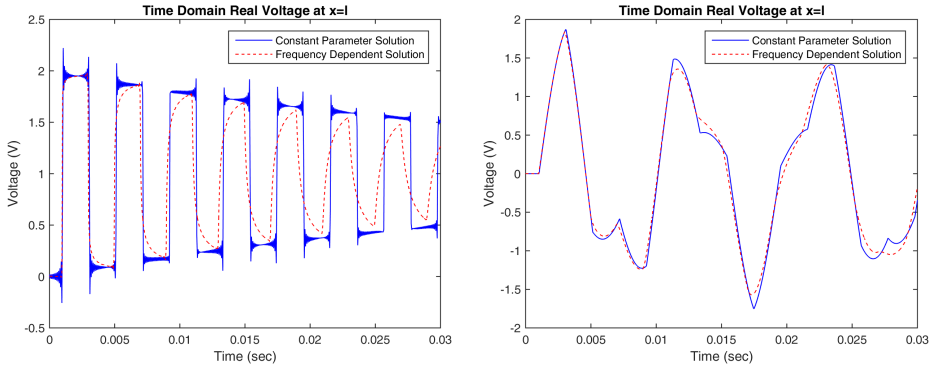

(a) Step Input (b) Sinusoidal Input

Figure 5.30: Comparison between constant parameters and frequency-dependent paramters for Falcon line

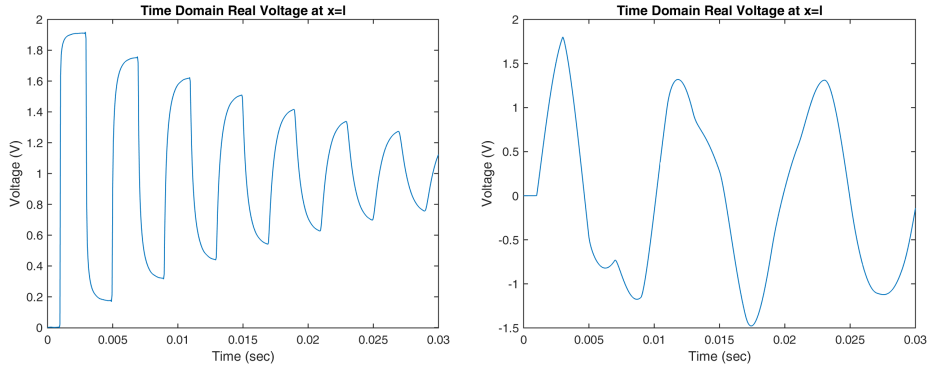

(a) Step Input (b) Sinusoidal Input

Figure 5.31: Time Response from PGD Solution with skin effects for Grosbeak line

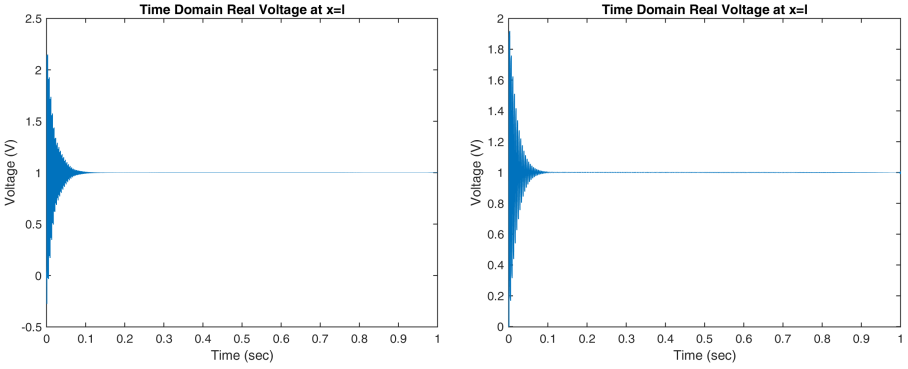

(a) Constant Parameters Model (b) Frequency-Depdendent Parameters Model

Figure 5.32: Time Response from PGD Solution without and with skin effects for Grosbeak line for a step input

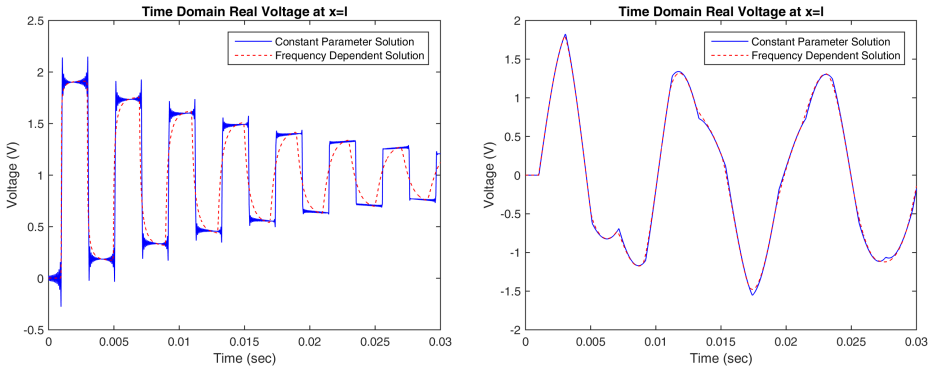

(a) Step Input (b) Sinusoidal Input

Figure 5.33: Comparison between constant parameters and frequency-dependent paramters for Grosbeak line

of skin depth to the radius of the conductor is not that big and the second reason is that the increase in resistance is more pronounced in the Falcon transmission line.

5.9 Conclusions

The main contribution of the study presented in this chapter is the development of a method to include transmission line effects like skin effects that render the parameters a function of frequency. The method is equally applicable on the ground return effect which has a similar effect on the parameters i.e. the frequency dependence. The work presented in this study, shows the effectiveness of frequency domain methods for problems involving frequency dependent parameters. In particular, harmonic analysis using PGD is both fast and accurate and provides results where the modal analysis methods are unable. There are methods available that include the parameters as a function of frequency and simulate the model in time domain but these methods are complicated to implement and as they use time integration it will be computationally costly and time consuming. The method we presented here involves PGD which has already been proved as a fast and accurate method. The method is also applicable to the fractional RLC circuits. The application of the said method on the commercially available transmission lines shows the effectiveness and proves that compared to time integration, this method is more practical.

Conclusions

This chapter provides an overall conclusion of the research conducted during this thesis and future directions this research can take based on our observations and conclusions. We group the conclusions from each chapter and summarize it as follows:

- The a priori method of fast non-linear solver of ASD proved to be a robust and efficient solver for static cases. However, the method of LATIN which was the basis for ASD method was unable to converge because of instability induced due to the separation of non-linear problem from the global part.

- The swing dynamics model involves non-linearity which involves neighboring nodes. This complex non-linearity must be handled carefully. The swing dynamics equations are hyperbolic partial differential equations and the system becomes linearly unstable if the linear approximation using Taylor series is adopted. Also, the separation of non-linearity from the global problem results in system becoming unstable.

- The method of TPWL which uses multiple linear approximations summed in a weighted convex combination. Using multiple linear approximations helps the system to remain stable. In the case, where we use only one linearization around the initial equilibrium point, the resulting linear equation becomes an unbounded function of δ, which was originally bounded in the non-linear sine function. This was avoided by using multiple linear approximations and the convex combination of these linear functions make sure that the contribution from any one linearization point is kept limited. The weighting functions based on the distance also biased the contribution of linear approximations towards the one closest and hence the system remains stable.

- The reduced-order model based on TPWL method proved to be accurate and computationally efficient. The method was able to provide reduced-order model that can be used for accurate and quick solutions for a wide range of input variables.

- The method of PGD was implemented in the construction of a reduced-order model of the DP model of transmission lines. The separated representation obtained from PGD was shown to be accurate compared with the analytical solution of the DP model in the frequency-domain. The number of enrichment

modes from PGD formulation are comparable to the size of the reduced basis from a posteriori POD method for the case where we separate only the space and frequency dimensions. The real advantage of PGD becomes apparent where we introduce other parameters in the separated representation.

- The method of PGD works efficiently for parametric problem. The results presented in Chapter 4 show that for achieving better performance of parametric solution, the range of parameters and the size of discretization hold the key. If the parameter range chosen is comparatively bigger then the number of enrichment modes become too many and also the accuracy suffers. This is due to the fact that there are a lot of resonances present in the problem and as the frequency increases the resonant modes introduce more and more waves which are difficult to capture with fewer enrichment modes. There is a solution however for reducing the number of modes and that is to use a post-PGD compression of modes using SVD or high order SVD (HOSVD) methods.

- In the last chapter, we discussed the problem where the parameters are function of one of the coordinates in PGD formulation. In this particular case, the parameters are frequency dependent which is a common occurrence in many real-life applications. We presented PGD based harmonic analysis solver for such problems. The method of PGD presents an efficient and fast method as well as accurate and reliable method for problems which are frequency dependent in time-domain representation or involve fractional derivatives of time.

Based on the results achieved during the research, we have published our results in various journals. These include

- Although the static problems were not the focus of the study, the solution using the ASD method of power flow analysis were published in a research paper.

  Borzacchiello D, Chinesta F, Malik MH, García-Blanco R, Diez P. Unified formulation of a family of iterative solvers for power systems analysis. Electric Power Systems Research, Volume 140, November 2016, Pages 201-208, ISSN 0378-7796, http://dx.doi.org/10.1016/j.epsr.2016.06.021

- The results of the TPWL method presented in Chapter 3 were also published.

  Malik MH, Borzacchiello D, Chinesta F, Diez P. Reduced order modeling for transient simulation of power systems using Trajectory Piece-Wise Linear approximation. Advanced Modeling and Simulation in Engineering Sciences 2016.

- A manuscript is submitted based on the results of Chapter 5 for frequency dependent parameters model.

  Malik MH, Borzacchiello D, Chinesta F, Diez P. Inclusion of Frequency Dependent Parameters in Power Transmission Lines Simulation using Harmonic Analysis and Proper Generalized Decomposition.

Further Developments

The research carried out during the current doctoral studies is just the beginning of an exciting research direction. There are several problems that can be studied further based on the studies we conducted, namely:

- Application of TPWL method on benchmark grids by IEEE and extension to real world grid networks which includes both types of load and generator buses and other power generation modeled by different models. Also, the network topology is complex and time dependent in real networks, the method offers great potential which should be utilized and can be developed into softwares specific to the power industry needs.
- Harmonic analysis of benchmark power grids and extension to real power networks based on the PGD formulation provided in the current study. This method also offers potential that should be developed further and can lead to industrial applications and patents.
- The results from the frequency-dependent parametric problem can be extended to fractional RLC circuits.

Bibliography

[1] P. Kundur, *Power System Stability and Control*. McGraw-Hill, 1994. *cited on page ix, 22, and 39*

[2] M. Reta-Hernández, "Transmission Line Parameters," in *Electric Power Generation, Transmission, and Distribution, Third Edition* (L. L. Grigsby, ed.), pp. 1–36, CRC Press, may 2012. *cited on page xi, 159, and 160*

[3] S. Massoud Amin, "Smart Grid: Overview, Issues and Opportunities. Advances and Challenges in Sensing, Modeling, Simulation, Optimization and Control," *European Journal of Control*, vol. 17, no. 5-6, pp. 547–567, 2011. *cited on page 6 and 7*

[4] Y. S. Qudaih and Y. Mitani, "Power Distribution System Planning for Smart Grid Applications using ANN," *Energy Procedia*, vol. 12, no. 0, pp. 3–9, 2011. *cited on page 6*

[5] M. Fadaeenejad, A. M. Saberian, M. Fadaee, M. A. M. Radzi, H. Hizam, and M. Z. A. Abkadir, "The present and future of smart power grid in developing countries," *Renewable and Sustainable Energy Reviews*, vol. 29, pp. 828–834, 2014. *cited on page 6*

[6] V. Gunderson, "2016 Top Markets Report Smart Grid," tech. rep., International Trade Administration, USA, April 2016. *cited on page 6*

[7] S.-W. Mei and J.-Q. Zhu, "Mathematical and Control Scientific Issues of Smart Grid and Its Prospects," *Acta Automatica Sinica*, vol. 39, no. 2, pp. 119–131, 2013. *cited on page 7*

[8] T. Ackermann, G. Andersson, and L. Söder, "Distributed generation: A definition," *Electric Power Systems Research*, vol. 57, no. 3, pp. 195–204, 2001. *cited on page 7*

[9] R. B. Deepak Sharma, "Distributed electricity generation in competitive energy markets: A case study in australia," *The Energy Journal*, vol. 18, pp. 17–39, 1997. *cited on page 8*

[10] G. Pepermans, J. Driesen, D. Haeseldonckx, R. Belmans, and W. D'haeseleer, "Distributed generation: Definition, benefits and issues," *Energy Policy*, vol. 33, no. 6, pp. 787–798, 2005. *cited on page 8*

[11] R. Preece, *Improving the Stability of Meshed Power Networks*. Springer Theses, Cham: Springer International Publishing, 2013. *cited on page 8*

[12] J. Nazarko, *Modeling of Electrical Power Distribution Systems*. Bialystok: Bialystok Technical University Publisher, 1993. *cited on page 8*

[13] S. Khaitan and A. Gupta, *High Performance Computing in Power and Energy Systems*. Power Systems, Berlin, Heidelberg: Springer Berlin Heidelberg, 2013. *cited on page 8*

[14] J. H. Chow, *Power System Coherency and Model Reduction*, vol. 94 of *Power Electronics and Power Systems*. New York, NY: Springer New York, 2013. *cited on page 9 and 12*

[15] R. Podmore, "Identification of Coherent Generators for Dynamic Equivalents," *IEEE Transactions on Power Apparatus and Systems*, vol. PAS-97, pp. 1344–1354, jul 1978. *cited on page 9 and 10*

[16] K. Tanaka and M. Takemura, "Development of reduction program for bulk power system stability study," *POWERCON '98. 1998 International Conference on Power System Technology. Proceedings (Cat. No.98EX151)*, vol. 2, no. 3, pp. 1305–1309, 1998. *cited on page 9*

[17] J. Yu, M. Zhang, and W. Li, "Static Equivalent Method Based on Component Particularity Representation and Sensitivity Consistency," *IEEE Transactions on Power Systems*, vol. 29, pp. 2400–2408, sep 2014. *cited on page 10*

[18] A. Debs, "Estimation of external network equivalents from internal system data," *IEEE Transactions on Power Apparatus and Systems*, vol. 94, no. 2, pp. 273–279, 1975. *cited on page 10*

[19] B. Stott, O. Alsaç, and A. Monticelli, "Studies on power system load flow equivalencing," *IEEE Transactions on Power Apparatus and Systems*, vol. PAS-99, no. 6, pp. 2301–2310, 1980. *cited on page 10*

[20] B. Stott, O. Alsaç, and A. Monticelli, "Numerical testing of power system load flow equivalents," *IEEE Transactions on Power Apparatus and Systems*, vol. PAS-99, no. 6, pp. 2292–2300, 1980. *cited on page 10*

[21] R. van Amerongen and H. van Meeteren, "A Generalised Ward Equivalent for Security Analysis," *IEEE Transactions on Power Apparatus and Systems*, vol. PAS-101, pp. 1519–1526, jun 1982. *cited on page 10*

[22] V. Müller and D. Nelles, "Application of neural networks to static equivalent networks," *European Transactions on Electrical Power*, vol. 12, pp. 217–223, may 2002. *cited on page 10*

[23] H. Altalib and P. Krause, "Dynamic equivalents by combination of reduced order models of system components," *IEEE Transactions on Power Apparatus and Systems*, vol. 95, pp. 1535–1544, sep 1976. *cited on page 10*

[24] H. Rudnick, R. Patino, and A. Brameller, "Power-system dynamic equivalents:coherency recognition via the rate of change of kinetic energy," *IEE Proceedings C Generation, Transmission and Distribution*, vol. 128, no. 6, p. 325, 1981. *cited on page 10*

[25] X. Feng, Z. Lubosny, and J. Bialek, "Dynamic equivalencing of distribution network with high penetration of distributed generation," *41st International Universities Power Engineering Conference, UPEC 2006, Conference Proceedings*, vol. 2, pp. 467–471, 2006. *cited on page 10 and 11*

[26] F. Ma, X. Luo, and V. Vittal, "Application of dynamic equivalencing in large-scale power systems," *2011 IEEE Power and Energy Society General Meeting*, pp. 1–10, 2011. *cited on page 11*

[27] J. E. Anderson and A. Chakrabortty, "PMU placement for dynamic equivalencing of power systems under flow observability constraints," *Electric Power Systems Research*, vol. 106, pp. 51–61, 2014. *cited on page 11*

[28] A. Chakrabortty, J. H. Chow, and A. Salazar, "A measurement-based framework for dynamic equivalencing of large power systems using wide-area phasor measurements," *IEEE Transactions on Smart Grid*, vol. 2, pp. 68–81, March 2011. *cited on page 11*

[29] A. Takimoto, "Power system dynamic equivalence based on a new model reduction technique," *Electrical Engineering in Japan*, vol. 114, no. 7, pp. 56–67, 1994. *cited on page 11 and 12*

[30] T. Singhavilai, O. Anaya-Lara, and K. Lo, "Identification of the dynamic equivalent of a power system," *Universities Power Engineering Conference (UPEC), 2009 Proceedings of the 44th International*, vol. 0, no. 1, pp. 1–5, 2009. *cited on page 11*

[31] R. Gueddouche and M. Boudour, "Nonlinear Estimation of External Power System," *Global Journal of Researches in Engineering*, vol. 12, no. 7, pp. 13–19, 2012. *cited on page 11*

[32] Y. Zhou, K. Wang, Y. Xiong, and B. Zhang, "Study of power system online dynamic equivalent based on wide area measurement system," *Energy Procedia*, vol. 16, no. PART C, pp. 1768–1775, 2012. *cited on page 12*

[33] A. Ahmed and M. Shahid Ullah, "Dynamic equivalence of a large power system using power system simulator for engineers (PSS / E)," *Journal of Engineering and Technology*, vol. 8, no. 2, pp. 13–31, 2010. *cited on page 12*

[34] H. Zhou, P. Ju, H. Yang, and R. Sun, "Dynamic equivalent method of interconnected power systems with consideration of motor loads," *Science China Technological Sciences*, vol. 53, no. 4, pp. 902–908, 2010. *cited on page 12*

[35] B. Hong, H. Hu, T. Chen, and Q. Li, "Dynamic Equivalent Method of Motor Loads for Power Systems Based on the Weighted," *Journal of Power and Energy Engineering*, vol. 02, no. 04, pp. 416–422, 2014. *cited on page 12*

[36] B. Porkar, M. Vakilian, and R. Feuillet, "Frequency-Dependent Network Equivalent for Electromagnetic Transient Studies by Vector Fitting," in *2005/2006 PES TD*, pp. 166–171, IEEE, 2006. *cited on page 12*

[37] A. Stankovicc, A. Saric, and M. Milosevic, "Identification of nonparametric dynamic power system equivalents with artificial neural networks," *IEEE Transactions on Power Systems*, vol. 18, pp. 1478–1486, nov 2003. *cited on page 12*

[38] S.-K. Joo, C.-C. Liu, L. Jones, and J.-W. Choe, "Coherency and Aggregation Techniques Incorporating Rotor and Voltage Dynamics," *IEEE Transactions on Power Systems*, vol. 19, pp. 1068–1075, may 2004. *cited on page 12*

[39] M. L. Ourari, L. A. Dessaint, and V.-Q. Do, "Dynamic equivalent modeling of large power systems using structure preservation technique," *IEEE Transactions on Power Systems*, vol. 21, pp. 1284–1295, Aug 2006. *cited on page 12*

[40] Z. Bai, P. M. Dewilde, and R. W. Freund, "Reduced-Order Modeling," in *Numerical Methods in Electromagnetics*, vol. 13 of *Handbook of Numerical Analysis*, pp. 825–895, Elsevier, 2005. *cited on page 12 and 44*

[41] D. Chaniotis and M. A. Pai, "Model Reduction in Power Systems Using Krylov Subspace Methods," *IEEE Transactions on Power Systems*, vol. 20, no. 2, pp. 888–894, 2005. *cited on page 12*

[42] P. Parrilo, S. Lall, F. Paganini, G. C. Verghese, B. Lesieutre, and J. Marsden, "Model reduction for analysis of cascading failures in power systems," in *American Control Conference, 1999. Proceedings of the 1999*, vol. 6, pp. 4208–4212 vol.6, 1999. *cited on page 12, 34, 42, 59, 61, and 62*

[43] C. Sturk, L. Vanfretti, F. Milano, and H. Sandberg, "Structured model reduction of power systems," in *2012 American Control Conference (ACC)*, pp. 2276–2282, IEEE, jun 2012. *cited on page 13*

[44] C. Sturk, L. Vanfretti, Y. Chompoobutrgool, and H. Sandberg, "Structured power system model reduction of non-coherent areas," *IEEE Power and Energy Society General Meeting*, pp. 1–8, 2012. *cited on page 13*

[45] M. Bettayeb and U. M. Al-Saggaf, "Practical model reduction techniques for power systems," *Electric Power Systems Research*, vol. 25, no. 3, pp. 169–176, 1992. *cited on page 13*

[46] U. M. Al-Saggaf and M. Bettayeb, "Techniques in optimized model reduction for high dimensional systems," in *Digital and Numeric Techniques and their Applications in Control Systems, Part 1 of 2* (C. LEONDES, ed.), vol. 55,

Part 1 of *Control and Dynamic Systems*, pp. 51 – 109, Academic Press, 1993. *cited on page 14*

[47] A. Cherid and M. Bettayeb, "Reduced-order models for the dynamics of a single-machine power system via balancing," *Electric Power Systems Research*, vol. 22, pp. 7–12, sep 1991. *cited on page 14*

[48] U. M. Al-Saggaf, "Reduced-order models for dynamic control of a power plant with an improved transient and steady-state behavior," *Electric Power Systems Research*, vol. 26, no. 1, pp. 79–85, 1993. *cited on page 14*

[49] N. Kashyap, S. Werner, T. Riihonen, and Y. F. Huang, "Reduced-order synchrophasor-assisted state estimation for smart grids," *2012 IEEE 3rd International Conference on Smart Grid Communications, SmartGridComm 2012*, pp. 605–610, 2012. *cited on page 14*

[50] B. Wille-Haussmann, J. Link, and C. Wittwer, "Simulation study of a "Smart Grid" approach: Model reduction, reactive power control," *IEEE PES Innovative Smart Grid Technologies Conference Europe, ISGT Europe*, pp. 1–7, 2010. *cited on page 14*

[51] A. Bergen and V. Vittal, *Power Systems Analysis*. Prentice Hall, 1999. *cited on page 27, 39, and 41*

[52] D. Borzacchiello, F. Chinesta, M. Malik, R. García-Blanco, and P. Diez, "Unified formulation of a family of iterative solvers for power systems analysis," *Electric Power Systems Research*, vol. 140, pp. 201–208, nov 2016. *cited on page 34 and 39*

[53] P. Ladevèze, *Nonlinear Computational Structural Mechanics*. Mechanical Engineering Series, New York, NY: Springer New York, 1999. *cited on page 34 and 49*

[54] P. Kundur, J. Paserba, V. Ajjarapu, G. Andersson, A. Bose, C. Canizares, N. Hatziargyriou, D. Hill, A. Stankovic, C. Taylor, T. Van Cutsem, and V. Vittal, "Definition and Classification of Power System Stability IEEE/CIGRE Joint Task Force on Stability Terms and Definitions," *IEEE Transactions on Power Systems*, vol. 19, pp. 1387–1401, aug 2004. *cited on page 39*

[55] Y. Susuki, I. Mezić, and T. Hikihara, "Coherent swing instability of power grids," *Journal of Nonlinear Science*, vol. 21, no. 3, pp. 403–439, 2011. *cited on page 43, 45, 88, and 93*

[56] P. Hines, K. Balasubramaniam, and E. Sanchez, "Cascading failures in power grids," *IEEE Potentials*, vol. 28, pp. 24–30, sep 2009. *cited on page 43*

[57] R. Baldick, B. Chowdhury, I. Dobson, Zhaoyang Dong, Bei Gou, D. Hawkins, H. Huang, M. Joung, D. Kirschen, Fangxing Li, Juan Li, Zuyi Li, Chen-Ching Liu, L. Mili, S. Miller, R. Podmore, K. Schneider, Kai Sun, D. Wang, Zhigang

Wu, Pei Zhang, Wenjie Zhang, and Xiaoping Zhang, "Initial review of methods for cascading failure analysis in electric power transmission systems IEEE PES CAMS task force on understanding, prediction, mitigation and restoration of cascading failures," in *2008 IEEE Power and Energy Society General Meeting - Conversion and Delivery of Electrical Energy in the 21st Century*, no. July, pp. 1–8, IEEE, jul 2008. *cited on page 43*

[58] P. C. Magnusson, "The Transient-Energy Method of Calculating Stability," *American Institute of Electrical Engineers, Transactions of the*, vol. 66, pp. 747–755, jan 1947. *cited on page 44*

[59] P. D. Aylett, "The energy-integral criterion of transient stability limits of power systems," *Proceedings of the IEE - Part C: Monographs*, vol. 105, no. 8, pp. 527–536, 1958. *cited on page 44*

[60] P. D. Z. Bai and R. Freund, "Reduced-order modeling," in *Handbook of Numerical Analysis Vol. XIII, Numerical Methods in Electromagnetics* (E. t. Schilders, W.Maten, ed.), vol. 13, pp. 825–895, 2005. *cited on page 44*

[61] W. Schilders, "Introduction to model order reduction," in *Model Order Reduction: Theory, Research Aspects and Applications* (W. H. Schilders, H. A. van der Vorst, and J. Rommes, eds.), vol. 13 of *Mathematics in Industry*, pp. 3–32, Springer Berlin Heidelberg, 2008. *cited on page 44*

[62] R. Pinnau, "Model reduction via proper orthogonal decomposition," in *Model Order Reduction: Theory, Research Aspects and Applications* (W. H. Schilders, H. A. van der Vorst, and J. Rommes, eds.), vol. 13 of *Mathematics in Industry*, pp. 95–109, Springer Berlin Heidelberg, 2008. *cited on page 44*

[63] F. Chinesta, A. Leygue, F. Bordeu, J. V. Aguado, E. Cueto, D. Gonzalez, I. Alfaro, A. Ammar, and A. Huerta, "PGD-Based Computational Vademecum for Efficient Design, Optimization and Control," *Archives of Computational Methods in Engineering*, vol. 20, no. 1, pp. 31–59, 2013. *cited on page 44, 110, 111, 143, and 149*

[64] L. Knockaert and D. D. Zutter, "Laguerre-svd reduced-order modeling," *IEEE Transactions on Microwave Theory and Techniques*, vol. 48, pp. 1469–1475, Sep 2000. *cited on page 44*

[65] D. González, F. Masson, F. Poulhaon, A. Leygue, E. Cueto, and F. Chinesta, "Proper Generalized Decomposition based dynamic data driven inverse identification," *Mathematics and Computers in Simulation*, vol. 82, no. 9, pp. 1677–1695, 2012. *cited on page 49*

[66] B. Vandoren, K. De Proft, A. Simone, and L. Sluys, "Mesoscopic modelling of masonry using weak and strong discontinuities," *Computer Methods in Applied Mechanics and Engineering*, vol. 255, pp. 167–182, mar 2013. *cited on page 54*

[67] L. N. Lowes, *Finite Element Modeling of Reinforced Concrete Beam-Column Bridge Connections*. PhD thesis, University of California, Berkeley, 1999. *cited on page 54*

[68] B. Vandoren, A. Simone, and L. J. Sluys, "A constrained Large Time Increment Method for a Gradient-Enhanced Damage Model," in *5th European Conference on Computational Mechanics (ECCM V)*, no. WCCM XI, (Barcelona, Spain), 2014. *cited on page 54*

[69] L. Montier, T. Henneron, S. Clénet, and B. Goursaud, "Transient simulation of an electrical rotating machine achieved through model order reduction," *Advanced Modeling and Simulation in Engineering Sciences*, vol. 3, no. 1, pp. 1–17, 2016. *cited on page 59*

[70] Y. Liang, H. Lee, S. Lim, W. Lin, K. Lee, and C. Wu, "Proper orthogonal decomposition and its applications - part I: Theory," *Journal of Sound and Vibration*, vol. 252, no. 3, pp. 527 – 544, 2002. *cited on page 60 and 61*

[71] G. Kerschen, J.-C. Golinval, A. F. Vakakis, and L. A. Bergman, "The method of proper orthogonal decomposition for dynamical characterization and order reduction of mechanical systems: An overview," *Nonlinear Dynamics*, vol. 41, no. 1-3, pp. 147–169, 2005. *cited on page 61*

[72] G. Berkooz, P. Holmes, and J. L. Lumley, "The proper orthogonal decomposition in the analysis of turbulent flows," *Annual Review of Fluid Mechanics*, vol. 25, no. 1, pp. 539–575, 1993. *cited on page 61*

[73] M. N. Albunni, *Model Order Reduction of Moving Nonlinear Electromagnetic Devices*. PhD thesis, Technical University of Munich, September 2010. *cited on page 77, 78, 82, 84, and 85*

[74] M. J. Rewieński, *A Trajectory Piecewise-Linear Approach to Model Order Reduction of Nonlinear Dynamical Systems*. PhD thesis, Massachusetts Institute of Technology, June 2003. *cited on page 77, 78, and 86*

[75] M. Barrault, Y. Maday, N. C. Nguyen, and A. T. Patera, "An 'empirical interpolation' method: application to efficient reduced-basis discretization of partial differential equations," *Comptes Rendus Mathematique*, vol. 339, no. 9, pp. 667–672, 2004. *cited on page 78*

[76] S. Chaturantabut and D. C. Sorensen, "Nonlinear Model Reduction via Discrete Empirical Interpolation," *SIAM Journal on Scientific Computing*, vol. 32, no. 5, pp. 2737–2764, 2010. *cited on page 78*

[77] Y. Liu, W. Yuan, and H. Chang, "A global maximum error controller-based method for linearization point selection in trajectory piecewise-linear model order reduction," *Computer-Aided Design of Integrated Circuits and Systems, IEEE Transactions on*, vol. 33, pp. 1100–1104, July 2014. *cited on page 78 and 85*

[78] Y. Chen and J. White, "A quadratic method for nonlinear model order reduction," in *Technical Proceedings of the 2000 International Conference on Modeling and Simulation of Microsystems*, pp. 477 – 480, 2000. *cited on page 78*

[79] D. Vasilyev, M. Rewieński, and J. White, "A tbr-based trajectory piecewise-linear algorithm for generating accurate low-order models for nonlinear analog circuits and mems," in *Design Automation Conference, 2003. Proceedings*, pp. 490–495, June 2003. *cited on page 78 and 79*

[80] L. Qu and P. Chapman, "A trajectory piecewise-linear approach to model order reduction for nonlinear stationary magnetic devices," in *Computers in Power Electronics, 2004. Proceedings. 2004 IEEE Workshop on*, pp. 15–19, Aug 2004. *cited on page 78*

[81] M. Rewieński and J. White, "A trajectory piecewise-linear approach to model order reduction and fast simulation of nonlinear circuits and micromachined devices," *Computer-Aided Design of Integrated Circuits and Systems, IEEE Transactions on*, vol. 22, pp. 155–170, Feb 2003. *cited on page 78*

[82] M. Farooq, L. Xia, F. Hussin, and A. Malik, "Automated model generation of analog circuits through modified trajectory piecewise linear approach with cheby shev newton interpolating polynomials," in *Intelligent Systems Modelling Simulation (ISMS), 2013 4th International Conference on*, pp. 605–609, Jan 2013. *cited on page 78 and 79*

[83] C. Long, L. Simonson, W. Liao, and L. He, "Floorplanning optimization with trajectory piecewise-linear model for pipelined interconnects," in *Design Automation Conference, 2004. Proceedings. 41st*, pp. 640–645, July 2004. *cited on page 78*

[84] M. Farooq and L. Xia, "Local approximation improvement of trajectory piecewise linear macromodels through chebyshev interpolating polynomials," in *Design Automation Conference (ASP-DAC), 2013 18th Asia and South Pacific*, pp. 767–772, Jan 2013. *cited on page 78*

[85] D. Maier, *On the Use of Model Order Reduction Techniques for the Elastohydrodynamic Contact Problem*. PhD thesis, Karlsruhe Institute of Technology, INSA Lyon, Febraury 2015. *cited on page 78*

[86] M. Rewieński and J. White, "A trajectory piecewise-linear approach to model order reduction and fast simulation of nonlinear circuits and micromachined devices," in *Computer Aided Design, 2001. ICCAD 2001. IEEE/ACM International Conference on*, pp. 252–257, Nov 2001. *cited on page 78 and 84*

[87] J. He, J. Sætrom, and L. Durlofsky, "Enhanced linearized reduced-order models for subsurface flow simulation," *Journal of Computational Physics*, vol. 230, no. 23, pp. 8313 – 8341, 2011. *cited on page 78 and 79*

[88] M. Cardoso and L. Durlofsky, "Linearized reduced-order models for subsurface flow simulation," *Journal of Computational Physics*, vol. 229, no. 3, pp. 681 – 700, 2010. *cited on page 78 and 79*

[89] D. Gratton, "Reduced-order, trajectory piece-wise linear models for nonlinear computational fluid dynamics," Master's thesis, Massachusetts Institute of Technology, USA, 2004. *cited on page 78*

[90] W. Xie and C. Theodoropoulos, "An off-line model reduction-based technique for on-line linear MPC applications for nonlinear large-scale distributed systems," in *20th European Symposium on Computer Aided Process Engineering* (S. Pierucci and G. B. Ferraris, eds.), vol. 28 of *Computer Aided Chemical Engineering*, pp. 409 – 414, Elsevier, 2010. *cited on page 78 and 79*

[91] S. Burgard, O. Farle, D. Klis, and R. Dyczij-Edlinger, "Order-reduction of fields-level models with affine and non-affine parameters by interpolation of subspaces," *IFAC-PapersOnLine*, vol. 48, no. 1, pp. 170 – 175, 2015. *cited on page 78*

[92] H. Panzer, J. Mohring, R. Eid, and B. Lohmann, "Parametric model order reduction by matrix interpolation," *at - Automatisierungstechnik*, vol. 58, no. 8, pp. 475 – 484, 2010. *cited on page 78*

[93] H. Yu, X. Liu, H. Wang, and S. Tan, "A fast analog mismatch analysis by an incremental and stochastic trajectory piecewise linear macromodel," in *Design Automation Conference (ASP-DAC), 2010 15th Asia and South Pacific*, pp. 211–216, Jan 2010. *cited on page 79*

[94] K. Zong, F. Yang, and X. Zeng, "A wavelet-collocation-based trajectory piecewise-linear algorithm for time-domain model-order reduction of nonlinear circuits," *Circuits and Systems I: Regular Papers, IEEE Transactions on*, vol. 57, pp. 2981–2990, Nov 2010. *cited on page 79*

[95] E. Acha, V. Agelidis, O. Anaya-Lara, and T. Miller, "4 - power flows in compensation and control studies," in *Power Electronic Control in Electrical Systems* (E. Acha, V. Agelidis, O. Anaya-Lara, and T. Miller, eds.), Newnes Power Engineering Series, pp. 106 – 152, Oxford: Newnes, 2002. *cited on page 87*

[96] M. H. Malik, D. Borzacchiello, F. Chinesta, and P. Diez, "Reduced order modeling for transient simulation of power systems using trajectory piecewise linear approximation," *Advanced Modeling and Simulation in Engineering Sciences*, vol. 3, no. 1, p. 31, 2016. *cited on page 102*

[97] A. Morched and V. Brandwajn, "Transmission Network Equivalents for Electromagnetic Transients Studies," *IEEE Transactions on Power Apparatus and Systems*, vol. PAS-102, pp. 2984–2994, sep 1983. *cited on page 104 and 106*

[98] M. Belhocine and B. Marinescu, "A mix balanced-modal truncations for power systems model reduction," in *Control Conference (ECC), 2014 European*, pp. 2721–2726, June 2014. *cited on page 104 and 133*

[99] M. Belhocine and B. Marinescu, "On the connections between used models of power transmission lines," in *2013 IEEE Power Energy Society General Meeting*, pp. 1–5, July 2013. *cited on page 104, 106, 132, 133, and 134*

[100] S. Lefebvre, "Reduced order transmission line models for power system analysis," *International Journal of Electrical Power & Energy Systems*, vol. 21, pp. 211–223, mar 1999. *cited on page 104*

[101] A. Clerici and L. Marzio, "Coordinated Use of TNA and Digital Computer for Switching-Surge Studies: Transient Equivalent of a Complex Network," *IEEE Transactions on Power Apparatus and Systems*, vol. PAS-89, pp. 1717–1726, nov 1970. *cited on page 104*

[102] X. P. Zhang and H. Chen, "Analysis and selection of transmission line models used in power system transient simulations," *International Journal of Electrical Power and Energy Systems*, vol. 17, no. 4, pp. 239–246, 1995. *cited on page 104*

[103] R. Ionutiu, S. Lefteriu, and A. C. Antoulas, "Comparison of Model Reduction Methods with Applications to Circuit Simulation," in *Scientific Computing in Electrical Engineering SCEE 2006*, vol. 11, pp. 3–24, 2007. *cited on page 104*

[104] A. Soysal and A. Semlyen, "Reduced order transmission line modeling for improved efficiency in the calculation of electromagnetic transients," *IEEE Transactions on Power Systems*, vol. 9, no. 3, pp. 1494–1498, 1994. *cited on page 104*

[105] R. F. Remis, "An efficient model-order reduction approach to low-frequency transmission line modeling," *Progress In Electromagnetics Research*, vol. 101, pp. 139–155, 2010. *cited on page 104*

[106] Youngsoo Jang, Jaesop Kong, and J. Seo, "Balanced model reduction with guaranteed performance in frequency ranges," in *Proceedings of 1994 33rd IEEE Conference on Decision and Control*, vol. 3, pp. 2732–2733, IEEE, 1984. *cited on page 104*

[107] M. R. Opmeer, "Model reduction for distributed parameter systems: A functional analytic view," in *2012 American Control Conference (ACC)*, pp. 1418–1423, June 2012. *cited on page 104*

[108] F. Chinesta, R. Keunings, and A. Leygue, *The Proper Generalized Decomposition for Advanced Numerical Simulations.* SpringerBriefs in Applied Sciences and Technology, Cham: Springer International Publishing, 2014. *cited on page 110*

[109] F. Chinesta, A. Ammar, A. Leygue, and R. Keunings, "An overview of the proper generalized decomposition with applications in computational rheology," *Journal of Non-Newtonian Fluid Mechanics*, vol. 166, no. 11, pp. 578–592, 2011. *cited on page 111, 143, and 149*

[110] P. Ladevèze and L. Chamoin, "On the verification of model reduction methods based on the proper generalized decomposition," *Computer Methods in Applied Mechanics and Engineering*, vol. 200, pp. 2032–2047, jun 2011. *cited on page 111*

[111] E. Pruliere, F. Chinesta, and A. Ammar, "On the deterministic solution of multidimensional parametric models using the Proper Generalized Decomposition," *Mathematics and Computers in Simulation*, vol. 81, no. 4, pp. 791–810, 2010. *cited on page 111*

[112] A. Ammar, B. Mokdad, F. Chinesta, and R. Keunings, "A new family of solvers for some classes of multidimensional partial differential equations encountered in kinetic theory modeling of complex fluids," *Journal of Non-Newtonian Fluid Mechanics*, vol. 139, no. 3, pp. 153–176, 2006. *cited on page 111*

[113] A. Ammar, B. Mokdad, F. Chinesta, and R. Keunings, "A new family of solvers for some classes of multidimensional partial differential equations encountered in kinetic theory modelling of complex fluids. Part II: Transient simulation using space-time separated representations," *Journal of Non-Newtonian Fluid Mechanics*, vol. 144, no. 2-3, pp. 98–121, 2007. *cited on page 111*

[114] D. Modesto, S. Zlotnik, and A. Huerta, "Proper generalized decomposition for parameterized Helmholtz problems in heterogeneous and unbounded domains: Application to harbor agitation," *Computer Methods in Applied Mechanics and Engineering*, vol. 295, pp. 127–149, 2015. *cited on page 111*

[115] P. Ladevèze, J.-C. Passieux, and D. Néron, "The LATIN multiscale computational method and the Proper Generalized Decomposition," *Computer Methods in Applied Mechanics and Engineering*, vol. 199, pp. 1287–1296, apr 2010. *cited on page 111*

[116] R. García-Blanco, P. Díez, D. Borzacchiello, and F. Chinesta, "A reduced order modeling approach for optimal allocation of distributed generation in power distribution systems," in *2016 IEEE International Energy Conference (ENERGYCON)*, pp. 1–6, April 2016. *cited on page 111*

[117] R. García-Blanco, D. Borzacchiello, F. Chinesta, and P. Díez, "Monitoring a pgd solver for parametric power flow problems with goal-oriented error assessment," *International Journal for Numerical Methods in Engineering*, pp. n/a–n/a, 2016. nme.5470. *cited on page 111*

[118] A. Bergen and V. Vittal, *Power Systems Analysis*. Upper Saddle River, New Jersey: Prentice Hall, 2nd ed., 1986. *cited on page 121 and 129*

[119] B. Y. Levin, *Lecture on entire functions.* USA: Academic Press, 2001. *cited on page 133*

[120] R. F. Curtain and H. Zwart, *An Introduction to Infinite-Dimensional Linear Systems Theory.* New York, USA: Springer-Verlag, 2001. *cited on page 133*

[121] S. Kurokawa, J. PissolatoFilho, M. Tavares, C. Portela, and A. Prado, "Behavior of Overhead Transmission Line Parameters on the Presence of Ground Wires," *IEEE Transactions on Power Delivery*, vol. 20, pp. 1669–1676, apr 2005. *cited on page 139, 141, and 142*

[122] M. Admane, M. Sorine, and Q. Zhang, "Simulation of electric transmission lines with skin effect based on a reduced order differential model," in *IET Colloquium on Reliability of Electromagnetic Systems*, vol. 2007, pp. 16–16, IEE, 2007. *cited on page 139, 141, and 145*

[123] E. C. M. da Costa, S. Kurokawa, A. J. do Prado, and J. Pissolato, "Proposal of an alternative transmission line model for symmetrical and asymmetrical configurations," *International Journal of Electrical Power & Energy Systems*, vol. 33, pp. 1375–1383, oct 2011. *cited on page 139, 140, and 141*

[124] D. Bormann and H. Tavakoli, "Reluctance Network Treatment of Skin and Proximity Effects in Multi-Conductor Transmission Lines," *IEEE Transactions on Magnetics*, vol. 48, pp. 735–738, feb 2012. *cited on page 139 and 141*

[125] J. R. Marti, "Accurate Modeling of Frequency-Dependent Transmission Lines in Electromagnetic Transient Simulations," *IEEE Transactions on Power Apparatus and Systems*, vol. PAS-101, no. 1, pp. 147–157, 1982. *cited on page 139, 140, 141, and 164*

[126] C. Nucci, F. Rachidi, and M. Rubinstein, "Derivation of telegrapher's equations and field-to-transmission line interaction," in *Electromagnetic Field Interaction with Transmission Lines*, vol. 29, pp. 3–22, WIT Press, feb 2008. *cited on page 140*

[127] H. Igarashi, "Semi-Analytical Approach for Finite Element Analysis of Multiturn Coil Considering Skin and Proximity Effects," *IEEE Transactions on Magnetics*, vol. 02, no. c, pp. 1–1, 2016. *cited on page 140*

[128] V. M. Machado, M. E. Pedro, J. B. Faria, and D. Van Dommelen, "Magnetic field analysis of three-conductor bundles in flat and triangular configurations with the inclusion of proximity and skin effects," *Electric Power Systems Research*, vol. 81, pp. 2005–2014, nov 2011. *cited on page 140 and 141*

[129] A. Semlyen and A. Dabuleanu, "Fast and accurate switching transient calculations on transmission lines with ground return using recursive convolutions," *IEEE Transactions on Power Apparatus and Systems*, vol. 94, pp. 561–571, Mar 1975. *cited on page 140 and 141*

[130] Chu-Sun Yen, Z. Fazarinc, and R. Wheeler, "Time-domain skin-effect model for transient analysis of lossy transmission lines," *Proceedings of the IEEE*, vol. 70, no. 7, pp. 750–757, 1982. *cited on page 140 and 141*

[131] Kyung Suk Oh, "Accurate transient simulation of transmission lines with the skin effect," *IEEE Transactions on Computer-Aided Design of Integrated Circuits and Systems*, vol. 19, pp. 389–396, mar 2000. *cited on page 140, 141, and 145*

[132] M. Dávila, J. L. Naredo, P. Moreno, and A. Ramirez, "Practical implementation of a transmission line model for transient analysis considering corona and skin effects," in *Power Tech Conference Proceedings, 2003 IEEE Bologna*, vol. 2, pp. 6 pp. Vol.2–, June 2003. *cited on page 141*

[133] W. S. Meyer and H. W. Dommel, "Numerical modelling of frequency-dependent transmission-line parameters in an electromagnetic transients program," *IEEE Transactions on Power Apparatus and Systems*, vol. PAS-93, pp. 1401–1409, Sept 1974. *cited on page 141 and 142*

[134] D. Wilcox and M. Condon, "A new transmission-line model for time-domain implementation," *COMPEL - The international journal for computation and mathematics in electrical and electronic engineering*, vol. 16, pp. 261–274, dec 1997. *cited on page 141 and 142*

[135] O. Gatous and J. Pissolato, "Frequency-dependent skin-effect formulation for resistance and internal inductance of a solid cylindrical conductor," *IEE Proceedings - Microwaves, Antennas and Propagation*, vol. 151, no. 3, p. 212, 2004. *cited on page 141 and 145*

[136] S. Kim and D. Neikirk, "Compact equivalent circuit model for the skin effect," in *1996 IEEE MTT-S International Microwave Symposium Digest*, vol. 3, pp. 1815–1818, IEEE, 1996. *cited on page 141*

[137] S. Crandall, "The role of damping in vibration theory," *Journal of Sound and Vibration*, vol. 11, no. 1, pp. 3 – IN1, 1970. *cited on page 143*

[138] C. Germoso, A. Fraile, E. Alarcon, J. Aguado, and F. Chinesta, "From standard to fractional structural visco-elastodynamics: Application to seismic site response," *Physics and Chemistry of the Earth, Parts A/B/C*, pp. –, 2016. *cited on page 143*

[139] R. A. Chipman, *Theory and Problems of Transmission Lines*. McGraw-Hill, 1968. *cited on page 144*

[140] P. Lucht, "Transmission Lines and Maxwell's Equations," tech. rep., 2014. *cited on page 145*

[141] J. H. A. Monteiro, E. C. M. Costa, A. J. G. Pinto, S. Kurokawa, O. M. O. Gatous, and J. Pissolato, "Simplified skin-effect formulation for power transmission lines," *IET Science, Measurement & Technology*, vol. 8, pp. 47–53, mar 2014. *cited on page 145*

[142] G.-A. J. Francisco, R.-G. Juan, G.-C. Manuel, and R.-H. J. Roberto, "Fractional RC and LC electrical circuits," *Ingenierìa, Investigación y Tecnología*, vol. 15, no. 2, pp. 311 – 319, 2014. *cited on page 151*

Appendix A

PGD Formulations

A.1 PGD for Current ODE

We need a separable solution to the eq. (4.12) in the form of

$$\hat{I}(x,\omega) = \sum_{i=1}^{n} X_i(x) O_i(\omega) \tag{A.1}$$

Eq. (4.12) along with the boundary conditions given in eq. (4.13) and eq. (4.14) represent the second order ODE for current along a transmission line. In order to develop a PGD formulation, first we must have a weak formulation of the problem.

Multiply eq. (4.12) with a test function $\delta I^*(x)$,

$$\int_{\Omega_x \times \Omega_\omega} \delta I^* \frac{\partial^2 \hat{I}}{\partial x^2}\, dx\, d\omega + \int_{\Omega_x \times \Omega_\omega} \delta I^* f(\omega) \hat{I}\, dx\, d\omega = 0 \tag{A.2}$$

where, $f(\omega) = (LC\omega^2 - \iota RC\omega)$.

Integrating by parts gives,

$$\begin{aligned} \int_{\Omega_x \times \Omega_\omega} \delta I^* \frac{\partial^2 \hat{I}}{\partial x^2}\, dx\, d\omega &= \int_{\Omega_\omega} \delta I^* \frac{\partial \hat{I}}{\partial x}\bigg|_{x=l} d\omega - \int_{\Omega_\omega} \delta I^* \frac{\partial \hat{I}}{\partial x}\bigg|_{x=0} d\omega \\ &- \int_{\Omega_x \times \Omega_\omega} \frac{\partial \delta I^*}{\partial x} \frac{\partial \hat{I}}{\partial x}\, dx\, d\omega \end{aligned} \tag{A.3}$$

With the boundary conditions given in eq. (4.13) or eq. (4.14), one of the terms in the eq. (A.3) becomes zero. For example, with boundary condition of eq. (4.13), we have

$$\int_{\Omega_x \times \Omega_\omega} \delta I^* \frac{\partial^2 \hat{I}}{\partial x^2}\, dx\, d\omega = -\int_{\Omega_\omega} \delta I^* \frac{\partial \hat{I}}{\partial x}\bigg|_{x=0} d\omega - \int_{\Omega_x \times \Omega_\omega} \frac{\partial \delta I^*}{\partial x} \frac{\partial \hat{I}}{\partial x}\, dx\, d\omega \tag{A.4}$$

Therefore, the weak form of eq. (A.2) becomes,

$$\int_{\Omega_x\times\Omega_\omega} \frac{\partial \delta I^*}{\partial x}\frac{\partial \hat{I}}{\partial x}\, dx\, d\omega - \int_{\Omega_x\times\Omega_\omega} f(\omega)\delta I^* \hat{I}\, dx\, d\omega = -\int_{\Omega_\omega} \delta I^*(x=0,\omega)\frac{\partial \hat{I}}{\partial x}\, d\omega \quad \text{(A.5)}$$

The PGD solution methodology is based upon an alternating strategy with the separated form of $\hat{I}(x,\omega)$ given above in eq. (A.1). We assume that the solution is converged until the step $n-1$, and the solution is during the enrichment step n in the p^{th} iteration,

$$\hat{I}(x,\omega) = \sum_{i=1}^{n-1} X_i(x)O_i(\omega) + X_n^p(x)O_n^{p-1}(\omega) \quad \text{(A.6)}$$

We assume the test function $\delta I(x,\omega)$ in the separated form as,

$$\delta I^*(x,\omega) = \delta X_n^*(x)O_n^{p-1*}(\omega) \quad \text{(A.7)}$$

Substituting eq. (A.6) and eq. (A.7) in eq. (A.5), we get

$$\begin{aligned}
&\int_{\Omega_x\times\Omega_\omega} \frac{d\delta X_n^*}{dx}\frac{dX_n^p}{dx} O_n^{p-1*}O_n^{p-1}\, dx\, d\omega - \int_{\Omega_x\times\Omega_\omega} f(\omega)\delta X_n^* X_n^p O_n^{p-1*}O_n^{p-1}\, dx\, d\omega = \\
&-\int_{\Omega_x\times\Omega_\omega} \sum_{i=1}^{n-1} \frac{d\delta X_n^*}{dx}\frac{dX_i}{dx} O_n^{p-1*}O_i\, dx\, d\omega + \int_{\Omega_x\times\Omega_\omega} f(\omega)\sum_{i=1}^{n-1} \delta X_n^* X_i O_n^{p-1*}O_i\, dx\, d\omega \\
&+\int_{\Omega_\omega} \delta X_n^* O_n^{p-1*}\hat{V}(\iota C\omega)\, d\omega
\end{aligned} \quad \text{(A.8)}$$

In the above equation, all functions of the parameter ω are known, and we can evaluate the corresponding one-dimensional integrals

$$\begin{aligned}
\alpha^x &= \int_{\Omega_\omega} O_n^{p-1*}O_n^{p-1}\, d\omega \\
\beta^x &= \int_{\Omega_\omega} f(\omega)O_n^{p-1*}O_n^{p-1}\, d\omega \\
\gamma_i^x &= \int_{\Omega_\omega} O_n^{p-1*}O_i\, d\omega \\
\delta_i^x &= \int_{\Omega_\omega} f(\omega)O_n^{p-1*}O_i\, d\omega \\
\mu^x &= \int_{\Omega_\omega} O_n^{p-1*}\hat{V}.(\iota C\omega)\, d\omega
\end{aligned} \quad \text{(A.9)}$$

Hence, we have a weighted residual form in the variable X_n^p,

$$\begin{aligned}
&\int_0^l \frac{d\delta X_n^*}{dx}\frac{dX_n^p}{dx}\alpha^x\, dx - \int_0^l \delta X_n^* X_n^p \beta^x\, dx = \\
&-\int_0^l \sum_{i=1}^{n-1} \frac{d\delta X_n^*}{dx}\frac{dX_i}{dx}\gamma_i^x\, dx + \int_0^l \sum_{i=1}^{n-1} \delta X_n^* X_i \delta_i^x\, dx + \delta X_n^*\mu^x|_{x=0}
\end{aligned} \quad \text{(A.10)}$$

The solution to eq. (A.10) can be found using finite elements which will give us X_n^p. The equation in terms of Finite Elements can be described as:

$$\begin{aligned}\alpha^x[K_x]\{X_n^p\} - \beta^x[M_x]\{X_n^p\} = -\sum_{i=1}^{n-1}(\gamma_i^x[K_x]\{X_i\} - \delta_i^x[M_x]\{X_i\}) \\ + \{1, 0, ..., 0\}^T\mu_x\end{aligned} \tag{A.11}$$

$$\begin{aligned}\alpha^x &= \{O_n^{p-1}\}^T[M_w^1]\{O_n^{p-1}\} \\ \beta^x &= \{O_n^{p-1}\}^T[M_w^2]\{O_n^{p-1}\} \\ \gamma_i^x &= \{O_n^{p-1}\}^T[M_w^1]\{O_i\} \\ \delta_i^x &= \{O_n^{p-1}\}^T[M_w^2]\{O_i\} \\ \mu^x &= \hat{V}\{O_n^{p-1}\}^T[M_w^1]\{(\iota C\omega)\}\end{aligned} \tag{A.12}$$

The next step will be to evaluate O_n^p,
We assume the solution in the separated form as:

$$\hat{I}(x,\omega) = \sum_{i=1}^{n-1} X_i(x)O_i(\omega) + X_n^p(x)O_n^p(\omega) \tag{A.13}$$

We assume the test function $I^*(x,\omega)$ in the separated form as

$$\delta I^*(x,\omega) = X_n^{p*}(x)\delta O_n^*(\omega) \tag{A.14}$$

Substituting eq. (A.13) and eq. (A.14) in eq. (A.5) and simplifying we get:

$$\begin{aligned}&\int_{\Omega_x\times\Omega_\omega} \frac{dX_n^{p*}}{dx}\frac{dX_n^p}{dx}\delta O_n^* O_n^p \; dx \; d\omega - \int_{\Omega_x\times\Omega_\omega} f(\omega)X_n^{p*}X_n^p\delta O_n^* O_n^p \; dx \; d\omega = \\ &-\int_{\Omega_x\times\Omega_\omega}\sum_{i=1}^{n-1}\frac{dX_i}{dx}O_i\frac{dX_n^{p*}}{dx}\delta O_n^* \; dx \; d\omega + \int_{\Omega_x\times\Omega_\omega} f(\omega)\sum_{i=1}^{n-1}X_iO_iX_n^{p*}\delta O_n^* \; dx \; d\omega \\ &+\int_{\Omega_\omega} X_n^{p*}|_{x=0}\delta O_n^*\hat{V}.(\iota C\omega) \; d\omega\end{aligned} \tag{A.15}$$

In this step, all the functions of the parameter x are known, and we can evaluate the following integrals,

$$\begin{aligned}\alpha^\omega &= \int_{\Omega_x}\frac{dX_n^{p*}}{dx}\frac{dX_n^p}{dx} \; dx \\ \beta^\omega &= \int_{\Omega_x} X_n^{p*}X_n^p \; dx \\ \gamma_i^\omega &= \int_{\Omega_x}\frac{dX_n^{p*}}{dx}\frac{dX_i}{dx} \; dx \\ \delta_i^\omega &= \int_{\Omega_x} X_n^{p*}X_i \; dx \\ \xi^\omega &= X_n^{p*}|_{x=0}\hat{V}\end{aligned} \tag{A.16}$$

Hence, we have eq. (A.15) as,

$$\int_{\Omega_\omega} \alpha^\omega O_n^p \delta O_n^* \, d\omega - \int_{\Omega_\omega} f(\omega)\beta^\omega O_n^p \delta O_n^* \, d\omega = -\int_{\Omega_\omega} \sum_{i=1}^{n-1} \gamma_i^\omega O_i \delta O_n^* \, d\omega + \int_{\Omega_\omega} f(\omega) \sum_{i=1}^{n-1} \delta_i^\omega O_i \delta O_n^* \, d\omega + \int_{\Omega_\omega} \xi^\omega \delta O_n^* (\iota C\omega) \, d\omega \tag{A.17}$$

The eq. (A.17) giving the weighted residual form doesn't involve any differential operators. The corresponding strong form results as:

$$\alpha^\omega O_n^p - f(\omega)\beta^\omega O_n^p = -\sum_{i=1}^{n-1} \gamma_i^\omega O_i + f(\omega) \sum_{i=1}^{n-1} \delta_i^\omega O_i + \xi^\omega (\iota C\omega) \tag{A.18}$$

$$(\alpha^\omega - f(\omega)\beta^\omega) O_n^p = -\sum_{i=1}^{n-1} (\gamma_i^\omega - f(\omega)\delta_i^\omega) O_i + \xi^\omega (\iota C\omega) \tag{A.19}$$

This is a set of algebraic equations solving which gives the unknown function $O_n^p(\omega)$.

Alternatively, we can solve eq. (A.17) using FEM.

$$(\alpha^\omega [M_\omega] - \beta^\omega [M_\omega^A])\{O_n^p\} = -\sum_{i=1}^{n-1} (\gamma_i^\omega [M_\omega] - \delta_i^\omega [M_\omega^A])\{O_i\} + \xi^\omega \{(\iota C\omega)\} \tag{A.20}$$

This is an algebraic equation solving which gives the unknown function $O_n^p(\omega)$.

A.2 PGD Formulation with Inductance L as an extra parameter

$$\hat{V}(x, \omega, L) = \sum_{i=1}^{n} X_i(x) O_i(\omega) L_i(L) \tag{A.21}$$

The test function is defined as,

$$\delta V(x, \omega, L) = \delta X(x) O(\omega) L(L)) + X(x) \delta O(\omega) L(L) + X(x) O(\omega) \delta L(L) \tag{A.22}$$

The term $LC\omega^2 - RC\omega$ has to be separated as well. Therefore, we define the following functions,

$$\begin{aligned} &f_1(\omega) = C\omega^2 \qquad f_2(\omega) = RC\omega\iota \\ &g_1(L) = L \qquad\quad g_2(L) = 1 \\ &F = LC\omega^2 - RC\omega\iota = f_1(\omega)g_1(L) - f_2(\omega)g_2(L) \end{aligned} \tag{A.23}$$

The generic bi-linear form is defined as,

$$\begin{aligned} &m_1(O,\tilde{O})a_1(X,\tilde{X})p_1(L,\tilde{L}) - m_2(O,\tilde{O})a_2(X,\tilde{X})p_2(L,\tilde{L}) \\ &+ m_3(O,\tilde{O})a_2(X,\tilde{X})p_3(L,\tilde{L}) = l_1^O(\tilde{O})l_1^X(\tilde{X})l_1^L(\tilde{L}) + l_2^O(\tilde{O})l_2^X(\tilde{X})l_2^L(\tilde{L}) \end{aligned} \tag{A.24}$$

With the following definitions

$$\begin{aligned} &a_1(X,\tilde{X}) = \int_{\Omega_x} \frac{d\tilde{X}^*(x)}{dx}\frac{dX(x)}{dx}dx \ , \quad a_2(X,\tilde{X}) = \int_{\Omega_x} \tilde{X}^*(x)X(x)dx \\ &m_1(O,\tilde{O}) = \int_{\Omega_\omega} \tilde{O}^*(\omega)O(\omega)d\omega \ , \quad m_2(O,\tilde{O}) = \int_{\Omega_\omega} f_1(\omega)\tilde{O}^*(\omega)O(\omega)d\omega \\ &m_3(O,\tilde{O}) = \int_{\Omega_\omega} f_2(\omega)\tilde{O}^*(\omega)O(\omega)d\omega \\ &p_1(L,\tilde{L}) = \int_{\Omega_L} \tilde{L}^*(L)L(L)dL \ , \quad p_2(L,\tilde{L}) = \int_{\Omega_L} g_1(L)\tilde{L}^*(L)L(L)dL \\ &p_3(L,\tilde{L}) = \int_{\Omega_L} g_2(L)\tilde{L}^*(L)L(L)dL \\ &l_1^O(\tilde{O}) = \int_{\Omega_\omega} \omega\tilde{O}^*(\omega)d\omega \ , \quad l_2^O(\tilde{O}) = \int_{\Omega_\omega} \tilde{O}^*(\omega)d\omega \\ &l_1^X(\tilde{X}) = \tilde{X}^*(x)(x=0).I_1\iota \ , \quad l_2^X(\tilde{X}) = \tilde{X}^*(x)(x=0).I_1.R \\ &l_1^L(\tilde{L}) = \int_{\Omega_L} L\tilde{L}^*(L)dL \ , \quad l_2^L(\tilde{L}) = \int_{\Omega_L} \tilde{L}^*(L)dL \end{aligned} \tag{A.25}$$

We now, define the alternating algorithm to calculate X_n assuming O_n and L_n known, the separated function and test function are,

$$\begin{aligned} \hat{V}^n &= \hat{V}^{n-1} + X_n O_n L_n \\ \delta V &= \delta X_n O_n L_n \end{aligned} \tag{A.26}$$

The bi-linear form reads,

$$\begin{aligned} &m_1(O_n,O_n)a_1(X_n,\delta X_n)p_1(L_n,L_n) - m_2(O_n,O_n)a_2(X_n,\delta X_n)p_2(L_n,L_n) \\ &+ m_3(O_n,O_n)a_2(X_n,\delta X_n)p_3(L_n,L_n) = -\sum_{i=1}^{n-1} m_1(O_i,O_n)a_1(X_i,\delta X_n)p_1(L_i,L_n) \\ &+ \sum_{i=1}^{n-1} m_2(O_i,O_n)a_2(X_i,\delta X_n)p_2(L_i,L_n) - \sum_{i=1}^{n-1} m_3(O_i,O_n)a_2(X_i,\delta X_n)p_3(L_i,L_n) \\ &+ l_1^O(O_n)l_1^X(\delta X_n)l_1^L(L_n) + l_2^O(O_n)l_2^X(\delta X_n)l_2^L(L_n) \end{aligned} \tag{A.27}$$

To calculate X_n^p, using the weak form

$$\begin{aligned}
&\int_{\Omega_x} \frac{d\delta X_n^*}{dx}\frac{dX_n}{dx}dx \int_{\Omega_\omega} O_n^* O_n d\omega \int_{\Omega_L} L_n^* L_n dL \\
&- \int_{\Omega_x} \delta X_n^* X_n dx \int_{\Omega_\omega} f_1(\omega) O_n^* O_n d\omega \int_{\Omega_L} g_1(L) L_n^* L_n dL \\
&+ \int_{\Omega_x} \delta X_n^* X_n dx \int_{\Omega_\omega} f_2(\omega) O_n^* O_n d\omega \int_{\Omega_L} g_2(L) L_n^* L_n dL = \\
&- \sum_{i=1}^{n-1} \int_{\Omega_x} \frac{d\delta X_n^*}{dx}\frac{dX_i}{dx}dx \int_{\Omega_\omega} O_n^* O_i d\omega \int_{\Omega_L} L_n^* L_i dL \\
&+ \sum_{i=1}^{n-1} \int_{\Omega_x} \delta X_n^* X_i dx \int_{\Omega_\omega} f_1(\omega) O_n^* O_i d\omega \int_{\Omega_L} g_1(L) L_n^* L_i dL \\
&- \sum_{i=1}^{n-1} \int_{\Omega_x} \delta X_n^* X_i dx \int_{\Omega_\omega} f_2(\omega) O_n^* O_i d\omega \int_{\Omega_L} g_2(L) L_n^* L_i dL \\
&+ \delta X_n^*(x=0).I_1 \iota \int_{\Omega_\omega} \omega O_n^* d\omega \int_{\Omega_L} L L_n^* dL \\
&+ \delta X_n^*(x=0).I_1.R \int_{\Omega_\omega} O_n^* d\omega \int_{\Omega_L} L_n^* dL
\end{aligned} \tag{A.28}$$

In matrix terms, we can write

$$\begin{aligned}
&\{X_n\}[K_x].\{O_n^*\}[M_\omega]\{O_n\}.\{L_n^*\}[M_L]\{L_n\} \\
&- \{X_n\}[M_x].\{O_n^*\}[M_\omega^2]\{O_n\}.\{L_n^*\}[M_L^1]\{L_n\} \\
&+ \{X_n\}[M_x].\{O_n^*\}[M_\omega^1]\{O_n\}.\{L_n^*\}[M_L]\{L_n\} = \\
&- \sum_{i=1}^{n-1} \{X_i\}[K_x].\{O_n^*\}[M_\omega]\{O_i\}.\{L_n^*\}[M_L]\{L_i\} \\
&+ \sum_{i=1}^{n-1} \{X_i\}[M_x].\{O_n^*\}[M_\omega^2]\{O_i\}.\{L_n^*\}[M_L^1]\{L_i\} \\
&- \sum_{i=1}^{n-1} \{X_i\}[M_x].\{O_n^*\}[M_\omega^1]\{O_i\}.\{L_n^*\}[M_L]\{L_i\} \\
&+ \{1,0,\cdots,0\}^T.I_1\iota\{O_n^*\}[M_\omega^1]\{1\}\{L_n^*\}[M_L^1]\{1\} \\
&+ \{1,0,\cdots,0\}^T.I_1.R\{O_n^*\}[M_\omega]\{1\}\{L_n^*\}[M_L]\{1\}
\end{aligned} \tag{A.29}$$

To calculate O_n assuming X_n and L_n known, the separated function and test function are,

$$\begin{aligned}
\hat{V}^n &= \hat{V}^{n-1} + X_n O_n L_n \\
\delta V &= X_n \delta O_n L_n
\end{aligned} \tag{A.30}$$

The bi-linear form reads

$$
\begin{aligned}
&m_1(O_n,\delta O_n)a_1(X_n,X_n)p_1(L_n,L_n) - m_2(O_n,\delta O_n)a_2(X_n,X_n)p_2(L_n,L_n)\\
&+ m_3(O_n,\delta O_n)a_2(X_n,X_n)p_3(L_n,L_n) = -\sum_{i=1}^{n-1} m_1(O_i,\delta O_n)a_1(X_i,X_n)p_1(L_i,L_n)\\
&+ \sum_{i=1}^{n-1} m_2(O_i,\delta O_n)a_2(X_i,X_n)p_2(L_i,L_n) - \sum_{i=1}^{n-1} m_3(O_i,\delta O_n)a_2(X_i,X_n)p_3(L_i,L_n)\\
&+ l_1^O(\delta O_n)l_1^X(X_n)l_1^L(L_n) + l_2^O(\delta O_n)l_2^X(X_n)l_2^L(L_n)
\end{aligned}
\tag{A.31}
$$

To calculate O_n^p, using the weak form

$$
\begin{aligned}
&\int_{\Omega_x}\frac{dX_n^*}{dx}\frac{dX_n}{dx}dx\int_{\Omega_\omega}\delta O_n^* O_n d\omega\int_{\Omega_L} L_n^* L_n dL\\
&-\int_{\Omega_x} X_n^* X_n dx\int_{\Omega_\omega} f_1(\omega)\delta O_n^* O_n d\omega\int_{\Omega_L} g_1(L)L_n^* L_n dL\\
&+\int_{\Omega_x} X_n^* X_n dx\int_{\Omega_\omega} f_2(\omega)\delta O_n^* O_n d\omega\int_{\Omega_L} g_2(L)L_n^* L_n dL =\\
&-\sum_{i=1}^{n-1}\int_{\Omega_x}\frac{dX_n^*}{dx}\frac{dX_i}{dx}dx\int_{\Omega_\omega}\delta O_n^* O_i d\omega\int_{\Omega_L} L_n^* L_i dL\\
&+\sum_{i=1}^{n-1}\int_{\Omega_x} X_n^* X_i dx\int_{\Omega_\omega} f_1(\omega)\delta O_n^* O_i d\omega\int_{\Omega_L} g_1(L)L_n^* L_i dL\\
&-\sum_{i=1}^{n-1}\int_{\Omega_x} X_n^* X_i dx\int_{\Omega_\omega} f_2(\omega)\delta O_n^* O_i d\omega\int_{\Omega_L} g_2(L)L_n^* L_i dL\\
&+X_n^*(x=0).I_1\iota\int_{\Omega_\omega}\omega\delta O_n^* d\omega\int_{\Omega_L} LL_n^* dL\\
&+X_n^*(x=0).I_1.R\int_{\Omega_\omega}\delta O_n^* d\omega\int_{\Omega_L} L_n^* dL
\end{aligned}
\tag{A.32}
$$

In matrix terms, we can write

$$
\begin{aligned}
&[M_\omega]\{O_n\}.\{X_n^*\}[K_x]\{X_n\}.\{L_n^*\}[M_L]\{L_n\}\\
&-[M_\omega^2]\{O_n\}.\{X_n^*\}[M_x]\{X_n\}.\{L_n^*\}[M_L^1]\{L_n\}\\
&+[M_\omega^1]\{O_n\}.\{X_n^*\}[M_x]\{X_n\}.\{L_n^*\}[M_L]\{L_n\} =\\
&-\sum_{i=1}^{n-1}[M_\omega]\{O_i\}.\{X_n^*\}[K_x]\{X_i\}.\{L_n^*\}[M_L]\{L_i\}\\
&+\sum_{i=1}^{n-1}[M_\omega^2]\{O_i\}.\{X_n^*\}[M_x]\{X_i\}.\{L_n^*\}[M_L^1]\{L_i\}\\
&-\sum_{i=1}^{n-1}[M_\omega^1]\{O_i\}.\{X_n^*\}[M_x]\{X_i\}.\{L_n^*\}[M_L]\{L_i\}\\
&+X_n^*(x=0).I_1\iota[M_\omega^1]\{1\}\{L_n^*\}[M_L^1]\{1\}\\
&+X_n^*(x=0).I_1.R[M_\omega]\{1\}\{L_n^*\}[M_L]\{1\}
\end{aligned}
\tag{A.33}
$$

To calculate L_n assuming X_n and O_n known, the separated function and test function are

$$\begin{aligned}\hat{V}^n &= \hat{V}^{n-1} + X_n O_n L_n \\ \delta V &= X_n O_n \delta L_n\end{aligned} \tag{A.34}$$

The bi-linear form reads

$$\begin{aligned}&m_1(O_n,O_n)a_1(X_n,X_n)p_1(L_n,\delta L_n) - m_2(O_n,O_n)a_2(X_n,X_n)p_2(L_n,\delta L_n) \\ &+ m_3(O_n,O_n)a_2(X_n,X_n)p_3(L_n,\delta L_n) = -\sum_{i=1}^{n-1} m_1(O_i,O_n)a_1(X_i,X_n)p_1(L_i,\delta L_n) \\ &+ \sum_{i=1}^{n-1} m_2(O_i,O_n)a_2(X_i,X_n)p_2(L_i,\delta L_n) - \sum_{i=1}^{n-1} m_3(O_i,O_n)a_2(X_i,X_n)p_3(L_i,\delta L_n) \\ &+ l_1^O(O_n)l_1^X(X_n)l_1^L(\delta L_n) + l_2^O(O_n)l_2^X(X_n)l_2^L(\delta L_n)\end{aligned} \tag{A.35}$$

To calculate L_n^p, using the weak form

$$\begin{aligned}&\int_{\Omega_x} \frac{dX_n^*}{dx}\frac{dX_n}{dx}dx \int_{\Omega_\omega} O_n^* O_n d\omega \int_{\Omega_L} \delta L_n^* L_n dL \\ &- \int_{\Omega_x} X_n^* X_n dx \int_{\Omega_\omega} f_1(\omega) O_n^* O_n d\omega \int_{\Omega_L} g_1(L)\delta L_n^* L_n dL \\ &+ \int_{\Omega_x} X_n^* X_n dx \int_{\Omega_\omega} f_2(\omega) O_n^* O_n d\omega \int_{\Omega_L} g_2(L)\delta L_n^* L_n dL = \\ &- \sum_{i=1}^{n-1} \int_{\Omega_x} \frac{dX_n^*}{dx}\frac{dX_i}{dx}dx \int_{\Omega_\omega} O_n^* O_i d\omega \int_{\Omega_L} \delta L_n^* L_i dL \\ &+ \sum_{i=1}^{n-1} \int_{\Omega_x} X_n^* X_i dx \int_{\Omega_\omega} f_1(\omega) O_n^* O_i d\omega \int_{\Omega_L} g_1(L)\delta L_n^* L_i dL \\ &- \sum_{i=1}^{n-1} \int_{\Omega_x} X_n^* X_i dx \int_{\Omega_\omega} f_2(\omega) O_n^* O_i d\omega \int_{\Omega_L} g_2(L)\delta L_n^* L_i dL \\ &+ X_n^*(x=0).I_1 \iota \int_{\Omega_\omega} \omega O_n^* d\omega \int_{\Omega_L} L\delta L_n^* dL \\ &+ X_n^*(x=0).I_1.R \int_{\Omega_\omega} O_n^* d\omega \int_{\Omega_L} \delta L_n^* dL\end{aligned} \tag{A.36}$$

In matrix terms, we can write

$$
\begin{aligned}
&[M_L]\{L_n\}.\{X_n^*\}[K_x]\{X_n\}.\{O_n^*\}[M_\omega]\{O_n\} \\
&- [M_L^1]\{L_n\}.\{X_n^*\}[M_x]\{X_n\}.\{O_n^*\}[M_\omega^2]\{O_n\} \\
&+ [M_L]\{L_n\}.\{X_n^*\}[M_x]\{X_n\}.\{O_n^*\}[M_\omega^1]\{O_n\} = \\
&- \sum_{i=1}^{n-1}[M_L]\{L_i\}.\{X_n^*\}[K_x]\{X_i\}.\{O_n^*\}[M_\omega]\{O_i\} \\
&+ \sum_{i=1}^{n-1}[M_L^1]\{L_i\}.\{X_n^*\}[M_x]\{X_i\}.\{O_n^*\}[M_\omega^2]\{O_i\} \\
&- \sum_{i=1}^{n-1}[M_L]\{L_i\}.\{X_n^*\}[M_x]\{X_i\}.\{O_n^*\}[M_\omega^1]\{O_i\} \\
&+ X_n^*(x=0).I_1\iota\{O_n^*\}[M_\omega^1]\{1\}[M_L^1]\{1\} \\
&+ X_n^*(x=0).I_1.R\{O_n^*\}[M_\omega]\{1\}[M_L]\{1\}
\end{aligned}
\tag{A.37}
$$

A.3 Parametric Solution with R, L, C included

For the fully parametric solution, we need the separated solution in the form as:

$$
V(x,\omega,L,R,C) = \sum_{i=1}^{n} X_i(x)O_i(\omega)L_i(L)R_i(R)C_i(C) \tag{A.38}
$$

As with the tradition, we assume that the solution is in the p^{th} iteration for the mode N and all the previous modes have converged. At this stage, the separated representation and the test functions are given as

$$
\begin{aligned}
V(x,\omega,L,R,C) = &\sum_{i=1}^{n-1} X_i(x)O_i(\omega)L_i(L)R_i(R)C_i(C) + \\
&X_n^p(x)O_n^{p-1}(\omega)L_n^{p-1}(L)R_n^{p-1}(R)C_n^{p-1}(C)
\end{aligned}
\tag{A.39}
$$

$$
\delta V^*(x,\omega,L,R,C) = \delta X_n^*(x)O_n^{p-1*}(\omega)L_n^{p-1*}(L)R_n^{p-1*}(R)C_n^{p-1*}(C) \tag{A.40}
$$

For the sake of simplicity we drop the superscript p and $p-1$ from eq. (A.39) and eq. (A.40).

$$
\begin{aligned}
V(x,\omega,L,R,C) = &\sum_{i=1}^{n-1} X_i(x)O_i(\omega)L_i(L)R_i(R)C_i(C) + \\
&X_n(x)O_n(\omega)L_n(L)R_n(R)C_n(C)
\end{aligned}
\tag{A.41}
$$

$$
\delta V^*(x,\omega,L,R,C) = \delta X_n^*(x)O_n^*(\omega)L_n^*(L)R_n^*(R)C_n^*(C) \tag{A.42}
$$

Let us define some definitions for the integrals we will be using in this section.

$$\begin{aligned} x_1 &= \int_{\Omega_x} \frac{\partial X_n^*}{\partial x}\frac{\partial X_n}{\partial x}\, dx \qquad x_2 = \int_{\Omega_x} X_n^* X_n\, dx \\ x_3^i &= \int_{\Omega_x} \frac{\partial X_n^*}{\partial x}\frac{\partial X_i}{\partial x}\, dx \qquad x_4^i = \int_{\Omega_x} X_n^* X_n\, dx \end{aligned} \tag{A.43}$$

$$\begin{aligned} o_1 &= \int_{\Omega_\omega} O_n^* O_n\, d\omega \quad o_2 = \int_{\Omega_\omega} \omega^2 O_n^* O_n\, d\omega \quad o_3 = \int_{\Omega_\omega} \omega O_n^* O_n\, d\omega \\ o_4^i &= \int_{\Omega_\omega} O_n^* O_i\, d\omega \quad o_5^i = \int_{\Omega_\omega} \omega^2 O_n^* O_i\, d\omega \quad o_6^i = \int_{\Omega_\omega} \omega O_n^* O_i\, d\omega \end{aligned} \tag{A.44}$$

$$\begin{aligned} l_1 &= \int_{\Omega_L} L_n^* L_n\, dL \qquad l_2 = \int_{\Omega_L} L L_n^* L_n\, dL \\ l_3^i &= \int_{\Omega_L} L_n^* L_i\, dL \qquad l_4^i = \int_{\Omega_L} L L_n^* L_i\, dL \end{aligned} \tag{A.45}$$

$$\begin{aligned} c_1 &= \int_{\Omega_C} C_n^* C_n\, dC \qquad c_2 = \int_{\Omega_C} C C_n^* C_n\, dC \\ c_3^i &= \int_{\Omega_C} C_n^* C_i\, dC \qquad c_4^i = \int_{\Omega_C} C C_n^* C_i\, dC \end{aligned} \tag{A.46}$$

$$\begin{aligned} r_1 &= \int_{\Omega_R} R_n^* R_n\, dR \qquad r_2 = \int_{\Omega_R} R R_n^* R_n\, dR \\ r_3^i &= \int_{\Omega_R} R_n^* R_i\, dR \qquad r_4^i = \int_{\Omega_R} R R_n^* R_i\, dR \end{aligned} \tag{A.47}$$

$$\begin{aligned} x_1^b &= Xn^*(x=0) \\ o_1^b &= \int_{\Omega_\omega} O_n^*\, d\omega \qquad o_2^b = \int_{\Omega_\omega} \omega O_n^*\, d\omega \\ l_1^b &= \int_{\Omega_L} L_n^*\, dL \qquad l_2^b = \int_{\Omega_L} L L_n^*\, dL \\ c_1^b &= \int_{\Omega_C} C_n^*\, dC \\ r_1^b &= \int_{\Omega_R} R R_n^*\, dR \qquad r_2^b = \int_{\Omega_R} R_n^*\, dR \end{aligned} \tag{A.48}$$

Inserting eq. (A.36) in the eq. (4.15) and multiply by the test function of eq. (A.37) and simplifying. Skipping the intermediate steps as it is similar to the previous sections and presenting the codifiable form

$$\begin{aligned} &\int_{\Omega_x} \frac{\partial \delta X_n^*}{\partial x}\frac{\partial X_n}{\partial x}.o_1.l_1.c_1.r_1\, dx - \int_{\Omega_x} \delta X_n^* X_n.o_2.l_2.c_2.r_1\, dx \\ &+ \int_{\Omega_x} \delta X_n^* X_n.o_3.l_1.c_2.r_2\, dx\ \iota = -\sum_{i=1}^{n-1} \int_{\Omega_x} \frac{\partial \delta X_n^*}{\partial x}\frac{\partial X_i}{\partial x}.o_4^i.l_3^i.c_3^i.r_3^i\, dx \\ &+ \sum_{i=1}^{n-1} \int_{\Omega_x} \delta X_n^* X_i.o_5^i.l_4^i.c_4^i.r_3^i\, dx - \sum_{i=1}^{n-1} \int_{\Omega_x} \delta X_n^* X_i.o_6^i.l_3^i.c_4^i.r_4^i\, dx\ \iota \\ &+ I_1 \delta X_n^*(x=0).o_1^b.l_1^b.c_1^b.r_1^b + I_1 \delta X_n^*(x=0).o_2^b.l_2^b.c_1^b.r_2^b\ \iota \end{aligned} \tag{A.49}$$

In matrix notation, the above equation is much easier to interpret and is,

$$
\begin{aligned}
&[K_x]\vec{X_n}.o_1.l_1.c_1.r_1 - [M_x]\vec{X_n}.o_2.l_2.c_2.r_1 + [M_x]\vec{X_n}.o_3.l_1.c_2.r_2\ \iota = \\
&-\sum_{i=1}^{n-1}[K_x]\vec{X_i}.o_4^i.l_3^i.c_3^i.r_3^i + \sum_{i=1}^{n-1}[M_x]\vec{X_i}.o_5^i.l_4^i.c_4^i.r_3^i - \sum_{i=1}^{n-1}[M_x]\vec{X_i}.o_6^i.l_3^i.c_4^i.r_4^i\ \iota \\
&+ I_1.\delta\vec{X}_n^*(x=0).o_1^b.l_1^b.c_1^b.r_1^b + I_1.\delta\vec{X}_n^*(x=0).o_2^b.l_2^b.c_1^b.r_2^b\ \iota
\end{aligned}
\tag{A.50}
$$

For calculating O_n,

$$
\begin{aligned}
&\int_{\Omega_\omega} O_n\delta O_n^*.x_1.l_1.c_1.r_1\ d\omega - \int_{\Omega_\omega}\omega^2.O_n\delta O_n^*.x_2.l_2.c_2.r_1\ d\omega \\
&+\int_{\Omega_\omega}\omega.O_n\delta O_n^*.x_2.l_1.c_2.r_2\ d\omega\ \iota = -\sum_{i=1}^{n-1}\int_{\Omega_\omega} O_i\delta O_n^*.x_3^i.l_3^i.c_3^i.r_3^i\ d\omega \\
&+\sum_{i=1}^{n-1}\int_{\Omega_\omega}\omega^2.O_i\delta O_n^*.x_4^i.l_4^i.c_4^i.r_3^i\ d\omega - \sum_{i=1}^{n-1}\int_{\Omega_\omega}\omega.O_i\delta O_n^*.x_4^i.l_3^i.c_4^i.r_4^i\ d\omega\ \iota \\
&+\int_{\Omega_\omega}\delta O_n^*.x_1^b.l_1^b.c_1^b.r_1^b\ d\omega + \int_{\Omega_\omega}\delta O_n^*.x_1^b.l_2^b.c_1^b.r_2^b\ d\omega\ \iota
\end{aligned}
\tag{A.51}
$$

In matrix notation, the above equation is much easier to interpret and is,

$$
\begin{aligned}
&[M_\omega]\vec{O_n}.x_1.l_1.c_1.r_1 - [M_\omega^2]\vec{O_n}.x_2.l_2.c_2.r_1 + [M_\omega^1]\vec{O_n}.x_2.l_1.c_2.r_2\ \iota = \\
&-\sum_{i=1}^{n-1}[M_\omega]\vec{O_i}.x_3^i.l_3^i.c_3^i.r_3^i + \sum_{i=1}^{n-1}[M_\omega^2]\vec{O_i}.x_4^i.l_4^i.c_4^i.r_3^i - \sum_{i=1}^{n-1}[M_\omega^1]\vec{O_i}.x_4^i.l_3^i.c_4^i.r_4^i\ \iota \\
&+[M_\omega]\vec{1}.x_1^b.l_1^b.c_1^b.r_1^b + [M_\omega^1]\vec{1}.x_1^b.l_2^b.c_1^b.r_2^b\ \iota
\end{aligned}
\tag{A.52}
$$

For calculating L_n,

$$
\begin{aligned}
&\int_{\Omega_L} L_n\delta L_n^*.x_1.\omega_1.c_1.r_1\ dL - \int_{\Omega_L} L.L_n\delta L_n^*.x_2.\omega_2.c_2.r_1\ dL \\
&+\int_{\Omega_L} L_n\delta L_n^*.x_2.\omega_3.c_2.r_2\ dL\ \iota = -\sum_{i=1}^{n-1}\int_{\Omega_L} L_i\delta L_n^*.x_3^i.\omega_4^i.c_3^i.r_3^i\ dL \\
&+\sum_{i=1}^{n-1}\int_{\Omega_L} L.L_i\delta L_n^*.x_4^i.\omega_5^i.c_4^i.r_3^i\ dL - \sum_{i=1}^{n-1}\int_{\Omega_L} L_i\delta L_n^*.x_4^i.\omega_6^i.c_4^i.r_4^i\ dL\ \iota \\
&+\int_{\Omega_L}\delta L_n^*.x_1^b.\omega_1^b.c_1^b.r_1^b\ dL + \int_{\Omega_L} L.\delta L_n^*.x_1^b.\omega_2^b.c_1^b.r_2^b\ dL\ \iota
\end{aligned}
\tag{A.53}
$$

In matrix notation, the above equation is much easier to interpret and is,

$$
\begin{aligned}
&[M_L]\vec{L_n}.x_1.\omega_1.c_1.r_1 - [M_L^1]\vec{L_n}.x_2.\omega_2.c_2.r_1 + [M_L]\vec{L_n}.x_2.\omega_3.c_2.r_2\ \iota = \\
&-\sum_{i=1}^{n-1}[M_L]\vec{L_i}.x_3^i.\omega_4^i.c_3^i.r_3^i + \sum_{i=1}^{n-1}[M_L^1]\vec{L_i}.x_4^i.\omega_5^i.c_4^i.r_3^i - \sum_{i=1}^{n-1}[M_L]\vec{L_i}.x_4^i.\omega_6^i.c_4^i.r_4^i\ \iota \\
&+[M_L]\vec{1}.x_1^b.\omega_1^b.c_1^b.r_1^b + [M_L^1]\vec{1}.x_1^b.\omega_2^b.c_1^b.r_2^b\ \iota
\end{aligned}
\tag{A.54}
$$

For calculating C_n,

$$\begin{aligned}
&\int_{\Omega_C} C_n \delta C_n^*.x_1.\omega_1.l_1.r_1 \; dC - \int_{\Omega_C} C.C_n \delta C_n^*.x_2.\omega_2.l_2.r_1 \; dC \\
&+ \int_{\Omega_C} C.C_n \delta C_n^*.x_2.\omega_3.l_1.r_2 \; dC \; \iota = -\sum_{i=1}^{n-1} \int_{\Omega_C} C_i \delta C_n^*.x_3^i.\omega_4^i.l_3^i.r_3^i \; dC \\
&+ \sum_{i=1}^{n-1} \int_{\Omega_C} C.C_i \delta C_n^*.x_4^i.\omega_5^i.l_4^i.r_3^i \; dC - \sum_{i=1}^{n-1} \int_{\Omega_C} C.C_i \delta C_n^*.x_4^i.\omega_6^i.l_3^i.r_4^i \; dC \; \iota \\
&+ \int_{\Omega_C} \delta C_n^*.x_1^b.\omega_1^b.l_1^b.r_1^b \; dC + \int_{\Omega_C} \delta C_n^*.x_1^b.\omega_2^b.l_2^b.r_2^b \; dC \; \iota
\end{aligned} \tag{A.55}$$

In matrix notation, the above equation is much easier to interpret and is,

$$\begin{aligned}
&[M_C]\vec{C_n}.x_1.\omega_1.l_1.r_1 - [M_C^1]\vec{C_n}.x_2.\omega_2.l_2.r_1 + [M_C^1]\vec{C_n}.x_2.\omega_3.l_1.r_2 \; \iota = \\
&-\sum_{i=1}^{n-1}[M_C]\vec{C_i}.x_3^i.\omega_4^i.l_3^i.r_3^i + \sum_{i=1}^{n-1}[M_C^1]\vec{C_i}.x_4^i.\omega_5^i.l_4^i.r_3^i - \sum_{i=1}^{n-1}[M_C^1]\vec{C_i}.x_4^i.\omega_6^i.l_3^i.r_4^i \; \iota \\
&+ [M_C]\vec{1}.x_1^b.\omega_1^b.l_1^b.r_1^b + [M_C]\vec{1}.x_1^b.\omega_2^b.l_2^b.r_2^b \; \iota
\end{aligned} \tag{A.56}$$

For calculating R_n,

$$\begin{aligned}
&\int_{\Omega_R} R_n \delta R_n^*.x_1.\omega_1.l_1.c_1 \; dR - \int_{\Omega_R} R_n \delta R_n^*.x_2.\omega_2.l_2.c_2 \; dR \\
&+ \int_{\Omega_R} R.R_n \delta R_n^*.x_2.\omega_3.l_1.c_2 \; dR \; \iota = -\sum_{i=1}^{n-1} \int_{\Omega_R} R_i \delta R_n^*.x_3^i.\omega_4^i.l_3^i.c_3^i \; dR \\
&+ \sum_{i=1}^{n-1} \int_{\Omega_R} R_i \delta R_n^*.x_4^i.\omega_5^i.l_4^i.c_4^i \; dR - \sum_{i=1}^{n-1} \int_{\Omega_R} R.R_i \delta R_n^*.x_4^i.\omega_6^i.l_3^i.c_4^i \; dR \; \iota \\
&+ \int_{\Omega_R} R \delta R_n^*.x_1^b.\omega_1^b.l_1^b.c_1^b \; dR + \int_{\Omega_R} \delta R_n^*.x_1^b.\omega_2^b.l_2^b.c_1^b \; dR \; \iota
\end{aligned} \tag{A.57}$$

In matrix notation, the above equation is much easier to interpret and is,

$$\begin{aligned}
&[M_R]\vec{R_n}.x_1.\omega_1.l_1.c_1 - [M_R]\vec{R_n}.x_2.\omega_2.l_2.c_2 + [M_R^1]\vec{R_n}.x_2.\omega_3.l_1.c_2 \; \iota = \\
&-\sum_{i=1}^{n-1}[M_R]\vec{R_i}.x_3^i.\omega_4^i.l_3^i.c_3^i + \sum_{i=1}^{n-1}[M_R]\vec{R_i}.x_4^i.\omega_5^i.l_4^i.c_4^i - \sum_{i=1}^{n-1}[M_R^1]\vec{R_i}.x_4^i.\omega_6^i.l_3^i.c_4^i \; \iota \\
&+ [M_R^1]\vec{1}.x_1^b.\omega_1^b.l_1^b.c_1^b + [M_R]\vec{1}.x_1^b.\omega_2^b.l_2^b.c_1^b \; \iota
\end{aligned} \tag{A.58}$$

UNIVERSITE BRETAGNE LOIRE

Thèse de Doctorat

Muhammad Haris MALIK

Reduced Order Modeling for Smart Grids' Simulation and Optimization

Modélisation à ordre réduit pour la simulation et l'optimisation des réseaux intelligents

Résumé

Cette thèse présente l'étude de la réduction de modèles pour les réseaux électriques et les réseaux de transmission. Un point de vue mathématique a été adopté pour la réduction de modèles. Les réseaux électriques sont des réseaux immenses et complexes, dont l'analyse et la conception nécessite la simulation et la résolution de grands modèles non-linéaires. Dans le cadre du développement de réseaux électriques intelligents (smart grids) avec une génération distribuée de puissance, l'analyse en temps réel de systèmes complexes tels que ceux-ci nécessite des modèles rapides, fiables et précis. Dans la présente étude, nous proposons des méthodes de réduction de de modèles à la fois a priori et a posteriori, adaptées aux modèles dynamiques des réseaux électriques.

Un accent particulier a été mis sur la dynamique transitoire des réseaux électriques, décrite par un modèle oscillant non-linéaire et complexe. La non-linéarité de ce modèle nécessite une attention particulière pour bénéficier du maximum d'avantages des techniques de réduction de modèles. Initialement, des méthodes comme POD et LATIN ont été adoptées avec des degrés de succès divers. La méthode de TPWL, qui combine la POD avec des approximations linéaires multiples, a été prouvée comme étant la méthode de réduction de modèles la mieux adaptée pour le modèle dynamique oscillant.

Pour les lignes de transmission, un modèle de paramètres distribués en domaine fréquentiel est utilisé. Des modèles réduits de type PGD sont proposés pour le modèle DP des lignes de transmission. Un problème multidimensionnel entièrement paramétrique a été formulé, avec les paramètres électriques des lignes de transmission inclus comme coordonnées additionnelles de la représentation séparée. La méthode a été étendue pour étudier la solution du modèle des lignes de transmission pour laquelle les paramètres dépendent de la fréquence.

Mots-clés
Réseaux Intelligents, Dynamique transitoire, Équations oscillantes, Lignes de transmission, Réduction de modèles, Décomposition orthogonale appropriée, Méthode d'incrémentation de grande longueur, Méthode linéaire par morceaux de trajectoire, Décomposition généralisée appropriée, Paramètres dépendants de la fréquence

Abstract

This thesis presents the study of the model order reduction for power grids and transmission networks. The specific focus has been the transient dynamics. A mathematical viewpoint has been adopted for model reduction. Power networks are huge and complex network, simulation for power grid analysis and design require large non-linear models to be solved. In the context of developing "Smart Grids" with the distributed generation of power, real time analysis of complex systems such as these needs fast, reliable and accurate models. In the current study we propose model order reduction methods both a-priori and a-posteriori suitable for dynamic models of power grids.

The model that describes the transient dynamics of the power grids is complex non-linear swing dynamics model. The non-linearity of the swing dynamics model necessitates special attention to achieve maximum benefit from the model order reduction techniques. In the current research, POD and LATIN methods were applied initially with varying degrees of success. The method of TPWL has been proved as the best-suited model reduction method for swing dynamics model; this method combines POD with multiple linear approximations.

For the transmission lines, a distributed parameters model in frequency-domain is used. PGD based reduced-order models are proposed for the DP model of transmission lines. A fully parametric problem with electrical parameters of transmission lines included as coordinates of the separated representation. The method was extended to present the solution of frequency-dependent parameters model for transmission lines.

Key Words
Smart Grids, Transient Dynamics, Swing Equations, Transmission Lines, Model Reduction, Proper Orthogonal Decomposition, Large Time Increment Method, Trajectory Piece-wise Linear Method, Proper Generalized Decomposition, Frequency-Dependent Parameters